Error Analyses for Nyström Methods for Solving Fredholm Integral and Integro-Differential Equations

Abigail Imogen Fairbairn

The University of Leeds

School of Mathematics

Submitted in accordance with the requirements for the degree of

Doctor of Philosophy

September 2018

The candidate confirms that the work submitted is her own, except where work which has formed part of jointly authored publications has been included. The contribution of the candidate and the other authors to this work has been explicitly indicated below. The candidate confirms that appropriate credit has been given within the thesis where reference has been made to the work of others.

The work in Chapter 4 of this thesis has appeared in the following (two, both published) jointly authored publications:

- [50] A. I. Fairbairn and M. A. Kelmanson. Computable theoretical error bounds for Nyström methods for Fredholm integral equations of the second kind. In P.J. Harris, editor, *Proc. 10th UK Conf. on Boundary Integral Methods (Brighton, UK)*, pages 85 – 94, 2015.

- [52] A. I. Fairbairn and M. A. Kelmanson. Spectrally accurate Nyström-solver error bounds for 1-D Fredholm integral equations of the second kind. *Appl. Math. Comput.*, 315:211 – 223, 2017.

The work in Chapter 5 of this thesis has appeared in the following (three, two published, one in press at time of thesis submission) jointly authored publications:

- [51] A.I. Fairbairn and M.A. Kelmanson. An exponentially convergent Volterra-Fredholm method for integro-differential equations. In D.J. Chappell, editor, *Proc. 11th UK Conf. on Boundary Integral Methods (Nottingham, UK)*, pages 53–63, 2017.

- [53] A.I. Fairbairn and M.A. Kelmanson. Error analysis of a spectrally accurate Volterra-transformation method for solving 1-D Fredholm integro-differential equations. *Int. J. Mech. Sci.*, 144:382–391, 2018.

- [54] A.I. Fairbairn and M.A. Kelmanson. A priori Nyström-method error bounds in approximate solutions of 1-D Fredholm integro-differential equations. *Int. J. Mech. Sci.*, 27pp. in press, 2018.

In the above publications the candidate did almost all of the computations and Prof. M. A. Kelmanson wrote all initial drafts of abstracts, introductions and conclusions, and acted as corresponding author. With the exception of those aspects relating to

the Euler-Bernoulli problem in [54], which were done by Prof. M. A. Kelmanson, all core aspects of the papers were shared, i.e. analysis, methods, implementation, novel error-formulae, presentation and discussion of results, and interpretations.

Acknowledgements

I cannot thank Prof. Mark Kelmanson enough. I could not have asked for a better supervisor. I thank him not only for his help and advice throughout the last four years, but also for encouraging me to pursue a PhD in the first place. He has been most generous with his time, and his constructive feedback has enabled me to develop my confidence in not only my mathematical skills, but also those in my written work. Mark has consistently pushed me to achieve the best of my abilities and I have learned a great deal from him. It has been a pleasure to work together. I am immensely grateful.

I would also like to thank Dr. Evy Kersalé for his helpful comments and feedback during annual review meetings. This too was valuable in assisting my progress.

In addition, I am grateful for the financial support from the EPSRC through the Doctoral Training Grant Studentship.

Finally, my thanks go to my parents Catherine and James, and my partner Adam, for their patience, encouragement and constant support. Together they have kept me going when times got tough.

Abstract

This thesis concerns the development and implementation of novel error analyses for ubiquitous Nyström-type methods used in approximating the solution in 1-D of both Fredholm integral- and integro-differential equations of the second-kind, (FIEs) and (FIDEs). The distinctive contribution of the present work is that it offers a new systematic procedure for predicting, to spectral accuracy, error bounds in the numerical solution of FIEs and FIDEs when the solution is, as in most practical applications, *a priori* unknown.

The classic Legendre-based Nyström method is extended through Lagrange interpolation to admit solution of FIEs by collocation on *any* nodal distribution, in particular, those that are optimal for not only integration but also differentiation. This offers a coupled extension of optimal-error methods for FIEs into those for FIDEs. The so-called FIDE-Nyström method developed herein motivates yet another approach in which (demonstrably ill-conditioned) numerical differentiation is bypassed by reformulating FIDEs as hybrid Volterra-Fredholm integral equations (VFIEs). A novel approach is used to solve the resulting VFIEs that utilises Lagrange interpolation and Gaussian quadrature for the Volterra and Fredholm components respectively.

All error bounds implemented for the above numerical methods are obtained from novel, often complex extensions of an established but hitherto-unimplemented theoretical Nyström-error framework. The bounds are computed using *only the available computed numerical solution*, making the methods of practical value in, e.g., engineering applications. For each method presented, the errors in the numerical solution converge (sometimes exponentially) to zero with N, the number of discrete collocation nodes; this rate of convergence is additionally confirmed via large-N asymptotic estimates. In many cases these bounds are spectrally accurate approximations of the true computed errors; in those cases that the bounds are not, the non-applicability of the theory can be predicted either *a priori* from the kernel or *a posteriori* from the numerical solution.

Contents

List of Figures

List of Tables

Abbreviations and Conventions

BC	Boundary condition
BVP	Boundary value problem
CNM	Classical Nyström method
ECNM	Extended classical Nyström method
EINM	Extended interpolated Nyström method
EVP	Eigenvalue problem
FIDE	Fredholm integro-differential equation
FIE	Fredholm integral equation
FIE2	Fredholm integral equation of the second kind
IC	Initial condition
IDE	Integro-differential equation
INM	Interpolated Nyström method
LGR	Left-Gauss-Radau
ODE	Ordinary differential equation
PDE	Partial differential equation
RGR	Right-Gauss-Radau
VFIE	Volterra-Fredholm integral equation
VIE	Volterra integral equation
$\overset{LH}{=}$	Terms either side of this are equivalent by L'Hôpital's rule
$\|\cdot\|$	The infinity norm $\|\cdot\|_\infty$ defined on $[-1,1]$

Chapter 1

Introduction

"An approximate answer to the right problem is worth a good deal more than an exact answer to an approximate problem."

– John Tukey

1.1 Background and Motivation

Many problems arising in applied sciences, engineering and social sciences can be modelled by mathematical equations. However, due to the complexity of modelling real-life problems, it is in practice difficult, if not impossible, to solve the corresponding equations analytically, so their solutions must be approximated using so-called numerical methods. Accordingly, a vast literature exists on the development of numerical methods for "solving" problems whose closed-form analytical solutions lie beyond the reach of mathematical techniques. Moreover, even in those cases for which closed-form solutions are attainable, the complexity of the resulting solutions and the actual cost of evaluating them may be sufficiently high as to render them little more than an academic exercise; a Pyrrhic victory, so to speak. This being said, numerical methods themselves are useful only if the errors in the approximate solutions they yield can be quantified; in engineering terms, it is essential to know the tolerances of the output. Therefore, the development of computable and accurate error estimates and bounds thereon is a subject of considerable importance in its own right, and the subject of *error analysis* is a crucial component in the

application of numerical methods to all problems whose exact solution is unknown. It is within this broad area that this thesis is focussed.

Specifically considered herein are two widely encountered, important classes of numerical methods, namely those for approximating the solutions of *integral equations* (IEs) and *integro-differential equations* (IDEs), both of which are ubiquitous in the modelling of many real-life problems. IEs, which are characterised by containing the integral of an unknown function, arise in the modelling of, for example, heat conduction [56], population dynamics [81], electromagnetism [123] and acoustics [127]. Similarly, IDEs, characterised by containing both the integral and derivative(s) of an unknown function, can be used to model, for example, water waves [101], viscoelasticity [86] and option pricing [36].

The examples cited comprise but a few of the diverse practical applications contained within the plethora of literature on the development of numerical methods for IEs and IDEs. However, despite this ubiquity of application, relatively little attention has been paid to the important matter of analysing the errors incurred in the approximations. Accordingly, the main goal of this thesis is to address this scarcity; specifically, to analyse, to develop and to implement closed-form predictions of errors that are highly distinctive insofar as they *can be computed relatively easily, and to high degree of accuracy, using only the approximate solution computed by the numerical method.* This aspect will be revisited in more detail below.

Many well-known approximation techniques have been deployed in numerical solvers for both IEs and IDEs, for example, within the context of IEs, methods are based on Taylor-series expansions [91, 70], discrete product integration [76], Adomian decomposition [11, 58], multigrids [63] and Haar wavelets [13]. Similarly, within the context of IDEs, commonly used methods are Taylor-series expansions [137], the Tau method [69], sine-cosine wavelets [121], Sinc methods [106], Shannon wavelets [92] and a reproducing-kernel Hilbert space approach [6]. The diversity of and time-span covered by this literature bear testimony to the importance of obtaining accurate solutions of both IEs and IDEs.

IEs and IDEs can be classified in many ways, the most general being based upon the limits of integration. There are two fundamental forms: Volterra IEs/IDEs contain an integral with a variable limit of integration whereas Fredholm IEs/IDEs contain an integral with fixed limits of integration. Volterra and Fredholm IEs/IDEs are respectively associated with the reformulation of initial-value and boundary-value

problems. This thesis is concerned with the solution of only Fredholm IEs (FIEs) and Fredholm IDEs (FIDEs), whose reformulation from the boundary-value problem (BVP) format is often beneficial. For example, the reformulation of a two-point second-order BVP to an FIE has the welcome advantage that all associated boundary conditions (BCs) are subsumed into the single IE, rather than imposed externally on the differential equation. Similarly, the FIDE reformulation of higher-order two-point BVPs, e.g. the fourth-order Euler-Bernoulli beam-deflection problem with varying flexural rigidity [54], explicitly incorporates all BCs imposed upon the BVP.

The one-dimensional FIEs studied in this thesis can be written in the canonical form

$$u(x) - \lambda \int_{-1}^{1} K(x,y)\, u(y)\, dy = f(x), \qquad x \in [-1,1], \tag{1.1.1}$$

and, similarly, the one-dimensional FIDEs studied have the canonical form

$$u(x) - \mu(x)\, \frac{du}{dx} - \lambda \int_{-1}^{1} K(x,y)\, u(y)\, dy = f(x), \qquad x \in [-1,1], \tag{1.1.2}$$

in both of which forms the kernel $K : [-1,1] \times [-1,1] \to \mathbb{R}$, source function $f : [-1,1] \to \mathbb{R}$ and constant $\lambda \in \mathbb{R}$ are known functions and $u(x)$ is the unknown function to be determined on $[-1,1]$. The coefficient function $\mu : [-1,1] \to \mathbb{R}$ in (1.1.2) is also known and, because of the first-order differential term, the FIDE (1.1.2) must be augmented by a single BC. Note that the rescaling of many practical problems leads to the canonical forms (1.1.1) and (1.1.2). This thesis considers only FIEs and FIDEs with non-singular kernels; the former of which arise in applications such as electrostatics [88] and current flow [96], and the latter of which have applications in engineering [54] and aerodynamics [49].

Many numerical methods have been developed for the solution of FIEs, including well-known approaches based on interpolation, projection, collocation and quadrature detailed in [10, 14, 60, 83]. However, perhaps the most widely used approach is the Nyström method [98], which provides the foundations for the numerical methods developed in this thesis. The Nyström method employs Gaussian quadrature [9] and discrete collocation for determining approximate solutions of FIE (1.1.1) for all $x \in [-1,1]$. In general, if the FIE kernel is smooth and non-singular, then the Nyström solution is a spectrally accurate approximation of the exact solution.

However, solving FIEs with a singular kernel requires modifications to the Nyström method. For example: [100] uses a smoothing change of variables and product-integration techniques; [80] incorporates an error estimate into the Nyström method *a priori* in order to accommodate kernels with challenging end-point singularities; [8] presents iterative variants of the Nyström method that can be applied to FIEs with singular kernels; and [77] develops a new discretisation technique based on Clenshaw-Curtis quadrature that is used for FIEs whose kernel is discontinuous along the main diagonal, e.g. the kernel $K(x,y) = \widetilde{K}(|x-y|)$ arising in the modelling of radiative transfer. The new analysis developed in this thesis quantifies the problem-dependent level of accuracy that can be expected from the Nyström method. This analysis confirms that, for smooth continuously differentiable kernels and solutions, spectral accuracy can be achieved. Not only does this analysis highlight the merits of the Nyström method, but it also enables (sometimes spectrally accurate) estimates to be computed of the error in the resulting numerical solutions.

Despite their demonstrable ubiquity in solving FIEs, Nyström-type numerical methods appear less frequently in the literature on FIDEs which, as stated in [77], *"are usually solved by iterative finite difference methods, or by orthogonal function expansion methods"*. For example: [7] uses backward-difference and repeated-trapezoidal formulae; a Chebyshev finite difference scheme is proposed in [42]; [136] uses a Chebyshev series expansion whose coefficients are found iteratively; [12] determines the coefficients of a Chebyshev-polynomial expansion via a fast Galerkin scheme; [55] approximates FIDE solutions by a finite expansion of Legendre basis functions whose coefficients are determined by a Galerkin-Legendre system; a Legendre-polynomial expansion is used in [138], in which the coefficients are determined by matrix collocation; and, [24] compares a variational iteration method to the Legendre-polynomial approximation given in [138]. These methods, which are of varying degrees of efficiency and accuracy, can be used to approximate not only the solution of (1.1.2) but also the solution of its extension to FIDEs involving higher-order derivatives.

Although Nyström-type methods rarely appear in the existing literature within the context of solving FIDEs, [12] states that the Nyström method does *"generalise readily"* when solving IDEs as *"it is natural to introduce a finite difference approximation for the derivative term(s)"*. By contrast, [108] demonstrates how a higher-order-derivative extension of (1.1.2) can be discretised using a combination

of Lagrange interpolation and Gauss-Legendre quadrature to form a system of algebraic equations in which the unknowns are nodal values of the FIDE solution. The system in [108] is numerically solved by Newton's method and the resulting nodal values are Lagrange-interpolated to approximate the FIDE solution throughout the domain.

As alluded to above, and despite ongoing research, exemplified above, into approximation methods for solving FIEs and FIDEs, techniques for determining corresponding computable error bounds remain relatively scarce. This scarcity is particularly notable for the Nyström method, for which it is acknowledged in [83, p. 188] that *"these bounds will be difficult to evaluate in applications"*, and noted in [9, p. 282] that *"it is difficult to estimate the error"*. Moreover, the frequently stated bound on the Nyström error [10, Eq. 4.1.33] is dependent upon the exact solution, which in practice is not only invariably unknown, but also contains a component that is purely theoretical. Other analyses of the Nyström error notably focus on only convergence rates, see e.g. [45, 113, 117]. Similarly, computable error bounds are rare in the error analyses of numerical methods for the solution of IDEs. For example, in the above-cited literature, [136, 121, 106, 137, 42, 24, 7, 108] strikingly contain no discussion whatsoever of errors; [92] gives an error bound for only the first derivative of the solution; the error estimates in [69, 138, 55] are themselves subject to an unquantified error; [6] proves only a convergence theorem; and [12] develops error estimates that do not always exceed the true computed error and so cannot be used as reliable error bounds.

Consequently, the aims of this thesis are twofold: to develop and to implement numerical methods that yield spectrally accurate approximations to the solutions of FIEs and FIDEs, and to derive corresponding error bounds that are explicitly computable using only the numerical solution, so that they require no knowledge of the exact solution. Achieving these goals requires a thorough understanding of the numerical techniques used in both FIE- and FIDE-approximation methods. Therefore, the initial focus of this thesis is on the establishment of the foundations required for approximating a function, its derivatives and its integral, including a comprehensive study of the resulting errors. Using this initial framework, novel numerical methods and implementable error analyses are then developed for both FIEs and FIDEs.

1.2 Thesis Overview

The numerical methods developed in this thesis are based upon the widely used Nyström method [98], which is presently extended through incorporation of interpolation and numerical differentiation. Additionally, the existing theoretical error analysis of the Nyström method is used as the basis for novel error analyses that yield spectrally accurate error predictions for the newly derived methods. The development of these numerical methods and error predictions requires analysis of not only the Nyström method and the numerical quadrature used therein, but also analysis of the implementation of interpolation techniques and numerical differentiation. Accordingly, the structure of the remainder of this thesis is as follows.

Chapter 2 presents the framework required for performing interpolation and differentiation of discrete data. This includes a thorough analysis of Lagrange interpolation [85], the foundation upon which the numerical techniques in all subsequent chapters rely, along with its more stable barycentric counterpart [22], whose implementation is computationally less expensive. The errors are analysed for both forms of interpolation through the derivation of error bounds and convergence rates that enable the accuracy of each approach to be predicted and quantified. Since the accuracy of interpolation is dependent on the nodal distribution upon which it is based, a variety of interpolating-node distributions are examined and compared. These nodal distributions include those that are optimal for numerical differentiation along with those that are optimal for numerical integration, since both of these are required when implementing IE and IDE numerical methods. For completeness, Tikhonov regularisation [26] is considered in order to demonstrate how to overcome the limitations of Lagrange and barycentric interpolation.

Chapter 3 develops the tools required for solving IEs and IDEs numerically. The interpolation techniques introduced in Chapter 2 are extended to methods for implementing numerical quadrature and numerical differentiation. The former is required for solving both IEs and IDEs, whilst the latter is required for solving only IDEs. In order to implement the numerical differentiation outlined in Chapter 2 efficiently and accurately, differentiation matrices [19, 116] are introduced and analysed. These use the nodal data of a function to approximate its derivative, at those nodes, in a way that bypasses the need for any intermediate interpolation. Chapter 3 also presents an overview of Gaussian quadrature [9], i.e. the fundamental

component of the Nyström method. Gaussian quadrature offers a spectrally accurate method for approximating the definite integral of a function using discrete nodal data. Accordingly, Chapter 3 provides methods for approximating the derivative and integral of a function using only its nodal data. These techniques comprise the foundation of the IE and IDE numerical methods used and developed in Chapters 4 and 5 respectively.

Overviews of IEs and the Nyström method are presented in Chapter 4. An extension is then developed of the Nyström method which uses the interpolation techniques described in Chapter 2 to approximate the solution of IEs on *any* set of nodes, for example those optimal for differentiation. This is done in preparation for a further extension, described in Chapter 5, for solving IDEs with the goal of minimising the overall error by projecting between optimal quadrature and optimal differentiation nodes. Error analyses are presented for both the Nyström method and its interpolated counterpart. These error analyses are founded upon the existing fundamental operator theory that underpins the Nyström method. The error bounds and asymptotic error estimates derived from this theoretical framework are explicitly computable using only the numerical IE solution. As discussed above, this constitutes a novel aspect of this thesis.

In Chapter 5, IDEs are introduced and two distinct methods are developed for approximating their solution. First, the Nyström methods used to solve IEs in Chapter 4 are extended by incorporating the numerical differentiation outlined in Chapters 2 and 3. The error analysis for this newly extended Nyström approach develops the operator theory used in the IE error analyses to obtain spectrally accurate error bounds and predictions that are explicitly computable without knowledge of an exact solution. This Nyström method is expanded upon in [54] to solve a novel IDE formulation of an Euler-Bernoulli beam-deflection problem in which the flexural rigidity varies along the beam. Since no exact solution is attainable for this engineering problem, [54] provides concrete corroboration of the practical relevance of the novel Nyström approach and error analysis developed in this thesis.

Second, a method is developed in which IDE solutions are obtained by first transforming the IDE into a hybrid Volterra-Fredholm integral equation (VFIE). The resulting VFIE is solved by a novel method that uses a combination of the Lagrange interpolation introduced in Chapter 2 and Gaussian quadrature introduced in Chapter 3. An approximate IDE solution is then recovered from the approximate

VFIE solution. This approach bypasses the need for differentiation matrices, used in the extended Nyström methods, which are well-known to be ill-conditioned [18, 29, 46]. Similar operator theory as that used for the Nyström approaches is used to develop spectrally accurate error bounds and estimates, for the VFIE reformulation method, that require no knowledge of the exact solution. Consequently, since both of the newly developed numerical methods yield error bounds that are computable in the absence of an exact solution, they differ distinctively from all related methods in the existing literature.

In summary, Chapters 2 and 3 present an overview of existing approximation techniques required for solving IEs and IDEs numerically, and these approximation techniques are incorporated into novel numerical methods for solving IEs and IDEs in Chapters 4 and 5 respectively. Correspondingly, the errors incurred in the approximation techniques considered in Chapters 2 and 3 are analysed and incorporated into novel error analyses for the newly developed numerical IE and IDE methods. General summaries of the numerical methods and error analyses are given in Chapter 6.

In addition to the novel work contained in the main chapters of this thesis, the appendices contain novel work that is hitherto unpublished.

In Appendix A, a proof is presented, of explicit formulae for the derivatives of Lagrange polynomials, that does not appear to have been considered in the previous literature.

Appendix C presents a non-trivial proof of the complex Legendre-polynomial expression used to derive interpolation error bounds in Chapter 2, quoted in [1] but not proved.

In Appendix D, *ab initio* derivations are given for two methods of converting a BVP to a FIE. The first method initially follows the conversion in [104]; however, the approach in [104] is incorrect, despite apparently never before having been recognised as such. Therefore, the conversion in Appendix D is augmented with an example that demonstrates not only the correctness of the new approach but also the source of the error in [104]. The second conversion method in Appendix D derives the FIE given in [75], whose derivation from a BVP is not shown therein.

Finally, Appendix E proves the assertion, used in the Nyström method analysis in Chapter 4, that all but one of the eigenvalues of the (separable kernel) Nyström method matrices are equal to 0.

Only Appendix B contains work that is not original; however, the non-intuitive proof therein of a bound on monic polynomials based upon regularly spaced nodes is provided for completeness.

Chapter 2

Interpolation of Discrete Data

A first step towards the main goal of this thesis – the development and error analysis of numerical methods for finding approximate solutions of both integral equations (IEs) and integro-differential equations (IDEs) – is the establishment of the foundations and framework required for performing stable and reliable interpolation and differentiation of discrete data. With this framework established, it is used in subsequent chapters both to understand and to explain the errors incurred in the numerical techniques used in both IE and IDE scenarios.

Accordingly, *Lagrange interpolation* [85, 120] is introduced in Section 2.1 along with its more stable (and perhaps lesser-known) counterpart, *barycentric interpolation* [22]; for both approaches, error bounds and convergence rates are derived so that the accuracy of both forms of interpolation may be predicted and quantified. The Lagrange interpolation in Section 2.1 provides the foundation on which the numerical differentiation and numerical quadrature methods, in Sections 3.1 and 3.2 respectively, are established.

A variety of interpolating-node distributions are examined in order to demonstrate, through numerical experiments on the different nodal sets, the advantages – e.g. uniform distribution of error – of so-called *clustered distributions* [124, 57]. Such nodal distributions include those that are optimal for both numerical differentiation and for numerical integration (NB these sets are generally different), since these are used to minimise the error within the IE and IDE numerical approximations. Finally, *Tikhonov regularisation* [129, 26] is also considered in order to demonstrate how to overcome the limitations of Lagrange and barycentric interpolation: for example,

the *Runge phenomenon*, [107, 27] which results from interpolation using regularly spaced nodes.

Throughout this chapter, unless otherwise stated, $i, j = 1(1)N$.

2.1 Interpolation Methods

2.1.1 Lagrange Interpolation

The action of Nth-order Lagrange-interpolation [85, 120] on a function $u : [a, b] \to \mathbb{R}$ that is N-times continuously differentiable on the interval $[a, b]$, at data nodes $x_{j,N}$ ordered so that $a \leq x_{1,N} < x_{2,N} < ... < x_{N,N} \leq b$, is defined by the numerical operator $\mathcal{L}_N$ as

$$\mathcal{L}_N u = (\mathcal{L}_N u)(x) \equiv \sum_{j=1}^{N} L_{j,N}(x)\, u(x_{j,N}), \tag{2.1.1}$$

wherein the Lagrange basis functions are defined by

$$L_{j,N}(x) \equiv \prod_{\substack{k=1 \\ k \neq j}}^{N} \frac{x - x_{k,N}}{x_{j,N} - x_{k,N}}. \tag{2.1.2}$$

The Lagrange approximation $\mathcal{L}_N u$ in (2.1.1) is therefore a polynomial of degree $N - 1$ in x. Let the Nth-degree monic polynomial whose N distinct real roots are the interpolation nodes $x_{j,N}$ be defined by

$$p_N(x) \equiv \prod_{j=1}^{N} (x - x_{j,N}), \tag{2.1.3}$$

which is equivalently

$$p_N(x) = (x - x_{j,N})\, q_N(x), \tag{2.1.4}$$

wherein

$$q_N(x) \equiv \prod_{\substack{k=1 \\ k \neq j}}^{N} (x - x_{k,N}). \tag{2.1.5}$$

Differentiation of (2.1.4) gives

$$p'_N(x) = q_N(x) + (x - x_{j,N})\, q'_N(x), \tag{2.1.6}$$

in which setting $x = x_{j,N}$ yields

$$p'_N(x_{j,N}) = q_N(x_{j,N}). \tag{2.1.7}$$

Therefore the Lagrange basis function $L_{j,N}(x)$, defined in (2.1.2), can also be written in the more succinct form

$$L_{j,N}(x) = \frac{p_N(x)}{(x - x_{j,N})\, p'_N(x_{j,N})}. \tag{2.1.8}$$

2.1.2 Barycentric Interpolation

The Lagrange interpolation formula (2.1.1), in which $L_{j,N}(x)$ is henceforth constructed using (2.1.8), can be expressed in an alternative, so-called *barycentric form*. This has computational advantages over the Lagrange form such as reduced workload and increased stability [109]. The barycentric form is derived as follows. Equations (2.1.1) and (2.1.8) can together be written as the *first form* of the barycentric interpolation formula [67] which is

$$(\mathcal{B}_N^{(1)} u)(x) = p_N(x) \sum_{j=1}^{N} \frac{W_{j,N}\, u(x_{j,N})}{x - x_{j,N}}, \tag{2.1.9}$$

wherein the weights $W_{j,N}$ are defined by

$$W_{j,N} = \frac{1}{p'_N(x_{j,N})} \tag{2.1.10}$$

so that, by construction,

$$(\mathcal{B}_N^{(1)} u)(x) = (\mathcal{L}_N u)(x). \tag{2.1.11}$$

If the constant function $u(x) \equiv 1$ is approximated in this way then $u(x_{j,N}) = 1$ for all values of j, hence (2.1.9) can be written as

$$1 = p_N(x) \sum_{j=1}^{N} \frac{W_{j,N}}{x - x_{j,N}}, \tag{2.1.12}$$

and so (2.1.9) and (2.1.12) together yield the *second form* of the barycentric interpolation formula as

$$(\mathcal{B}_N^{(2)} u)(x) = \frac{\displaystyle\sum_{j=1}^{N} \frac{W_{j,N}\, u(x_{j,N})}{x - x_{j,N}}}{\displaystyle\sum_{j=1}^{N} \frac{W_{j,N}}{x - x_{j,N}}}. \tag{2.1.13}$$

By construction, (2.1.1), (2.1.9) and (2.1.13) are equivalent approximations of the function $u(x)$ so that

$$(\mathcal{L}_N u)(x) = (\mathcal{B}_N^{(1)} u)(x) = (\mathcal{B}_N^{(2)} u)(x). \tag{2.1.14}$$

2.2 Differentiation of Interpolation Formulae

The derivative $u'(x)$ of a function can also be approximated using the nodal data $u(x_{j,N})$. By first defining the differential operator $\mathcal{D}$ by

$$\mathcal{D}u = (\mathcal{D}u)(x) \equiv u'(x), \tag{2.2.1}$$

wherein a prime denotes differentiation with respect to x, the numerical differential operator $\mathcal{D}_N$ is defined as

$$\mathcal{D}_N \equiv \mathcal{D}\mathcal{L}_N. \tag{2.2.2}$$

Therefore, differentiating (2.1.1) with respect to x yields

$$\mathcal{D}_N u = (\mathcal{D}_N u)(x) \equiv \sum_{j=1}^{N} L'_{j,N}(x)\, u(x_{j,N}) \tag{2.2.3}$$

in which differentiation with respect to x of (2.1.8) gives

$$L'_{j,N}(x) = \frac{p'_N(x)\,(x - x_{j,N}) - p_N(x)}{(x - x_{j,N})^2\, p'_N(x_{j,N})}. \tag{2.2.4}$$

In a similar way, higher derivatives of $u(x)$ are approximated by defining

$$\mathcal{D}_N^{(M)} \equiv \mathcal{D}^M \mathcal{L}_N, \qquad M \geq 1, \tag{2.2.5}$$

so that the Mth derivative $u^{(M)}(x)$ is approximated by differentiating $\mathcal{L}_N u(x)$ in (2.1.1) M times to give

$$\mathcal{D}_N^{(M)} u = (\mathcal{D}_N^{(M)} u)(x) \equiv \sum_{j=1}^{N} L_{j,N}^{(M)}(x)\, u(x_{j,N}). \tag{2.2.6}$$

Since $\mathcal{L}_N u(x)$ is a polynomial of degree $N-1$ in x, the right-most term in (2.2.6) is a polynomial of degree $N-1-M$ in x for $M \leq N-1$. For $M \geq N$, (2.2.6) therefore

gives $\mathcal{D}_N^{(M)} u \equiv 0$. A formula for the functions $L_{j,N}^{(M)}(x)$ is found by differentiating (2.2.4) to give

$$L''_{j,N}(x) = \frac{p''_N(x)(x - x_{j,N})^2 - 2p'_N(x)(x - x_{j,N}) + 2p_N(x)}{(x - x_{j,N})^3 \, p'_N(x_{j,N})}, \tag{2.2.7}$$

and

$$L'''_{j,N}(x) = \frac{p'''_N(x)(x - x_{j,N})^3 - 3p''_N(x)(x - x_{j,N})^2 + 6p'_N(x)(x - x_{j,N}) - 6p_N(x)}{(x - x_{j,N})^4 \, p'_N(x_{j,N})}, \tag{2.2.8}$$

from which the general formula for the Mth derivative of $L_{j,N}(x)$ is postulated to be

$$L_{j,N}^{(M)}(x) = \frac{\displaystyle\sum_{k=0}^{M} (-1)^{M+k} \frac{M!}{k!} (x - x_{j,N})^k \, p_N^{(k)}(x)}{(x - x_{j,N})^{M+1} \, p'_N(x_{j,N})}, \tag{2.2.9}$$

which is proved by induction on M in Appendix A. This establishes the framework by which numerical differentiation can be implemented for finding approximate solutions of ODEs and IDEs. It is shown in Section 2.5 that this differentiation is readily achieved to spectral accuracy for sufficiently smooth solutions.

2.3 Nodal Distributions

The Lagrange and barycentric interpolation formulae (2.1.1) and (2.1.13) and the derivative interpolation formulae (2.2.3) and (2.2.6) apply to any nodal distribution $x_{j,N}$. In this section, several nodal distributions are defined on the interval $[-1, 1]$ and, where possible, explicit forms of the barycentric weights (2.1.10) are given. A regularly spaced distribution is introduced along with a range of *clustered distributions* [57, 124]; these are later shown, in Section 2.4, to yield more accurate approximations than the regularly spaced distribution. Due to their intended use within the numerical methods for IEs and IDEs, the clustered nodal distributions considered include those that are optimal for numerical differentiation and those that are optimal for numerical integration. For consistency, all of the nodal distributions are defined such that $-1 \leq x_{1,N} < x_{2,N} < \ldots < x_{N,N} \leq 1$; this ordering admits direct comparisons between the distributions and also simplifies comparisons between the numerical methods for IDEs in Chapter 5.

2.3.1 Specific Nodal Distributions

Regular Nodes

Regularly spaced nodal locations on $[-1, 1]$ are given by

$$x_{j,N} = -1 + \frac{2\,(j-1)}{N-1}, \tag{2.3.1}$$

using which the barycentric weights $W_{j,N}$ are derived from (2.1.10) as

$$W_{j,N} = \frac{(-1)^{N-j}}{(N-1)!}\binom{N-1}{j-1}\left(\frac{2}{N-1}\right)^{N-1}, \tag{2.3.2}$$

wherein the middle term in brackets denotes a binomial coefficient. However, since $W_{j,N}$ occurs in both the numerator and denominator of the barycentric interpolation formula (2.1.13), any factor common to all weights $W_{j,N}$ that is independent of j cancels out and so it is sufficient to define the weights as [22, Eq. 5.1]

$$W_{j,N} = (-1)^{j-1}\binom{N-1}{j-1}. \tag{2.3.3}$$

Note that, for the same reasoning, the subsequent barycentric weights defined in (2.3.8), (2.3.11), (2.3.17), (2.3.24), (2.3.25) and (2.3.28) do not contain any common factors that are independent of j.

Chebyshev Nodes

The Chebyshev nodes on $[-1, 1]$ are the roots of the Chebyshev polynomial of the first kind of degree N [93, Eq. 1.1], defined by

$$T_N(x) \equiv \cos(N \cos^{-1} x), \tag{2.3.4}$$

which satisfies Chebyshev's differential equation

$$(1 - x^2)\,T''_N(x) - x\,T'_N(x) + N^2\,T_N(x) = 0. \tag{2.3.5}$$

The monic polynomial $p_N(x)$ in (2.1.3) with roots at the Chebyshev nodes is therefore given by

$$p_N(x) = \frac{T_N(x)}{2^{N-1}} \tag{2.3.6}$$

and the Chebyshev nodes are given by

$$x_{j,N} = \cos\frac{2N-2j+1}{2N}\pi. \tag{2.3.7}$$

The barycentric weights $W_{j,N}$ in (2.1.10) are given explicitly [22, Eq. 5.3] as

$$W_{j,N} = (-1)^j \sin\frac{2j-1}{2N}\pi. \tag{2.3.8}$$

Chebyshev-Gauss-Lobatto Nodes

The Chebyshev-Gauss-Lobatto nodes are located at the endpoints ± 1 and the extrema in $(-1,1)$ of the Chebyshev polynomial $T_{N-1}(x)$ defined in (2.3.4). The monic polynomial with roots at these nodes is

$$p_N(x) = \frac{(x^2-1)\,T'_{N-1}(x)}{2^{N-2}\,(N-1)}, \tag{2.3.9}$$

giving

$$x_{j,N} = \cos\frac{N-j}{N-1}\pi. \tag{2.3.10}$$

The barycentric weights $W_{j,N}$ in (2.1.10) are given [22, Eq. 5.4] as

$$W_{j,N} = \frac{(-1)^j}{1+\delta_{1j}+\delta_{Nj}}, \tag{2.3.11}$$

wherein the *Kronecker delta* δ_{ij} is defined by

$$\delta_{ij} \equiv \begin{cases} 1 & i = j \\ \\ 0 & i \neq j. \end{cases} \tag{2.3.12}$$

Legendre Nodes

The Legendre nodes on $[-1,1]$ are the roots of the Legendre polynomial of degree N that is expressed using Rodrigues' formula [2, Eq. 8.6.18] as

$$P_N(x) = \frac{1}{2^N\,N!}\frac{d^N}{dx^N}\,(x^2-1)^N, \tag{2.3.13}$$

which satisfies Legendre's differential equation [133, p. 304]

$$(1-x^2)\,P''_N(x) - 2x\,P'_N(x) + N(N+1)P_N(x) = 0. \tag{2.3.14}$$

The monic polynomial with roots at the Legendre nodes is given by

$$p_N(x) = \frac{2^N (N!)^2}{(2N)!} P_N(x) \tag{2.3.15}$$

and the nodes are then defined by $P_N(x_{j,N}) = 0$, i.e.

$$x_{j,N} = j\text{th zero of } P_N(x). \tag{2.3.16}$$

The barycentric weights $W_{j,N}$ in (2.1.10) follow from (2.3.15) as

$$W_{j,N} = \frac{1}{P'_N(x_{j,N})}. \tag{2.3.17}$$

Legendre-Gauss-Radau Nodes

Legendre-Gauss-Radau distributions [68] are non-symmetric nodal distributions that include only one of the interval endpoints; $x = 1$ or $x = -1$. The monic polynomial $p_N(x)$ in (2.1.3) with these roots is

$$p_N^-(x) = \frac{2^N (N!)^2}{(2N)!} \Big(P_N(x) + P_{N-1}(x) \Big) \tag{2.3.18}$$

when $x = -1$ is included, or

$$p_N^+(x) = \frac{2^N (N!)^2}{(2N)!} \Big(P_N(x) - P_{N-1}(x) \Big) \tag{2.3.19}$$

when $x = +1$ is included; here $P_N(x)$ is the Legendre polynomial of degree N given in (2.3.13). The two nodal distributions (2.3.18) and (2.3.19) are reflections of each other about the y-axis, hence their monic polynomials satisfy the symmetry relationship

$$p_N^-(x) = (-1)^N \, p_N^+(-x). \tag{2.3.20}$$

The nodal distributions are hereafter named as the "Left-Gauss-Radau" (LGR) distribution when $x = -1$ is included, and the "Right-Gauss-Radau" (RGR) distribution when $x = 1$ is included. The LGR nodes are given by

$$x_{j,N}^- = \begin{cases} -1 & j = 1 \\ (j-1)\text{st zero of } P_N(x) - \dfrac{x-1}{N} P'_N(x) & j = 2(1)N, \end{cases} \tag{2.3.21}$$

wherein the expression for the nodes $x_{j,N}$ for $j = 2(1)N$ is derived using the relationship [65, Eq. 6.42]

$$P_{N-1}(x) = x\,P_N(x) - \frac{x^2-1}{N}\,P'_N(x), \tag{2.3.22}$$

and the RGR nodes are given by

$$x^+_{j,N} = \begin{cases} j\text{th zero of } P_N(x) - \dfrac{x+1}{N}P'_N(x) & j = 1(1)N-1 \\ 1 & j = N. \end{cases} \tag{2.3.23}$$

The LGR barycentric weights $W_{j,N}$ in (2.1.10) follow from (2.3.18) as

$$W^-_{j,N} = \begin{cases} \dfrac{(-1)^{N+1}}{N} & j = 1 \\ \dfrac{1}{P'_N(x^-_{j,N}) + P'_{N-1}(x^-_{j,N})} & j = 2(1)N, \end{cases} \tag{2.3.24}$$

and the RGR barycentric weights follow from (2.3.19) as

$$W^+_{j,N} = \begin{cases} \dfrac{1}{P'_N(x^+_{j,N}) - P'_{N-1}(x^+_{j,N})} & j = 1(1)N-1 \\ \dfrac{1}{N} & j = N. \end{cases} \tag{2.3.25}$$

Legendre-Gauss-Lobatto Nodes

The Legendre-Gauss-Lobatto nodes are located at the endpoints ± 1 and the extrema in $(-1,1)$ of the Legendre polynomial $P_{N-1}(x)$ defined in (2.3.13). The monic polynomial with these roots is

$$p_N(x) = \frac{2^N\,(N!)^2\,(2N-1)}{(2N)!\,N\,(N-1)}(x^2-1)\,P'_{N-1}(x) \tag{2.3.26}$$

which gives the nodes

$$x_{j,N} = \begin{cases} -1 & j = 1 \\ 1 & j = N \\ (j-1)\text{st zero of } P'_{N-1}(x) & j = 2(1)N-1. \end{cases} \tag{2.3.27}$$

The barycentric weights $W_{j,N}$ in (2.1.10) are found from (2.3.26) as

$$W_{j,N} = \begin{cases} (-1)^{N-1} & j = 1 \\ 1 & j = N \\ \dfrac{1}{P_{N-1}(x_{j,N})} & j = 2(1)N-1. \end{cases} \tag{2.3.28}$$

2.3.2 Comparison of Nodal Distributions

It is now shown that, as N increases, the different nodal distributions presented in Section 2.3.1 converge in an identical sense that can be quantified. Consider the number of points $n_{[a,b]}$ in the subset interval $[a,b] \subseteq [-1,1]$ as the integral

$$n_{[a,b]} = N \int_a^b \rho(x)dx \tag{2.3.29}$$

wherein $\rho(x)$ is the nodal density distribution function with, by definition,

$$\int_{-1}^{1} \rho(x)dx = 1. \tag{2.3.30}$$

The density function can be derived explicitly for the Chebyshev-Gauss-Lobatto nodes $x_{j,N}$ defined in (2.3.10) since they are projections onto the x-axis of points that are equally spaced along the upper half of a unit circle. Let C_a and C_b be the projections of points a and b onto the upper half of the unit circle, and let l be the length of the arc between C_a and C_b; these positions are illustrated in Figure 2.3.1.

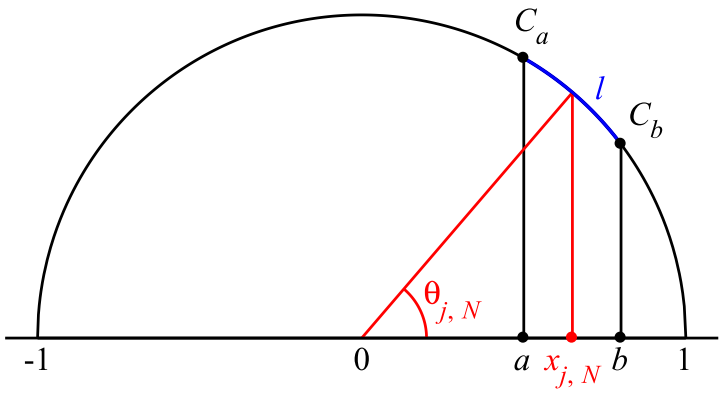

Figure 2.3.1: Positions of C_a, C_b, a, b, $\theta_{j,N}$ and $x_{j,N}$ (see text).

The probability of a point on the half unit circle with polar angle $\theta_{j,N}$ lying between C_a and C_b, and hence (by direct projection) the probability of the corresponding node $x_{j,N}$ lying in $[a, b]$, is clearly

$$p(\theta_{j,N}) = \frac{l}{\pi}. \tag{2.3.31}$$

Therefore, of the total N nodes, Nl/π lie in the interval $[a, b]$. By direct calculation, l is given by

$$l = \int_a^b \frac{dx}{\sqrt{1-x^2}} \tag{2.3.32}$$

so that the number of points $n_{[a,b]}$ in the interval $[a, b]$ of the total N in $[-1, 1]$ is

$$n_{[a,b]} = \frac{N}{\pi} \int_a^b \frac{dx}{\sqrt{1-x^2}}. \tag{2.3.33}$$

That is, by comparison with (2.3.29), the probability density function $\rho(x)$ is given by

$$\rho(x) = \frac{1}{\pi\sqrt{1-x^2}}. \tag{2.3.34}$$

Thus the points are distributed with the density per unit length

$$\text{density} \sim \frac{N}{\pi\sqrt{1-x^2}}, \qquad N \to \infty, \tag{2.3.35}$$

as given in [124, p. 42], in which it is asserted that this is a common property for various clustered nodal distributions upon which polynomial interpolation is effective. In particular, the density function (2.3.34) is common to not only all Jacobi polynomials [57, p. 26] but also other grids associated with the zeros and extrema of orthogonal polynomials such as Legendre polynomials [125, p. 91]. If $x_{j,N}$ represent the Chebyshev-Gauss-Lobatto nodes and $y_{j,N}$ represent the nodes of an alternative distribution then, for a given N, the maximum difference between the corresponding nodes of each distribution is

$$d_N = \max_{1 \le j \le N} |y_{j,N} - x_{j,N}|. \tag{2.3.36}$$

This nodal difference is plotted against N in Figure 2.3.2.

Since the nodal difference d_N in (2.3.36) is seen in Figure 2.3.2 to be a decreasing function of N for each of the clustered nodal distributions as $N \to \infty$, the density

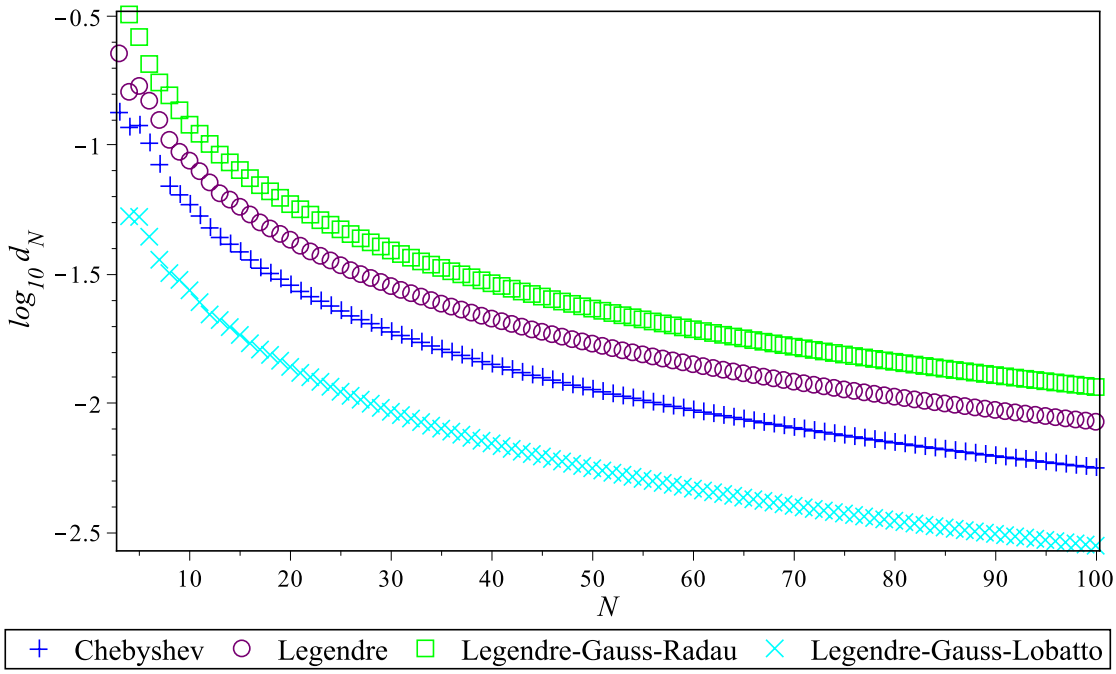

Figure 2.3.2: Logarithmic plot showing the decrease with N of the maximum difference, d_N in (2.3.36), between the Chebyshev-Gauss-Lobatto distribution and the other clustered nodal distributions considered in Section 2.3.1.

(2.3.35) is observed to be true for not only the Chebyshev-Gauss-Lobatto distribution but also for the other distributions whose nodes are contained within d_N, as asserted in [124, p. 42]. Figure 2.3.2 also shows that the Legendre-Gauss-Lobatto nodes are located the closest to the Chebyshev-Gauss-Lobatto nodes; this observation is augmented by the fact that asymptotic estimates of Legendre-Gauss-Lobatto nodes (for the purposes of Gauss quadrature) can be initiated on the Chebyshev-Gauss-Lobatto grid [128]. Furthermore, the convergence of the Legendre-Gauss-Lobatto grid to the Chebyshev-Gauss-Lobatto grid can be anticipated from the result in [30, Lemma 1, p. 23] and the visual comparison in [57, p. 24], in which it is stated that "there is hardly any noticeable difference"; a similar visual comparison in [125, p. 128] of the Legendre and Chebyshev distributions demonstrates the convergence of their respective nodes, which are stated to cluster near ± 1 with the same density as $N \to \infty$.

The convergence of the nodal distributions can also be shown by considering

contours of the potential function of the monic polynomials $p_N(x)$ in (2.1.3). These are given by different values of C, in the level sets of $p_N(z)$ computed from [124, MATLAB "Program 10"]

$$C = \sqrt{\Big(\Re(p_N(z))\Big)^2 + \Big(\Im(p_N(z))\Big)^2} = |p_N(z)|, \tag{2.3.37}$$

where $z = x + iy$ is a field-point in the complex potential plane. Figure 2.3.3 shows the constant value $C = 1$ for each of the nodal distributions based upon various values of N.

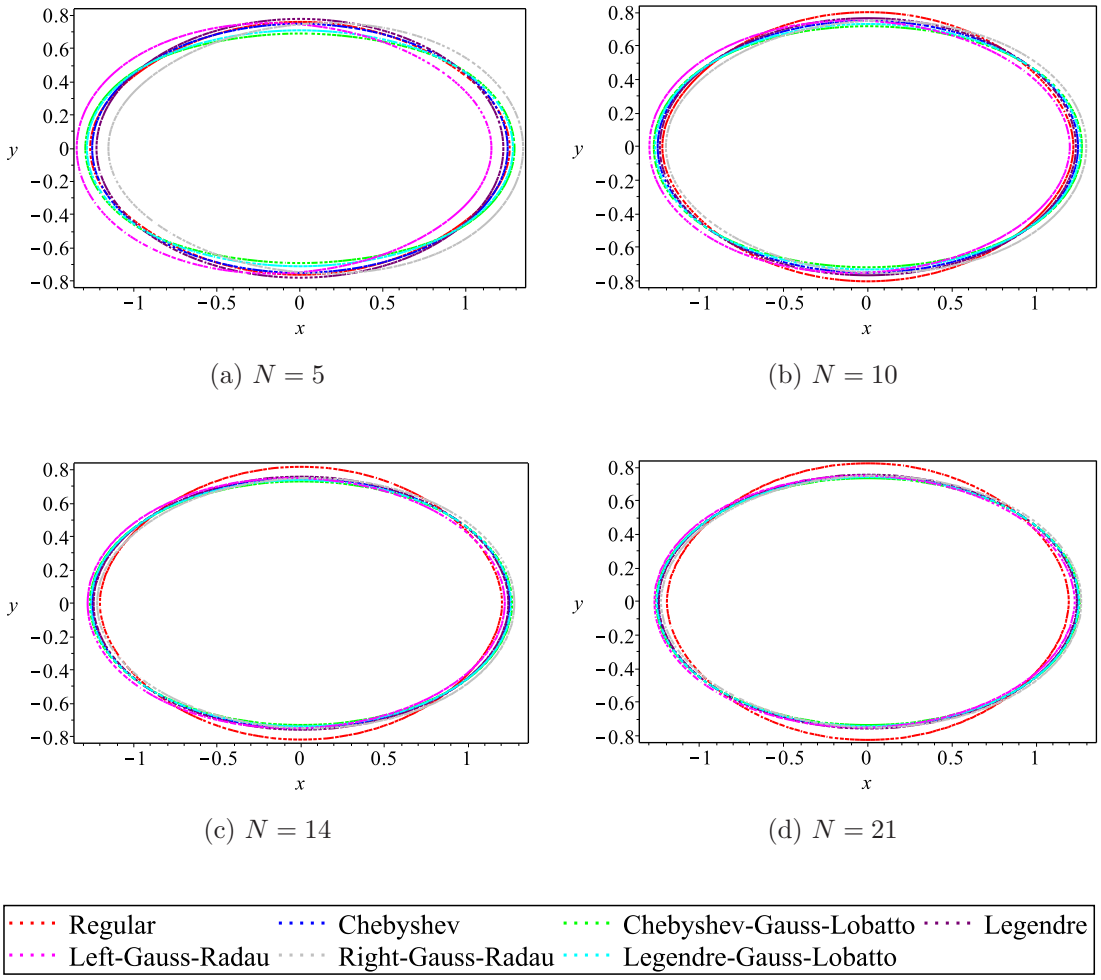

(a) $N = 5$ (b) $N = 10$

(c) $N = 14$ (d) $N = 21$

Figure 2.3.3: Contours $C = 1$ given by (2.3.37) for different nodal distributions and number of nodes N.

Figure 2.3.3 shows (visually) that, as N increases, the disparity between the contours of the different nodal distributions reduces, with the exception of the regular-nodes contour which remains "rounded". The orthogonal polynomial nodal distributions show an approximately uniform potential field for $C = 1$ and have been shown, as in Figure 2.3.2, to converge to the Chebyshev-Gauss-Lobatto distribution as $N \to \infty$. That is, the density function given by (2.3.35) applies to all of the clustered nodal distributions considered in Section 2.3.1, thus verifying the assertion in [124, p. 42].

Now that the interpolation techniques have been introduced, along with a selection of nodal distributions upon which the techniques can be applied, the corresponding interpolation-error formulae can be determined.

2.4 Error Analysis

2.4.1 Interpolation-Error Bounds

Without loss of generality it is assumed that $x \in [-1, 1]$ and that interpolation is based upon the nodes summarised in Section 2.3.1 and analysed in Section 2.3.2.

The error between a function u and its Lagrange interpolant $\mathcal{L}_N u$ in (2.1.1) is [27, p. 85]

$$u(x) - \mathcal{L}_N u(x) = \frac{u^{(N)}(\xi)}{N!} p_N(x), \tag{2.4.1}$$

for some $\xi \in [-1, 1]$ that depends on x. That is, for any $x \in [-1, 1]$ there is some value ξ for which (2.4.1) is satisfied. In (2.4.1) $p_N(x)$ is the monic polynomial given by (2.1.3) and $u^{(N)}(\xi)$ is the Nth derivative of $u(x)$ evaluated at $x = \xi$. Note that the exact solution u cannot be replaced by its Lagrange interpolant $\mathcal{L}_N u$ on the right-hand side of (2.4.1) since $\mathcal{L}_N u$ is a polynomial of degree $N - 1$ (see comment below (2.1.2)) and therefore its Nth derivative is 0. A bound on the interpolation error follows from (2.4.1) as

$$\|u - \mathcal{L}_N u\| \leq \frac{\left\|u^{(N)}\right\|}{N!} \|p_N\|, \tag{2.4.2}$$

which is finite when $u(x)$ is N-times continuously differentiable. Here, and throughout this thesis, it is assumed that $\|\cdot\|$ is the infinity norm $\|\cdot\|_\infty$ defined on $[-1, 1]$.

The error between the derivative of a function (2.2.1) and its numerical approximation (2.2.3) is given by [9, Eq. 5.7.5]

$$(\mathcal{D} - \mathcal{D}_N)u(x) \leq \frac{u^{(N)}(\xi_1)}{N!} p'_N(x) + \frac{u^{(N+1)}(\xi_2)}{(N+1)!} p_N(x), \tag{2.4.3}$$

in which $\xi_1, \xi_2 \in [-1, 1]$ both depend on x. The error in (2.4.3) is therefore bounded by

$$\|(\mathcal{D} - \mathcal{D}_N)u\| \leq \frac{\left\|u^{(N)}\right\|}{N!} \|p'_N\| + \frac{\left\|u^{(N+1)}\right\|}{(N+1)!} \|p_N\|, \tag{2.4.4}$$

the left-hand side of which is henceforth referred to as the *differentiation error*. The error formulae (2.4.1) and (2.4.2) demonstrate that the interpolation error is dependent on the monic polynomial p_N, whilst the error formulae (2.4.3) and (2.4.4) demonstrate that the differentiation error is dependent on not only p_N, but also its first derivative. In a similar way, for higher values of M, the error between $u^{(M)}(x)$ and its numerical approximation (2.2.6) depends upon $p_N^{(k)}$ for $k = 0(1)M$. Knowledge of how the maximum value of the monic polynomial and its derivatives behave therefore enables predictions of the corresponding bounds.

A comparison of $\left\|p_N^{(M)}\right\|$ for each of the nodal distributions for $M = 0(1)2$ is presented in Figure 2.4.1, which shows a hierarchy of norms in a decreasing sequence of magnitude, the smallest of which reveals those nodal distributions giving the most accurate interpolation results. For example, the best interpolation approximation of a function $u(x)$ is predicted on the Chebyshev nodes, and the worst on the regular nodes. The minimality of $\|p_N\|$ based on the Chebyshev nodes can be anticipated from [89, Thm. 1, p.303] which states that, of all monic polynomials of degree N, that with the smallest (infinity) norm in $[-1, 1]$ is the Chebyshev polynomial $2^{1-N}T_N(x)$, as given in (2.3.6). Of all orthogonal polynomial distributions, the Gauss-Radau distributions are predicted to give the least accurate interpolation approximations since $\|p_N\|$ is seen to be approximately 10 times larger than on the Chebyshev nodes. When the derivatives $u'(x)$ and $u''(x)$ are approximated, it is the Chebyshev-Gauss-Lobatto nodes that are now predicted to be the best, and the Gauss-Radau distributions are again predicted to be the worst of the clustered grids. The hierarchy of nodal distributions is seen to be preserved for both $\|p'_N\|$ and $\|p''_N\|$. It is also apparent that, for all distributions, the convergence of $\left\|p_N^{(M)}\right\|$ with increasing N is faster the lower that M is. Therefore, for a given value of N, the

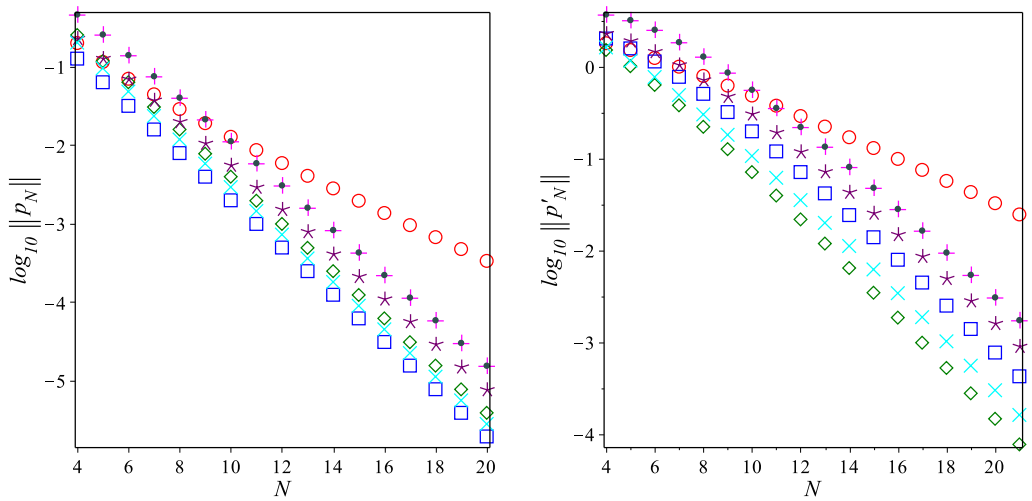

(a) Norms $\|p_N\|$ (b) Norms $\|p'_N\|$

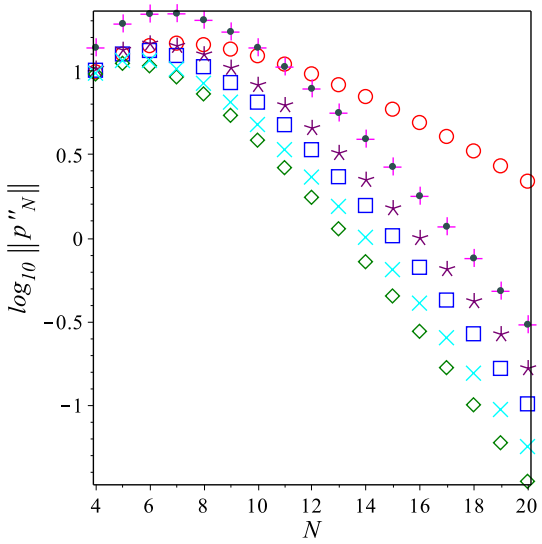

(c) Norms $\|p''_N\|$

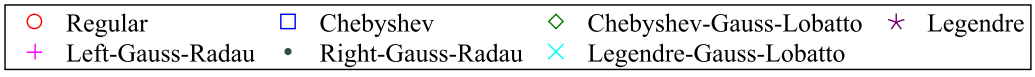

Figure 2.4.1: Logarithmic plot of norms $\|p_N\|$, $\|p'_N\|$ and $\|p''_N\|$, plotted against N for $p_N(x)$ in (2.1.3) based upon various nodal distributions. The logarithmic vertical scales indicate spectral convergence of all norms with N.

approximation of a function is predicted to be more accurate than the approximation of its first derivative, which in turn is predicted to be more accurate than the approximation of its second derivative. For each M the rate of convergence, with increasing N, of the norm $\left\| p_N^{(M)} \right\|$ is seen to be the same for each of the clustered nodal distributions; this rate is derived for each nodal distribution in Section 2.4.2. The second derivatives have been included herein as these are commonly used in elliptic, parabolic and hyperbolic problems arising in mathematical physics.

The accuracy of interpolation on each nodal distribution can also by examined by considering potential fields generated by level sets (constant values of C in (2.3.37)) for each of the monic polynomials. Figures 2.4.2–2.4.8 show the monic polynomial $p_N(x)$ in (2.1.3) and the corresponding level sets of C in (2.3.37) for each of the nodal distributions so far considered.

The definition of C in (2.3.37) is equivalent to [124, Eqns. 5.3–5.4]

$$C \equiv \mathrm{e}^{N\phi_N(z)}, \tag{2.4.5}$$

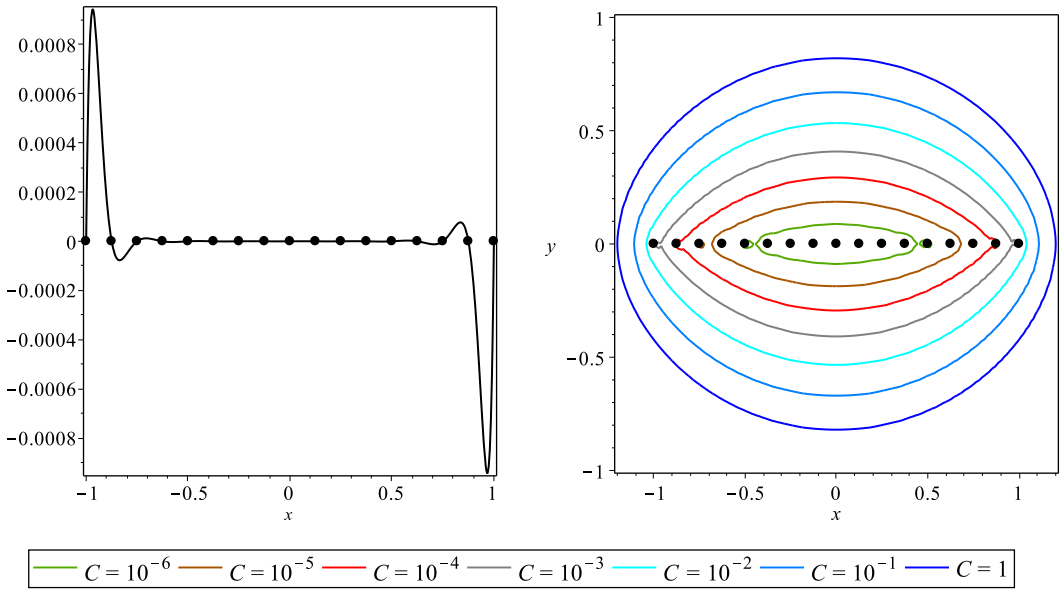

Figure 2.4.2: Monic polynomial (2.1.3) (left) for $N = 17$ on regularly spaced nodes, and corresponding level sets of potential (right) for $C = 10^{-k}$ for $k = 0(1)6$. Note "angular" contours as $C \to 0$.

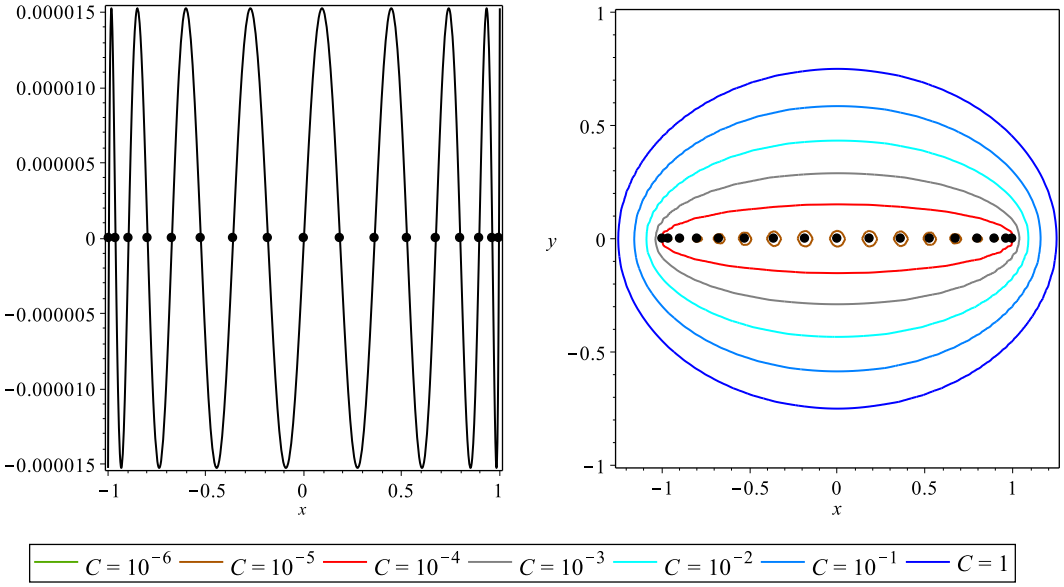

Figure 2.4.3: As for Figure 2.4.2, on Chebyshev nodes. Note disappearance of "angularity" in contours as $C \to 0$, in noteworthy contrast to Figure 2.4.2.

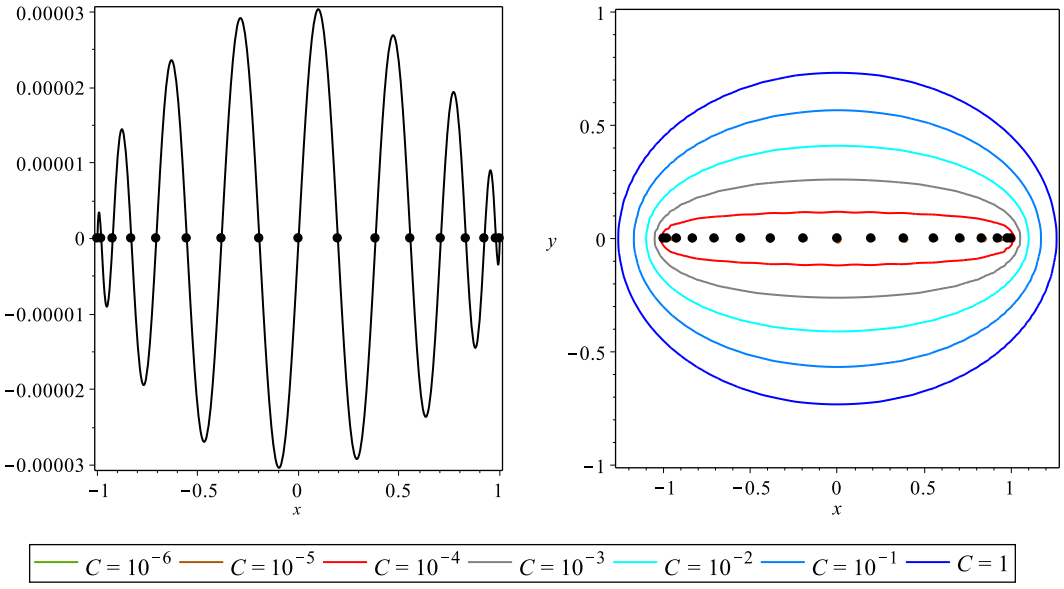

Figure 2.4.4: As for Figure 2.4.2, on Chebyshev-Gauss-Lobatto nodes. Note "optimality" of contours as $C \to 0$: equipotentials remain smooth and "flatten out".

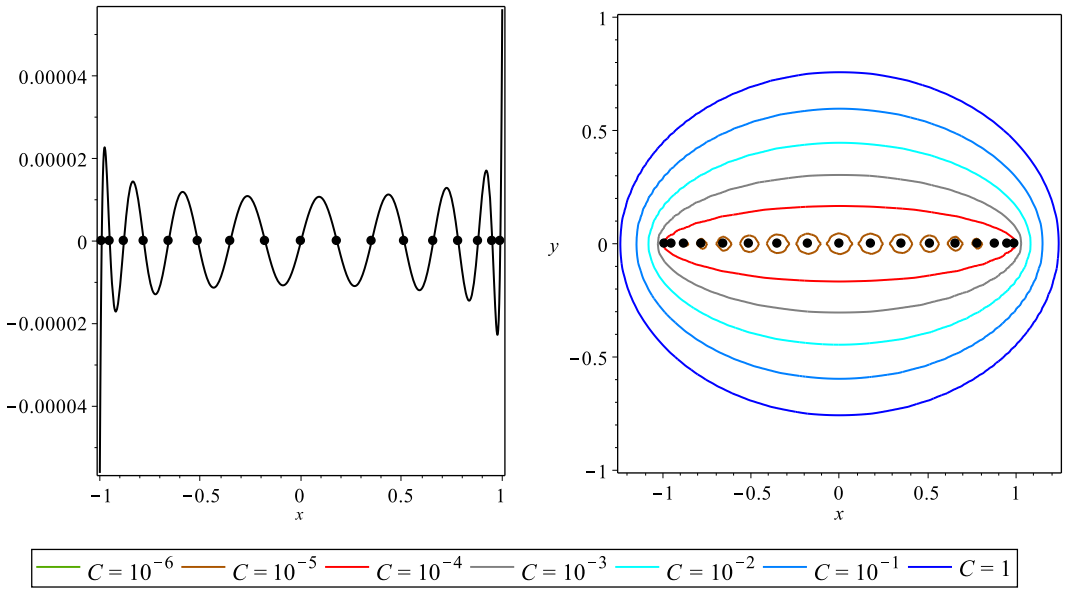

Figure 2.4.5: As for Figure 2.4.2, on Legendre nodes. Note that these contours appear more angular than those for the Chebyshev nodes in Figure 2.4.3.

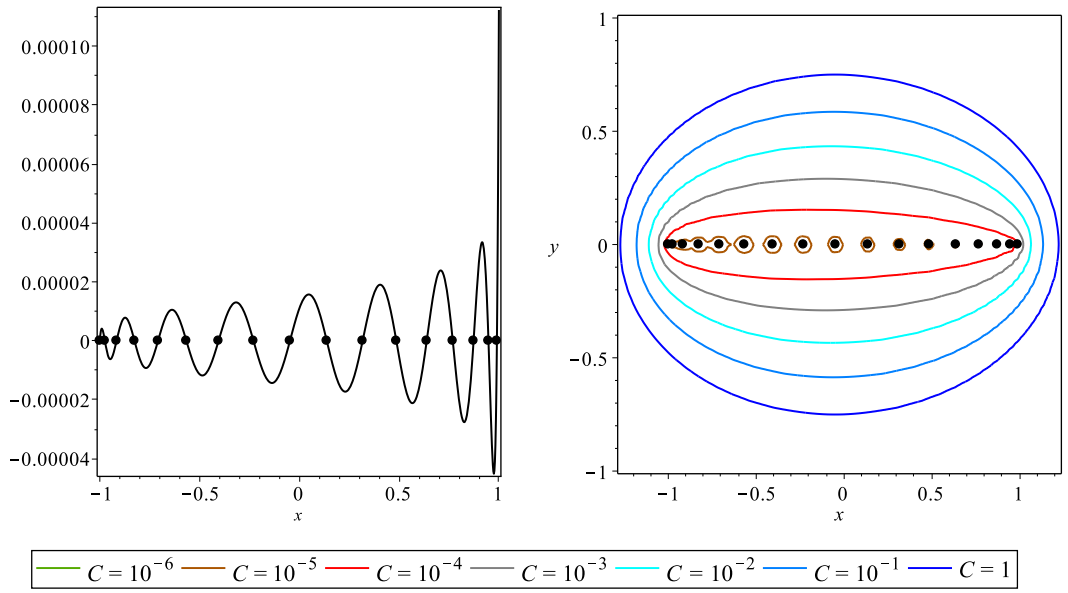

Figure 2.4.6: As for Figure 2.4.2, on Left-Gauss-Radau nodes. Note that these contours are more angular on the right-hand side: that is, towards the end with no fixed node.

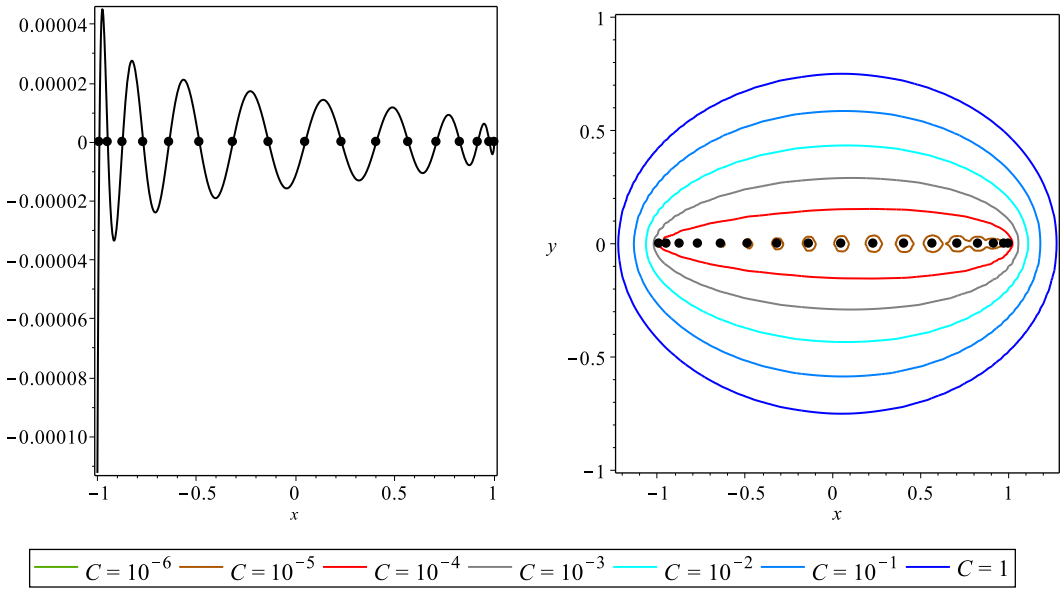

Figure 2.4.7: As for Figure 2.4.2, on Right-Gauss-Radau nodes. Note that these contours are more angular on the left-hand side

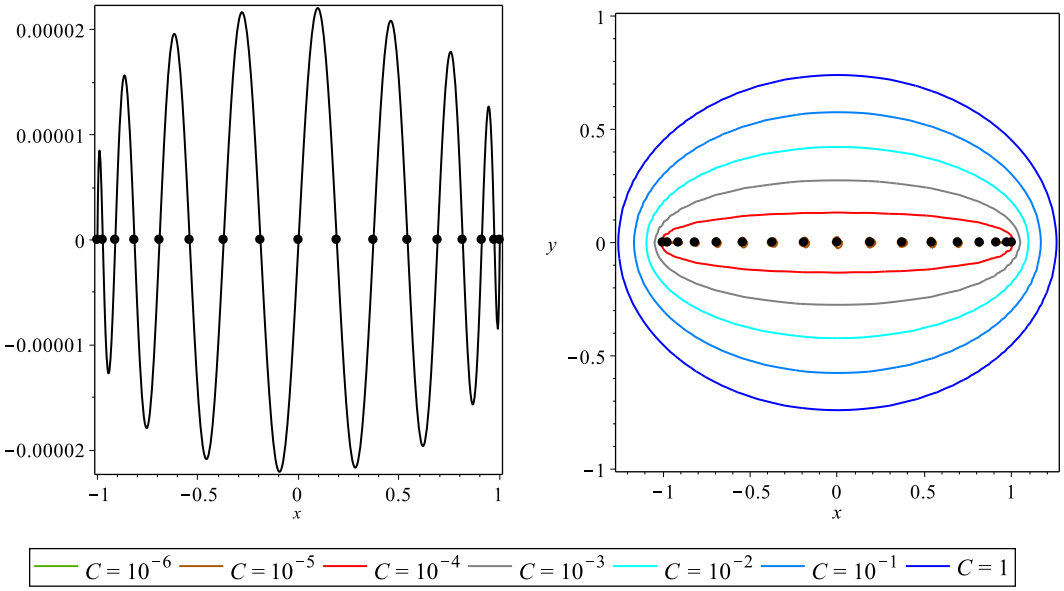

Figure 2.4.8: As for Figure 2.4.2, on Legendre-Gauss-Lobatto nodes. Note that these contours appear to be smooth and flat as $C \to 0$.

in which

$$\phi_N(z) = N^{-1} \sum_{j=1}^{N} \log |z - x_{j,N}| \tag{2.4.6}$$

is the potential at z due to point charges at the nodes $x_{j,N}$. If $\phi_N(z)$ varies along $[-1, 1]$ then $|p_N(z)|$ grows exponentially with N. However, if $\phi_N(z)$ is approximately constant for $z \in [-1, 1]$, then so is $p_N(z)$ [124, p.45]. In this case, the corresponding contours C (2.3.37) are generated by points z that have approximately the same imaginary part; these contours therefore appear to be flatter. Consequently, the flatter the contour C is, the closer to an equipotential curve $p_N(x)$ is. As $\|p_N\|$ is used to bound the interpolation error in (2.4.2), the roundedness of the contours in Figure 2.4.2 supports the prediction based on Figure 2.4.1 that interpolation on the regular nodes is the least accurate as N increases. Note also that, within the region bounded by the smallest contour containing ± 1, if a function $u(x)$ is analytic then it may be approximated by polynomial interpolation (2.1.1) with spectral accuracy [124, p. 48]. When $|p_N(x)|$ increases for x at, or near to, ± 1 to a magnitude that is much larger than any of the oscillations in the interior of $[-1, 1]$, e.g. as on the regular, Legendre and Gauss-Radau distributions, the corresponding contours are angular at the end(s) at which this increase occurs. The distributions without this phenomenon have contours that are flatter in shape, which suggests that the most accurate interpolation possible is on those distributions is when $p_N(x)$ oscillates between near-equal and opposite values. Specifically, the optimality of interpolation using the Chebyshev nodes, for which $p_N(x)$ oscillates between exactly-equal and opposite values, can effectively be anticipated from the *Chebyshev alternation theorem* [93, Thm. 3.4].

Expanded details of Figures 2.4.2–2.4.8 are presented in Figures 2.4.9–2.4.15 respectively, in each of which the zoomed regions are centered on $x = -1$ (left) and on $x = 0$ (right): that is, the nodes in each of the plots are respectively $x_{1,N}$ and $x_{2,N}$ (left) and $x_{9,N}$ (right) because $N = 17$. Note that the zoom factor in the first figure is half of that in the remaining six.

The contours represent equipotential field strengths generated by equal charges placed at the nodes. For larger values of $|z|$, the corresponding value of C dictated by (2.3.37) forms a closed convex contour in the complex plane that is influenced by all of the charges. The smaller values of C correspond to smaller values of $|z|$ in the neighbourhood of a node $x_{i,N}$ say, for some $i = 1(1)N$, whereat the charge at that

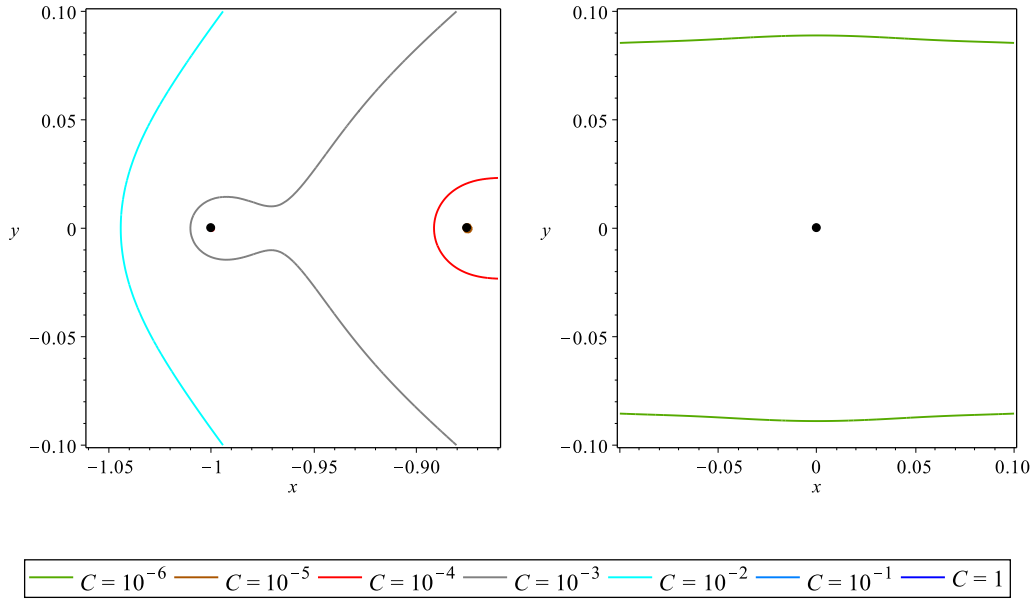

Figure 2.4.9: Expanded view of contours in Figure 2.4.2 in the neighbourhood of $x = -1$ and $x = 0$ for $N = 17$ (regular nodes).

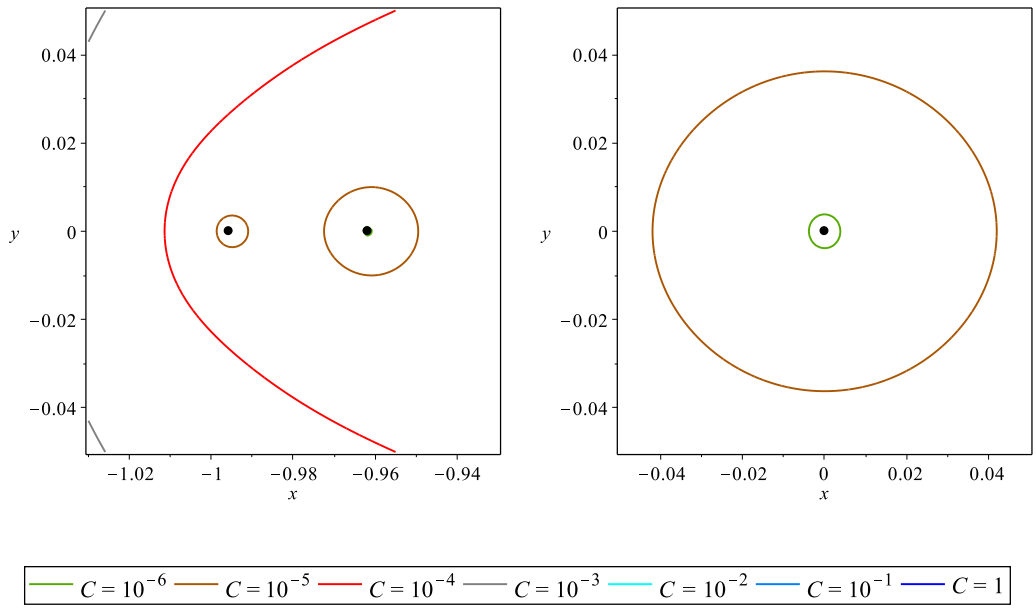

Figure 2.4.10: Expanded view of contours in Figure 2.4.3 in the neighbourhood of $x = -1$ and $x = 0$ for $N = 17$ (Chebyshev nodes).

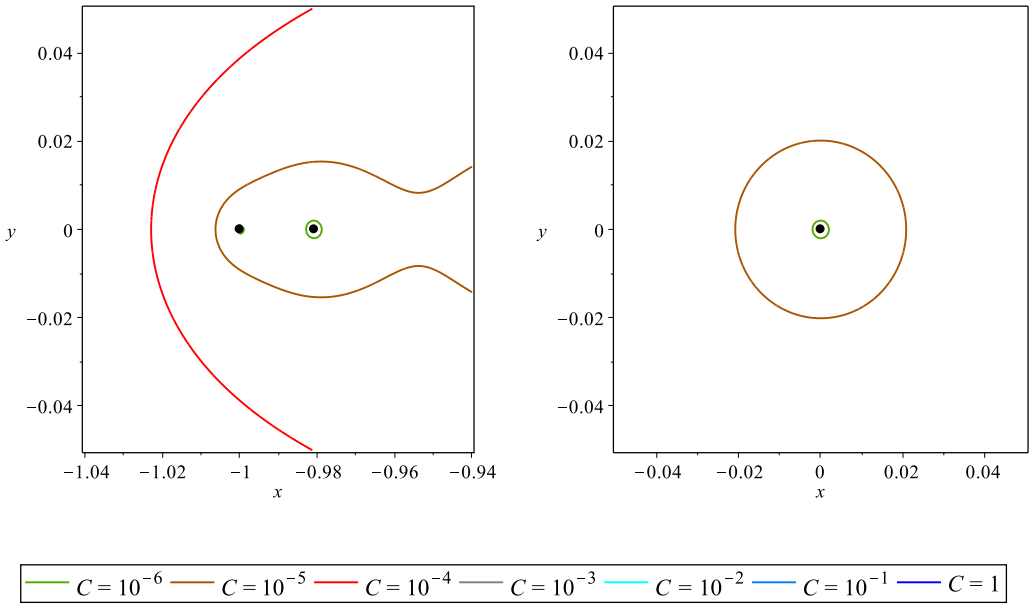

Figure 2.4.11: Expanded view of contours in Figure 2.4.4 in the neighbourhood of $x = -1$ and $x = 0$ for $N = 17$ (Chebyshev-Gauss-Lobatto nodes).

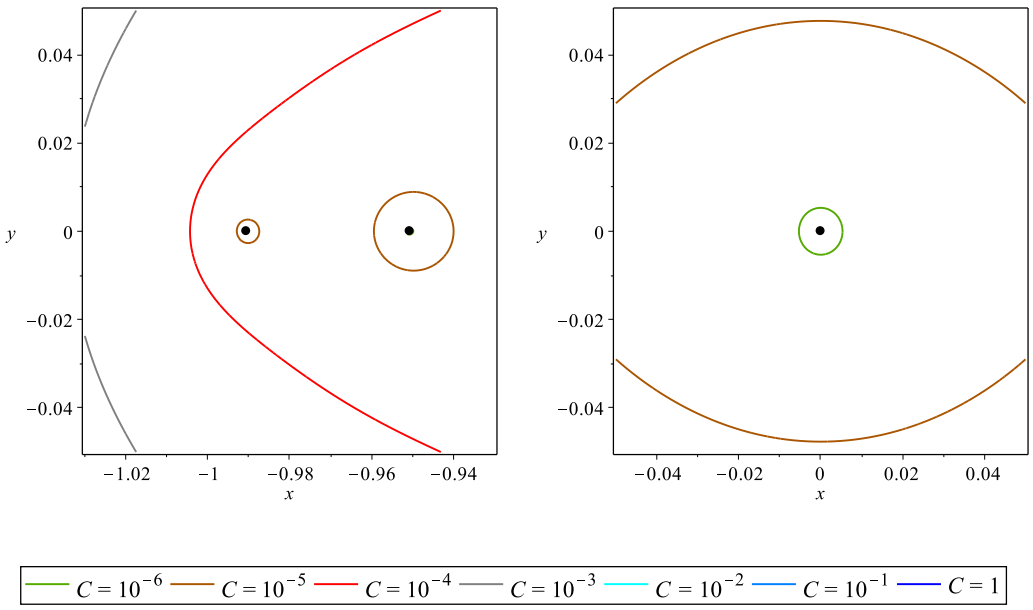

Figure 2.4.12: Expanded view of contours in Figure 2.4.5 in the neighbourhood of $x = -1$ and $x = 0$ for $N = 17$ (Legendre nodes).

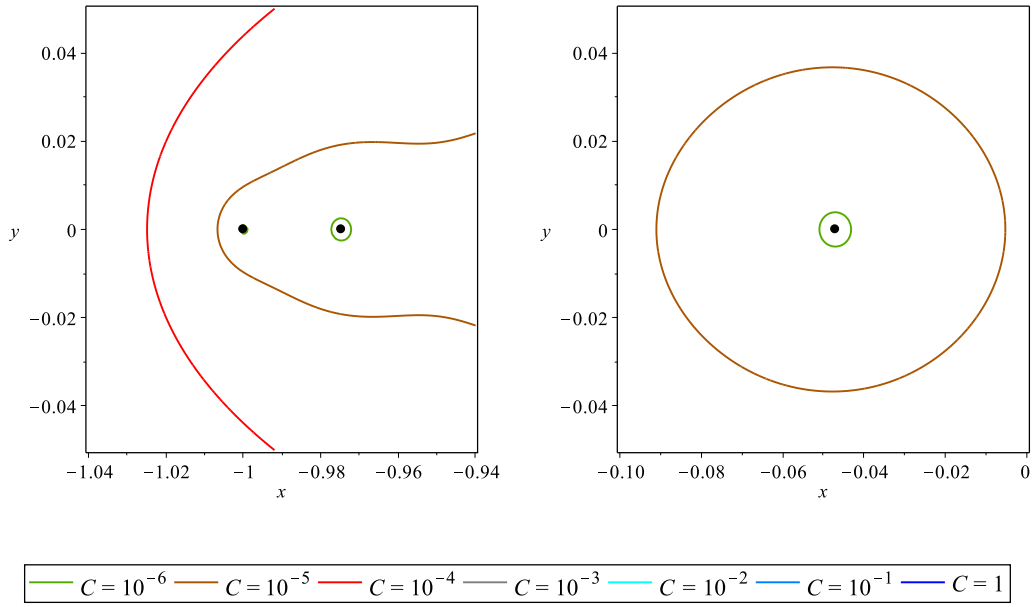

Figure 2.4.13: Expanded view of contours in Figure 2.4.6 in the neighbourhood of $x = -1$ and $x = 0$ for $N = 17$ (Left-Gauss-Radau nodes).

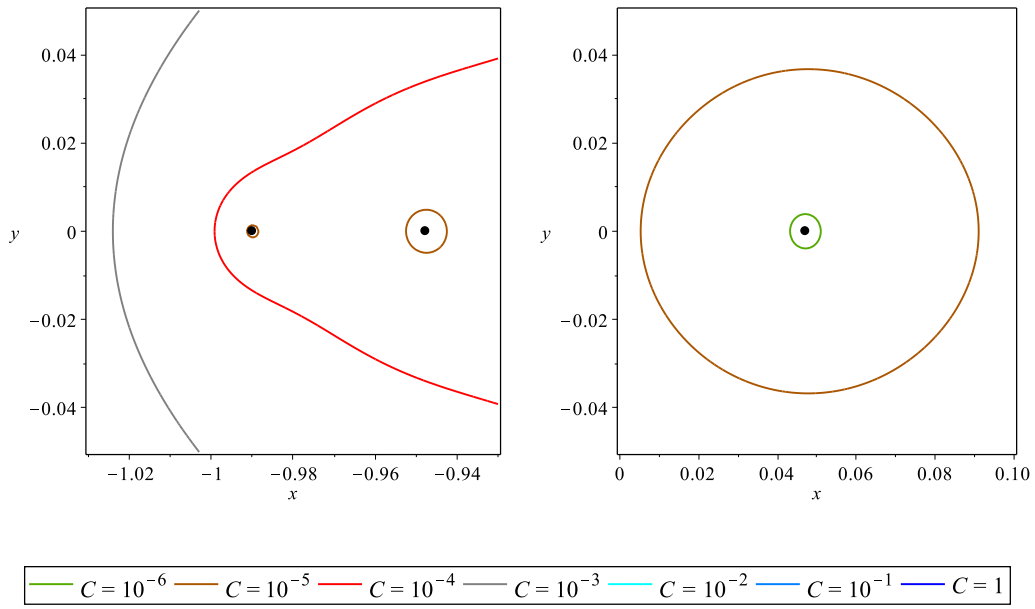

Figure 2.4.14: Expanded view of contours in Figure 2.4.7 in the neighbourhood of $x = -1$ and $x = 0$ for $N = 17$ (Right-Gauss-Radau nodes).

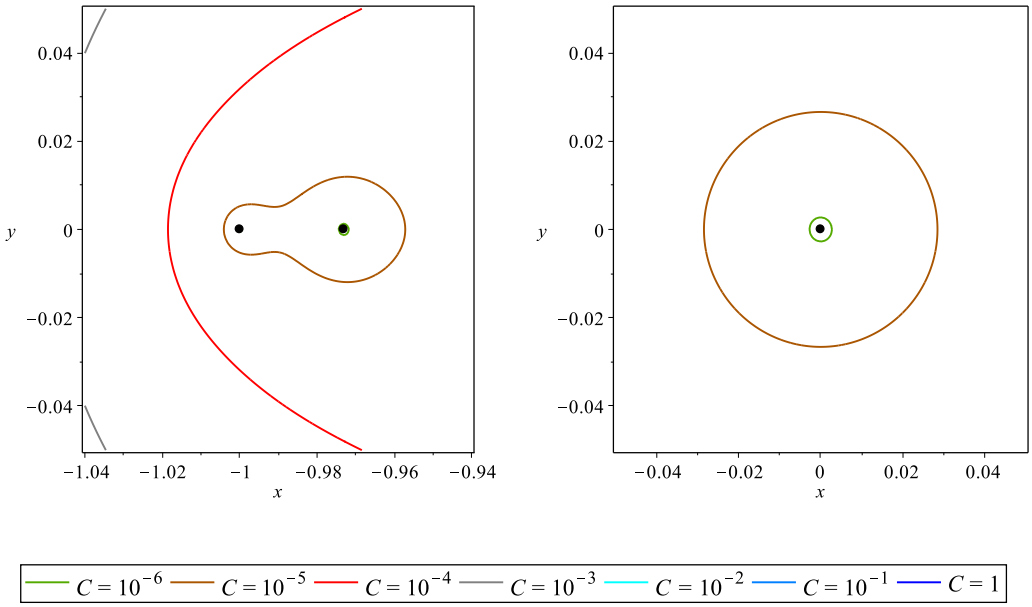

Figure 2.4.15: Expanded view of contours in Figure 2.4.8 in the neighbourhood of $x = -1$ and $x = 0$ for $N = 17$ (Legendre-Gauss-Lobatto nodes).

node is dominant and the influence of the others weaker so that C forms a contour that is local (looped around one node). The smallest contours in Figures 2.4.9–2.4.15 correspond to $C = 10^{-6}$ and so correspond to the weakest of the potential fields. Comparison of the Legendre and Legendre-Gauss-Lobatto contours about the outer nodes $x_{1,N}$ and $x_{2,N}$ in Figures 2.4.12 and 2.4.15 shows that the contours with $C = 10^{-5}$ are local about each Legendre node but enclose both of the outer Legendre-Gauss-Lobatto nodes. This is because the outer two nodes are further apart in the Legendre distribution than in the Legendre-Gauss-Lobatto distribution and so the charges from the Legendre nodes are not strong enough to interact over that distance. The same can be said for the contour corresponding to $C = 10^{-5}$ for the Chebyshev and Chebyshev-Gauss-Lobatto distributions in Figures 2.4.10 and 2.4.11. It is clear that, for all nodal distributions, the right-hand figures are symmetric, or near-symmetric in the Gauss-Radau cases, although the size of the contours vary around the central node $x_{9,N}$. This suggests that, on all distributions, interpolants are most accurate towards the centre of the interval $[-1, 1]$.

Figures 2.4.1–2.4.15 demonstrate the accuracy that can be expected from interpolation on each nodal distribution. Specifically Figure 2.4.1 presents a hierarchy of

norms that illustrates which nodal distributions give the best interpolation results; this hierarchy is consolidated by the contours in Figures 2.4.2–2.4.15, from which the most accurate interpolants are expected to be on those distributions whose contours are approximately the level curves discussed above. The accuracy of each distribution can now be determined explicitly via exact formulae for the interpolation-error bounds in (2.4.2) and (2.4.4).

2.4.2 Theoretical Interpolation- and Differentiation-Error Bounds

In this section explicit formulae for bounding the interpolation error (2.4.2) and differentiation error (2.4.4) are found for the nodal distributions introduced in Section 2.3. Asymptotic convergence rates of the bounds as $N \to \infty$ are computed using Stirling's formula [9, p.279]. Many of the results presented here are new, or at least not given so explicitly elsewhere.

Regular Nodes

When the interpolation nodes in (2.1.1) are the regularly spaced nodes (2.3.1), the bound on $\|p_N\|$ is given as [41, 103]

$$\|p_N\| \leq \frac{(N-1)!}{4}\, h^N, \tag{2.4.7}$$

in which

$$h = \frac{2}{N-1} \tag{2.4.8}$$

is the equal spacing between the nodes. A proof of (2.4.7) is given in Appendix B. Substitution of (2.4.7) into (2.4.2) gives the interpolation-error bound as

$$\|u - \mathcal{L}_N u\| \leq \left(\frac{2}{N-1}\right)^N \frac{\left\|u^{(N)}\right\|}{4N}. \tag{2.4.9}$$

By the product rule, differentiating the monic polynomial $p_N(x)$ in (2.1.3) yields

$$p'_N(x) = \sum_{j=1}^{N} \left(\prod_{\substack{i=1 \\ i \neq j}}^{N} (x - x_{i,N}) \right), \tag{2.4.10}$$

which is equivalently

$$p'_N(x) = \sum_{j=1}^{N} \frac{p_N(x)}{x - x_{j,N}}. \tag{2.4.11}$$

By inspection, $|p'_N(x)|$ for the regular nodes is maximised at $x = \pm 1$ and so

$$\|p'_N\| = |p'_N(\pm 1)|. \tag{2.4.12}$$

Substitution of $x = x_{1,N} = -1$ into (2.4.10) gives

$$p'_N(-1) = \prod_{i=2}^{N} (x_{1,N} - x_{i,N}) \tag{2.4.13}$$

which, by expressing the nodes in (2.3.1) using h in (2.4.8) as

$$x_{j,N} = -1 + (j-1)\,h, \tag{2.4.14}$$

is equivalently

$$\begin{aligned} p'_N(-1) &= \prod_{i=2}^{N} \Big(-1 - (-1 + (i-1)\,h) \Big) \\ &= \prod_{i=2}^{N} \Big(-(i-1)\,h \Big) \\ &= (-h)^{N-1}\,(N-1)!\,. \end{aligned} \tag{2.4.15}$$

Substitution of (2.4.15) into (2.4.12) then gives

$$\|p'_N\| = h^{N-1}\,(N-1)! \tag{2.4.16}$$

which is substituted into (2.4.4) with (2.4.7) to give the differentiation-error bound as

$$\|(\mathcal{D} - \mathcal{D}_N)u\| \le \left(\frac{2}{N-1}\right)^{N-1} \frac{1}{N} \left(\|u^{(N)}\| + \frac{\|u^{(N+1)}\|}{2\,(N-1)(N+1)} \right). \tag{2.4.17}$$

Chebyshev Nodes

By definition (2.3.4), $\|T_N\| = 1$ and therefore (2.3.6) gives

$$\|p_N\| = \frac{1}{2^{N-1}}, \tag{2.4.18}$$

so that the interpolation-error bound (2.4.2) becomes

$$\|u - \mathcal{L}_N u\| \leq \frac{\left\|u^{(N)}\right\|}{2^{N-1}N!} \sim \left(\frac{\mathrm{e}}{2N}\right)^N \sqrt{\frac{2}{\pi N}} \left\|u^{(N)}\right\|, \qquad N \to \infty. \tag{2.4.19}$$

Differentiating (2.3.6) and using the property [2, Eq. 22.14.5]

$$\|T'_N\| = N^2 \tag{2.4.20}$$

gives the differentiation-error bound (2.4.4), via (2.4.18), as

$$\begin{aligned} \|(\mathcal{D} - \mathcal{D}_N)u\| &\leq \frac{1}{2^{N-1}N!}\left(N^2 \left\|u^{(N)}\right\| + \frac{\left\|u^{(N+1)}\right\|}{N+1}\right) \\ &\sim \left(\frac{\mathrm{e}}{2N}\right)^N \sqrt{\frac{2}{\pi N}}\left(N^2 \left\|u^{(N)}\right\| + \frac{\left\|u^{(N+1)}\right\|}{N+1}\right), \quad N \to \infty. \end{aligned} \tag{2.4.21}$$

Chebyshev-Gauss-Lobatto Nodes

Using the substitution $x = \cos\theta$ the Chebyshev polynomial (2.3.4) is rewritten as

$$T_N(x) = T_N(\cos\theta) = \cos N\theta \tag{2.4.22}$$

which, when differentiated with respect to x, yields

$$T'_N(x) = \frac{-1}{\sin\theta}\frac{d}{d\theta}T_N(\cos\theta) = \frac{N\sin N\theta}{\sin\theta}. \tag{2.4.23}$$

Therefore, defining

$$\Psi_N(x) \equiv (x^2 - 1)\, T'_{N-1}(x) \tag{2.4.24}$$

and setting $x = \cos\theta$ gives

$$\Psi_N(\cos\theta) = -(N-1)\sin\theta\sin(N-1)\theta \tag{2.4.25}$$

so that

$$\|\Psi_N\| \leq N - 1. \tag{2.4.26}$$

Together (2.3.9), (2.4.24) and (2.4.26) give

$$\|p_N\| \leq \frac{1}{2^{N-2}}, \tag{2.4.27}$$

and so the interpolation-error bound (2.4.2) becomes

$$\|u - \mathcal{L}_N u\| \leq \frac{\|u^{(N)}\|}{2^{N-2}N!} \sim \left(\frac{\mathrm{e}}{2N}\right)^N \sqrt{\frac{8}{\pi N}}\, \|u^{(N)}\|, \qquad N \to \infty. \tag{2.4.28}$$

Differentiating (2.3.9) gives

$$p'_N(x) = \frac{1}{2^{N-2}(N-1)}\Big((x^2-1)\,T''_{N-1}(x) + 2x\,T'_{N-1}(x)\Big) \tag{2.4.29}$$

which is simplified using Chebyshev's differential equation (2.3.5) to give

$$p'_N(x) = \frac{1}{2^{N-2}(N-1)}\Big((N-1)^2\,T_{N-1}(x) + x\,T'_{N-1}(x)\Big). \tag{2.4.30}$$

As $T_{N-1}(x)$, x and $T'_{N-1}(x)$ attain their maximum moduli at $x = 1$, (2.4.30) is maximised at $x = 1$ so that

$$\|p'_N\| = p'_N(1) = \frac{1}{2^{N-2}(N-1)}\Big((N-1)^2 + (N-1)^2\Big) = \frac{N-1}{2^{N-3}}. \tag{2.4.31}$$

Therefore, by (2.4.27) and (2.4.31), the differentiation-error bound (2.4.4) becomes

$$\begin{aligned} \|(\mathcal{D} - \mathcal{D}_N)u\| &\leq \frac{1}{2^{N-2}N!}\left(2(N-1)\,\|u^{(N)}\| + \frac{\|u^{(N+1)}\|}{N+1}\right) \\ &\sim \left(\frac{\mathrm{e}}{2N}\right)^N \sqrt{\frac{8}{\pi N}}\left(2(N-1)\,\|u^{(N)}\| + \frac{\|u^{(N+1)}\|}{N+1}\right), \quad N \to \infty. \end{aligned} \tag{2.4.32}$$

Legendre Nodes

As $\|P_N\| = 1$ [2, Eq. 22.14.7], (2.3.15) gives

$$\|p_N\| = \frac{2^N (N!)^2}{(2N)!}, \tag{2.4.33}$$

which gives the interpolation-error bound (2.4.2) as

$$\|u - \mathcal{L}_N u\| \leq \frac{2^N N!\,\|u^{(N)}\|}{(2N)!} \sim \left(\frac{\mathrm{e}}{2N}\right)^N \frac{\|u^{(N)}\|}{\sqrt{2}}, \qquad N \to \infty. \tag{2.4.34}$$

Differentiating (2.3.15) and using the definition [2, Eq. 22.14.8]

$$\|P'_N\| = \frac{N(N+1)}{2} \tag{2.4.35}$$

gives the differentiation-error bound (2.4.4), via (2.4.33), as

$$\begin{aligned} \|(\mathcal{D} - \mathcal{D}_N)u\| &\leq \frac{2^N N!}{(2N)!}\left(\frac{N(N+1)\left\|u^{(N)}\right\|}{2} + \frac{\left\|u^{(N+1)}\right\|}{N+1}\right) \\ &\sim \left(\frac{\mathrm{e}}{2N}\right)^N \frac{1}{\sqrt{2}}\left(\frac{N(N+1)\left\|u^{(N)}\right\|}{2} + \frac{\left\|u^{(N+1)}\right\|}{N+1}\right), \quad N \to \infty. \end{aligned} \tag{2.4.36}$$

Legendre-Gauss-Radau Nodes

The Gauss-Radau bounds are derived using the Left-Gauss-Radau nodal distribution; as the Right-Gauss-Radau distribution is a reflection of this about the y-axis, both distributions have the same norms $\|p_N\|$ and $\|p'_N\|$.

Legendre polynomials attain their maximum modulus of 1 at $x = 1$ [59, p. 162] so that

$$\|P_{N-1} + P_N\| = P_N(1) + P_{N-1}(1) = 2 \tag{2.4.37}$$

and hence, from (2.3.18),

$$\|p_N\| = \frac{2^{N+1}(N!)^2}{(2N)!}. \tag{2.4.38}$$

Substitution of (2.4.38) into the interpolation-error bound (2.4.2) gives

$$\|u - \mathcal{L}_N u\| \leq \frac{2^{N+1}N!\left\|u^{(N)}\right\|}{(2N)!} \sim \left(\frac{\mathrm{e}}{2N}\right)^N \sqrt{2}\left\|u^{(N)}\right\|, \qquad N \to \infty. \tag{2.4.39}$$

Differentiating (2.3.18) gives

$$p'_N(x) = \frac{2^N(N!)^2}{(2N)!}\Big(P'_N(x) + P'_{N-1}(x)\Big), \tag{2.4.40}$$

so that

$$\|p'_N\| = \frac{2^N(N!)^2}{(2N)!}\left\|P'_N + P'_{N-1}\right\|. \tag{2.4.41}$$

Given [27, p. 500] that

$$\|P'_N\| = |P'_N(\pm 1)| = P'_N(1) = \frac{N(N+1)}{2} \tag{2.4.42}$$

it follows that

$$\left\|P'_{N-1}\right\| = |P'_{N-1}(\pm 1)| = P'_{N-1}(1) = \frac{(N-1)N}{2}, \tag{2.4.43}$$

and therefore

$$\left\|P'_{N} + P'_{N-1}\right\| = P'_{N}(1) + P'_{N-1}(1) = \frac{N}{2}(N+1+N-1) = N^2. \tag{2.4.44}$$

Substitution of (2.4.38), (2.4.41) and (2.4.44) into the differentiation-error bound (2.4.4) then gives

$$\begin{aligned} \|(\mathcal{D} - \mathcal{D}_N)u\| &\leq \frac{2^N N!}{(2N)!}\left(N^2\left\|u^{(N)}\right\| + \frac{2\left\|u^{(N+1)}\right\|}{N+1}\right) \\ &\sim \left(\frac{\mathrm{e}}{2N}\right)^N \frac{1}{\sqrt{2}}\left(N^2\left\|u^{(N)}\right\| + \frac{2\left\|u^{(N+1)}\right\|}{N+1}\right), \quad N \to \infty. \end{aligned} \tag{2.4.45}$$

Legendre-Gauss-Lobatto Nodes

To evaluate the interpolation-error bound first define

$$\psi_N(x) \equiv (x^2 - 1)\, P'_{N-1}(x) \tag{2.4.46}$$

so that, via (2.3.26),

$$\|p_N\| = \frac{2^N\,(N!)^2\,(2N-1)}{(2N)!\,N\,(N-1)}\,\|\psi_N\|\,. \tag{2.4.47}$$

Note that $\psi_N(\pm 1) = 0$ and so the maximum of $|\psi_N(x)|$ occurs when $\psi'_N(x) = 0$ for some $x \in (-1, 1)$. Differentiating (2.4.46) and using Legendre's differential equation (2.3.14) yields

$$\psi'_N(x) = (N-1)NP_{N-1}(x) \tag{2.4.48}$$

so that $\|\psi_N\|$ is attained at an (internal) root of $P_{N-1}(x)$. By inspection, $\|\psi_N\|$ occurs at $x = 0$ when N is even and at the root of $P_{N-1}(x)$ that is closest to $x = 0$ when N is odd. Therefore

$$\|\psi_N\| = \begin{cases} |P'_{N-1}(0)| & N \text{ even} \\ \left|P'_{N-1}(y_{\frac{N-1}{2},N-1})\left((y_{\frac{N-1}{2},N-1})^2 - 1\right)\right| & N \text{ odd} \end{cases} \tag{2.4.49}$$

wherein $y_{\frac{N-1}{2},N-1}$ is the $\frac{N-1}{2}$-th root of $P_{N-1}(x)$. The Legendre polynomial can be written in the form (derived in Appendix C)

$$P_N(x) = 2^N \sum_{k=0}^{N} \binom{N}{k} \binom{\frac{N+k-1}{2}}{N} x^k \tag{2.4.50}$$

so that differentiation of (2.4.50) yields

$$P'_N(x) = 2^N \sum_{k=0}^{N} k \binom{N}{k} \binom{\frac{N+k-1}{2}}{N} x^{k-1}. \tag{2.4.51}$$

When N is even, this form of $P'_N(x)$ can be used to find an explicit expression for $|P'_{N-1}(0)|$ and hence $\|\psi_N\|$. When $x = 0$ in (2.4.51) the only non-zero term in the sum is when $k = 1$, whence (2.4.51) becomes

$$\begin{aligned} P'_N(0) \quad &= 2^N \binom{N}{1} \binom{\frac{N}{2}}{N} \\ &= 2^N N \frac{\frac{N}{2}!}{N!(-\frac{N}{2})!}. \end{aligned} \tag{2.4.52}$$

Half-integer factorials are evaluated as (see Appendix C)

$$\left(-\frac{1}{2} + n\right)! = \frac{(2n)!}{4^N n!}\sqrt{\pi} \tag{2.4.53}$$

and

$$\left(-\frac{1}{2} - n\right)! = \frac{(-4)^N n!}{(2n)!}\sqrt{\pi}, \tag{2.4.54}$$

for $n \in \mathbb{N}$. To evaluate $\frac{N}{2}!$ let $n = \frac{N+1}{2}$ in (2.4.53) so that

$$\left(\frac{N}{2}\right)! = \frac{(N+1)!}{4^{\frac{N+1}{2}}\left(\frac{N+1}{2}\right)!}\sqrt{\pi} \tag{2.4.55}$$

and to evaluate $(-\frac{N}{2})!$ let $n = \frac{N-1}{2}$ in (2.4.54) so that

$$\left(-\frac{N}{2}\right)! = \frac{(-4)^{\frac{N-1}{2}}\left(\frac{N-1}{2}\right)!}{(N-1)!}\sqrt{\pi}. \tag{2.4.56}$$

Substituting (2.4.55) and (2.4.56) into (2.4.52) gives

$$\begin{aligned} P'_N(0) \quad &= \quad 2^N \frac{N}{N!} \cdot \frac{(N+1)!\sqrt{\pi}}{4^{\frac{N+1}{2}}\left(\frac{N+1}{2}\right)!} \cdot \frac{(N-1)!}{(-4)^{\frac{N-1}{2}}\left(\frac{N-1}{2}\right)!\sqrt{\pi}} \\ &= \quad \frac{(N+1)!(-1)^{\frac{N-1}{2}}}{2^N\left(\frac{N+1}{2}\right)!\left(\frac{N-1}{2}\right)!} \end{aligned} \tag{2.4.57}$$

and so

$$P'_{N-1}(0) = \frac{N!(-1)^{\frac{N-2}{2}}}{2^{N-1}\left(\frac{N}{2}\right)!\left(\frac{N-2}{2}\right)!}. \tag{2.4.58}$$

Therefore, by (2.4.49) and (2.4.58),

$$\|\psi_N\| = \frac{N!\,N}{2^N\left(\left(\frac{N}{2}\right)!\right)^2}, \qquad N \text{ even}, \tag{2.4.59}$$

and so (2.4.47) becomes

$$\|p_N\| = \frac{(N!)^3\,(2N-1)}{(2N)!\,(N-1)\left(\left(\frac{N}{2}\right)!\right)^2}, \qquad N \text{ even}. \tag{2.4.60}$$

Substitution of (2.4.60) into (2.4.2) then gives the interpolation-error bound as

$$\|u - \mathcal{L}_N u\| \le \frac{(N!)^2\,(2N-1)\,\|u^{(N)}\|}{(2N)!\,(N-1)\left(\left(\frac{N}{2}\right)!\right)^2} \sim \left(\frac{\mathrm{e}}{2N}\right)^N \frac{(2N-1)\,\|u^{(N)}\|}{\sqrt{\pi N}(N-1)},$$

$$N \text{ even} \to \infty. \tag{2.4.61}$$

It is evident from Figure 2.4.1(a) that $\|p_N\|$ on the Legendre-Gauss-Lobatto nodes decreases at a constant rate with N, therefore the convergence rate in (2.4.61) is postulated to hold for N odd as well as N even.

Differentiation of (2.3.26) gives

$$p'_N(x) = \frac{2^N\,(N!)^2\,(2N-1)}{(2N)!\,N\,(N-1)}\Big((x^2-1)\,P''_{N-1}(x) + 2xP'_{N-1}(x)\Big) \tag{2.4.62}$$

which, by Legendre's differential equation (2.3.14), simplifies to

$$p'_N(x) = \frac{2^N\,(N!)^2\,(2N-1)}{(2N)!}\,P_{N-1}(x). \tag{2.4.63}$$

As $\|P_N\| = 1$, (2.4.63) gives

$$\|p'_N\| = \frac{2^N\,(N!)^2\,(2N-1)}{(2N)!} \tag{2.4.64}$$

which is substituted into (2.4.4) with (2.4.60) to give the differentiation-error bound

$$\|(\mathcal{D} - \mathcal{D}_N)u\| \le \frac{N!\,(2N-1)}{(2N)!}\left(2^N\,\|u^{(N)}\| + \frac{N!\,\|u^{(N+1)}\|}{(N^2-1)\left(\left(\frac{N}{2}\right)!\right)^2}\right), \; N \text{ even} \tag{2.4.65}$$

$$\sim \left(\frac{\mathrm{e}}{2N}\right)^N (2N-1)\left(\frac{\|u^{(N)}\|}{\sqrt{2}} + \frac{\|u^{(N+1)}\|}{\sqrt{\pi\,N}\,(N^2-1)}\right), \; N \to \infty.$$

2.4.3 Comparison of Error Bounds Calculated So Far

The interpolation-error and differentiation-error bounds determined in Section 2.4.2 on each of the nodal distributions are now compared.

For simplicity, denote the nodally-dependent bound on $\|p_N\|/N!$ by σ_N so that

$$\frac{\|p_N\|}{N!} \leq \sigma_N \tag{2.4.66}$$

and that on $\|p'_N\|/N!$ by ϕ_N so that

$$\frac{\|p'_N\|}{N!} \leq \phi_N. \tag{2.4.67}$$

Then (2.4.2) becomes

$$\|u - \mathcal{L}_N u\| \leq \sigma_N \left\|u^{(N)}\right\| \tag{2.4.68}$$

and (2.4.4) becomes

$$\|(\mathcal{D} - \mathcal{D}_N)u\| \leq \phi_N \left\|u^{(N)}\right\| + \frac{\sigma_N \left\|u^{(N+1)}\right\|}{N+1}. \tag{2.4.69}$$

Additionally, let $\widetilde{\sigma}_N$ and $\widetilde{\phi}_N$ respectively be the asymptotic formulae for σ_N and ϕ_N as $N \to \infty$, so that

$$\|u - \mathcal{L}_N u\| \sim \widetilde{\sigma}_N \left\|u^{(N)}\right\|, \qquad N \to \infty, \tag{2.4.70}$$

and

$$\|(\mathcal{D} - \mathcal{D}_N)u\| \sim \widetilde{\phi}_N \left\|u^{(N)}\right\| + \frac{\widetilde{\sigma}_N \left\|u^{(N+1)}\right\|}{N+1}., \qquad N \to \infty. \tag{2.4.71}$$

Formulae for σ_N, ϕ_N, $\widetilde{\sigma}_N$ and $\widetilde{\phi}_N$ derived in Section 2.4.2 for the various nodal distributions are summarised in Table 2.1.

As seen from Table 2.1, the values of $\widetilde{\sigma}_N$ and $\widetilde{\phi}_N$ for all orthogonal-polynomial distributions have a leading-order term of $\left(\frac{\mathrm{e}}{2N}\right)^N$ whereas σ_N and ϕ_N for the regular nodes have leading-order terms of $\left(\frac{2}{N-1}\right)^N$ and $\left(\frac{2}{N-1}\right)^{N-1}$ respectively. This reveals why $\|p_N\|$ and $\|p'_N\|$ converge at approximately the same rate on each of the orthogonal-polynomial distributions as $N \to \infty$, as observed in Figure 2.4.1. The accuracy of the bounds and convergence rates predicted in this section are now verified on a test problem.

	σ_N	ϕ_N	$\widetilde{\sigma}_N$	$\widetilde{\phi}_N$
Regular	$\left(\frac{2}{N-1}\right)^N \frac{1}{4N}$	$\left(\frac{2}{N-1}\right)^{N-1} \frac{1}{N}$	-	-
Chebyshev	$\frac{1}{2^{N-1}N!}$	$\frac{N}{2^{N-1}(N-1)!}$	$\left(\frac{\mathrm{e}}{2N}\right)^N \sqrt{\frac{2}{\pi N}}$	$\left(\frac{\mathrm{e}}{2N}\right)^N \sqrt{\frac{2N^3}{\pi}}$
Chebyshev-Gauss-Lobatto	$\frac{1}{2^{N-2}N!}$	$\frac{N-1}{2^{N-3}N!}$	$\left(\frac{\mathrm{e}}{2N}\right)^N \sqrt{\frac{8}{\pi N}}$	$\left(\frac{\mathrm{e}}{2N}\right)^N \sqrt{\frac{32}{\pi N}}(N-1)$
Legendre	$\frac{2^N N!}{(2N)!}$	$\frac{2^{N-1}N(N+1)!}{(2N)!}$	$\left(\frac{\mathrm{e}}{2N}\right)^N \frac{1}{\sqrt{2}}$	$\left(\frac{\mathrm{e}}{2N}\right)^N \frac{N(N+1)}{\sqrt{8}}$
Legendre-Gauss-Radau	$\frac{2^{N+1}N!}{(2N)!}$	$\frac{2^N N^2\, N!}{(2N)!}$	$\left(\frac{\mathrm{e}}{2N}\right)^N \sqrt{2}$	$\left(\frac{\mathrm{e}}{2N}\right)^N \frac{N^2}{\sqrt{2}}$
Legendre-Gauss-Lobatto	$\frac{(N!)^2\,(2N-1)}{(2N)!(N-1)\left(\left(\frac{N}{2}\right)!\right)^2}$	$\frac{2^N\, N!\,(2N-1)}{(2N)!}$	$\left(\frac{\mathrm{e}}{2N}\right)^N \frac{(2N-1)}{\sqrt{\pi N}(N-1)}$	$\left(\frac{\mathrm{e}}{2N}\right)^N \frac{(2N-1)}{\sqrt{2}}$

Table 2.1: The coefficients σ_N, ϕ_N, $\widetilde{\sigma}_N$ and $\widetilde{\phi}_N$ that scale the bounds on both interpolation and differentiation errors, and respective asymptotic convergence rates, for various nodal distributions.

2.5 Numerical Experiments

In the previous section, explicit bounds and convergence rates were found for the interpolation error and differentiation error on various nodal distributions. The error bounds and convergence rates for the interpolation error are now validated by comparison with the true error computed using both Lagrange interpolation (2.1.1) and barycentric interpolation (2.1.13) on the smooth test function

$$u(x) = \cos x - 2x + 1, \qquad x \in [-1, 1]; \tag{2.5.1}$$

a more challenging test function is considered later in this section. The interpolation errors, bounds (2.4.68) and convergence rates (2.4.70) are computed for each nodal distribution with the corresponding values of σ_N and $\widetilde{\sigma}_N$ found in Table 2.1 and the results are presented in Figures 2.5.1–2.5.3.

Since the barycentric formula (2.1.13) is simply an exact algebraic manipulation of the standard Lagrange formula (2.1.1), identical errors are achieved by both methods on a given set of nodes. For each distribution the bounds and convergence rates are found to be spectrally accurate with respect to the true computational errors. The vertical scales of the plots in Figures 2.5.1–2.5.3 show that a similar error is achieved for each value of N on the clustered distributions; convergence on the regular nodes is seen to be slower.

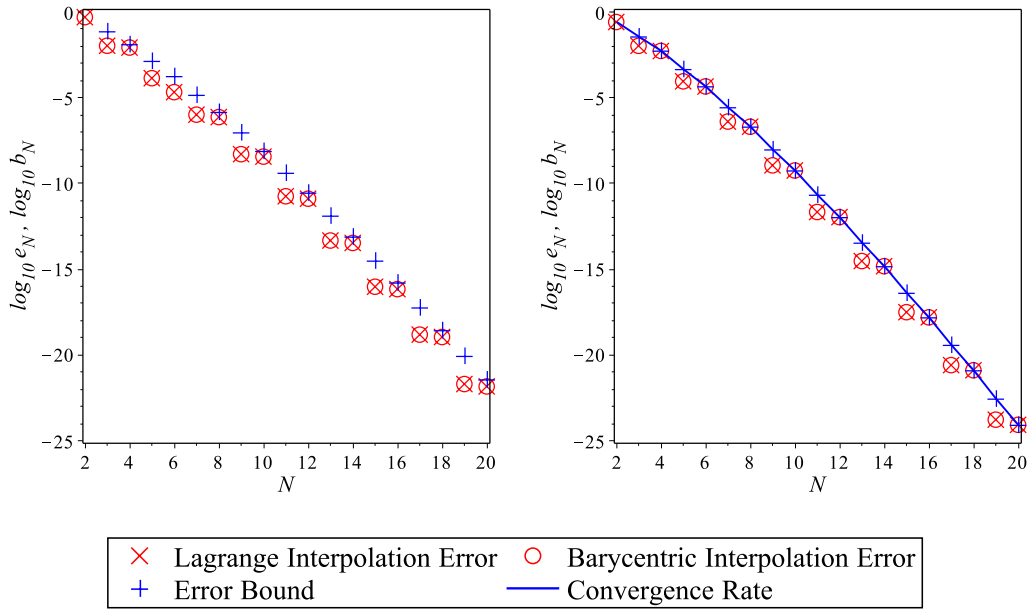

Figure 2.5.1: Logarithmic plots of the Lagrange interpolation errors $e_N = \|u - \mathcal{L}_N u\|$ and barycentric interpolation errors $e_N = \left\|u - \mathcal{B}_N^{(2)} u\right\|$, for $u(x)$ given by (2.5.1), computed using the regular nodes (left) and Chebyshev nodes (right). Error bounds (b_N, $+$) and asymptotic convergence rates (solid lines) derived in Section 2.4 are compared to the true (computed) Lagrange ($\times$) and barycentric ($\circ$) errors. The Lagrange and barycentric errors are indistinguishable, as expected from the construction of the barycentric formula.

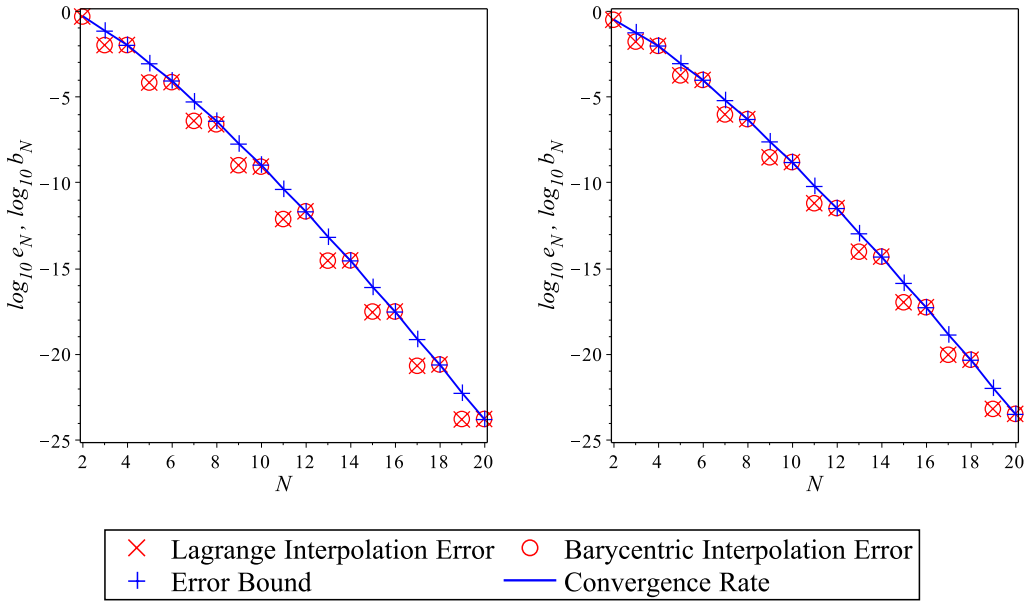

Figure 2.5.2: As for Figure 2.5.1 on the Chebyshev-Gauss-Lobatto nodes (left) and Legendre nodes (right).

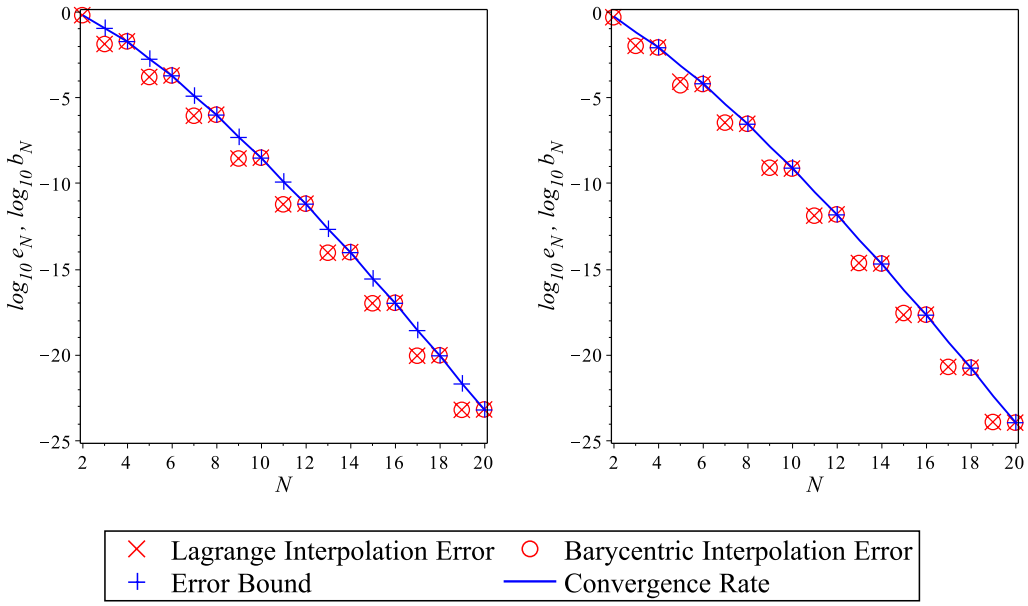

Figure 2.5.3: As for Figure 2.5.1 on the Legendre-Gauss-Radau nodes (left) and Legendre-Gauss-Lobatto nodes (right).

As stated in Section 2.1.2, one advantage of using barycentric interpolation (2.1.13) rather than standard Lagrange interpolation (2.1.1) is a reduction in computational work required to obtain solutions of comparable accuracy. Using the `time()` command in `Maple` to quantify the workload required by each method, a comparison can be made for test example (2.5.1); the results are presented in Figure 2.5.4.

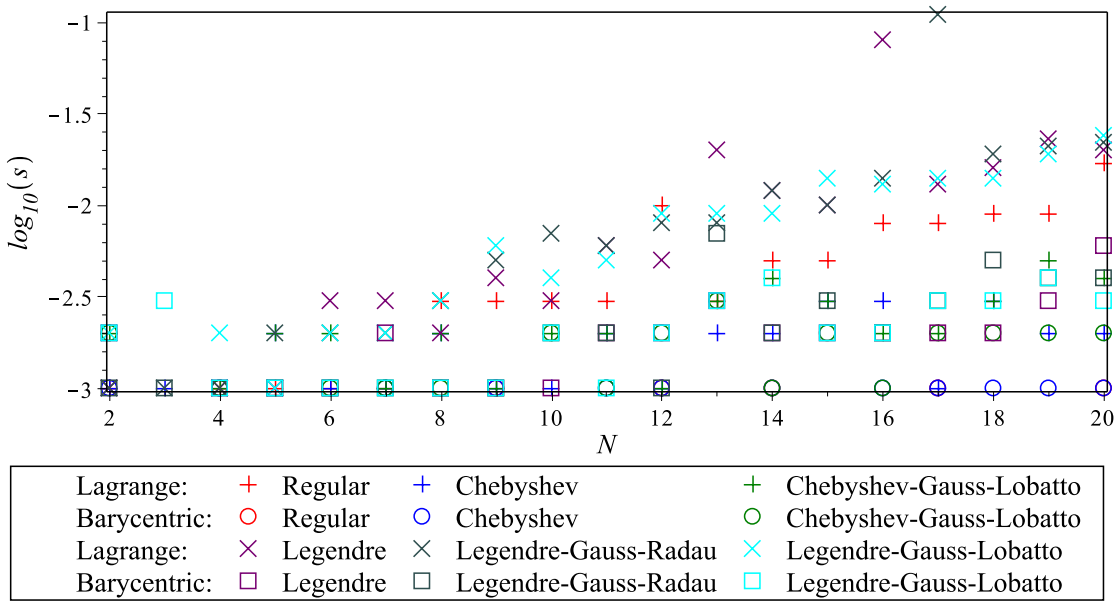

Figure 2.5.4: Logarithmic plot of workloads, given in seconds (s), associated with different interpolation methods on different node sets, for example (2.5.1). The barycentric implementation (2.1.13) (circles and squares) is clearly more economical than the Lagrange implementation (2.1.1) (crosses).

On each node set, and for each N, more CPU is required to compute an approximation using the standard Lagrange form of interpolation. This is consistent with the results and findings in [22], which states that there are $O(N^2)$ additions and multiplications required to obtain a Lagrange interpolant, whereas by using barycentric interpolation this is reduced to $O(N)$. A more detailed breakdown of the respective sub-costs in terms of N, of both set-up and evaluation, associated with Lagrange and barycentric interpolation is given in [135]; this breakdown includes estimates of the costs associated with floating-point operations.

Bounds and convergence rates for the differentiation error are now considered for example (2.5.1), for which the derivative is

$$u'(x) = -\sin x - 2. \tag{2.5.2}$$

The true computational errors, bounds (2.4.69) and convergence rates (2.4.71) are computed for each nodal distribution with the corresponding values of ϕ_N, σ_N, $\widetilde{\phi}_N$ and $\widetilde{\sigma}_N$ found in Table 2.1; results are presented in Figures 2.5.5–2.5.7.

The vertical scales of the plots in Figures 2.5.5–2.5.7 show that the smallest differentiation errors arise on either of the Gauss-Lobatto distributions, whilst the regular nodes again yield the largest errors. On all nodal distributions the error bounds and convergence rates are seen to be an accurate prediction of the true computed errors, and so may be used to predict the error for higher values of N.

Note that, irrespective of whether or not Lagrange or barycentric interpolation is used, the convergence of the computed errors to zero, as N increases, is not

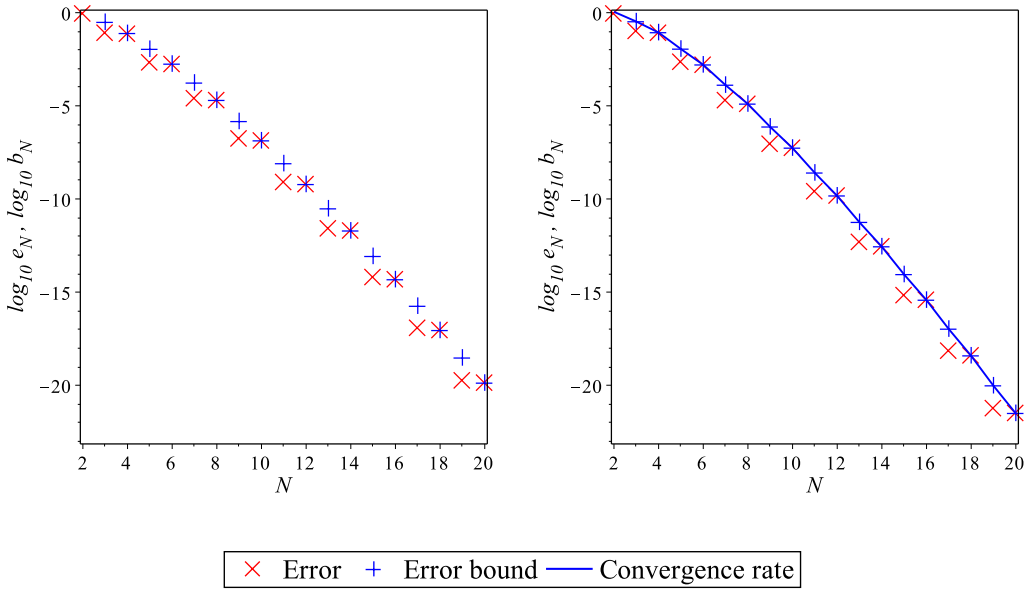

Figure 2.5.5: Logarithmic plot of the differentiation error $e_N = \|(\mathcal{D} - \mathcal{D}_N)u\|$ for $u(x)$ given by (2.5.1), using the regular nodes (left) and Chebyshev nodes (right). Error bounds (b_N, $+$) and convergence rates (solid lines) derived in Section 2.4 are compared to the actual computational errors ($\times$).

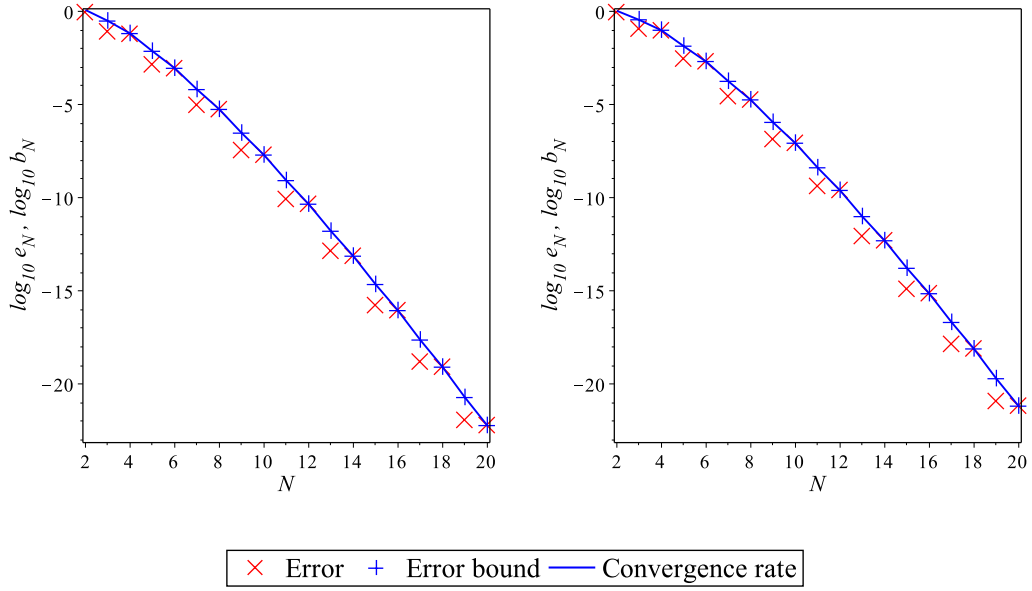

Figure 2.5.6: As for Figure 2.5.5 on the Chebyshev-Gauss-Lobatto nodes (left) and the Legendre nodes (right).

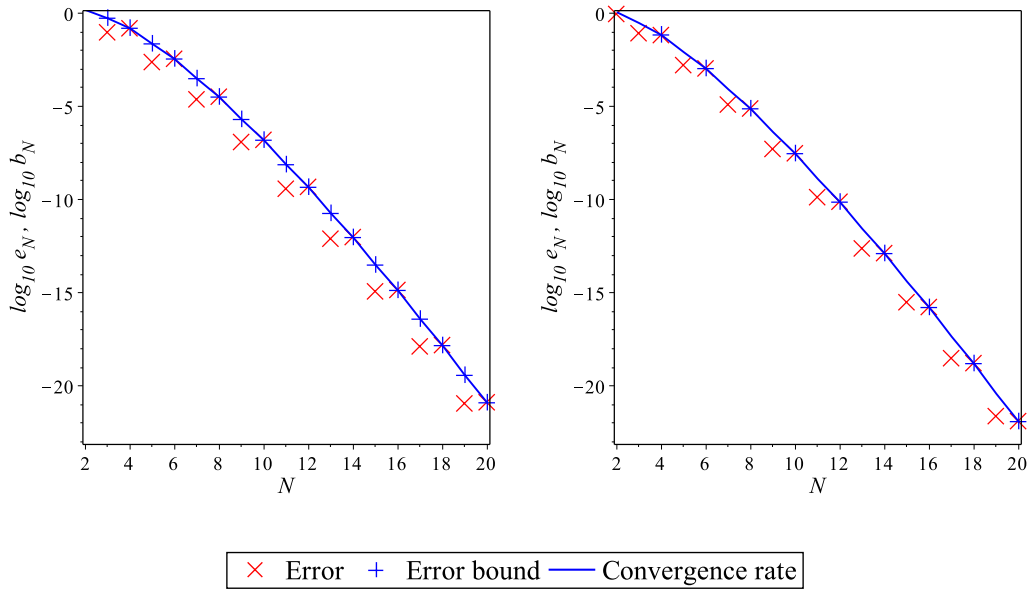

Figure 2.5.7: As for Figure 2.5.5 on the Legendre-Gauss-Radau nodes (left) and the Legendre-Gauss-Lobatto nodes (right).

guaranteed for certain node distributions. This is illustrated by the following well-known "Runge-phenomenon" example [27, Eq. 4.9]

$$u(x) = \frac{1}{1+25x^2}, \qquad x \in [-1,1], \tag{2.5.3}$$

for which the errors resulting from both Lagrange interpolation (2.1.1) and barycentric interpolation (2.1.13) are shown in Figures 2.5.8–2.5.10.

Interpolation polynomials based on regular nodes oscillate with increasing modulus towards the edges of the interval as the degree of the interpolation polynomial increases: this is known as the Runge Phenomenon [27]. Figure 2.5.8 shows that both Lagrange and barycentric interpolation on regularly spaced nodes yield exponentially divergent errors with increasing N, which is an illustration of the Runge phenomenon. This can be explained by considering the contours shown in Figure 2.4.2, for which [124, p. 48] states that, if a function $u(x)$ is analytic within the region bounded by the smallest contour containing $[-1,1]$, then it may be approximated by polynomial interpolation (2.1.1) with spectral accuracy. Comparison of Figures 2.4.2 and 2.4.9 shows that the contour with $C = 10^{-3}$ is approximately the

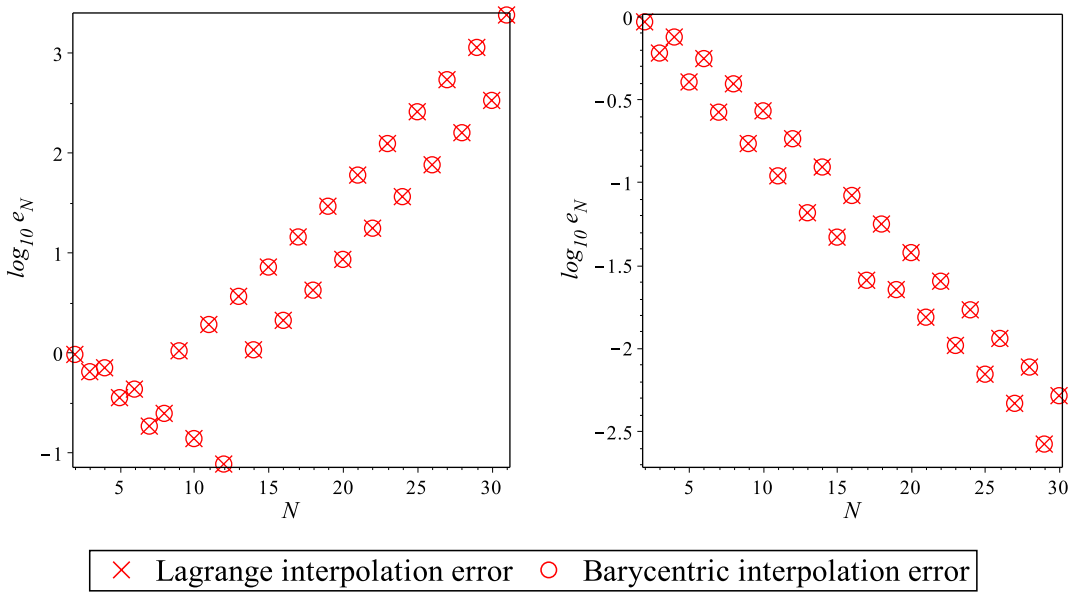

Figure 2.5.8: Logarithmic plots of the Lagrange interpolation errors $e_N = \|u - \mathcal{L}_N u\|$ and barycentric interpolation errors $e_N = \left\|u - \mathcal{B}_N^{(2)} u\right\|$, for $u(x)$ given by (2.5.3), computed using the regular nodes (left) and Chebyshev nodes (right). Note the exponential divergence of the error arising on the regularly spaced nodes.

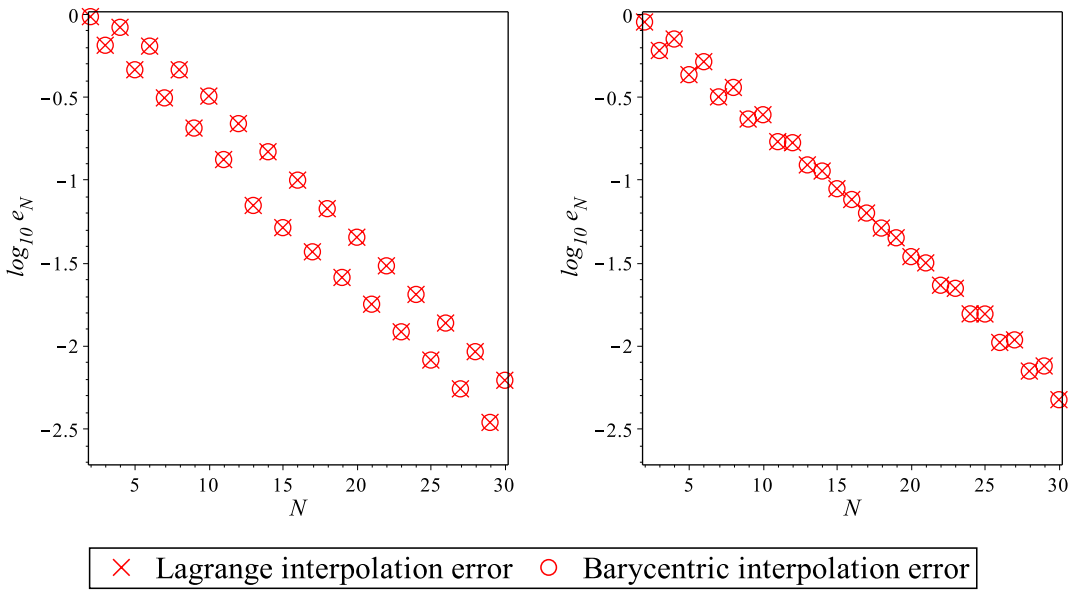

Figure 2.5.9: As for Figure 2.5.8 on the Chebyshev-Gauss-Lobatto nodes (left) and Legendre nodes (right).

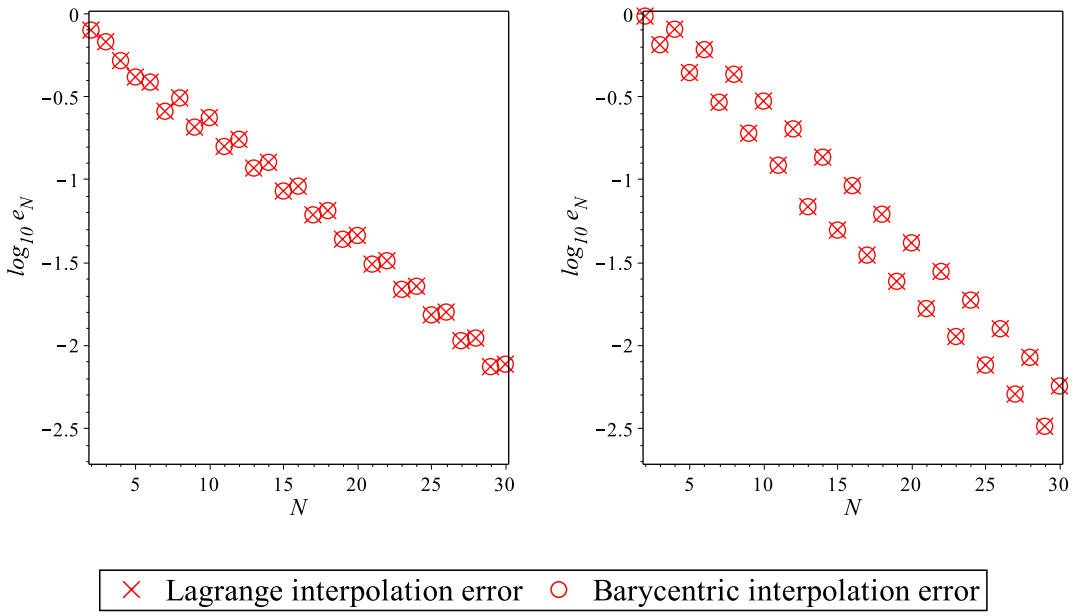

Figure 2.5.10: As for Figure 2.5.8 on the Legendre-Gauss-Radau nodes (left) and Legendre-Gauss-Lobatto nodes (right).

smallest contour containing $[-1,1]$; however, this contour also contains the poles of the function $u(x)$ in (2.5.3) which are at $\pm\frac{i}{5}$, and hence polynomial interpolation of (2.5.3) is expected to be inaccurate. Regarding the regular-nodal distribution, [125, p. 99] states that, in the limit $N \to \infty$, the smallest contour that contains $[-1,1]$, known as the "Runge region" [28], crosses the real axis at ± 1 and the imaginary axis at $\pm 0.52552491457i$; it is within this Runge region that a function must be analytic for polynomial interpolation to be convergent. Figures 2.4.3–2.4.7 show that, for the clustered nodal distributions, the smallest contours containing ± 1 are approximately $C = 10^{-4}$; on each of these distributions, the poles $\pm\frac{i}{5}$ lie outside this contour and so spectrally accurate interpolation errors are obtained that converge to zero as N increases. That is, by interpolating on a set of nodes that cluster more densely towards the ends of the interval, the Runge phenomenon is averted when using both Lagrange and barycentric interpolation. However, a comparison of the vertical scales of Figures 2.5.8–2.5.10 with Figures 2.5.1–2.5.3 shows that, although the clustered nodal distributions yield convergent errors with increasing N when approximating the Runge function, convergence is much slower than when approximating a smooth function.

The error bounds and convergence rates have been omitted in Figures 2.5.8–2.5.10 as, for this example, the term $\left\|u^{(N)}\right\|$ diverges rapidly with N. Specifically, any function of the form

$$\widetilde{u}(x) = \frac{1}{1+(\beta\, x)^2}, \tag{2.5.4}$$

wherein $\beta \in \mathbb{R}$ is a constant, satisfies [50, p. 93]

$$\left\|\widetilde{u}^{(N)}\right\| \leq N!\,\beta^N \sim \sqrt{2\pi N}\left(\frac{\beta N}{\mathrm{e}}\right)^N. \tag{2.5.5}$$

Table 2.1 shows that the orthogonal polynomial nodal distributions have $\widetilde{\sigma}_N \sim \left(\frac{\mathrm{e}}{2N}\right)^N$ which, when combined with (2.4.70) and (2.5.5), gives the asymptotic error estimate

$$\left\|\widetilde{u} - \mathcal{L}_N\widetilde{u}\right\| \sim \left(\frac{\beta}{2}\right)^N, \tag{2.5.6}$$

and hence the interpolation-error prediction diverges for $\beta > 2$ and converges for $\beta < 2$ as $N \to \infty$. Since $\beta = 5$ in Example (2.5.3), the error bounds given by (2.4.70) and Table 2.1 diverge and hence fail to predict the convergence of the true computed errors. This is because the value of ξ in the formula (2.4.1) that gives the

true error is unknown and so the error bound (2.4.2), and those given explicitly for the different node sets, maximises $|u^{(N)}|$ for all possible choices of ξ. This example shows a limitation on the applicability of the error formulae for certain "badly behaved" functions.

Note that (2.5.4) has poles at $\pm\frac{i}{\beta}$ and so, when $\beta = 2$, the poles lie approximately on the boundary of the Runge region. In addition, if $\beta > 2$ the poles lie within the Runge region and if $\beta < 2$ the poles lie outside the Runge region. That is, the values of β that cause the error estimate (2.5.6) to diverge also cause the true interpolation error on the regular nodes to diverge.

Figure 2.5.8 shows that interpolation of (2.5.3) on the regular nodes has divergent errors due to the Runge phenomenon. To circumvent this apparent shortfall, a method is now considered which uses the nodal data of a function at the *regular* nodes but in which, even for the test function (2.5.3), the Runge phenomenon is averted.

2.6 Tikhonov Regularisation

It is shown above that, when interpolating $u(x)$ in (2.5.3), the Runge phenomenon can be averted simply by choosing clustered nodes. However, the question posed in [26] is whether or not the *spectral* accuracy of Chebyshev interpolation can be achieved by using *regularly* spaced nodes. This question is answered in the affirmative by employing Tikhonov regularisation [129]. The Tikhonov polynomial approximating a function $u(x)$ on the interval $[-1, 1]$ is given as

$$u_N(x;\alpha) = \sum_{j=1}^{N} b_{j,N}\, C_{j,N}(x), \tag{2.6.1}$$

wherein the functions $C_{j,N}(x)$ are the standard Chebyshev cardinal functions, which are equivalent to the Lagrange basis functions $L_{j,N}(x)$, defined in (2.1.2), computed on Chebyshev nodes (2.3.7). For the remainder of this section, the Chebyshev nodes (2.3.7) are relabelled as $y_{k,N}$, and the regular nodes (2.3.1) are denoted by $x_{k,N}$ for $k = 1(1)N$. The Tikhonov approximation is *not* an interpolant since the constants $b_{j,N}$ in (2.6.1) are chosen in such a way as to minimise the sum

$$\rho = R + \alpha\, S, \tag{2.6.2}$$

in which the interpolation residual R is computed on the *regular* nodes as

$$R = \sum_{k=1}^{N} \Big(u(x_{k,N}) - u_N(x_{k,N}) \Big)^2 \tag{2.6.3}$$

whereas the accompanying *smoothness norm* S is computed on the *Chebyshev* nodes as

$$S = \sum_{k=1}^{N} \left(\frac{d^2 u_N}{dx^2}(y_{k,N}) \right)^2 . \tag{2.6.4}$$

In (2.6.2), α is a constant, known as the Tikhonov parameter, that is to be determined as part of the regularisation process.

The constants $b_{j,N}$ in (2.6.1) must be chosen so as to minimise the sums implicit in (2.6.2). Therefore, to determine these constants, (2.6.2) is partially differentiated with respect to each of the $b_{i,N}$. First, ρ in (2.6.2) is written explicitly in terms of the constants $b_{j,N}$ as

$$\begin{aligned} \rho &= \sum_{k=1}^{N} \Big(u(x_{k,N}) - u_N(x_{k,N}) \Big)^2 + \alpha \sum_{k=1}^{N} \left(\frac{d^2 u_N}{dx^2}(y_{k,N}) \right)^2 \\ &= \sum_{k=1}^{N} \Big(u(x_{k,N}) - \sum_{j=1}^{N} b_{j,N} C_{j,N}(x_{k,N}) \Big)^2 + \alpha \sum_{k=1}^{N} \left(\sum_{j=1}^{N} b_{j,N}\, C''_{j,N}(y_{k,N}) \right)^2 , \end{aligned} \tag{2.6.5}$$

thereby giving

$$\begin{aligned} \frac{\partial \rho}{\partial b_{i,N}} = \; & 2 \sum_{k=1}^{N} \Big(- C_{i,N}(x_{k,N}) \Big) \Big(u(x_{k,N}) - \sum_{j=1}^{N} b_{j,N}\, C_{j,N}(x_{k,N}) \Big) \\ & + 2\,\alpha \sum_{k=1}^{N} \sum_{j=1}^{N} b_{j,N} C''_{i,N}(y_{k,N})\, C''_{j,N}(y_{k,N}). \end{aligned} \tag{2.6.6}$$

The stationary value of ρ, here a minimum due to ρ being a sum of squares, is found by setting $\dfrac{\partial \rho}{\partial b_{i,N}} = 0$ so that

$$\begin{aligned} & 2 \sum_{k=1}^{N} \Big(- C_{i,N}(x_{k,N}) \Big) \Big(u(x_{k,N}) - \sum_{j=1}^{N} b_{j,N}\, C_{j,N}(x_{k,N}) \Big) \\ & \qquad + 2\,\alpha \sum_{k=1}^{N} \sum_{j=1}^{N} b_{j,N}\, C''_{i,N}(y_{k,N})\, C''_{j,N}(y_{k,N}) = 0, \end{aligned} \tag{2.6.7}$$

which is equivalently

$$\sum_{j=1}^{N}\left(\sum_{k=1}^{N} C_{i,N}(x_{k,N})\,C_{j,N}(x_{k,N}) + \alpha\sum_{k=1}^{N} C''_{i,N}(y_{k,N})\,C''_{j,N}(y_{k,N})\right) b_{j,N} = \sum_{k=1}^{N} C_{i,N}(x_{k,N})\,u(x_{k,N}). \tag{2.6.8}$$

That is, (2.6.8) is a system of N linear equations

$$\mathbf{H}_N\,\mathbf{b}_N = \mathbf{g}_N \tag{2.6.9}$$

in which

$$\{\mathbf{H}_N\}_{i,j} = \sum_{k=1}^{N} C_{i,N}(x_{k,N})\,C_{j,N}(x_{k,N}) + \alpha\sum_{k=1}^{N} C''_{i,N}(y_{k,N})\,C''_{j,N}(y_{k,N}), \tag{2.6.10}$$

and

$$\{\mathbf{g}_N\}_i = \sum_{k=1}^{N} C_{i,N}(x_{k,N})\,u(x_{k,N}) \tag{2.6.11}$$

are known, whilst

$$\{\mathbf{b}_N\}_i = b_{i,N} \tag{2.6.12}$$

is yet to be determined.

Knowing the function $u(x)$, the cardinal functions $C_{i,N}(x)$, and the sets of regular and Chebyshev nodes, system (2.6.9) can be solved for the required coefficients $b_{j,N}$ in (2.6.1). It remains only to determine the Tikhonov constant α in (2.6.2), which can be done only experimentally using the so-called *L-shaped curve* method [61]. This involves evaluating $u_N(x;\alpha)$ for a fixed value of N and a range of values α. The log of the residual R is then plotted against the log of the smoothness norm S which gives a curve in an L-shape (see Figure 2.6.1). The Tikhonov constant α is then chosen so that it is the value corresponding to the elbow of the curve, where the residual and the smoothness norm are both low values. The example approximated in [26] is

$$u(x) = \frac{1}{1+x^2} \qquad x \in [-5,5], \tag{2.6.13}$$

using Chebyshev and regular nodes scaled onto the interval $[-5,5]$; this is equivalent to approximating (2.5.3) using nodes on $[-1,1]$. The advantage of scaling onto

$[-1, 1]$ is that standard second-order Chebyshev differentiation matrices (see Chapter 3) can be used to construct the matrices $\mathbf{H}_N$. The L-shaped curve for $N = 31$ is shown in Figure 2.6.1.

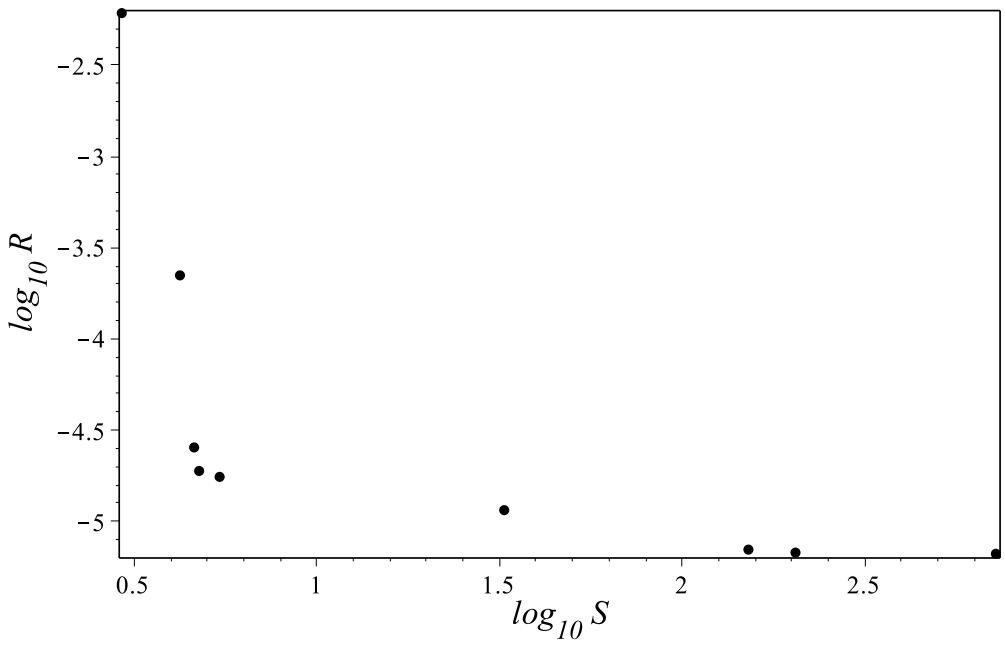

Figure 2.6.1: L-shaped curve for $N = 31$ and $u(x)$ as given by (2.5.3). From top-left to bottom-right the dots correspond to (S, R) pairs obtained using $\alpha = 10^{-k}$, $k = 2(1)10$. The elbow of the curve is obtained for $\alpha \in (10^{-6}, 10^{-4})$, in accordance with [26].

The error of the scaled Tikhonov approximation (2.6.1) for $N = 31$ and $\alpha = 10^{-6}$ is shown in Figure 2.6.2; it is compared with the errors of the Chebyshev and regular Lagrange interpolation polynomials (2.1.1) also computed with $N = 31$.

Figure 2.6.2 shows that the error of the Tikhonov approximation (2.6.1) on regularly spaced nodes is of comparable size with the error of Lagrange interpolation (2.1.1) on Chebyshev nodes. The minimal difference between the errors of the Tikhonov approximation and the Chebyshev Lagrange interpolant is also seen in [26, Fig.1b] which shows the errors (not on a logarithmic scale) on $[-5, 5]$; note that $N = 30$ in [26] as the nodes are labeled $x_{k,N}$, $y_{k,N}$ for $k = 0(1)N$. In contrast, the error of Lagrange interpolation on regular nodes is seen in Figure 2.6.2 to be orders of magnitude larger than both the Tikhonov and Chebyshev Lagrange approximations

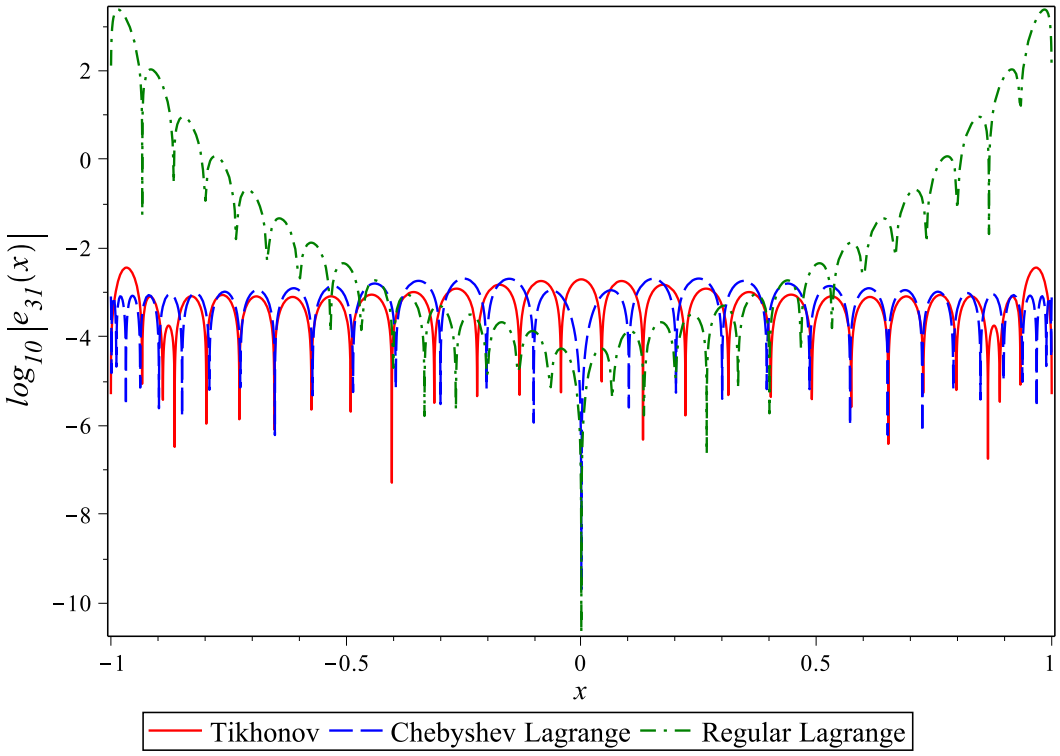

Figure 2.6.2: The Tikhonov approximation (2.6.1) error $e_{31}(x) = u(x) - u_{31}(x; 10^{-6})$ on regularly spaced nodes (solid line) is compared with the Lagrange interpolation errors $e_{31}(x) = u(x) - \mathcal{L}_{31}u(x)$ on Chebyshev nodes (dashed line) and on regular nodes (dash-dot line).

towards the ends of the interval $[-1, 1]$; this is expected from Figure 2.5.8, which shows that the regular Lagrange errors are divergent with increasing N.

2.7 Summary

The purpose of this chapter was to introduce accurate numerical methods, for interpolating a function and its derivative, that can later be incorporated into numerical methods for solving both IEs and IDEs. The Lagrange interpolation introduced in Section 2.1 provides the basis on which all of the component numerical methods required to solve IEs and IDEs are founded. Specifically, it is shown in Chapter 3 how the Lagrange interpolation formula and basis functions can be used to implement, respectively, spectrally accurate numerical differentiation and numerical quadrature.

By considering interpolation on a variety of nodal distributions, including those that are optimal for numerical differentiation and numerical quadrature, the numerical methods derived in Chapters 4 and 5 may be implemented in such a way that the overall IE and IDE error can be minimised. Furthermore, by analysing and comparing on each of the node sets considered in this chapter the errors incurred through interpolation of a function and its derivative, a framework has been accordingly provided from which the IE and IDE error analyses can be built. Barycentric interpolation was additionally implemented in order to offer advantages in terms of both workload and stability, and Tikhonov regularisation was considered in order to overcome the limitations of standard Lagrange interpolation for certain classes of functions.

Chapter 3

Spectrally Accurate Numerical Differentiation and Numerical Quadrature

The techniques developed in Chapter 2 are now extended to numerical methods for robust quadrature and differentiation of discrete data, the former of which is required for solving both integral equations (IEs) and integro-differential equations (IDEs), and the latter of which is required for solving IDEs. It is therefore necessary to have a comprehensive understanding of the errors incurred in both numerical quadrature and differentiation.

In Chapter 2 several nodal distributions were considered on which both interpolation and differentiation errors were analysed and, germane to the goals of this thesis, quantified. In this chapter, an efficient and accurate means of implementing the numerical differentiation studied in Section 2.2 is considered. Specifically, *differentiation matrices* [19, 116] are used to perform spectrally accurate [27] differentiation of discrete data in a way that effectively bypasses initial interpolation of that data. Furthermore, this chapter introduces *Gaussian quadrature* [9] which uses discrete nodal data to accurately approximate the definite integral of a function; it is included herein as the numerical methods introduced in later chapters are based upon the well-known *Nyström method* [98, 10] which utilises several forms of Gaussian quadrature.

In Section 3.1, simplified entries for differentiation matrices based upon a variety of nodal distributions are derived and properties of differentiation matrices based

upon symmetric nodal distributions are discussed. Theoretically and computationally determined eigenvalues of the differentiation matrices are then considered. In Section 3.2 Gaussian quadrature rules based upon three of the nodal distributions examined in Chapter 2 are introduced, and the errors associated with each rule are compared by determining theoretical bounds on each.

Unless otherwise stated, throughout Section 3.1, $i, j = 1(1)N$ and, throughout Section 3.2, $i, j = 1(1)M$.

3.1 Differentiation Matrices

In Chapter 2 it was shown, by (2.2.3) and (2.2.4), how the derivative of a function can be approximated for all $x \in [-1, 1]$ by differentiating the Lagrange interpolation formula (2.1.1). Now suppose that the derivative is required at only the nodal values, rather than throughout the interval $[-1, 1]$, which is exactly what is required for the subsequent collocation of a discretised IDE in Chapter 5, as only the nodal data of a function is needed in order to form an interpolating polynomial. By setting $x = x_{i,N}$ in (2.2.3) and (2.2.4), the nodal data of the derivative $u'(x)$ can be approximated by

$$u'(x_{i,N}) = (\mathcal{D}u)(x_{i,N}) \approx (\mathcal{D}_N u)(x_{i,N}) = \sum_{j=1}^{N} L'_{j,N}(x_{i,N})\, u(x_{j,N}), \tag{3.1.1}$$

in which

$$L'_{j,N}(x_{i,N}) = \frac{p'_N(x_{i,N})(x_{i,N} - x_{j,N}) - p_N(x_{i,N})}{(x_{i,N} - x_{j,N})^2\, p'_N(x_{j,N})}. \tag{3.1.2}$$

The summation in (3.1.1) effectively defines a matrix-vector product in which the $N \times N$ matrix $\mathbf{D}_N$ has elements

$$\{\mathbf{D}_N\}_{i,j} = L'_{j,N}(x_{i,N}). \tag{3.1.3}$$

Using (3.1.3) a matrix-vector form of (3.1.1) is

$$\mathbf{u}'_N = \mathbf{D}_N\, \mathbf{u} \tag{3.1.4}$$

wherein the vectors containing differentiated and original nodal data are respectively

$$\{\mathbf{u}'_N\}_i = (\mathcal{D}_N u)(x_{i,N}) \quad \text{and} \quad \{\mathbf{u}\}_i = u(x_{i,N}). \tag{3.1.5}$$

The matrix $\mathbf{D}_N$ evaluated using (3.1.3) is then, by (3.1.4), the so-called $N \times N$ *differentiation matrix*. That is, the matrix-vector multiplication (3.1.4) clearly approximates discrete differentiation without first having to construct the interpolating polynomial (2.2.3).

The right-hand side of (3.1.2), which by (3.1.3) defines the entries of the differentiation matrix, can be simplified for both $i = j$ and $i \neq j$. Since $p_N(x_{i,N}) = 0$ by (2.1.3), when $i \neq j$ (3.1.2) simplifies to

$$L'_{j,N}(x_{i,N}) = \frac{p'_N(x_{i,N})}{(x_{i,N} - x_{j,N})\, p'_N(x_{j,N})}, \qquad i \neq j. \tag{3.1.6}$$

When $i = j$ the definition (2.2.4), from which (3.1.2) originates, must be used along with L'Hôpital's rule, which is represented by the symbol $\overset{LH}{=}$. Letting $x \to x_{j,N}$ in (2.2.4) therefore gives

$$\begin{aligned} L'_{j,N}(x_{j,N}) &= \lim_{x \to x_{j,N}} \frac{p'_N(x)(x - x_{j,N}) - p_N(x)}{(x - x_{j,N})^2\, p'_N(x_{j,N})}, \\ &\overset{LH}{=} \lim_{x \to x_{j,N}} \frac{p''_N(x)(x - x_{j,N}) + p'_N(x) - p'_N(x)}{2\,(x - x_{j,N})\, p'_N(x_{j,N})}, \\ &= \frac{p''_N(x_{j,N})}{2\, p'_N(x_{j,N})}. \end{aligned} \tag{3.1.7}$$

By (3.1.6) and (3.1.7), the entries of the differentiation matrix (3.1.3) are therefore given by

$$\{\mathbf{D}_N\}_{i,j} = \begin{cases} \dfrac{p'_N(x_{i,N})}{(x_{i,N} - x_{j,N})\, p'_N(x_{j,N})} & i \neq j \\[2ex] \dfrac{p''_N(x_{j,N})}{2\, p'_N(x_{j,N})} & i = j. \end{cases} \tag{3.1.8}$$

Nodal data of higher derivatives of $u(x)$ can be approximated in a similar way. Consider multiplying (3.1.4) by $\mathbf{D}_N^{M-1}$, which yields

$$\mathbf{D}_N^{M-1}\, \mathbf{u}'_N = \mathbf{D}_N^M\, \mathbf{u} \tag{3.1.9}$$

wherein, by (3.1.5) and (2.2.5), the ith element on the left-hand side of (3.1.9) is equivalently

$$\{\mathbf{D}_N^{M-1}\, \mathbf{u}'_N\}_i = \mathcal{D}_N^{(M-1)}(\mathcal{D}_N u)(x_{i,N}) = (\mathcal{D}_N^{(M)} u)(x_{i,N}). \tag{3.1.10}$$

Therefore, the nodal data of the Mth derivative of $u(x)$ can be found from (3.1.9) as

$$\mathbf{u}_N^{(M)} = \mathbf{D}_N^M \, \mathbf{u}, \qquad M \geq 1, \tag{3.1.11}$$

wherein

$$\{\mathbf{u}_N^{(M)}\}_i = (\mathcal{D}_N^{(M)} u)(x_{i,N}). \tag{3.1.12}$$

That is, the product of the Mth power of a differentiation matrix with an N-vector containing nodal data of a function yields an N-vector whose elements are the nodal data of the Mth derivative of the original function. Comparison of (3.1.11) with (2.2.6), in which $x = x_{i,N}$ in the latter gives the entries of the matrix $\mathbf{D}_N^M$ as

$$\{\mathbf{D}_N^M\}_{i,j} = L_{j,N}^{(M)}(x_{i,N}), \tag{3.1.13}$$

which avoids the computational expense of raising $\mathbf{D}_N$ to the Mth power. Evaluating $L_{j,N}^{(M)}(x)$, in (2.2.9), at the nodes gives

$$L_{j,N}^{(M)}(x_{i,N}) = \frac{\displaystyle\sum_{k=1}^{M} (-1)^{M+k} \, \frac{M!}{k!} (x_{i,N} - x_{j,N})^{k-1} \, p_N^{(k)}(x_{i,N})}{(x_{i,N} - x_{j,N})^M \, p'_N(x_{j,N})}, \qquad i \neq j \tag{3.1.14}$$

and

$$L_{j,N}^{(M)}(x_{j,N}) = \frac{p_N^{(M+1)}(x_{j,N})}{(M+1)\, p'_N(x_{j,N})}, \tag{3.1.15}$$

proofs of which are in Appendix A. Together, (3.1.13), (3.1.14) and (3.1.15) can be used to construct Mth-order $N \times N$ differentiation matrices using *any* set of nodes $x_{i,N}$ for $i = 1(1)N$.

The matrix-vector product in (3.1.11) effectively emulates the differentiation of a continuous function at discrete points in the interval $[-1, 1]$. The specific effect of changing those points is now examined by looking at the nodal distributions considered in Chapter 2. Since only first-order IDEs are studied in this thesis, only the specific properties of the first-order differentiation matrix, defined by (3.1.8), are considered. The entries of the differentiation matrix in (3.1.8) can, for some nodal distributions, be simplified further to yield explicit forms; for example, simplified forms of the entries of differentiation matrices based upon Chebyshev, Chebyshev-Gauss-Lobatto and Legendre-Gauss-Lobatto distributions are given in [27, Appx. F.8,F.9,F.10] and those for Legendre and Legendre-Gauss-Radau distributions are

given in [78, p. 67]. It is now shown how these entries are derived from (3.1.6) and (3.1.7). The regular nodal distribution is omitted from this chapter due to its limited interpolation accuracy highlighted in Chapter 2. The next few subsections, which detail the derivation of the differentiation-matrix entries, are unavoidably repetitive in structure although not in detailed content.

3.1.1 Chebyshev Nodes

The entries of the differentiation matrix based upon Chebyshev nodes are first considered. The derivatives of $p_N(x)$ as defined by (2.3.6) are substituted into (3.1.6) and (3.1.7) respectively to give

$$L'_{j,N}(x_{i,N}) = \frac{T'_N(x_{i,N})}{(x_{i,N} - x_{j,N})T'_N(x_{j,N})}, \qquad i \neq j, \tag{3.1.16}$$

and

$$L'_{j,N}(x_{j,N}) = \frac{T''_N(x_{j,N})}{2\,T'_N(x_{j,N})}. \tag{3.1.17}$$

Therefore, to simplify the differentiation-matrix entries, the values of $T'_N(x_{j,N})$ and $T''_N(x_{j,N})$ are required. To evaluate $T'_N(x_{j,N})$ the substitution $x = \cos\theta$ is used to rewrite the Chebyshev polynomial defined by (2.3.4) as

$$T_N(x) = T_N(\cos\theta) = \cos N\theta \tag{3.1.18}$$

and the nodes, defined by (2.3.7), as

$$x_{j,N} = \cos\theta_{j,N} \quad \text{wherein} \quad \theta_{j,N} = \frac{2N - 2j + 1}{2N}\pi. \tag{3.1.19}$$

Differentiating both sides of (3.1.18) with respect to x yields

$$T'_N(x) = \frac{-1}{\sin\theta}\frac{d}{d\theta}T_N(\cos\theta) = \frac{N\sin N\theta}{\sin\theta} \tag{3.1.20}$$

which, upon substitution of (3.1.19), gives

$$T'_N(x_{j,N}) = \frac{N\sin N\theta_{j,N}}{\sin\theta_{j,N}}. \tag{3.1.21}$$

Since

$$\sin\theta_{j,N} = \sqrt{1 - \cos^2\theta_{j,N}} = \sqrt{1 - x_{j,N}^2}, \tag{3.1.22}$$

and, by simple algebra,

$$\sin N\theta_{j,N} = \sin\left(N - j + \tfrac{1}{2}\right)\pi = (-1)^{N-j}, \tag{3.1.23}$$

then (3.1.21) can be rewritten as

$$T'_N(x_{j,N}) = \frac{(-1)^{N-j}\,N}{\sqrt{1-x_{j,N}^2}}. \tag{3.1.24}$$

To evaluate $T''_N(x_{j,N})$, the Chebyshev differential equation (2.3.5) is rewritten as

$$T''_N(x) = \frac{x\,T'_N(x) - N^2\,T_N(x)}{1-x^2} \tag{3.1.25}$$

which, when evaluated at the nodes, yields

$$T''_N(x_{j,N}) = \frac{x_{j,N}\,T'_N(x_{j,N})}{1-x_{j,N}^2} = \frac{(-1)^{N-j}\,x_{j,N}\,N}{(1-x_{j,N}^2)^{3/2}} \tag{3.1.26}$$

since, by construction, $T_N(x_{j,N}) = 0$. Therefore, by (3.1.3), (3.1.16), (3.1.17), (3.1.24) and (3.1.26), the explicit forms of the entries for the $N \times N$ differentiation matrix based upon the Chebyshev nodes are

$$\{\mathbf{D}_N\}_{i,j} = \begin{cases} \dfrac{(-1)^{i+j}}{x_{i,N}-x_{j,N}}\sqrt{\dfrac{1-x_{j,N}^2}{1-x_{i,N}^2}} & i \neq j \\[2ex] \dfrac{x_{j,N}}{2\,(1-x_{j,N}^2)} & i = j, \end{cases} \tag{3.1.27}$$

in accordance with [27, Eq. F.50].

3.1.2 Chebyshev-Gauss-Lobatto Nodes

The entries of the differentiation matrix based upon Chebyshev-Gauss-Lobatto nodes are now considered. Substitution of the derivatives of $p_N(x)$ defined by (2.3.9), the first of which is given by (2.4.30), into (3.1.6) and (3.1.7) respectively yields

$$L'_{j,N}(x_{i,N}) = \frac{(N-1)^2\,T_{N-1}(x_{i,N}) + x_{i,N}\,T'_{N-1}(x_{i,N})}{(x_{i,N}-x_{j,N})\Big((N-1)^2\,T_{N-1}(x_{j,N}) + x_{j,N}\,T'_{N-1}(x_{j,N})\Big)}, \qquad i \neq j, \tag{3.1.28}$$

and

$$L'_{j,N}(x_{j,N}) = \frac{\left((N-1)^2+1\right)T'_{N-1}(x_{j,N}) + x_{j,N}\,T''_{N-1}(x_{j,N})}{2\left((N-1)^2\,T_{N-1}(x_{j,N}) + x_{j,N}\,T'_{N-1}(x_{j,N})\right)}. \tag{3.1.29}$$

The values of $T_{N-1}(x_{j,N})$, $T'_{N-1}(x_{j,N})$ and $T''_{N-1}(x_{j,N})$ are therefore required to simplify the differentiation-matrix entries. The values of $T_{N-1}(x_{j,N})$ are considered first. Using the substitution $x = \cos\theta$ the nodes $x_{j,N}$ defined by (2.3.10) become

$$x_{j,N} = \cos\theta_{j,N} \quad \text{wherein} \quad \theta_{j,N} = \frac{N-j}{N-1}\pi. \tag{3.1.30}$$

Evaluating the Chebyshev polynomial $T_N(x)$ defined by (2.3.4) at the nodes therefore yields

$$T_{N-1}(x_{j,N}) = \cos((N-j)\pi) = (-1)^{N-j}. \tag{3.1.31}$$

The values of $T'_{N-1}(x_{j,N})$ are now found. By definition, the interior nodes, $x_{j,N}$ with $j = 2(1)N-1$, satisfy

$$T'_{N-1}(x_{j,N}) = 0, \qquad j = 2(1)N-1, \tag{3.1.32}$$

and so it remains to find $T'_{N-1}(x)$ evaluated at the exterior nodes $x_{1,N} = -1$ and $x_{N,N} = 1$. By (3.1.20), the substitution $x = \cos\theta$ yields

$$T'_{N-1}(x) = \frac{(N-1)\sin(N-1)\theta}{\sin\theta} \tag{3.1.33}$$

which, upon substitution of (3.1.30) for $j = 1$, yields, by L'Hôpital's rule,

$$\begin{aligned} T'_{N-1}(x_{1,N}) &= \lim_{j\to 1}\left(\frac{(N-1)\,\sin(N-j)\pi}{\sin\frac{N-j}{N-1}\pi}\right) \\ &\overset{LH}{=} \lim_{j\to 1}\left(\frac{-(N-1)\,\pi\,\cos(N-j)\pi}{-\frac{\pi}{N-1}\cos\frac{N-j}{N-1}\pi}\right) = (-1)^N\,(N-1)^2. \end{aligned} \tag{3.1.34}$$

Similarly, substitution of (3.1.30) into (3.1.33) for $j = N$ yields, by L'Hôpital's rule,

$$T'_{N-1}(x_{N,N}) = (N-1)^2. \tag{3.1.35}$$

The nodal values of $T''_{N-1}(x)$, which by (3.1.25) is given by

$$T''_{N-1}(x) = \frac{x\,T'_{N-1}(x) - (N-1)^2\,T_{N-1}(x)}{1-x^2}, \tag{3.1.36}$$

must now be found. Substitution of the interior nodes $x_{j,N}$, $j = 2(1)N-1$, into (3.1.36) yields, via (3.1.31) and (3.1.32),

$$T''_{N-1}(x_{j,N}) = \frac{(-1)^{N-j+1}\,(N-1)^2}{1-x_{j,N}^2}, \qquad j = 2(1)N-1. \tag{3.1.37}$$

To evaluate $T''_{N-1}(x)$ at the exterior nodes, $x = -1$ is substituted into (3.1.36) to yield, by L'Hôpital's rule,

$$\begin{aligned} T''_{N-1}(-1) &= \lim_{x\to -1}\left(\frac{x\,T'_{N-1}(x) - (N-1)^2\,T_{N-1}(x)}{1-x^2}\right) \\ &\overset{LH}{=} \lim_{x\to -1}\left(\frac{x\,T''_{N-1}(x) + \left(1-(N-1)^2\right)T'_{N-1}(x)}{-2x}\right) \\ &= \frac{-T''_{N-1}(-1) + \left(1-(N-1)^2\right)T'_{N-1}(-1)}{2} \end{aligned} \tag{3.1.38}$$

which, using (3.1.34), is rearranged to give

$$T''_{N-1}(x_{1,N}) = T''_{N-1}(-1) = \frac{(-1)^N(N-1)^2\left(1-(N-1)^2\right)}{3}. \tag{3.1.39}$$

Similarly, substitution of $x = 1$ into (3.1.36) yields, by L'Hôpital's rule and (3.1.35),

$$T''_{N-1}(x_{N,N}) = T''_{N-1}(1) = \frac{(N-1)^2\left((N-1)^2-1\right)}{3}. \tag{3.1.40}$$

Together, (3.1.3) and (3.1.28)–(3.1.40) provide the explicit entries of the $N \times N$ differentiation matrix based upon the Chebyshev-Gauss-Lobatto distribution as

$$\{\mathbf{D}_N\}_{i,j} = \begin{cases} \dfrac{(-1)^{i+j}(1+\delta_{i1}+\delta_{iN})}{(x_{i,N}-x_{j,N})(1+\delta_{j1}+\delta_{jN})} & i \neq j \\ \dfrac{-x_{j,N}}{2(1-x_{j,N}^2)} & i = j = 2(1)N-1 \\ -\dfrac{2(N-1)^2+1}{6} & i = j = 1 \\ \dfrac{2(N-1)^2+1}{6} & i = j = N, \end{cases} \tag{3.1.41}$$

wherein δ_{ij} is the Kronecker delta defined in (2.3.12); these entries are in agreement with [27, Eq. F.45].

3.1.3 Legendre Nodes

The entries of the differentiation matrix based upon Legendre nodes are now considered. The derivatives of $p_N(x)$ defined by (2.3.15) are substituted into (3.1.6) and (3.1.7) respectively to give

$$L'_{j,N}(x_{i,N}) = \frac{P'_N(x_{i,N})}{(x_{i,N} - x_{j,N})P'_N(x_{j,N})}, \qquad i \neq j, \tag{3.1.42}$$

and

$$L'_{j,N}(x_{j,N}) = \frac{P''_N(x_{j,N})}{2P'_N(x_{j,N})}. \tag{3.1.43}$$

Since $P'_N(x_{j,N})$ cannot be further simplified, only the diagonal entries of the differentiation matrix can be simplified by finding $P''_N(x_{j,N})$. By Legendre's differential equation (2.3.14), the second derivative of the Legendre polynomial is

$$P''_N(x) = \frac{2\,x\,P'_N(x) - N(N+1)\,P_N(x)}{1 - x^2} \tag{3.1.44}$$

which, when evaluated at the nodes $x_{j,N}$, gives

$$P''_N(x_{j,N}) = \frac{2\,x_{j,N}\,P'_N(x_{j,N})}{1 - x_{j,N}^2} \tag{3.1.45}$$

since, by definition (2.3.16), $P_N(x_{j,N}) = 0$. Therefore (3.1.3), (3.1.42), (3.1.43) and (3.1.45) give the entries of the $N \times N$ differentiation matrix based upon the Legendre nodes as

$$\{\mathbf{D}_N\}_{i,j} = \begin{cases} \dfrac{P'_N(x_{i,N})}{(x_{i,N} - x_{j,N})P'_N(x_{j,N})} & i \neq j \\ \dfrac{x_{j,N}}{1 - x_{j,N}^2} & i = j, \end{cases} \tag{3.1.46}$$

as stated in [78, p. 67].

3.1.4 Legendre-Gauss-Radau Nodes

The entries of the differentiation matrix based upon the Left-Gauss-Radau distribution, whose nodes including $x_{1,N} = -1$ are defined in (2.3.21), are considered

first. The entries of the differentiation matrix based upon the Right-Gauss-Radau distribution are then found through the anti-symmetry of the two Gauss-Radau distributions. Let

$$\Psi_{N}(x) = P_{N}(x) + P_{N-1}(x) \tag{3.1.47}$$

so that $p_{N}(x)$ defined by (2.3.18) is given by

$$p_{N}(x) = \frac{2^{N}(N!)^{2}}{(2N)!}\,\Psi_{N}(x). \tag{3.1.48}$$

Substituting the derivatives of (3.1.48) into (3.1.6) and (3.1.7) respectively gives

$$L'_{j,N}(x_{i,N}) = \frac{\Psi'_{N}(x_{i,N})}{(x_{i,N} - x_{j,N})\,\Psi'_{N}(x_{j,N})}, \qquad i \neq j, \tag{3.1.49}$$

and

$$L'_{j,N}(x_{j,N}) = \frac{\Psi''_{N}(x_{j,N})}{2\,\Psi'_{N}(x_{j,N})}, \tag{3.1.50}$$

hence $\Psi'_{N}(x_{j,N})$ and $\Psi''_{N}(x_{j,N})$ are required to simplify the differentiation matrix entries; the former is considered first. Using (2.3.22), $\Psi_{N}(x)$ in (3.1.47) can be written in terms of only $P_{N}(x)$ as

$$\Psi_{N}(x) = (1+x)\,P_{N}(x) - \frac{x^{2}-1}{N}P'_{N}(x) \tag{3.1.51}$$

which is differentiated to give

$$\Psi'_{N}(x) = P_{N}(x) + (1+x)\,P'_{N}(x) - \frac{1}{N}\Big((x^{2}-1)P''_{N}(x) + 2x\,P'_{N}(x)\Big). \tag{3.1.52}$$

By Legendre's differential equation (2.3.14), $\Psi'_{N}(x)$ in (3.1.52) simplifies to

$$\begin{aligned}\Psi'_{N}(x) &= P_{N}(x) + (1+x)\,P'_{N}(x) - \frac{1}{N}\Big(N\,(N+1)\,P_{N}(x)\Big)\\ &= (1+x)\,P'_{N}(x) - N\,P_{N}(x).\end{aligned} \tag{3.1.53}$$

The Legendre polynomial derivative in (3.1.53) can be eliminated by noting that, by (2.3.22),

$$(1+x)\,P'_{N}(x) = \frac{N\,x\,P_{N}(x) - N\,P_{N-1}(x)}{x-1} \tag{3.1.54}$$

hence (3.1.53) becomes

$$\begin{aligned}\Psi'_N(x) &= \frac{N\,x\,P_N(x) - N\,P_{N-1}(x) - N\,(x-1)\,P_N(x)}{x-1} \\ &= \frac{N\left(P_N(x) - P_{N-1}(x)\right)}{x-1},\end{aligned} \tag{3.1.55}$$

which is equivalently

$$\Psi'_N(x) = \frac{N\left(2P_N(x) - \Psi_N(x)\right)}{x-1} \tag{3.1.56}$$

wherein $\Psi_N(x)$ is given by (3.1.47). Since by (3.1.48) $\Psi_N(x_{j,N}) = 0$, (3.1.56) gives

$$\Psi'_N(x_{j,N}) = \frac{2N\,P_N(x_{j,N})}{x_{j,N}-1}, \tag{3.1.57}$$

which for $j = 1$ simplifies to

$$\Psi'_N(x_{1,N}) = (-1)^{N+1}\,N. \tag{3.1.58}$$

To find $\Psi''_N(x_{j,N})$ (3.1.56) is differentiated to give

$$\Psi''_N(x) = \frac{N\left(2P'_N(x) - \Psi'_N(x)\right)}{x-1} - \frac{N\left(2P_N(x) - \Psi_N(x)\right)}{(x-1)^2}. \tag{3.1.59}$$

The second term on the right-hand side of (3.1.59) can be rewritten using (3.1.56) to give

$$\Psi''_N(x) = \frac{N\left(2P'_N(x) - \Psi'_N(x)\right)}{x-1} - \frac{\Psi'_N(x)}{x-1}, \tag{3.1.60}$$

which simplifies to

$$\Psi''_N(x) = \frac{2NP'_N(x) - (N+1)\,\Psi'_N(x)}{x-1}. \tag{3.1.61}$$

Therefore, by (3.1.57), the nodal values of (3.1.61) are given by

$$\Psi''_N(x_{j,N}) = \frac{2N\left((x_{j,N}-1)\,P'_N(x_{j,N}) - (N+1)\,P_N(x_{j,N})\right)}{(x_{j,N}-1)^2}. \tag{3.1.62}$$

Since [27, Eq. A.31]

$$P_N(-1) = (-1)^N \quad \text{and} \quad P'_N(-1) = (-1)^{N+1}\,\frac{N(N+1)}{2}, \tag{3.1.63}$$

when $j = 1$ (3.1.62) readily yields

$$\begin{aligned} \Psi''_N(x_{1,N}) &= \frac{2N\Big((-1)^N N(N+1) - (-1)^N(N+1)\Big)}{4} \\ &= \frac{(-1)^N N(N+1)(N-1)}{2}. \end{aligned} \tag{3.1.64}$$

When $j = 2(1)N$ (2.3.21) gives

$$(x_{j,N} - 1)\, P'_N(x_{j,N}) - N\, P_N(x_{j,N}) = 0, \tag{3.1.65}$$

which when substituted into (3.1.62) yields

$$\Psi''_N(x_{j,N}) = -\frac{2N\, P_N(x_{j,N})}{(x_{j,N} - 1)^2}. \tag{3.1.66}$$

By (3.1.3), and (3.1.49)–(3.1.66), the entries of the $N \times N$ differentiation matrix based upon the Left-Gauss-Radau distribution are therefore

$$\{\mathbf{D}_N\}_{i,j} = \begin{cases} \dfrac{(x_{j,N} - 1)\, P_N(x_{i,N})}{(x_{i,N} - x_{j,N})\,(x_{i,N} - 1)\, P_N(x_{j,N})} & i \neq j \\ -\dfrac{(N-1)(N+1)}{4} & i = j = 1 \\ \dfrac{1}{2\,(1 - x_{j,N})} & i = j \neq 1 \\ \dfrac{(-1)^N (x_{j,N} - 1)}{2\,(x_{j,N} + 1)\, P_N(x_{j,N})} & i = 1, j \neq 1 \\ \dfrac{2\,(-1)^N P_N(x_{i,N})}{1 - x_{i,N}^2} & j = 1, i \neq 1, \end{cases} \tag{3.1.67}$$

the last two of which are simplified specific forms of $i \neq j$ entries, and the first three of which are in agreement with the entries given by [78, p. 67], since by (2.3.18)

$$P_N(x_{j,N}) = -P_{N-1}(x_{j,N}). \tag{3.1.68}$$

Since the LGR and RGR distributions are reflections of each other about the y-axis their monic polynomials satisfy

$$p_N^{-(r)}(x) = (-1)^{N+r}\, p_N^{+(r)}(-x), \qquad r \geq 0, \tag{3.1.69}$$

wherein a '$-$' superscript refers to the LGR distribution and a '$+$' superscript refers to the RGR distribution and in which a bracketed superscript $r \in \mathbb{N}$ denotes the rth derivative of a function, with $r = 0$ corresponding to the original, non-differentiated function. Furthermore, the Gauss-Radau nodes satisfy

$$x^{-}_{j,N} = -x^{+}_{N+1-j,N}. \tag{3.1.70}$$

Substitution of (3.1.69) into (3.1.6) yields

$$\begin{aligned} L^{-'}_{j,N}(x^{-}_{i,N}) &= \frac{p_N^{-'}(x^{-}_{i,N})}{(x^{-}_{i,N} - x^{-}_{j,N})\, p_N^{-'}(x^{-}_{j,N})} \\ &= \frac{-p_N^{+'}(x^{+}_{N+1-i,N})}{(x^{+}_{N+1-i,N} - x^{+}_{N+1-j,N})\, p_N^{+'}(x^{+}_{N+1-j,N})} \\ &= -L^{+'}_{N+1-j,N}(x^{+}_{N+1-i,N}), \qquad i \neq j, \end{aligned} \tag{3.1.71}$$

and substitution of (3.1.69) into (3.1.7) yields

$$\begin{aligned} L^{-'}_{j,N}(x^{-}_{j,N}) &= \frac{p_N^{-''}(x^{-}_{j,N})}{2\, p_N^{-'}(x^{-}_{j,N})} \\ &= \frac{p_N^{+''}(x^{+}_{N+1-j,N})}{-2\, p_N^{+'}(x^{+}_{N+1-j,N})} \\ &= -L^{+'}_{N+1-j,N}(x^{+}_{N+1-j,N}). \end{aligned} \tag{3.1.72}$$

Therefore, by (3.1.71) and (3.1.72), the LGR and RGR differentiation matrices satisfy the relationship

$$\{\mathbf{D}^{-}_{N}\}_{i,j} = -\{\mathbf{D}^{+}_{N}\}_{N+1-i,\, N+1-j}. \tag{3.1.73}$$

By the anti-symmetry arguments (3.1.69)–(3.1.73) applied to the analysis leading up to (3.1.67), the entries of the $N \times N$ differentiation matrix based upon the Right-

Gauss-Radau distribution are

$$\{\mathbf{D}_N\}_{i,j} = \begin{cases} \dfrac{(x_{j,N}+1)\,P_N(x_{i,N})}{(x_{i,N}-x_{j,N})\,(x_{i,N}+1)\,P_N(x_{j,N})} & i \neq j \\ \dfrac{(N-1)(N+1)}{4} & i = j = N \\ -\dfrac{1}{2\,(1+x_{j,N})} & i = j \neq N \\ \dfrac{1+x_{j,N}}{2\,(1-x_{j,N})\,P_N(x_{j,N})} & i = N, j \neq N \\ \dfrac{2\,P_N(x_{i,N})}{x_{i,N}^2-1} & j = N, i \neq N, \end{cases} \tag{3.1.74}$$

the last two of which are again simplified specific forms of $i \neq j$ entries.

3.1.5 Legendre-Gauss-Lobatto Nodes

To evaluate the entries of the differentiation matrix based upon the Legendre-Gauss-Lobatto nodes, the derivatives of $p_N(x)$ defined by (2.3.26), the first of which is given by (2.4.63), are substituted into (3.1.6) and (3.1.7) respectively to give

$$L'_{j,N}(x_{i,N}) = \frac{P_{N-1}(x_{i,N})}{(x_{i,N}-x_{j,N})P_{N-1}(x_{j,N})}, \qquad i \neq j, \tag{3.1.75}$$

and

$$L'_{j,N}(x_{j,N}) = \frac{P'_{N-1}(x_{j,N})}{2\,P_{N-1}(x_{j,N})}. \tag{3.1.76}$$

To simplify the differentiation-matrix entries, the values of $P_{N-1}(x_{j,N})$ and $P'_{N-1}(x_{j,N})$ are therefore required; the former of which can only be simplified for $j = 1$ and $j = N$. Trivially, [27, Eq. A.31] gives

$$(-1)^N\,P_{N-1}(x_{1,N}) = P_{N-1}(x_{N,N}) = 1, \tag{3.1.77}$$

and so it remains to find $P'_{N-1}(x_{j,N})$. By their definition (2.3.27), the interior nodes, $x_{j,N}$ with $j = 2(1)N-1$, yield the property

$$P'_{N-1}(x_{j,N}) = 0, \qquad j = 2(1)N-1 \tag{3.1.78}$$

and, by definition [27, Eq. A.31], the exterior nodes $x_{1,N} = -1$ and $x_{N,N} = 1$ yield

$$(-1)^{N+1} P'_N(x_{1,N}) = P'_N(x_{N,N}) = \frac{N(N+1)}{2}. \tag{3.1.79}$$

Therefore, (3.1.3) and (3.1.75)–(3.1.79) give the entries of the $N \times N$ differentiation matrix based upon the Legendre-Gauss-Lobatto distribution as

$$\{\mathbf{D}_N\}_{i,j} = \begin{cases} \dfrac{P_{N-1}(x_{i,N})}{(x_{i,N} - x_{j,N})P_{N-1}(x_{j,N})} & i \neq j \\ \dfrac{(1-N)N}{4} & i = j = 1 \\ 0 & i = j = 2(1)N-1 \\ \dfrac{(N-1)N}{4} & i = j = N, \\ \dfrac{(-1)^N}{2} & i = 1,\ j = N \\ \dfrac{(-1)^{N-1}}{2} & i = N,\ j = 1 \\ \dfrac{(-1)^N}{(1+x_{j,N})P_{N-1}(x_{j,N})} & i = 1,\ j \neq 1 \\ \dfrac{1}{(1-x_{j,N})P_{N-1}(x_{j,N})} & i = N,\ j \neq N \\ \dfrac{(-1)^{N-1}P_{N-1}(x_{i,N})}{(x_{i,N}+1)} & j = 1,\ i \neq 1 \\ \dfrac{P_{N-1}(x_{i,N})}{(x_{i,N}-1)} & j = N,\ i \neq N, \end{cases} \tag{3.1.80}$$

the first four of which are given in [27, Eq. F.55] and the last six of which are simplified specific forms of $i \neq j$ entries.

3.1.6 Differentiation-Matrix Properties

The previous sections have shown how differentiation matrices are structured. Properties of differentiation matrices are now examined in order to facilitate the ex-

planation of errors when differentiation matrices are incorporated into numerical methods for integro-differential equations. First, a property is considered for differentiation matrices based upon nodal distributions that are symmetrically distributed about the origin; these include the above-considered Chebyshev, Chebyshev-Gauss-Lobatto, Legendre and Legendre-Gauss-Lobatto distributions, whose nodes all satisfy

$$x_{i,N} = -x_{N+1-i,N}. \tag{3.1.81}$$

The monic polynomials $p_N(x)$, defined in (2.1.3), are therefore odd functions of x if N is odd and even functions of x if N is even and so

$$p_N^{(r)}(x_{i,N}) = (-1)^{N+r}\, p_N^{(r)}(x_{N+1-i,N}), \qquad r \geq 0, \tag{3.1.82}$$

wherein a bracketed superscript $r \in \mathbb{N}$ denotes the rth derivative of a function, with $r = 0$ corresponding to the original, non-differentiated function. By (3.1.3), (3.1.6), (3.1.81) and (3.1.82) the non-diagonal entries of $\mathbf{D}_N$ satisfy

$$\begin{aligned} \{\mathbf{D}_N\}_{i,j} &= \frac{p'_N(x_{i,N})}{(x_{i,N} - x_{j,N})p'_N(x_{j,N})} = \frac{p'_N(x_{N+1-i,N})}{-(x_{N+1-i,N} - x_{N+1-j,N})p'_N(x_{N+1-j,N})} \\ &= -\{\mathbf{D}_N\}_{N+1-i,\,N+1-j}, \qquad i \neq j, \end{aligned} \tag{3.1.83}$$

and, by (3.1.3), (3.1.7) and (3.1.82), the diagonal entries satisfy

$$\{\mathbf{D}_N\}_{j,j} = \frac{p''_N(x_{j,N})}{2p'_N(x_{j,N})} = -\frac{p''_N(x_{N+1-j,N})}{p'_N(x_{N+1-j,N})} = -\{\mathbf{D}_N\}_{N+1-j,\,N+1-j}, \tag{3.1.84}$$

and so combining (3.1.83) and (3.1.84) gives

$$\{\mathbf{D}_N\}_{i,j} = -\{\mathbf{D}_N\}_{N+1-i,\,N+1-j}. \tag{3.1.85}$$

The next property to note is that, for all differentiation matrices,

$$\sum_{j=1}^{N} \{\mathbf{D}_N\}_{i,j} = 0, \tag{3.1.86}$$

which follows from approximating the constant function $\widetilde{u}(x) \equiv 1$ by Lagrange interpolation (2.1.1). In this case $\widetilde{u}(x_{j,N}) = 1$ for all $j = 1(1)N$, whence (2.1.1) becomes

$$(\mathcal{L}_N \widetilde{u})(x) = \sum_{j=1}^{N} L_{j,N}(x). \tag{3.1.87}$$

As $\widetilde{u}^{(N)}(x) = 0$ for $N \geq 1$, the Lagrange interpolation error formula (2.4.1) gives

$$\widetilde{u}(x) - \mathcal{L}_N \widetilde{u}(x) = 0 \tag{3.1.88}$$

so that

$$\sum_{j=1}^{N} L_{j,N}(x) = 1. \tag{3.1.89}$$

Differentiating (3.1.89) then gives

$$\sum_{j=1}^{N} L'_{j,N}(x) = 0, \tag{3.1.90}$$

which is equivalent to (3.1.86) when $x = x_{i,N}$.

3.1.7 Eigenvalue Analysis

It is well-known [18, 29, 46] that differentiation matrices are ill-conditioned. This is illustrated by Figure 3.1.1 in which the Chebyshev-Gauss-Lobatto differentiation matrices $\mathbf{D}_{15}$, $\mathbf{D}_{15}^2$, $\mathbf{D}_{20}$ and $\mathbf{D}_{20}^2$ are plotted. The behaviour exhibited by the differentiation matrices in Figure 3.1.1 portends ill-conditioning and so it is clear that the second-order differentiation matrices are more ill-conditioned than the first-order differentiation matrices. Comparison of the vertical scales in Figure 3.1.1 demonstrates that both $\mathbf{D}_N$ and $\mathbf{D}_N^2$ become more ill-conditioned as N increases. In particular it is the moduli $|\{\mathbf{D}_N\}_{1,2}| = |\{\mathbf{D}_N\}_{N,N-1}|$ and $|\{\mathbf{D}_N^2\}_{1,2}| = |\{\mathbf{D}_N^2\}_{N,N-1}|$ that are the greatest, the former of which can be evaluated from (3.1.41) as

$$\{\mathbf{D}_N\}_{1,2} = \frac{2}{1 - \cos\frac{\pi}{N-1}} = O(N^2). \tag{3.1.91}$$

Similarly, it is clear from (3.1.41) that $|\{\mathbf{D}_N\}_{1,1}| = |\{\mathbf{D}_N\}_{N,N}| = O(N^2)$ and hence, in general, the largest entries of $\mathbf{D}_N^M$ are $O(N^{2M})$. This behaviour is qualitatively similar for differentiation matrices based upon the other nodal distributions discussed.

The eigenvalues of a differentiation matrix can be analysed in order to quantify its ill-conditioning. A detailed analysis of the eigenvalues of differentiation matrices with and without the imposition of a boundary condition is performed in [126], in the former of which $\mathbf{D}_N$ is reduced to an $N-1 \times N-1$ matrix by removing the row and column that correspond to the location of the boundary condition, i.e. for

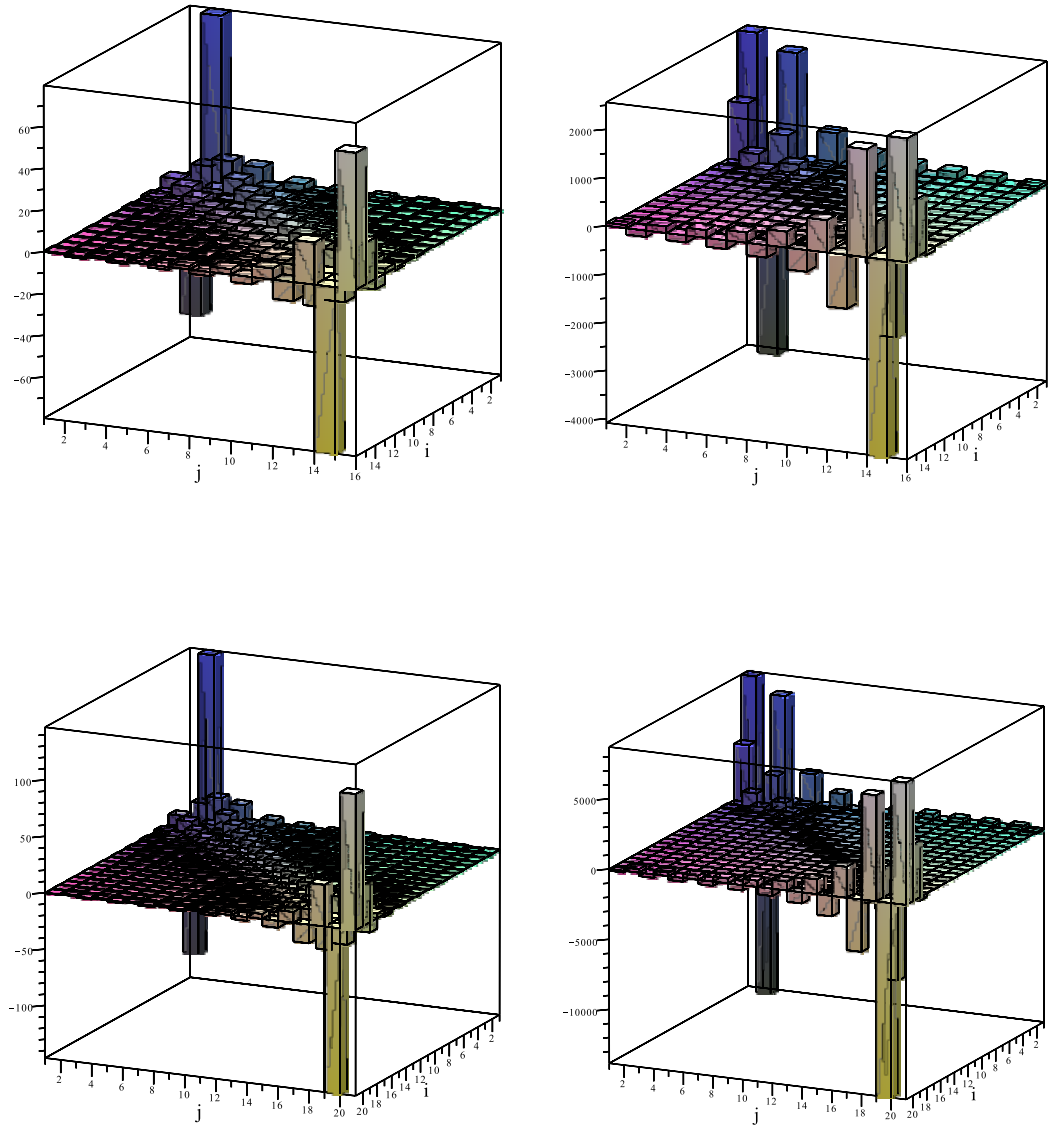

Figure 3.1.1: Plots of the Chebyshev-Gauss-Lobatto differentiation matrices $\mathbf{D}_{15}$ (top left), $\mathbf{D}_{15}^2$ (top right), $\mathbf{D}_{20}$ (bottom left) and $\mathbf{D}_{20}^2$ (bottom right).

a boundary condition given at point $x_{j,N}$ the jth row and jth column of $\mathbf{D}_N$ are removed. It is shown in [126] that the differentiation matrix $\mathbf{D}_N$, in the absence of boundary conditions, is nilpotent whence all eigenvalues of $\mathbf{D}_N$ are zero. This can be shown by considering the matrix-vector equation (3.1.11). As stated below (2.2.6),

$\mathcal{D}_N^{(M)} u \equiv 0$ when $M \geq N$, therefore setting $M = N$ in (3.1.11) gives, for arbitrary $\mathbf{u}$,

$$\mathbf{0} = \mathbf{D}_N^N \mathbf{u} \tag{3.1.92}$$

and so

$$\mathbf{D}_N^N = \mathbf{0}, \tag{3.1.93}$$

in which $\mathbf{0}$ denotes the zero vector in (3.1.92) and the zero matrix in (3.1.93). By (3.1.93), $\mathbf{D}_N$ is nilpotent and so its eigenvalues are all zero: equivalently, its characteristic polynomial is

$$\lambda^N = 0. \tag{3.1.94}$$

However, due to rounding errors, the computed characteristic polynomial (3.1.94) is in practice augmented by lower-order terms whose coefficients are the order of the machine precision: that is, the computed eigenvalues of $\mathbf{D}_N$ are not all identically zero. Instead, the eigenvalues lie on a circle centered at the origin in the complex eigenvalue plane. This is a similar effect to that seen for the ill-conditioned 20th-order *Wilkinson polynomial* [20] whose roots are perturbed by $O(1)$ when the coefficient of the x^{19} term is perturbed by 10^{-9}. Here, the displacement from the origin of the computed eigenvalues is dependent upon the value of N and also the machine precision. This is illustrated in Figures 3.1.2–3.1.4, in which plots of the eigenvalues are shown for differentiation matrices with $N = 15$ and $N = 20$, both of which are evaluated for machine precisions set at both 20 and 40 digits.

Figures 3.1.2–3.1.4 show, *cf.* [126], that the computed eigenvalues lie on a circle about the origin due to rounding errors of the machine, hence the differentiation matrices are ill-conditioned rather than singular. Furthermore, the figures demonstrate that the computed eigenvalues are most accurate when N is low and when a high number of digits are used in computations. This is quantified in [126], which states that, when the lower-order coefficients of the characteristic polynomial are perturbed by ϵ, the computed eigenvalues move distances of order $\epsilon^{1/N}$. Therefore, since the coefficients of the lower-order terms are the order of machine precision, i.e. $O(\epsilon)$, a high number of digits used in computations yields a smaller perturbation to the eigenvalues, as does a low value of N.

It is noted [29] that, although exact formulae *cf.* (3.1.8) are used to compute a differentiation matrix, its entries $\{\mathbf{D}_N\}_{1,2}$ and $\{\mathbf{D}_N\}_{N,N-1}$ are computed with an

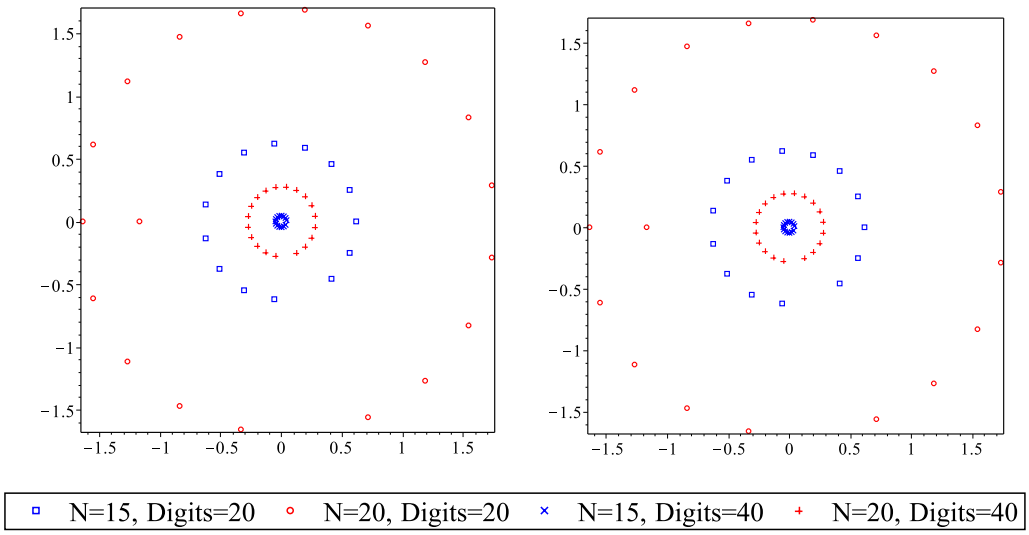

Figure 3.1.2: Computed eigenvalues of differentiation matrices based upon the Chebyshev nodes (left) and the Chebyshev-Gauss-Lobatto nodes (right) are plotted in the complex eigenvalue plane. Theoretically all eigenvalues should lie at zero, and so the plots show that the accuracy of the computed eigenvalues decreases with increasing N and with decreasing machine precision.

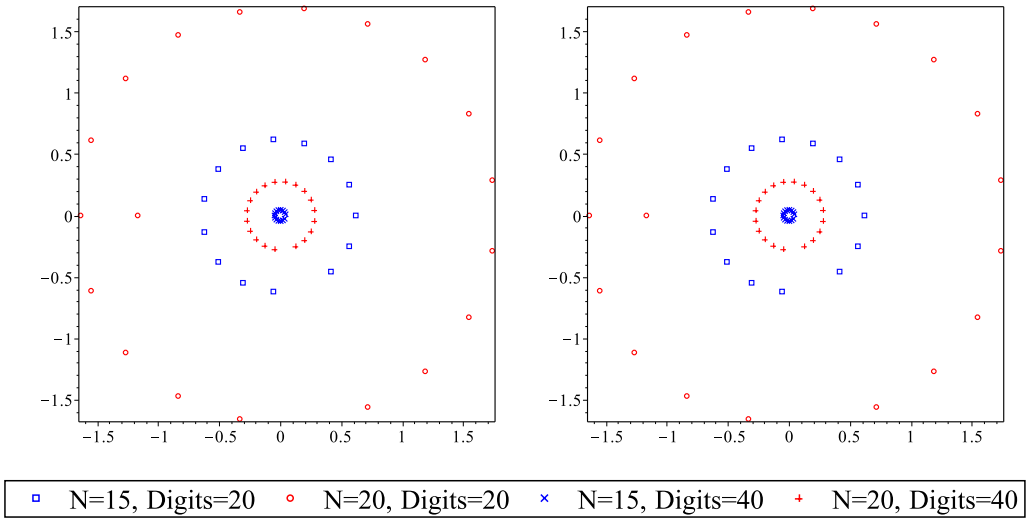

Figure 3.1.3: As for Figure 3.1.2 for matrices based upon the Legendre nodes (left) and Legendre-Gauss-Lobatto nodes (right).

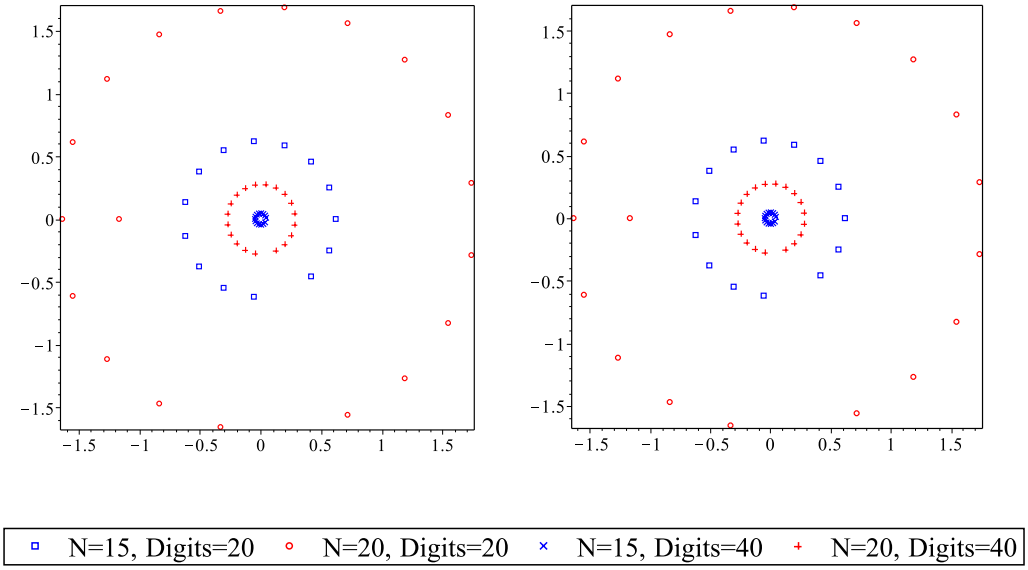

Figure 3.1.4: As for Figure 3.1.2 for matrices based upon the Left-Gauss-Radau nodes (left) and Right-Gauss-Radau nodes (right).

$O(N^4\epsilon)$ error due to the difference $x_{i,N} - x_{j,N}$ in the denominator of the non-diagonal entries; this is a result of the roundoff error ϵ in the computed nodes and the $O(N^{-2})$ nodal spacing near the boundaries of $[-1, 1]$ [116] for the orthogonal polynomials whose nodes are distributed with density (2.3.35). For a second-order differentiation matrix the error in $\{\mathbf{D}_N^2\}_{1,2}$ and $\{\mathbf{D}_N^2\}_{N,N-1}$ increases to $O(N^6\epsilon)$ [29]. Several methods have been considered to overcome the loss of accuracy incurred by the error in the differentiation-matrix entries. In [29] a preconditioning technique is employed so that the function that the differentiation matrix is acting upon vanishes at the boundaries, hence the error in the differentiation matrix is suppressed. In order to avoid the errors within the differentiation matrix itself, when the nodal distribution is either Chebyshev or Chebyshev-Gauss-Lobatto, trigonometric identities can be used [15, 46, 47] to decrease the error incurred when subtracting two numbers that are very close together. Specifically, the identities

$$x_{i,N} - x_{j,N} = \cos\theta_{i,N} - \cos\theta_{j,N} = -2\sin\left(\frac{\theta_{i,N} + \theta_{i,N}}{2}\right)\sin\left(\frac{\theta_{i,N} - \theta_{i,N}}{2}\right) \tag{3.1.95}$$

and

$$1 - x_{j,N}^2 = 1 - \cos^2\theta_{j,N} = \sin^2\theta_{j,N}, \tag{3.1.96}$$

in which the nodes are either Chebyshev (3.1.19) or Chebyshev-Gauss-Lobatto (3.1.30), can be used to alleviate the above-mentioned $O(N^4\epsilon)$ error incurred through computing the reciprocals of $x_{i,N} - x_{j,N}$ and $1 - x_{j,N}^2$. Using (3.1.95) and (3.1.96), the Chebyshev differentiation matrix (3.1.27) is rewritten as

$$\{\mathbf{D}_N\}_{i,j} = \begin{cases} \dfrac{(-1)^{i+j+1}\,\sin\left(\dfrac{2N-2j+1}{2N}\pi\right)}{2\sin\left(\dfrac{2N-i-j+1}{2N}\pi\right)\sin\left(\dfrac{j-i}{2N}\pi\right)\sin\left(\dfrac{2N-2i+1}{2N}\pi\right)} & i \neq j \\ \dfrac{\cos\left(\dfrac{2N-2j+1}{2N}\pi\right)}{2\,\sin^2\left(\dfrac{2N-2j+1}{2N}\pi\right)} & i = j, \end{cases} \tag{3.1.97}$$

and the Chebyshev-Gauss-Lobatto differentiation matrix (3.1.41) is rewritten as

$$\{\mathbf{D}_N\}_{i,j} = \begin{cases} \dfrac{(-1)^{i+j+1}(1+\delta_{i1}+\delta_{iN})}{2\,(1+\delta_{j1}+\delta_{jN})\,\sin\left(\dfrac{2N-i-j}{2(N-1)}\pi\right)\sin\left(\dfrac{j-i}{2(N-1)}\pi\right)} & i \neq j \\ \dfrac{-\cos\left(\dfrac{N-j}{N-1}\pi\right)}{2\,\sin^2\left(\dfrac{N-j}{N-1}\pi\right)} & i = j = 2(1)N-1 \\ -\dfrac{2(N-1)^2+1}{6} & i = j = 1 \\ \dfrac{2(N-1)^2+1}{6} & i = j = N. \end{cases} \tag{3.1.98}$$

For any differentiation matrix, if the ratio $p'_N(x_{i,N})/p'_N(x_{j,N})$ cannot be simplified within the non-diagonal terms of (3.1.8) e.g. as in the Legendre (3.1.46), Legendre-Gauss-Radau (3.1.67), (3.1.74) and Legendre-Gauss-Lobatto (3.1.80) matrices, it accumulates error due to the product of terms given by (2.1.5) and (2.1.7); to reduce this build up of roundoff error the ratio can be computed as [37]

$$\frac{p'_N(x_{i,N})}{p'_N(x_{j,N})} = (-1)^{i+j}\mathrm{e}^{b_i-b_j} \quad \text{wherein} \quad b_i = \sum_{\substack{k=1\\k\neq i}}^{N} \ln|x_{i,N} - x_{k,N}|. \tag{3.1.99}$$

To reduce the roundoff errors for higher values of N, a method is presented in [18, 15, 37] for preserving property (3.1.86) by computing diagonal entries using

$$\{\mathbf{D}_N\}_{i,i} = -\sum_{\substack{j=1 \\ j\neq i}}^{N} \{\mathbf{D}_N\}_{i,j}, \tag{3.1.100}$$

which clearly enforces the property in (3.1.86). Furthermore, this technique can be extended to higher powers of $\mathbf{D}_N$ since differentiation of (3.1.90), and comparison with (3.1.13), yields

$$\sum_{j=1}^{N} \{\mathbf{D}_N^M\}_{i,j} = 0. \tag{3.1.101}$$

A similar technique can also be used to replace the entry that has the largest magnitude in a row of $\mathbf{D}_N$, however this is found to have no significant improvement on (3.1.100) [18]. It has also been found [46] that the error in matrix entries corresponding to nodes near $x = -1$ is larger than that in entries corresponding to nodes near $x = 1$. To overcome this, the anti-symmetry relation (3.1.85) can be used so that the more accurate bottom half of the differentiation matrix (3.1.3) can be used to populate the less accurate top half [16, 46] using

$$\{\mathbf{D}_N\}_{i,j} = -\{\mathbf{D}_N\}_{N+1-i,\,N+1-j}, \qquad i = 1(1)\frac{N}{2}. \tag{3.1.102}$$

This method can be extended to higher powers of $\mathbf{D}_N$ since, for symmetrically distributed nodal sets, one finds [37]

$$\{\mathbf{D}_N^M\}_{i,j} = (-1)^M \{\mathbf{D}_N^M\}_{N+1-i,\,N+1-j}, \qquad M \geq 1. \tag{3.1.103}$$

Other techniques for improving the accuracy of differentiation matrices include an *even-odd decomposition algorithm* [37, 46, 115], which exploits the anti-symmetry (3.1.85) of $\mathbf{D}_N$; a recursive formula for computing higher-order differentiation matrices [37, 132] utilizing barycentric representations *cf.* (2.1.13) [15, 16]; pre-conditioning schemes [39, 40]; a coordinate transformation [47, 82]; and, in [48], the accuracy of higher-order Chebyshev-Gauss-Lobatto differentiation matrices is improved by using the periodic properties of the cosine function. Figure 3.1.5 shows a comparison of the eigenvalues of Chebyshev and Chebyshev-Gauss-Lobatto differentiation matrices computed using the original formulae (3.1.27) and (3.1.41), the trigonometric

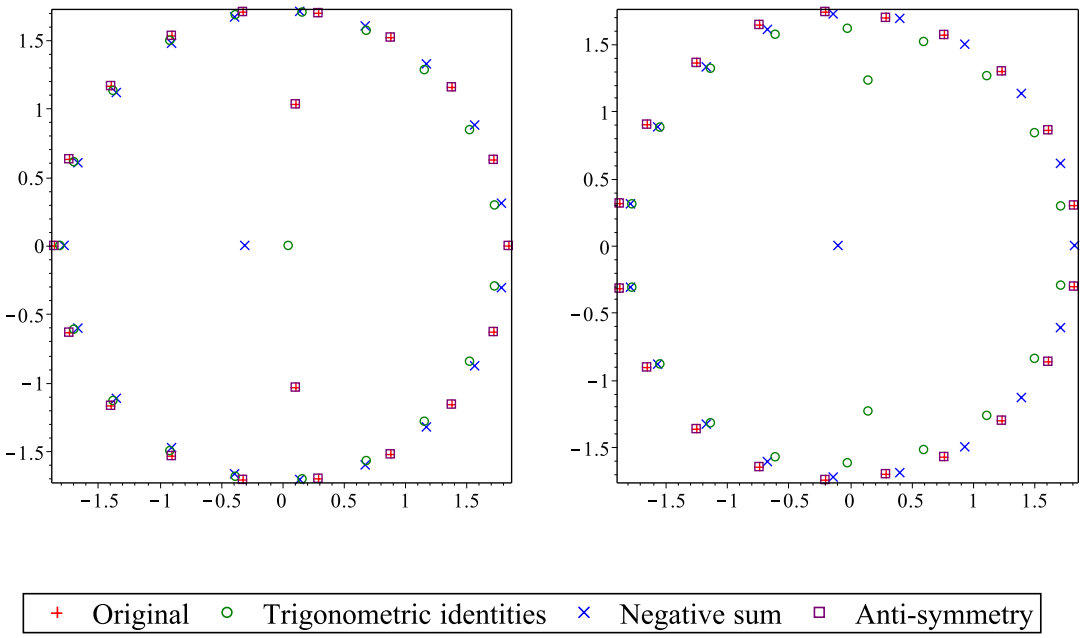

Figure 3.1.5: Eigenvalues of Chebyshev (left) and Chebyshev-Gauss-Lobatto (right) differentiation matrices, computed using the original formulae (3.1.27) and (3.1.41), are compared to the eigenvalues of the altered differentiation matrices, computed using the trigonometric identities (3.1.97) and (3.1.98), the negative-sum for the diagonal entries (3.1.100), and the anti-symmetry relation (3.1.102). Eigenvalues are computed with $N = 20$ and 20 digits.

identities (3.1.97) and (3.1.98), the negative-sum for the diagonal entries (3.1.100), and the anti-symmetry relation (3.1.102).

Figure 3.1.5 reveals that there is a negligible effect on the eigenvalues when the anti-symmetry relation is used, however using either the trigonometric identities or the negative-sum technique moves the eigenvalues so that they lie on a circle whose radius is slightly smaller than that of the eigenvalues computed using the original differentiation-matrix formulae (3.1.27) and (3.1.41). Therefore, the differentiation matrices computed using the trigonometric identities and the negative-sum technique are better representations of the theoretical differentiation matrix whose eigenvalues are all zero, and hence these yield the most accurate differentiation errors for a given N.

Although the eigenvalue analysis in this section has highlighted that the differen-

tiation matrix $\mathbf{D}_N$ is singular, and so theoretically not invertible, this is not so [126] when the differentiation matrix is amended to include a boundary condition; this is done by effectively replacing one row and one column of $\mathbf{D}_N$, yielding a matrix that has non-zero eigenvalues and so is invertible. It is an analogy of this procedure that is used in Chapter 5 to circumvent the presence of the unbounded differential operator $\mathcal{D}$, defined in (2.2.1), in the error analysis for integro-differential equation (IDE) methods. Furthermore, the simplified differentiation matrices introduced in this section will, for all nodal distributions, significantly reduce the computational workload required when implementing differentiation matrices into numerical methods for IDEs in Chapter 5. Now that the framework for spectrally accurate numerical differentiation has been established, it remains to consider a spectrally accurate method for the numerical quadrature required in Chapters 4 and 5.

3.2 Gaussian Quadrature

There are many well-known numerical methods for computing a definite integral; the trapezoidal rule [134], Simpson's rule [14], Boole's rule [2], Clenshaw-Curtis quadrature [35], and Gaussian quadrature [9], the last two of which are generally the most accurate. For this reason, Gaussian quadrature is commonly used in the Nyström method [98, 10], which is introduced in Chapter 4 and developed in Chapter 5. Accordingly, this section introduces the fundamentals of Gaussian quadrature.

An M-point Gaussian quadrature rule on the interval $[-1, 1]$ is defined by [68, Eq. 8.4.6]

$$\int_{-1}^{1} \omega(x) f(x) dx = \sum_{j=1}^{M} w_{j,M} f(y_{j,M}) + E_M \tag{3.2.1}$$

for a suitable set of quadrature abscissae $y_{j,M} \in [-1, 1]$ and corresponding weights $w_{j,M}$ computed as [68, Eq. 8.4.8]

$$w_{j,M} = \int_{-1}^{1} \omega(x)\, L_{j,M}(x)\, dx, \tag{3.2.2}$$

in which the functions $L_{j,M}(x)$ are the Lagrange basis functions (2.1.8) computed using the nodes $y_{j,M}$. The error E_M is given by [68, Eq. 8.4.7]

$$E_M = \frac{f^{(2M)}(\xi)}{(2M)!} \int_{-1}^{1} \omega(x) \Big(p_M(x)\Big)^2 dx, \tag{3.2.3}$$

in which $\xi \in (-1,1)$ is an unknown constant and $p_M(x)$ is the monic polynomial (2.1.3) with roots at nodes $y_{j,M}$. Since ξ in (3.2.3) is unknown, in practice $f^{(2M)}(\xi)$ must be replaced by $\left\|f^{(2M)}\right\|$ in order to bound E_M. Although the quadrature rule (3.2.1) and (3.2.2) can be obtained by integrating the Lagrange interpolation formula (2.1.1), the error term E_M in (3.2.3) does not result from integrating the Lagrange interpolation error (2.4.1). This is because Gaussian quadrature is derived from integrating a *Hermite interpolation formula* [105] with the necessary condition that $p_M(x)$ is orthogonal to all polynomials of inferior degree over $[-1,1]$, relative to $\omega(x)$ [68, p. 388].

Gaussian quadrature has a degree of precision $2M-1$ when M nodes are used, this degree being reduced by one [68, p. 402] for each arbitrarily prescribed abscissa; that is, if there are ν arbitrarily prescribed nodes, the degree of precision is $2M-1-\nu$. Since an IDE is augmented by a boundary condition, a nodal distribution that contains a prescribed node at an interval endpoint simplifies the implementation of that boundary condition within the numerical methods in Chapter 5. Therefore, in view of the ultimate goal of solving IDEs, three types of Gaussian quadrature are considered which can be used when the weight function $\omega(x)$ equals 1 and in which the nodes include ν endpoints. Specifically $\nu = 0, 1, 2$ respectively correspond to the Gauss-Legendre, Legendre-Gauss-Radau and Legendre-Gauss-Lobatto distributions defined in Section 2.3; the following subsections present the nodes, weights and error functions that are required to implement Gaussian quadrature on these node sets.

3.2.1 Gauss-Legendre Quadrature

Gauss-Legendre quadrature uses abscissae $y_{j,M}$ at the Legendre nodes (2.3.16) so that

$$P_M(y_{j,M}) = 0. \tag{3.2.4}$$

Standard theory on orthogonal polynomials [105] determines the weights $w_{j,M}$ in (3.2.2) as

$$w_{j,M} = \frac{-2}{(M+1)P'_M(y_{j,M})P_{M+1}(y_{j,M})}, \tag{3.2.5}$$

and the error term (3.2.3) as

$$E_M = \frac{2^{2M+1}\,(M!)^4}{(2M+1)\,((2M)!)^3}\,f^{(2M)}(\xi), \qquad -1 < \xi < 1. \tag{3.2.6}$$

That is, Gauss-Legendre quadrature integrates $f(x)$ exactly on $[-1,1]$ if $f(x)$ is a polynomial in x of degree less than or equal to $2M-1$, since on the Gauss-Legendre nodes $\nu = 0$ are arbitrarily prescribed.

3.2.2 Legendre-Gauss-Radau Quadrature

Quadrature based upon the Left-Gauss-Radau nodes defined in (2.3.21) uses abscissae given by

$$y_{j,M} = \begin{cases} -1 & j = 1 \\ (j-1)\text{st zero of } P_{M-1}(x) + \frac{x-1}{M} P'_{M-1}(x) & j = 2(1)M \end{cases} \tag{3.2.7}$$

and weights $w_{j,M}$ in (3.2.2) given by [68, p. 407–408]

$$w_{j,M} = \begin{cases} \dfrac{2}{M^2} & j = 1 \\ \dfrac{1 - y_{j,M}}{M^2 \left(P_{M-1}(y_{j,M})\right)^2} & j = 2(1)M. \end{cases} \tag{3.2.8}$$

Quadrature based upon the Right-Gauss-Radau nodal distribution has nodes $\widetilde{y}_{j,M} = -y_{M+1-j,M}$ and weights $\widetilde{w}_{j,M} = w_{M+1-j,M}$ in which $y_{j,M}$ and $w_{j,M}$ are given by (3.2.7) and (3.2.8). The error term E_M in (3.2.3) for Legendre-Gauss-Radau quadrature is the same for both the LGR and RGR distributions and is given [68, Eq. 8.11.15] as

$$E_M = \frac{2^{2M-1}\, M\, ((M-1)!)^4}{((2M-1)!)^3} f^{(2M-1)}(\xi), \qquad -1 < \xi < 1. \tag{3.2.9}$$

Since on the Legendre-Gauss-Radau nodes $\nu = 1$ are arbitrarily prescribed, M-node Legendre-Gauss-Radau quadrature integrates $f(x)$ on $[-1,1]$ exactly if $f(x)$ is a polynomial in x of degree less than or equal to $2M-2$.

3.2.3 Legendre-Gauss-Lobatto Quadrature

Quadrature based upon the Legendre-Gauss-Lobatto nodes defined in (2.3.27) uses abscissae

$$y_{j,M} = \begin{cases} -1 & j = 1 \\ 1 & j = M \\ (j-1)\text{st zero of } P'_{M-1}(x) & j = 2(1)M-1 \end{cases} \tag{3.2.10}$$

and weights $w_{j,M}$ in (3.2.2) given [68, Eqns. 8.12.7–8.12.8] by

$$w_{j,M} = \begin{cases} \dfrac{2}{M(M-1)} & j = 1, M \\ \dfrac{2}{M(M-1)\big(P_{M-1}(y_{j,M})\big)^2} & j = 2(1)M-1. \end{cases} \tag{3.2.11}$$

The error term E_M in (3.2.3) for Legendre-Gauss-Lobatto quadrature is given [68, Eq. 8.12.9] as

$$E_M = -\frac{2^{2M-1}\, M\, (M-1)^3\, ((M-2)!)^4}{(2M-1)\, ((2M-2)!)^3}\, f^{(2M-2)}(\xi), \qquad -1 < \xi < 1, \tag{3.2.12}$$

so that if $f(x)$ is a polynomial in x of degree less than or equal to $2M-3$, M-node Legendre-Gauss-Lobatto quadrature integrates $f(x)$ on $[-1,1]$ exactly, since on the Legendre-Gauss-Lobatto nodes $\nu = 2$ are arbitrarily prescribed.

3.2.4 Quadrature Error Bounds

The error terms E_M (3.2.6), (3.2.9) and (3.2.12) can be written in the general form

$$E_M = (-1)^{\nu(\nu-1)/2}\, \psi_M^{(\nu)}\, f^{(2M-\nu)}(\xi), \qquad -1 < \xi < 1, \tag{3.2.13}$$

in which $\nu = 0, 1, 2$ correspond to Gauss-Legendre, Legendre-Gauss-Radau and Legendre-Gauss-Lobatto quadrature respectively and the error factors $\psi_M^{(\nu)}$ are found from simplifying (3.2.6), (3.2.9) and (3.2.12) to be

$$\psi_M^{(0)} = \frac{2^{2M+1}\, (M!)^4}{(2M+1)\, ((2M)!)^3}, \tag{3.2.14}$$

$$\psi_M^{(1)} = \frac{2^{2M+2}(M!)^4}{((2M)!)^3} \tag{3.2.15}$$

and

$$\psi_M^{(2)} = \frac{2^{2M+2}(2M-1)^2(M!)^4}{(M-1)((2M)!)^3}. \tag{3.2.16}$$

Bounding E_M in (3.2.13) then gives

$$\|E_M\| \leq B_M^{(\nu)} \equiv \psi_M^{(\nu)}\, \mathbb{F}_{2M-\nu} \tag{3.2.17}$$

wherein

$$\mathbb{F}_{2M-\nu} \equiv \max_{x\in[-1,1]} \left| f^{(2M-\nu)}(x) \right|. \tag{3.2.18}$$

As $M \to \infty$ (3.2.14), (3.2.15) and (3.2.16) reveal that

$$\psi_M^{(\nu)} \simeq \frac{2^{2(M+\nu)} M^{\nu-1} (M!)^4}{((2M)!)^3}, \tag{3.2.19}$$

which is exact for $\nu = 1$ and in error by less than 10^{-10} for $M \geq 7$ when $\nu = 0, 2$. By Stirling's formula [9, p.279],

$$\psi_M^{(\nu)} \sim \widetilde{\psi}_M^{(\nu)} = \frac{2^{2\nu-1}\sqrt{\pi}}{M^{(1-2\nu)/2}} \left(\frac{\mathrm{e}}{4M}\right)^{2M}, \qquad M \to \infty, \tag{3.2.20}$$

and therefore the asymptotic convergence rate for the quadrature error is

$$\|E_M\| \sim \widetilde{\psi}_M^{(\nu)} \, \mathbb{F}_{2M-\nu}, \qquad M \to \infty. \tag{3.2.21}$$

It is clear from (3.2.20) that $\widetilde{\psi}_M^{(\nu)} \sim O(M^{-2M})$ and so, by (3.2.21), the error is predicted to converge to zero provided that $\mathbb{F}_{2M-\nu} \sim o(M^{2M})$ as $M \to \infty$.

3.2.5 Numerical Experiments

The three discussed quadrature methods are tested on the example

$$f(x) = \cos(x) + \sin(x), \tag{3.2.22}$$

for which the computational errors $e_M = \|E_M\| = \left\| \int_{-1}^{1} f(x)dx - \sum_{j=1}^{M} w_{j,M} f(y_{j,M}) \right\|$, the error bounds $B_M^{(\nu)}$ given by (3.2.17), and the convergence rates given by (3.2.21), are shown in Figure 3.2.1 for $\nu = 0, 1, 2$.

Figure 3.2.1 shows that, as expected from the number of assigned abscissae, Gauss-Legendre is the most accurate quadrature method and Legendre-Gauss-Lobatto quadrature is the least accurate. On each node set, the bounds yield accurate approximations of the true errors; moreover the convergence rate (3.2.21) provides accurate approximations of the bounds for relatively low values of M. All calculations were performed on `Maple` using 50 digits, i.e. with a machine precision of 10^{-50}. The ratio between the bounds, $B_M^{(\nu)}$ in (3.2.17), for $\nu = 0$ and $\nu = 2$ can be written, via (3.2.14) and (3.2.16), as

$$\begin{aligned} \frac{B_M^{(0)}}{B_{M+1}^{(2)}} &= \frac{2^{2M+1} (M!)^4 \, \mathbb{F}_{2M}}{(2M+1) ((2M)!)^3} \cdot \frac{M ((2M+2)!)^3}{2^{2M+4} (2M+1)^2 ((M+1)!)^4 \, \mathbb{F}_{2M}} \\ &= \frac{M}{M+1} \sim 1 \quad \text{as} \quad M \to \infty. \end{aligned} \tag{3.2.23}$$

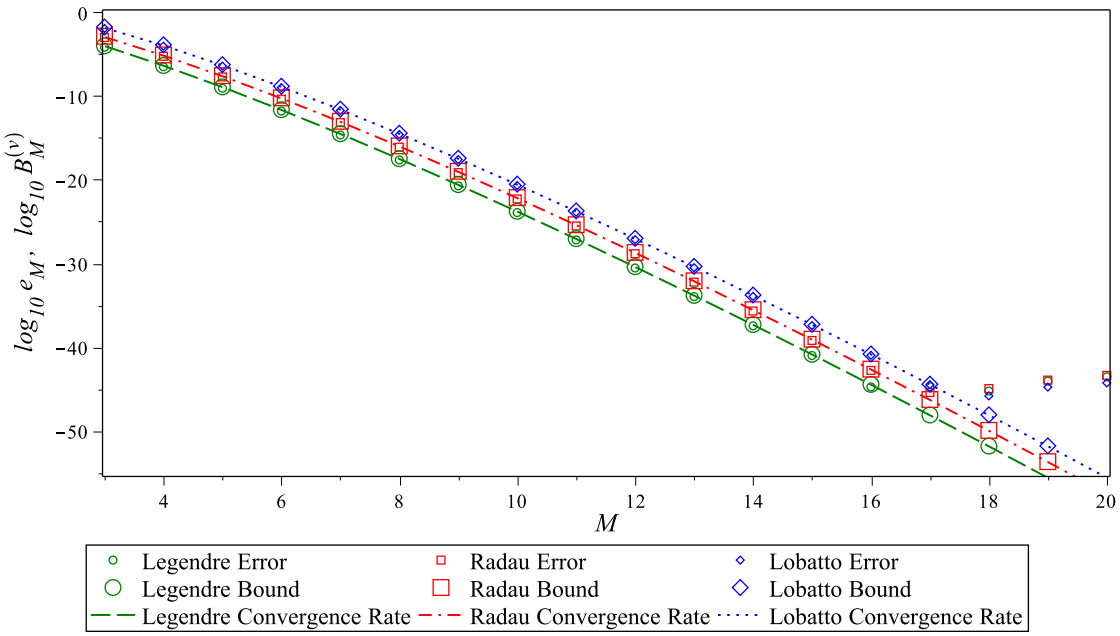

Figure 3.2.1: Logarithmic plot of the errors, bounds and predicted convergence rates associated with Gauss-Legendre ("Legendre"), Legendre-Gauss-Radau ("Radau") and Legendre-Gauss-Lobatto ("Lobatto") quadrature rules. The errors, bounds and convergence rates are, for this example, in close agreement due to the infinite differentiability of the test function in (3.2.22).

Therefore $B_M^{(0)} \simeq B_{M+1}^{(2)}$ as $M \to \infty$, which corroborates the results presented in Figure 3.2.1, in which it is clear that Gauss-Legendre quadrature with M nodes and Legendre-Gauss-Lobatto quadrature with $M+1$ nodes yield approximately the same error.

3.3 Summary

Spectrally accurate numerical methods for differentiation and integration have been presented, and their inherent errors analysed. The error analyses in both Chapters 2 and 3 provide a framework from which the error analyses of numerical methods for integral and integro-differential equations (IEs and IDEs) are developed in Chapters 4 and 5 respectively.

It is well-known that the differentiation matrices of Section 3.1 are an efficient and

accurate way of implementing the spectrally accurate differentiation introduced in Chapter 2; their accuracy can be improved further through the use of the techniques described in Section 3.1.7. The differentiation matrices have been introduced here with the goal of incorporating them into numerical methods for IDEs; by using the simplified matrix entries derived for the various nodal distributions in Sections 3.1.1–3.1.5, the required setup workload in the IDE methods in Chapter 5 is reduced. Additionally, a comparison of the eigenvalue analyses in Section 3.1.7 and [126] provides the arguments from which the error analyses for the IDE numerical methods in Chapter 5 are based.

The framework of Gaussian quadrature introduced in Section 3.2 is expanded upon in Chapters 4 and 5 in order to implement numerical methods for approximating the solution of IEs and IDEs. Although the Gauss-Legendre quadrature rule is, due to its maximal degree of precision, predicted to be the most accurate theoretically (and confirmed computationally), the Legendre-Gauss-Radau and Legendre-Gauss-Lobatto rules have computational advantages when incorporated into IDE numerical methods for which the governing IDE is augmented by a boundary condition at $x = \pm 1$.

3. SPECTRALLY ACCURATE NUMERICAL DIFFERENTIATION AND NUMERICAL QUADRATURE

Chapter 4

Integral Equations

An *integral equation* (IE) is an equation that contains the integral of an unknown function. Many problems arising in the physical sciences can be modelled using IEs. For example, IEs can be used to model population growth [81], biological systems [119], elastohydrodynamic lubrication [66], quantum scattering [17], and heat transfer [95]. Furthermore, ordinary and partial differential equations (ODEs and PDEs), which also arise in a wide range of physical problems, can be reformulated as IEs. The advantage of the IE reformulation is that associated boundary and initial conditions (BCs and ICs) are incorporated within the IE, in contrast to ODEs and PDEs on which BCs and ICs are imposed.

This chapter begins with an overview of integral equations: Section 4.1 introduces and classifies IEs and gives the IE representations of both initial and boundary value problems (IVPs and BVPs); Section 4.2 then presents an analytical method for solving IEs. However, since in general IEs cannot be solved analytically, the main focus of this chapter is numerical methods for finding approximate solutions. In Section 4.3 the well-known *Nyström method* [98, 10] is introduced which builds upon the Gaussian quadrature presented in Section 3.2. The Nyström method is then extended to incorporate the interpolation techniques introduced in Chapter 2 so that integral equations can be solved using *any* of the nodal distributions examined in Section 2.3. Specifically, the interpolation in the new *interpolated Nyström method* can be used to project between optimal quadrature and optimal differentiation nodes; when extended to solve integro-differential equations (IDEs) in Chapter 5 this enables the total error to be minimised.

Despite the wide use of the Nyström method, the development of computable, error bounds that require no knowledge of an exact solution remains relatively scarce. For example, the standard form of the Nyström error, see [10, Eq. 4.1.33] and [60, Eq. 4.7.16d], is dependent upon the exact solution and also contains a component that is bounded theoretically, see [10, Eq. 4.1.32] and [60, Eq. 4.7.16b]. Furthermore, the error analysis in, for example, [45, 113, 117] focuses on only convergence rates. Thus motivated, and in accordance with the goal of this thesis, in Section 4.4 there follow error analyses for both the Nyström method and its new interpolated counterpart. Error bounds are derived for both methods that are computable using only the numerical solution, therefore requiring no knowledge of the exact solution. The error analysis is founded on existing operator theory; specifically, the theoretical bound [60, Eq. 4.7.17b] on a component inherent in the Nyström error is developed into a computable quantity. Asymptotic error estimates are then developed from the interpolation and quadrature error analyses respectively detailed in Sections 2.4 and 3.2; these analyses quantify the disparity between the standard and interpolated Nyström-error accuracies.

The numerical methods and error analyses are validated on a diverse range of test problems with known solutions, some of which are designed to be challenging to approximation methods.

4.1 Classification of Integral Equations

An equation in which an unknown function (to be determined) appears under an integral sign is known as an integral equation (IE); this can be classified in many ways. IEs that have a variable limit of integration are classified as *Volterra integral equations* (VIEs) and those with fixed limits of integration are classified as *Fredholm integral equations* (FIEs) [10]. Additionally, IEs are classified as linear/nonlinear depending on whether the unknown function appears linearly or nonlinearly. An IE is of the *first kind* if the unknown function appears only inside the integral, whereas if the unknown function also appears outside the integral then the IE is of the *second kind*. For example,

$$\lambda \int_a^x K(x,y)\, u(y)\, dy = f(x), \qquad a \le x \le b, \tag{4.1.1}$$

is a *linear Volterra integral equation of the first kind* (VIE1);

$$u(x) - \lambda \int_a^x K(x,y)\, u(y)\, dy = f(x), \qquad a \le x \le b, \tag{4.1.2}$$

is a *linear Volterra integral equation of the second kind* (VIE2);

$$\lambda \int_a^b K(x,y)\, u(y)\, dy = f(x), \qquad a \le x \le b, \tag{4.1.3}$$

is a *linear Fredholm integral equation of the first kind* (FIE1); and

$$u(x) - \lambda \int_a^b K(x,y)\, u(y)\, dy = f(x), \qquad a \le x \le b \tag{4.1.4}$$

is a *linear Fredholm integral equation of the second kind* (FIE2). In each of the integral equations (4.1.1)–(4.1.4) the function $K : [a,b] \times [a,b] \to \mathbb{R}$ is the kernel, $f : [a,b] \to \mathbb{R}$ is the source function, $a, b, \lambda \in \mathbb{R}$ are constants, and $u(x)$ is the unknown function to be determined on $[a,b]$. *Nonlinear* IEs corresponding to their linear counterparts in (4.1.1)–(4.1.4) have the integrand $K(x,y)\,u(y)$ replaced by $K(x,y,u(y))$ or $K(x,y,u(x),u(y))$.

Volterra integral equations commonly arise from the reformulation of initial value problems (IVPs); this is advantageous since the VIE reformulation incorporates the initial conditions (ICs) directly. For example, the first-order IVP

$$\frac{du}{dx} = F\big(x, u(x)\big), \qquad u(a) = \alpha, \qquad x \ge a \tag{4.1.5}$$

can be reformulated as

$$u(x) = \alpha + \int_a^x F\big(y, u(y)\big)\, dy, \qquad x \ge a, \tag{4.1.6}$$

and the second order IVP

$$u''(x) + A(x)\, u'(x) + B(x)\, u(x) = g(x), \qquad u(a) = \alpha, \qquad u'(a) = \beta, \qquad x \ge a \tag{4.1.7}$$

can be written as [75]

$$u(x) = f(x) + \int_a^x K(x,y)\, u(y)\, dy, \qquad x \ge a, \tag{4.1.8}$$

in which the kernel $K(x,y)$ is given by

$$K(x,y) = (y-x)\big(B(y) - A'(y)\big) - A(y), \tag{4.1.9}$$

and the source function $f(x)$ is given by

$$f(x) = \int_a^x (x-y)\, g(y)\, dy + (x-a)\big(A(a)\,\alpha + \beta\big) + \alpha. \tag{4.1.10}$$

Fredholm integral equations arise frequently in the reformulation of two-point boundary value problems (BVPs) and eigenvalue problems (EVPs). For example, the BVP

$$y''(x) + A(x)\, y'(x) + B(x)\, y(x) = g(x), \qquad y(a) = \alpha, \qquad y(b) = \beta, \tag{4.1.11}$$

can be solved in the integral form (note the Volterra-type variable limit on the integral)

$$y(x) = \alpha + (x-a)\, y'(a) + \int_a^x (x-t)\, y''(t)\, dt \tag{4.1.12}$$

by converting the BVP (4.1.11) to the FIE2

$$u(x) = f(x) + \int_a^b K(x,t)\, u(t)\, dt \tag{4.1.13}$$

wherein

$$u(x) = y''(x), \tag{4.1.14}$$

the source function is given by

$$f(x) = g(x) - \alpha\, B(x) - \frac{\beta - \alpha}{b-a}\big(A(x) + (x-a)\, B(x)\big) \tag{4.1.15}$$

and the kernel is given by

$$K(x,t) = \begin{cases} \dfrac{a-t}{b-a}\big(A(x) + (x-b)\, B(x)\big) & a \le t \le x, \\[2ex] \dfrac{b-t}{b-a}\big(A(x) + (x-a)\, B(x)\big) & x \le t \le b. \end{cases} \tag{4.1.16}$$

The details of the conversion from the BVP (4.1.11) to the FIE2 (4.1.13), following the approach in [104], are in Appendix D. It is noted in passing that the approach presented in [104] is in error, which is corrected in Appendix D. Alternatively, the BVP (4.1.11) can be rewritten in terms of $y(x)$ as the FIE2 [75]

$$y(x) = f(x) + \int_a^b K(x,t)\, y(t)\, dt \tag{4.1.17}$$

with source function

$$f(x) = \alpha + \int_a^x (x-t)\, g(t)\, dt + \frac{x-a}{b-a}\left(\beta - \alpha - \int_a^b (b-t)\, g(t)\, dt\right), \tag{4.1.18}$$

and kernel

$$K(x,t) = \begin{cases} \dfrac{x-b}{b-a}\Big(A(t) - (a-t)\big(A'(t) - B(t)\big)\Big) & a \le t \le x, \\ \dfrac{x-a}{b-a}\Big(A(t) - (b-t)\big(A'(t) - B(t)\big)\Big) & x \le t \le b. \end{cases} \tag{4.1.19}$$

The derivation of (4.1.17)–(4.1.19), which is not presented in [75], is given in Appendix D.

The remainder of this chapter considers only Fredholm integral equations of the second kind (FIE2s). Integral equations of this form arise in many scientific applications [131] including electrostatics [88], polymer physics [102] and astrophysics [32]; however, FIE2s most commonly arise from reformulating a BVP as shown in (4.1.11)–(4.1.19).

4.2 Degenerate Kernel: Analytical Solution

An integral equation has a *degenerate kernel* [75, p. 123], otherwise known as a *separable kernel*, if it is of the form

$$K(x,y) = \sum_{j=1}^{m} P_j(x)\, Q_j(y), \tag{4.2.1}$$

in which case the IE (4.1.4) can be solved analytically by rewriting it as

$$u(x) - \lambda \sum_{j=1}^{m} P_j(x) \int_a^b Q_j(y)\, u(y)\, dy = f(x). \tag{4.2.2}$$

By defining constants C_i as

$$C_i \equiv \int_a^b Q_i(y)\, u(y)\, dy, \qquad i = 1(1)m, \tag{4.2.3}$$

the integral equation (4.2.2) becomes

$$u(x) = f(x) + \lambda \sum_{j=1}^{m} P_j(x)\, C_j \tag{4.2.4}$$

which is substituted into (4.2.3) to give

$$C_i = \int_a^b Q_i(y)\, f(y)\, dy + \lambda \sum_{j=1}^{m} C_j \int_a^b Q_i(y)\, P_j(y)\, dy. \tag{4.2.5}$$

In matrix-vector form (4.2.5) is

$$(\mathbf{I} - \lambda \mathbf{Q_m})\, \mathbf{C} = \mathbf{F} \tag{4.2.6}$$

wherein the elements, for $i, j = 1(1)m$, are given by

$$\{\mathbf{C}\}_i = C_i, \quad \{\mathbf{F}\}_i = \int_a^b Q_i(y)\, f(y)\, dy, \quad \{\mathbf{Q_m}\}_{i,j} = \int_a^b Q_i(y)\, P_j(y)\, dy. \tag{4.2.7}$$

Now denote by λ_0 the *singular value* of λ in (4.2.6) for which

$$\det(\mathbf{I} - \lambda_0\, \mathbf{Q_m}) = 0, \tag{4.2.8}$$

i.e. for which $\mathbf{I} - \lambda \mathbf{Q_m}$ in (4.2.6) is not invertible: then the integral equation (4.2.2) has either an infinite number of solutions or no solution. In general, there is a maximum of m singular values associated with the degenerate kernel (4.2.1). If $\lambda \neq \lambda_0$ then the system (4.2.6) can be inverted to give

$$\mathbf{C} = (\mathbf{I} - \lambda \mathbf{Q_m})^{-1}\, \mathbf{F}. \tag{4.2.9}$$

Using (4.2.9) the unique solution of the integral equation (4.2.2) is found from (4.2.4) as

$$u(x) = f(x) + \lambda\, \mathbf{P}\, (\mathbf{I} - \lambda \mathbf{Q_m})^{-1}\, \mathbf{F} \tag{4.2.10}$$

wherein the row vector $\mathbf{P}$ is computed by

$$\{\mathbf{P}\}_j = P_j(x), \qquad j = 1(1)m. \tag{4.2.11}$$

For example, when $m = 1$ in (4.2.1) the kernel can be written as

$$K(x, y) = P(x)\, Q(y), \tag{4.2.12}$$

the simplest degenerate kernel. In this case, the system (4.2.6) is equivalently

$$\left(1 - \lambda \int_a^b P(y)\, Q(y)\, dy\right) C = \int_a^b Q(y)\, f(y)\, dy, \tag{4.2.13}$$

wherein

$$C \equiv \int_a^b Q(y)\, u(y)\, dy, \tag{4.2.14}$$

and the singular value λ_0 is therefore

$$\lambda_0 = \frac{1}{\int_a^b K(y,y)\, dy}. \tag{4.2.15}$$

If $\int_a^b Q(y)\, f(y)\, dy \neq 0$ and $\lambda = \lambda_0$ then (4.2.13) becomes $C \cdot 0 \neq 0$ which is inconsistent and so there are no solutions. If $\lambda = \lambda_0$ and $\int_a^b Q(y)\, f(y)\, dy = 0$ then (4.2.13) becomes $C \cdot 0 = 0$ which has an infinite number of solutions for C and hence for $u(x)$. Finally, if $\lambda \neq \lambda_0$ then the unique solution is found from (4.2.10) as

$$u(x) = f(x) + \frac{\lambda\, P(x) \int_a^b Q(y)\, f(y) dy}{1 - \lambda \int_a^b P(y)\, Q(y) dy}. \tag{4.2.16}$$

When $\lambda \approx \lambda_0$ it is clear from (4.2.13) that $|C| \gg 1$, hence the FIE2 with kernel (4.2.12) is ill-conditioned. This is also the case for non-separable kernel FIE2s whose associated singular values λ_0 will not, in general, be explicitly derivable [79].

4.3 Numerical Methods

Since it is not always possible to solve integral equations analytically, numerical methods must be used to determine approximate numerical solutions. The numerical solution of an FIE2 of the form (4.1.4) is considered in a large body of literature; some of the most well-known approximation techniques based upon interpolation, quadrature, projection and collocation are covered in [10, 14, 60, 83]. Other numerical methods developed for the solution of an FIE2 include a degenerate-kernel approach [114] in which the FIE2 kernel is approximated by a kernel of the form (4.2.1), a multiple-grid method [63], a Taylor-series expansion [70, 91], Adomian decomposition [11], a Chebyshev-series expansion [102], Haar wavelets [13], and a discrete product-integration scheme [76].

This section presents an overview of the ubiquitous *Nyström method* [98, 10, 60] which utilises the Gaussian quadrature presented in Section 3.2. The well-known

classical version of the Nyström method is presented in Section 4.3.1, which is then extended in Section 4.3.2 to form a new *interpolated* version that uses the interpolation techniques from Chapter 2 to project between the Nyström quadrature nodes and, for example, optimal differentiation nodes. The interpolated Nyström method is developed in preparation for extension into a form that computes approximate solutions of integro-differential equations (IDEs) with the aim of minimising the combined error incurred through the approximation of both integral and derivative components. In Section 4.3.3 the Nyström methods are validated and analysed on a range of test problems with known solutions.

It is henceforth assumed that the FIE2 (4.1.4) has been scaled onto the interval $[-1, 1]$ so that it is of the canonical form

$$u(x) - \lambda \int_{-1}^{1} K(x, y)\, u(y)\, dy = f(x), \qquad -1 \leq x \leq 1. \tag{4.3.1}$$

For simplicity, (4.3.1) can be written in symbolic form as

$$u - \lambda\, \mathcal{K}\, u = f \tag{4.3.2}$$

in which the action of the linear integral operator $\mathcal{K}$ on u is defined by

$$\mathcal{K}\, u = (\mathcal{K}\, u)(x) \equiv \int_{-1}^{1} K(x, y)\, u(y)\, dy. \tag{4.3.3}$$

4.3.1 Classical Nyström Method

In the Nyström method the action of the integral operator $\mathcal{K}$ in (4.3.3) is approximated by the numerical operator $\mathcal{K}_M$ defined by

$$\mathcal{K}\, u \approx \mathcal{K}_M\, u = (\mathcal{K}_M\, u)(x) \equiv \sum_{j=1}^{M} w_{j,M}\, K(x, y_{j,M})\, u(y_{j,M}) \tag{4.3.4}$$

which represents an M-node quadrature rule with weights $w_{j,M}$ and nodes $y_{j,M}$. Since the weighting function in the integral in (4.3.3) is unity, the quadrature rule can be any of those defined in Section 3.2, namely Gauss-Legendre, Legendre-Gauss-Radau and Legendre-Gauss-Lobatto; the Nyström method is most commonly based upon Gauss-Legendre quadrature due to its maximal degree of precision.

Using (4.3.4), the approximate solution $u_M(x)$ of the FIE2 (4.3.1) satisfies the discrete equation

$$u_M(x) - \lambda \sum_{j=1}^{M} w_{j,M}\, K(x, y_{j,M})\, u_M(y_{j,M}) = f(x), \qquad x \in [-1, 1], \tag{4.3.5}$$

which has the corresponding symbolic form

$$u_M - \lambda\, \mathcal{K}_M\, u_M = f. \tag{4.3.6}$$

Collocation of (4.3.5) at the M quadrature nodes yields

$$u_M(y_{i,M}) - \lambda \sum_{j=1}^{M} w_{j,M}\, K(y_{i,M}, y_{j,M})\, u_M(y_{j,M}) = f(y_{i,M}), \qquad i = 1(1)M, \tag{4.3.7}$$

which is an $M \times M$ linear system for the nodal values $u_M(y_{i,M})$, $i = 1(1)M$, of the approximate solution. That is, (4.3.7) can be written in matrix-vector form as

$$(\mathbf{I}_M - \lambda\, \mathbf{K}_M)\, \mathbf{u}_M = \mathbf{f}_M \tag{4.3.8}$$

wherein, for $i, j = 1(1)M$,

$$\{\mathbf{u}_M\}_i = u_M(y_{i,M}), \quad \{\mathbf{f}_M\}_i = f(y_{i,M}), \quad \{\mathbf{K}_M\}_{i,j} = w_{j,M}\, K(y_{i,M}, y_{j,M}) \tag{4.3.9}$$

and $\mathbf{I}_M$ is the $M \times M$ identity matrix. Inversion of the system (4.3.8) yields the nodal values $u_M(y_{i,M})$, $i = 1(1)M$, which are substituted into (4.3.5) to give the Nyström inversion formula

$$u_M(x) = f(x) + \lambda \sum_{j=1}^{M} w_{j,M}\, K(x, y_{j,M})\, u_M(y_{j,M}), \qquad x \in [-1, 1], \tag{4.3.10}$$

that approximates $u(x)$ for all $x \in [-1, 1]$. Note that (4.3.10) recovers $u(x)$ exactly if $K(x, y)\, u(y)$ is a polynomial in y of degree less than or equal to $2M - 1 - \nu$, where $\nu = 0, 1, 2$ respectively correspond to quadratures based upon Legendre, Legendre-Gauss-Radau and Legendre-Gauss-Lobatto nodes. This method will hereafter be referred to as the *classical Nyström method* (CNM).

4.3.1.1 Matrix and Singular-Value Analysis

To determine the vector of nodal values $\mathbf{u}_M$ for use in (4.3.10), the system matrix $\mathbf{I}_M - \lambda\,\mathbf{K}_M$ in (4.3.8) must be inverted. It is therefore useful to understand the linear algebra of the sub-matrices within that system. Specifically, by investigating the eigenvalues of the matrices $\mathbf{K}_M$ the singular values λ_0 can be determined. Here the separable kernel of the form $K(x,y) = P(x)\,Q(y)$ is considered where, for simplicity, the entries of the matrix $\mathbf{K}_M$ in (4.3.9) are denoted by $K_{i,j}$ such that

$$K_{i,j} = \{\mathbf{K}_M\}_{i,j} = w_{j,M}\,K(y_{i,M}, y_{j,M}) = w_{j,M}\,P(y_{i,M})\,Q(y_{j,M}). \tag{4.3.11}$$

The matrix entries therefore satisfy

$$K_{i,j}\,K_{l,m} = w_{j,M}\,w_{m,M}\,P(y_{i,M})\,P(y_{l,M})\,Q(y_{j,M})\,Q(y_{m,M}) = K_{i,m}\,K_{l,j}. \tag{4.3.12}$$

Inspection of the matrix $\mathbf{K}_M$ leads to the assertion that its eigenvalues, denoted by Λ, satisfy

$$\det(\mathbf{K}_M - \Lambda\mathbf{I}_M) = (-\Lambda)^{M-1}\left(\sum_{i=1}^{M} K_{i,i} - \Lambda\right) = 0 \tag{4.3.13}$$

wherein $\mathbf{I}_M$ is the $M \times M$ identity matrix. Using property (4.3.12), assertion (4.3.13) is proved by induction in Appendix E. It is clear from (4.3.13) that all but one of the eigenvalues of $\mathbf{K}_M$ are equal to 0 and the non-zero eigenvalue is equivalent to the trace of $\mathbf{K}_M$. Therefore the matrix $\mathbf{K}_M$ based upon the kernel $K(x,y) = P(x)\,Q(y)$ is singular, hence

$$\det(\mathbf{K}_M) = 0. \tag{4.3.14}$$

It follows from (4.3.13) that the eigenvalues of the system matrix $\mathbf{I}_M - \lambda\mathbf{K}_M$, denoted by $\widetilde{\Lambda}$, satisfy

$$\det(\mathbf{I}_M - \lambda\mathbf{K}_M - \widetilde{\Lambda}\mathbf{I}_M) = (1-\widetilde{\Lambda})^{M-1}\left(1 - \widetilde{\Lambda} - \lambda\sum_{i=1}^{M} K_{i,i}\right) = 0, \tag{4.3.15}$$

hence one eigenvalue of $\mathbf{I}_M - \lambda\mathbf{K}_M$ is equal to $1 - \lambda\mathrm{Tr}\,(\mathbf{K}_M)$ whilst all others are equal to unity. The matrix $\mathbf{I}_M - \lambda\mathbf{K}_M$ is therefore singular only when $\lambda = \widetilde{\lambda}_0$ defined by

$$\widetilde{\lambda}_0 \equiv \frac{1}{\mathrm{Tr}\,(\mathbf{K}_M)} \tag{4.3.16}$$

in which case the Nyström method will fail.

Section 4.2 showed that an FIE2 with a separable kernel of the form (4.2.12) has no solution when $\lambda = \lambda_0$ as given by (4.2.15). The singular value λ_0 of the FIE2 is related to the singular value $\widetilde{\lambda}_0$ of the system matrix $\mathbf{I}_M - \lambda \mathbf{K}_M$ by

$$\frac{1}{\lambda_0} = \frac{1}{\widetilde{\lambda}_0} + E_M, \tag{4.3.17}$$

wherein E_M is the quadrature error term (3.2.13), since (4.2.15) gives

$$\frac{1}{\lambda_0} = \int_a^b K(y,y)dy = \sum_{i=1}^{M} w_{i,M}\, K(y_{i,M}, y_{i,M}) + E_M \tag{4.3.18}$$

and (4.3.16) gives

$$\frac{1}{\widetilde{\lambda}_0} = \mathrm{Tr}\,(\mathbf{K}_M) = \sum_{i=1}^{M} w_{i,M}\, K(y_{i,M}, y_{i,M}). \tag{4.3.19}$$

Therefore $\lambda_0 = \widetilde{\lambda}_0$ when $K(y,y)$ is a polynomial in y of degree less than or equal to $2M-1-\nu$, where $\nu = 0, 1, 2$ correspond to Gauss-Legendre, Legendre-Gauss-Radau and Legendre-Gauss-Lobatto quadratures respectively.

To quantify the effect on the exact solution of an FIE2 with kernel (4.2.12) as $\lambda \to \lambda_0$ first define

$$\mathbb{P} \equiv \int_a^b P(y)\, Q(y)dy \tag{4.3.20}$$

and

$$\mathbb{Q} \equiv \int_a^b Q(y)\, f(y)dy \tag{4.3.21}$$

so that (4.2.16) can be written as

$$u(x) = \frac{\lambda\, P(x)\, \mathbb{Q}}{1 - \lambda\, \mathbb{P}} + f(x). \tag{4.3.22}$$

Now let

$$\lambda = \lambda_0 + \epsilon, \qquad 0 < |\epsilon| \ll 1 \tag{4.3.23}$$

which, by (4.2.15), is equivalently

$$\lambda = \frac{1}{\mathbb{P}} + \epsilon. \tag{4.3.24}$$

Substitution of (4.3.24) into (4.3.22) yields

$$\begin{aligned} u(x) &= \frac{\left(\frac{1}{\mathbb{P}}+\epsilon\right) P(x)\,\mathbb{Q}}{1-(1+\epsilon\,\mathbb{P})} + f(x) \\ &= \frac{\frac{P(x)\,\mathbb{Q}}{\mathbb{P}} + \epsilon\, P(x)\,\mathbb{Q}}{-\epsilon\,\mathbb{P}} + f(x) \\ &= f(x) - \frac{P(x)\,\mathbb{Q}}{\mathbb{P}} - \frac{P(x)\,\mathbb{Q}}{\epsilon\,\mathbb{P}^2} \\ &= f(x) - \frac{P(x)\,\mathbb{Q}}{\mathbb{P}} + O(\epsilon^{-1}), \end{aligned} \tag{4.3.25}$$

which demonstrates that $\|u\| \to \infty$ as $|\epsilon| \to 0$.

The effect of $\lambda \to \lambda_0$ on the numerical solution $u_{_M}(x)$ in (4.3.10) can be similarly considered. Substituting λ, as given by (4.3.24), into the CNM numerical solution (4.3.10) yields

$$\begin{aligned} u_{_M}(x) &= f(x) + \left(\frac{1}{\mathbb{P}}+\epsilon\right) \sum_{j=1}^{M} w_{j,M}\, K(x, y_{j,M})\, u_{_M}(y_{j,M}) \\ &= f(x) + \frac{1}{\mathbb{P}} \sum_{j=1}^{M} w_{j,M}\, K(x, y_{j,M})\, u_{_M}(y_{j,M}) + \epsilon \sum_{j=1}^{M} w_{j,M}\, K(x, y_{j,M})\, u_{_M}(y_{j,M}) \\ &= f(x) + \frac{1}{\mathbb{P}} \sum_{j=1}^{M} w_{j,M}\, K(x, y_{j,M})\, u_{_M}(y_{j,M}) + O(\epsilon). \end{aligned} \tag{4.3.26}$$

Subtraction of (4.3.26) from (4.3.25) yields the error

$$u(x) - u_{_M}(x) = -\frac{1}{\mathbb{P}}\left(P(x)\,\mathbb{Q} + \sum_{j=1}^{M} w_{j,M}\, K(x, y_{j,M})\, u_{_M}(y_{j,M})\right) + O(\epsilon) + O(\epsilon^{-1}) \tag{4.3.27}$$

which, as $|\epsilon| \to 0$, gives

$$\|u - u_{_M}\| \sim O(\epsilon^{-1}). \tag{4.3.28}$$

Therefore the error between the exact and numerical solutions of the integral equation (4.3.1) satisfies

$$\|u - u_{_M}\| \to \infty \qquad \text{as } \lambda \to \lambda_0. \tag{4.3.29}$$

4.3.2 Interpolated Nyström Method

Since the integral weighting function in (4.3.1) is unity, the CNM utilises Legendre, Legendre-Gauss-Radau or Legendre-Gauss-Lobatto nodes. To approximate integration using a different set of nodes, for example in the context of an integro-differential equation that uses Chebyshev-Gauss-Lobatto points to optimise the differentiation error (see Figure 2.4.1), the Nyström method can be combined with Lagrange interpolation (2.1.1) to yield a new *interpolated Nyström method* (INM). Existing methods for solving FIE2s using Chebyshev-Gauss-Lobatto points are discussed in [31, 93].

In the INM, $\mathcal{K}\,u$ is approximated by Lagrange interpolating the nodal values $u(y_{j,M})$ in the quadrature rule (4.3.4) through a distinct set of nodes $x_{j,N}$, $j = 1(1)N$, so that

$$\mathcal{K}\,u \approx \mathcal{K}_M\,\mathcal{L}_N\,u = (\mathcal{K}_M\,\mathcal{L}_N\,u)(x) \equiv \sum_{j=1}^{M}\sum_{k=1}^{N} w_{j,M}\,K(x, y_{j,M})\,L_{k,N}(y_{j,M})\,u(x_{k,N}) \tag{4.3.30}$$

wherein the actions of the operators $\mathcal{K}_M$ and $\mathcal{L}_N$ are respectively defined by (4.3.4) and (2.1.1). Using (4.3.30), the approximate solution $\widetilde{u}_{M,N}(x)$ of the FIE2 (4.3.1) satisfies

$$\widetilde{u}_{M,N}(x) - \lambda \sum_{j=1}^{M}\sum_{k=1}^{N} w_{j,M}\,K(x, y_{j,M})\,L_{k,N}(y_{j,M})\,\widetilde{u}_{M,N}(x_{k,N}) = f(x), \qquad x \in [-1, 1], \tag{4.3.31}$$

which can be written in symbolic form as

$$\widetilde{u}_{M,N} - \lambda\,\mathcal{K}_M\,\mathcal{L}_N\,\widetilde{u}_{M,N} = f. \tag{4.3.32}$$

Collocating (4.3.31) at the N interpolation nodes $x_{i,N}$, $i = 1(1)N$ and interchanging the subscripts j and k yields the matrix-vector equation

$$(\mathbf{I}_N - \lambda\,\widetilde{\mathbf{K}}_{M,N})\,\widetilde{\mathbf{u}}_{M,N} = \widetilde{\mathbf{f}}_N, \tag{4.3.33}$$

wherein

$$\{\widetilde{\mathbf{u}}_{M,N}\}_i = \widetilde{u}_{M,N}(x_{i,N}), \qquad \{\widetilde{\mathbf{f}}_N\}_i = f(x_{i,N}),$$

$$\{\widetilde{\mathbf{K}}_{M,N}\}_{i,j} = \sum_{k=1}^{M} w_{k,M}\,K(x_{i,N}, y_{k,M})\,L_{j,N}(y_{k,M}), \qquad i, j = 1(1)N, \tag{4.3.34}$$

and $\mathbf{I}_N$ is the $N \times N$ identity matrix. Inversion of (4.3.33) yields the nodal values $\widetilde{u}_{M,N}(x_{i,N})$, $i = 1(1)N$, which are substituted into (4.3.31) to give the INM inversion formula

$$\widetilde{u}_{M,N}(x) = f(x) + \lambda \sum_{k=1}^{M} \sum_{j=1}^{N} w_{k,M}\, K(x, y_{k,M})\, L_{j,N}(y_{k,M})\, \widetilde{u}_{M,N}(x_{j,N}), \tag{4.3.35}$$

that approximates $u(x)$ for all $x \in [-1, 1]$. The nodal values recovered from (4.3.33) can alternatively be substituted into the Lagrange interpolation formula (2.1.1) yielding the *Lagrange-INM* approximation

$$\widetilde{u}_{M,N}(x) = \sum_{j=1}^{N} L_{j,N}(x)\, \widetilde{u}_{M,N}(x_{j,N}), \tag{4.3.36}$$

that also approximates $u(x)$ for all $x \in [-1, 1]$. The double sum in (4.3.35) indicates that the INM inversion formula is $O(M)$ times more computationally expensive than the Lagrange-INM approximation and $O(N)$ times more computationally expensive than the CNM (4.3.10) for a given M.

Since Lagrange interpolation, and its associated error, is inevitable in the INM it is, as yet, unknown whether the INM inversion formula (4.3.35) or Lagrange-INM approximation (4.3.36) is the most accurate. However, it is clear from the error formulae in Table 2.1 and (3.2.20) that a CNM equivalent to the Lagrange-INM approximation, i.e. Lagrange interpolating the nodal values obtained from inversion of the CNM system (4.3.8), yields a greater error than that of the CNM inversion formula (4.3.10). This is because the error of M-node Lagrange interpolation is $O(M^{-M})$ (see Table 2.1), and the error of M-node quadrature is $O(M^{-2M})$ (see (3.2.20)), provided the derivatives $u^{(M)}(x)$ and $\frac{\partial^M}{\partial y^M} K(x, y)\, u(y)$ do not grow exponentially with M. A *Lagrange-CNM* approximation is therefore not pursued further.

Note that, if $M = N$ and $x_{j,N} = y_{j,N}$, for all $j = 1(1)N$, i.e. the quadrature nodes are also the interpolation nodes, then the INM inversion formula (4.3.35) is equivalent to the CNM approximation (4.3.10) since $L_{j,N}(y_{k,N}) = \delta_{jk}$ where δ_{jk} is the Kronecker delta defined in (2.3.12).

4.3.2.1 Matrix and Singular Value Analysis

Let $\widetilde{K}_{i,j}$ denote the entries of the matrix $\widetilde{\mathbf{K}}_{M,N}$ in (4.3.34) based upon the separable kernel $K(x,y) = P(x)\,Q(y)$ such that

$$\begin{aligned}\widetilde{K}_{i,j} &= \{\widetilde{\mathbf{K}}_{M,N}\}_{i,j} = \sum_{k=1}^{M} w_{k,M}\, K(x_{i,N}, y_{k,M})\, L_{j,N}(y_{k,M}) \\ &= \sum_{k=1}^{M} w_{k,M}\, P(x_{i,N})\, Q(y_{k,M})\, L_{j,N}(y_{k,M}). \end{aligned} \tag{4.3.37}$$

Therefore, *cf.* (4.3.12),

$$\begin{aligned}\widetilde{K}_{i,j}\,\widetilde{K}_{l,m} &= \sum_{k=1}^{M}\sum_{n=1}^{M} w_{k,M}\, w_{n,M}\, P(x_{i,N})\, P(x_{l,N})\, Q(y_{k,M})\, Q(y_{n,M})\, L_{j,N}(y_{k,M})\, L_{m,N}(y_{n,M}) \\ &= \widetilde{K}_{l,j}\,\widetilde{K}_{i,m}. \end{aligned} \tag{4.3.38}$$

Since the entries of $\widetilde{\mathbf{K}}_{M,N}$ satisfy the same relationship as those of $\mathbf{K}_{M,N}$, the eigenvalues of $\widetilde{\mathbf{K}}_{M,N}$, denoted by Λ, are given by (*cf.* (4.3.13))

$$\det(\widetilde{\mathbf{K}}_{M,N} - \Lambda \mathbf{I}_N) = (-\Lambda)^{N-1}\left(\sum_{i=1}^{N}\widetilde{K}_{i,i} - \Lambda\right) = 0 \tag{4.3.39}$$

and the eigenvalues of $\mathbf{I}_N - \lambda\widetilde{\mathbf{K}}_{M,N}$, denoted by $\widetilde{\Lambda}$, are given by (*cf.* (4.3.15))

$$\det(\mathbf{I}_N - \lambda\widetilde{\mathbf{K}}_{M,N} - \widetilde{\Lambda}\mathbf{I}_N) = (1-\widetilde{\Lambda})^{N-1}\left(1 - \widetilde{\Lambda} - \lambda\sum_{i=1}^{N}\widetilde{K}_{i,i}\right) = 0. \tag{4.3.40}$$

The effect on the numerical solution $\widetilde{u}_{M,N}(x)$ in (4.3.35) as $\lambda \to \lambda_0$ follows in the same way as shown for the CNM by (4.3.20)–(4.3.29). Therefore, for λ given as in (4.3.23), the INM error satisfies

$$\|u - \widetilde{u}_{M,N}\| \sim O(\epsilon^{-1}), \qquad \text{as } |\epsilon| \to 0, \tag{4.3.41}$$

so that

$$\|u - \widetilde{u}_{M,N}\| \to \infty, \qquad \text{as } \lambda \to \lambda_0. \tag{4.3.42}$$

4.3.2.2 Barycentric Interpolated Nyström Method

Figures 2.5.1–2.5.4 demonstrate that, when Lagrange interpolation (2.1.1) is replaced by its barycentric counterpart (2.1.13), approximations of equivalent accuracy are obtained whilst the computational workload is significantly reduced. The computational efficiency of the INM can therefore be improved by replacing $\mathcal{L}_N$ in (4.3.30) by the barycentric operator $\mathcal{B}_N^{(2)}$, defined in (2.1.13), so that $\mathcal{K}\,u$ is approximated by

$$\mathcal{K}\,u \approx \mathcal{K}_M\,\mathcal{B}_N^{(2)}\,u = (\mathcal{K}_M\,\mathcal{B}_N^{(2)}\,u)(x) = \sum_{j=1}^{M}\left(\frac{\displaystyle\sum_{k=1}^{N}\frac{w_{j,M}\,W_{k,N}\,K(x,y_{j,M})\,u(x_{k,N})}{y_{j,M}-x_{k,N}}}{\displaystyle\sum_{l=1}^{N}\frac{W_{l,N}}{y_{j,M}-x_{l,N}}}\right) \tag{4.3.43}$$

using which (4.3.31) is adjusted to

$$\widetilde{u}_{M,N}(x) - \lambda\sum_{j=1}^{M}\left(\frac{\displaystyle\sum_{k=1}^{N}\frac{w_{j,M}\,W_{k,N}\,K(x,y_{j,M})\,\widetilde{u}_{M,N}(x_{k,N})}{y_{j,M}-x_{k,N}}}{\displaystyle\sum_{l=1}^{N}\frac{W_{l,N}}{y_{j,M}-x_{l,N}}}\right) = f(x). \tag{4.3.44}$$

Collocating (4.3.44) at the interpolation nodes $x_{i,N}$, $i = 1(1)N$, and interchanging the subscripts j and k then gives the matrix-vector equation

$$(\mathbf{I}_N - \lambda\,\widetilde{\mathbf{K}}_{M,N}^{\mathbf{B}})\,\widetilde{\mathbf{u}}_{M,N} = \widetilde{\mathbf{f}}_N, \tag{4.3.45}$$

wherein $\widetilde{\mathbf{u}}_{M,N}$ and $\widetilde{\mathbf{f}}_N$ are given by (4.3.34) and $\widetilde{\mathbf{K}}_{M,N}^{\mathbf{B}}$ is computed by

$$\{\widetilde{\mathbf{K}}_{M,N}^{\mathbf{B}}\}_{i,j} = \sum_{k=1}^{M}\left(\frac{w_{k,M}\,W_{j,N}\,K(x_{i,N},y_{k,M})}{\displaystyle\sum_{l=1}^{N}\frac{W_{l,N}\,(y_{k,M}-x_{j,N})}{y_{k,M}-x_{l,N}}}\right) \tag{4.3.46}$$

which is implicitly dependent on M and N. Note that, by construction, (4.3.34) and (4.3.46) yield $\widetilde{\mathbf{K}}_{M,N} \equiv \widetilde{\mathbf{K}}_{M,N}^{\mathbf{B}}$. Inversion of (4.3.45) yields the nodal elements

$\widetilde{u}_{M,N}(x_{j,N})$, $j = 1(1)N$, which are used to form the *barycentric INM* inversion formula

$$\widetilde{u}_{M,N}(x) = f(x) + \lambda \sum_{k=1}^{M} \left(\frac{\displaystyle\sum_{j=1}^{N} \frac{w_{k,M}\, W_{j,N}\, K(x, y_{k,M})\, \widetilde{u}_{M,N}(x_{j,N})}{y_{k,M} - x_{j,N}}}{\displaystyle\sum_{l=1}^{N} \frac{W_{l,N}}{y_{k,M} - x_{l,N}}} \right), \tag{4.3.47}$$

and the *barycentric Lagrange-INM* approximation

$$\widetilde{u}_{M,N}(x) = \frac{\displaystyle\sum_{j=1}^{N} \frac{W_{j,N}\, \widetilde{u}_{M,N}(x_{j,N})}{x - x_{j,N}}}{\displaystyle\sum_{j=1}^{N} \frac{W_{j,N}}{x - x_{j,N}}}. \tag{4.3.48}$$

Since (4.3.45)–(4.3.48) are undefined if $y_{k,M} = x_{j,N}$ for any $k = 1(1)M$ and $j = 1(1)N$, the interpolation nodes and quadrature nodes must be chosen so that they do not coincide. Table 4.1 shows the common nodes between the quadrature and interpolation distributions, and hence demonstrates the combination of node sets that cannot be used within the barycentric INM.

$x_{j,N}$ \ $y_{k,M}$	Gauss-Legendre	Legendre-Gauss-Radau	Legendre-Gauss-Lobatto
Regular	$x_{\frac{N+1}{2},N} = y_{\frac{M+1}{2},M} = 0,$ $\forall M,\ N$ odd	$x_{1,N} = y_{1,M} = -1$ or $x_{N,N} = y_{M,M} = 1$ $\forall M,\ N$	$x_{1,N} = y_{1,M} = -1$ and $x_{N,N} = y_{M,M} = 1$ $\forall M,\ N$
Chebyshev	$x_{\frac{N+1}{2},N} = y_{\frac{M+1}{2},M} = 0,$ $\forall M,\ N$ odd	$x_{j,N} \neq y_{k,M}$ $\forall j,\ k,\ M,\ N$	$x_{\frac{N+1}{2},N} = y_{\frac{M+1}{2},M} = 0,$ $\forall M,\ N$ odd
Chebyshev-Gauss-Lobatto	$x_{\frac{N+1}{2},N} = y_{\frac{M+1}{2},M} = 0,$ $\forall M,\ N$ odd	$x_{1,N} = y_{1,M} = -1$ or $x_{N,N} = y_{M,M} = 1$ $\forall M,\ N$	$x_{1,N} = y_{1,M} = -1$ and $x_{N,N} = y_{M,M} = 1$ $\forall M,\ N$

Table 4.1: Summary of coincident nodes between the quadrature and interpolation distributions; when there is a node in common the distributions cannot be used together within the barycentric INM.

Table 4.1 shows that, if Gauss-Legendre quadrature is used, M and N must either both be even or of different parity. When Legendre-Gauss-Radau quadrature is used only the Chebyshev nodes can be used for interpolation and, when Legendre-Gauss-Lobatto quadrature is used, only the Chebyshev nodes can be used for interpolation and M and N must either both be even or of different parity.

4.3.3 Numerical Experiments

The CNM, INM and Lagrange-INM thus described are now validated on a quartet of test problems with known solutions, three of which are chosen to test the theory on problems with potentially challenging solutions. The components of the FIE2 (4.3.1) for the test problems are summarised in Table 4.2.

Problem	Name	Solution $u(x)$	Kernel $K(x,y)$	λ
1	Smooth	$\cos x - 2x + 1$	$(3x+2)(y+1)$	$\frac{1}{10}$
2	Runge	$\frac{1}{1+25x^2}$	$3x + 2 + (2x-1)(25y^2+1)$	$\frac{1}{10}$
3	Steep	e^{12x}	$5xy + 2x + y$	$-\frac{1}{5}$
4	Oscillatory	$\sin 10x$	$(x^3-1)(y^5+2)$	$-\frac{1}{3}$

Table 4.2: Test problems with solutions of four qualitatively distinct forms. The Runge function [27, Eq. 4.9] in problem 2 has been shown in Figures 2.5.8–2.5.10 to be challenging to approximate and the extreme gradient and highly oscillatory solutions of problems 3 and 4 also offer well-documented challenges to approximation methods (see e.g. [21, 72]). The source function $f(x)$ is readily computed directly from (4.3.1).

In order for systems of the same dimension to be compared, in the following examples $M = N$ in both the CNM and INM so that both methods use N quadrature nodes and N collocation nodes. Gauss-Legendre quadrature is used within the INM due to its maximal degree of precision and Lagrange interpolation is used since the barycentric INM implementation is restricted; see Table 4.1.

Figure 4.3.1 shows the CNM errors $e_N = \|u - u_N\|$ computed using a selection of quadrature nodes and the INM and Lagrange-INM errors $e_N = \|u - \widetilde{u}_{N,N}\|$ computed using a selection of interpolation nodes.

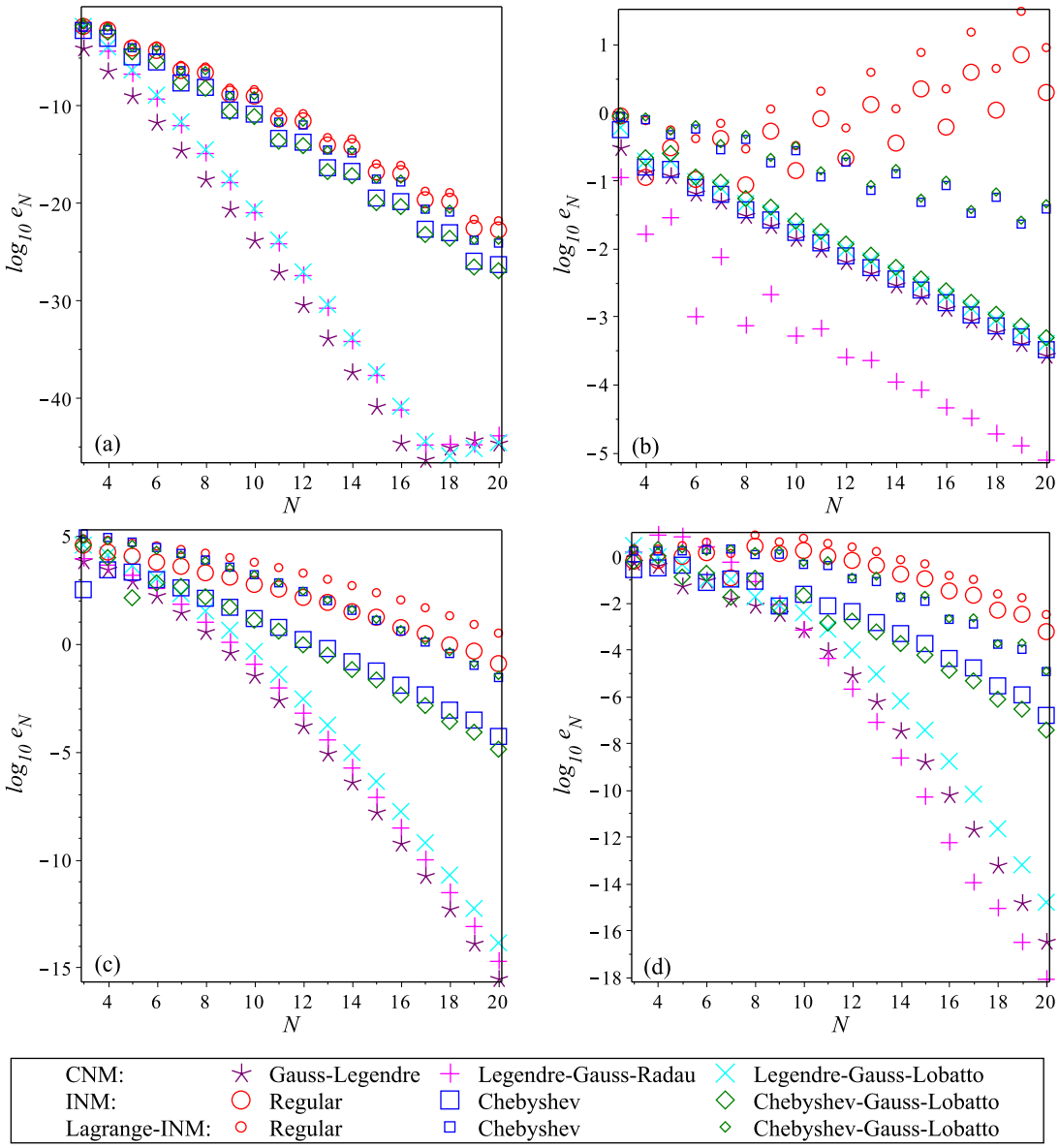

Figure 4.3.1: Spectral convergence of the CNM errors $e_N = \|u - u_N\|$, INM and Lagrange-INM errors $e_N = \|u - \widetilde{u}_{N,N}\|$ for Problems (a) 1 ("smooth"), (b) 2 ("Runge"), (c) 3 ("steep") and (d) 4 ("oscillatory") using a variety of node sets.

The disparate vertical scales of the sub-plots in Figure 4.3.1 demonstrate that, as expected, the error convergence is fastest for the smooth problem and slowest for the Runge problem, whilst the steep and oscillatory problems have errors of similar magnitude. The superior performance of the CNM is evident; however, contrary to the asymptotic convergence rate (3.2.21) for the quadrature error, the magnitudes

of the CNM errors do not always increase with ν for a given N. For example, it is the Gauss-Radau CNM that is the most accurate for problems 2 and 4. The errors obtained by the CNM for problem 1 are seen to increase slowly for $N > 17$ as calculations reach the roundoff plateau of the machine, wherein the marginally positive gradient reflects an accumulation of rounding errors as larger matrices are processed.

It was noted, following (4.3.36), that the error in a numerical solution of an FIE2 is increased by the introduction of Lagrange interpolation, therefore the convergence of the INM is slower than that of the CNM. However, despite being slower, spectral convergence with increasing N is achieved for the INM, as required by its intended extension to solve IDEs. Lagrange interpolation is inevitable in the extension to IDEs since it is the basis of the differentiation matrices introduced in Section 3.1. Figure 4.3.1 also shows that for each problem, and on each node set, the INM is uniformly more accurate than the Lagrange-INM, demonstrating that a Nyström-type inversion formula is more accurate than the standard Lagrange interpolation formula. Whether or not the INM or Lagrange-INM is used, the Runge phenomenon always plagues the solution of problem 2 on the regular nodes, causing divergence of the errors with increasing N; this is expected from the divergent errors shown in Figure 2.5.8 for Lagrange interpolation of the Runge function. Although the CNM, INM and Lagrange-INM on the orthogonal-polynomial nodal distributions do not fail to approximate the Runge function, the resulting errors are greater in magnitude than those of the other test problems; this is demonstrated by comparing the vertical scales of the subplots in Figure 4.3.1. Furthermore, Figure 4.3.1(b) shows that, when approximating the Runge function, the Gauss-Legendre CNM and Legendre-Gauss-Lobatto CNM no longer have superiority over the INM on the Chebyshev and Chebyshev-Gauss-Lobatto distributions; an explanation for this observation, based on asymptotic error estimates, is given in Section 4.4.3.

The error distribution in $[-1, 1]$ of the numerical methods is now considered. The errors incurred in the numerical solutions of problems 3 and 4 are compared against x; observations for problems 1 and 2 are qualitatively similar. The subsequent error analysis in Section 4.4.1 shows that the CNM error can be written in the form

$$u(x) - u_N(x) = \sum_{j=1}^{N} A_{j,N}\, K(x, y_{j,N}) + B_N \frac{\partial^{2N-\nu}}{\partial y^{2N-\nu}} \Big[K(x,y)u(y) \Big]_{y=\xi}, \qquad (4.3.49)$$

in which $\xi \in (-1,1)$ is an unknown constant and $A_{j,N}$, $j = 1(1)N$ and B_N are also constants. For problem 3, (4.3.49) gives

$$\begin{aligned} u(x) - u_N(x) &= (5x+1)\sum_{j=1}^{N} A_{j,N}\, y_{j,N} + 2x\sum_{j=1}^{N} A_{j,N} \\ &\quad + B_N\, x\, \frac{\partial^{2N-\nu}}{\partial y^{2N-\nu}}\Big[(5y+2)\,\mathrm{e}^{12y}\Big]_{y=\xi} + B_N \frac{\partial^{2N-\nu}}{\partial y^{2N-\nu}}\Big[y\,\mathrm{e}^{12y}\Big]_{y=\xi} \\ &= a_N x + b_N, \end{aligned} \tag{4.3.50}$$

for constants $|a_N| \ll 1$ and $|b_N| \ll 1$, whilst for problem 4 (4.3.49) gives

$$\begin{aligned} u(x) - u_N(x) &= (x^3-1)\sum_{j=1}^{N} A_{j,N}\,(y_{j,N}^5 + 2) \\ &\quad + B_N(x^3-1)\frac{\partial^{2N-\nu}}{\partial y^{2N-\nu}}\Big[(y^5+2)\sin 10y\Big]_{y=\xi} \\ &= c_N(x^3-1), \end{aligned} \tag{4.3.51}$$

for the constant $|c_N| \ll 1$. Therefore, (4.3.50) and (4.3.51) show that the variation of the error against x for the CNM is dependent upon the x component of the kernel $K(x,y)$. The error formulae (4.3.50) and (4.3.51) are verified in Figure 4.3.2.

The ensuing error analysis in Section 4.4.2 shows that the INM error can be written in the form

$$u(x) - \widetilde{u}_{N,N}(x) = \sum_{j=1}^{N} \widetilde{A}_{j,N,N}\, K(x, y_{j,N}) + \widetilde{B}_N \frac{\partial^{2N-\nu}}{\partial y^{2N-\nu}}\Big[K(x,y)u(y)\Big]_{y=\xi}, \tag{4.3.52}$$

in which $\xi \in (-1,1)$ is an unknown constant and $\widetilde{A}_{j,N,N}$, $j = 1(1)N$ and $\widetilde{B}_N$ are also constants. Comparison of (4.3.52) with (4.3.49) shows that for problem 3 the INM error is also a linear function of x so that

$$u(x) - \widetilde{u}_{N,N}(x) = \widetilde{a}_N x + \widetilde{b}_N, \tag{4.3.53}$$

for the unknown constants $|\widetilde{a}_N| \ll 1$ and $|\widetilde{b}_N| \ll 1$, and for problem 4 the INM error is of the form

$$u(x) - \widetilde{u}_{N,N}(x) = \widetilde{c}_N(x^3-1) \tag{4.3.54}$$

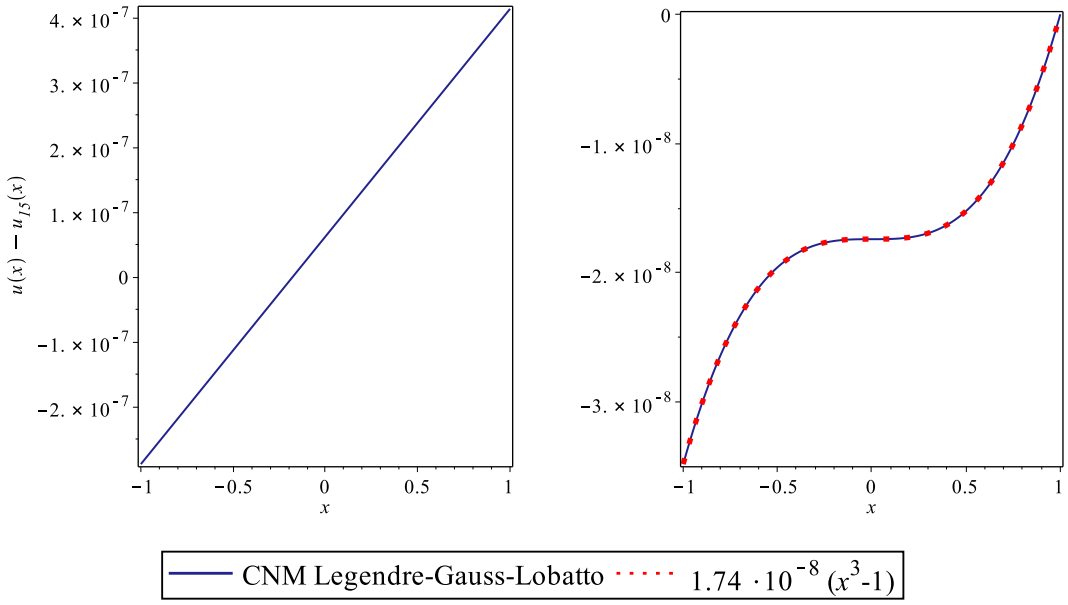

Figure 4.3.2: The CNM errors $u(x) - u_N(x)$ on the interval $[-1, 1]$ for problem 3 (left) and problem 4 (right) evaluated with $N = 15$. The error for problem 3 is linear, as predicted by (4.3.50) in which $a_N \approx 3.51 \cdot 10^{-7}$ and $b_N \approx 6.30 \cdot 10^{-8}$, whilst the problem 4 error, by comparison to the dotted line, is proportional to $(x^3 - 1)$ as predicted by (4.3.51) in which $c_N \approx 1.74 \cdot 10^{-8}$. The magnitudes of the constants a_N, b_N, c_N are therefore confirmed to be much smaller than 1. Such accurate and informative error predictions are possible through the subsequent theory of Section 4.4.1.

for the constant $|\widetilde{c}_N| \ll 1$. Therefore the INM error is also shown to be dependent upon the x component of the kernel $K(x, y)$. The error formulae (4.3.53) and (4.3.54) are verified in Figure 4.3.3.

The Lagrange-INM error is now considered. Since, through inversion of the system (4.3.33), the nodal values satisfy $\widetilde{u}_{N,N}(x_{i,N}) \approx u(x_{i,N})$, Lagrange interpolation of the exact and numerical nodal values yields $\mathcal{L}_N \widetilde{u}_{N,N} \approx \mathcal{L}_N u$. Therefore $u - \mathcal{L}_N \widetilde{u}_{N,N} \approx u - \mathcal{L}_N u$ and hence, by (2.4.1), the x dependence of the Lagrange-INM error is proportional to a perturbation of the monic polynomial $p_N(x)$ in (2.1.3) with roots at the interpolation nodes $x_{j,N}$, $j = 1(1)N$. This is verified in Figure 4.3.4 wherein the Lagrange-INM error is plotted along with the monic polynomial $p_N(x)$ for comparison.

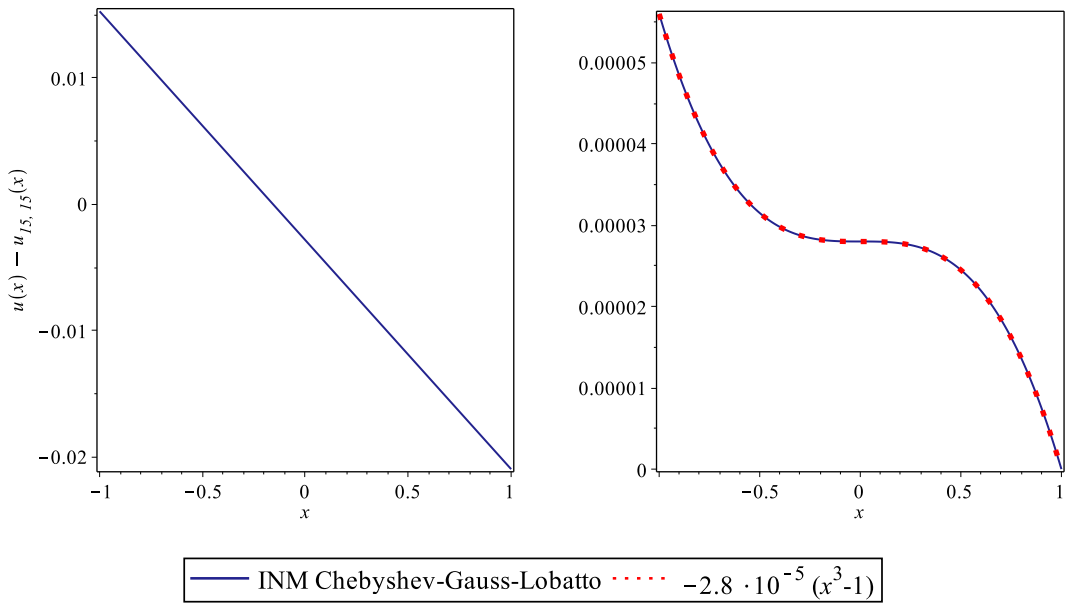

Figure 4.3.3: Result as per caption of Figure 4.3.2, for INM errors $u(x) - \widetilde{u}_{N,N}(x)$ and predictions (4.3.53) and (4.3.54), in which $\widetilde{a}_N \approx -0.018$, $\widetilde{b}_N \approx -0.0028$ and $\widetilde{c}_N \approx -2.8 \cdot 10^{-5}$ thereby confirming $|\widetilde{a}_N|$, $|\widetilde{b}_N|$, $|\widetilde{c}_N| \ll 1$. These error predictions are possible through the theory of Section 4.4.2.

The numerical experiments conducted thus far are computed with $M = N$ within the INM. It has been shown that the errors $\|u - \widetilde{u}_{N,N}\|$ decrease with increasing N; the exception to this is the regular nodes INM for problem 2. The INM errors $\|u - \widetilde{u}_{M,N}\|$ are now considered for $M \neq N$ to determine the extent to which the errors are dependent upon the M quadrature nodes and N interpolation nodes. Figure 4.3.5 shows the problem 1 errors $e_{M,N} = \|u - \widetilde{u}_{M,N}\|$ against M for fixed values of N solved on the Chebyshev-Gauss-Lobatto nodes; the results are qualitatively similar using alternative interpolation node sets.

Figure 4.3.5 demonstrates that, provided M is sufficiently high, the INM errors are dictated by N, since for each N the errors are approximately constant for $M \geq \frac{N}{2}$. This is consistent with the M-node quadrature and N-node Lagrange interpolation errors which, by (3.2.20) and Table 2.1, are seen to have leading-order terms of order $\left(\frac{\mathrm{e}}{4M}\right)^{2M}$ and $\left(\frac{\mathrm{e}}{2N}\right)^{N}$ respectively, provided that the derivatives of $u(x)$ and $K(x,y)\,u(y)$ do not grow exponentially. Therefore when $M = \frac{N}{2}$ the quadrature error and the interpolation error are of comparable accuracy and so the magnitudes

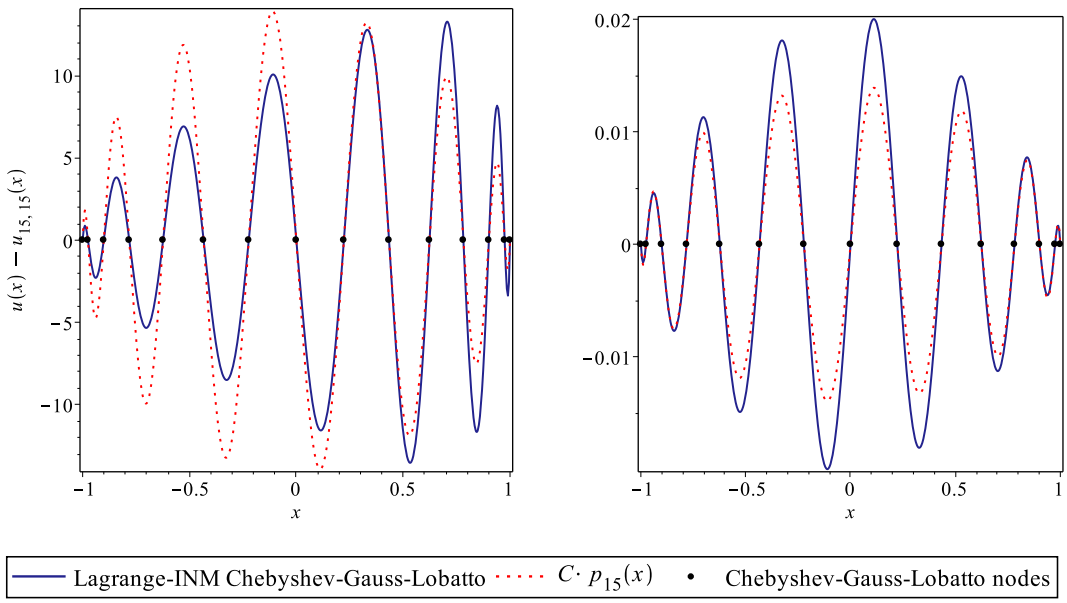

Figure 4.3.4: The Lagrange-INM errors $u(x) - \widetilde{u}_{N,N}(x)$ on the interval $[-1, 1]$ for problem 3 (left) and problem 4 (right) evaluated with $N = 15$. The errors are shown to be oscillatory with roots near those of the scaled monic polynomial $p_N(x)$, where the scaling factors are respectively $C = -1$ (left) and $C = 0.001$ (right). The Lagrange-INM error is seen to be approximately 0 at the interpolation nodes; its greatest magnitude at a node is $|u(x_{N,N}) - \widetilde{u}_{N,N}(x_{N,N})| \approx 0.021$ for problem 3 and $|u(x_{1,N}) - \widetilde{u}_{N,N}(x_{1,N})| \approx 5.6 \cdot 10^{-5}$ for problem 4.

of the INM errors are predominantly dependent upon M for $M < \frac{N}{2}$, and upon N for $M > \frac{N}{2}$; this verifies that it is sufficient to set $M = N$ in the INM.

The INM (4.3.35) and Lagrange-INM (4.3.36) are now compared to their barycentric counterparts (4.3.47) and (4.3.48). Problem 1 is solved using Gauss-Legendre quadrature nodes and Chebyshev-Gauss-Lobatto interpolation nodes which, by Table 4.1, requires M and N to be of different parity. Therefore, $M = N - 1$ is chosen and the resulting errors $e_N = \|u - \widetilde{u}_{N-1,N}\|$ and workloads, in seconds (s), are shown in Figure 4.3.6. For comparison, the Legendre CNM workloads are also shown in Figure 4.3.6. Observations are qualitatively similar when different quadrature and interpolation nodes are chosen.

As expected from the results shown in Figures 2.5.1–2.5.4, incorporating the barycentric implementation into the INM and Lagrange-INM has an imperceptible

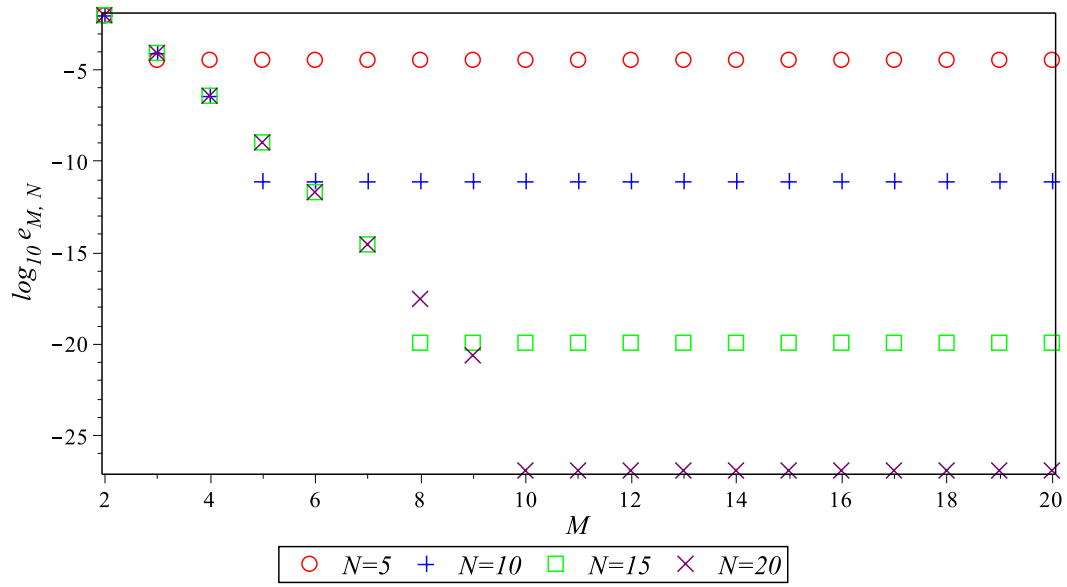

Figure 4.3.5: A logarithmic plot of the INM errors $e_{M,N} = \|u - \widetilde{u}_{M,N}\|$ for varying M and fixed N for problem 1 using Chebyshev-Gauss-Lobatto interpolation nodes.

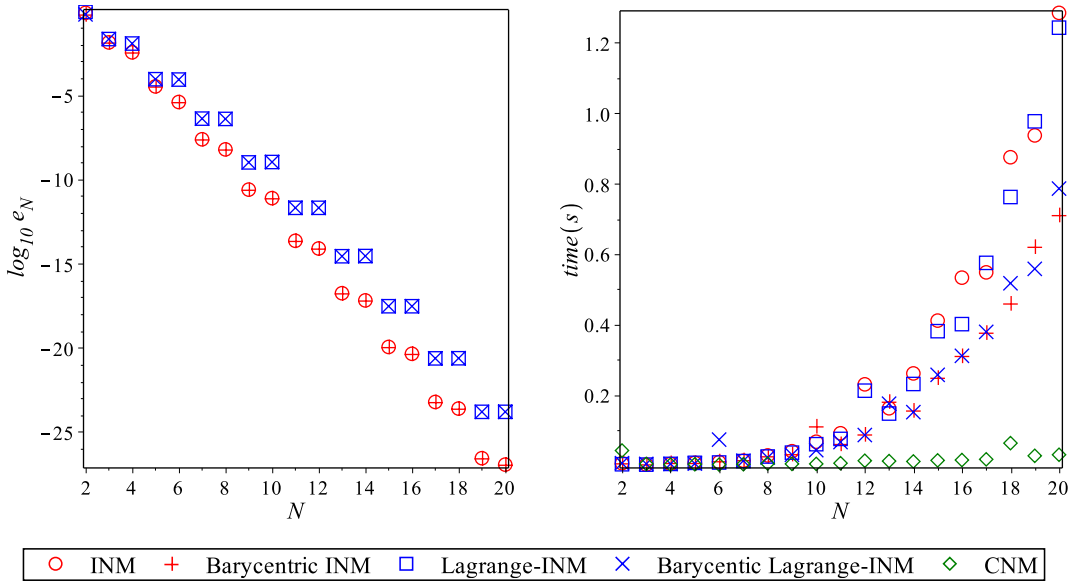

Figure 4.3.6: A comparison of errors $e_N = \|u - \widetilde{u}_{N-1,N}\|$ (left) and computational workloads, in seconds (s), (right) for the INM (4.3.35), Lagrange-INM (4.3.36) and their barycentric counterparts (4.3.47) and (4.3.48) for problem 1 solved using Gauss-Legendre quadrature nodes and Chebyshev-Gauss-Lobatto interpolation nodes. The Legendre CNM workloads are included for comparison (right).

effect on the errors whereas the workload for each N is significantly reduced. Despite this reduction, the CNM remains the most computationally efficient method as shown by the comparison of workloads in Figure 4.3.6. This is also expected since the double summation within the INM formulation causes the INM to be $O(N)$ times more computationally expensive than the CNM; this is seen by comparing (4.3.4) with (4.3.30). Figure 4.3.6 shows that the barycentric INM and barycentric Lagrange-INM have computational advantages in terms of workload over the INM and Lagrange-INM; however, since the quadrature and interpolation node combinations are limited, as shown in Table 4.1, the barycentric methods are less widely applicable.

Finally, to validate the "divergent" predictions (4.3.28) and (4.3.41), the errors as $\lambda \to \lambda_0$ are considered for problem 1 for which the singular value, computed from (4.2.15), is $\lambda_0 = \frac{1}{6}$. Figure 4.3.7 shows the CNM errors $e_N = \|u - u_N\|$ and INM errors $e_N = \|u - \widetilde{u}_{M,N}\|$, in which $M = N = 11$, plotted on a logarithmic scale against $\epsilon \equiv \lambda - \lambda_0$.

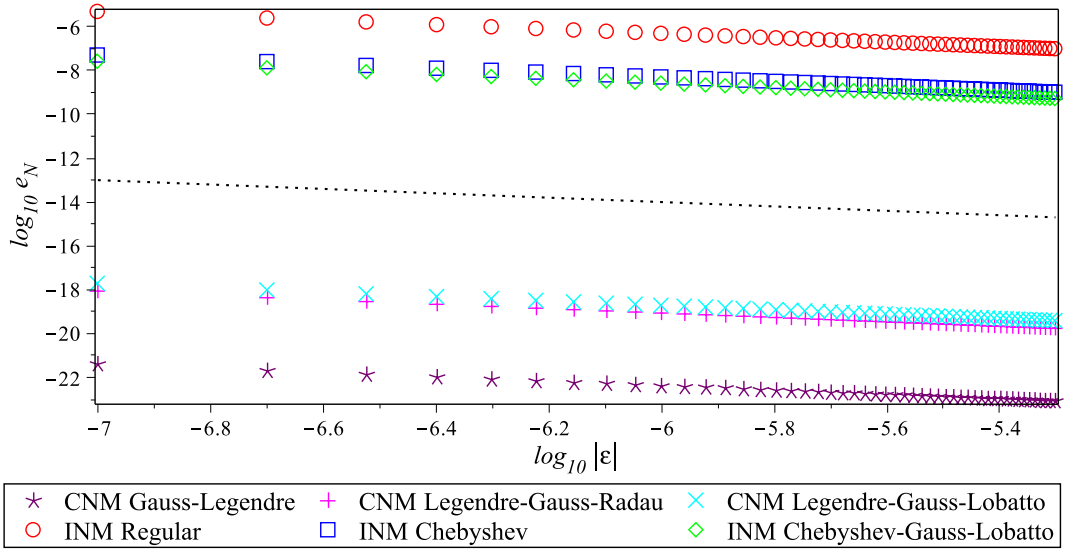

Figure 4.3.7: A logarithmic plot of the CNM errors $e_N = \|u - u_N\|$ and INM errors $e_N = \|u - \widetilde{u}_{N,N}\|$ with $N = 11$ against $\epsilon = \lambda - \lambda_0$. Here the dotted line shows a gradient of -1 thereby validating the $O(\epsilon^{-1})$ predictions of (4.3.28) and (4.3.41).

The error formulae (4.3.28) and (4.3.41) predict that both the CNM and INM errors diverge as $O(\epsilon^{-1})$ as $\epsilon \to 0$ and so, on a logarithmic scale, the errors should decrease with gradient -1 as $|\epsilon|$ increases; this is verified in Figure 4.3.7.

4.4 Error Analysis

In this section error predictions for both the classical and interpolated Nyström method are developed from existing theoretical Nyström error bounds. These error predictions differ from those given in literature which, although being theoretical, require the exact solution to be known; for example [10, Eq. 4.1.33] and [60, Eq. 4.7.16d]. That is, existing error estimates are based upon the unknown exact solution whereas in the present approach error estimates are based upon the available, numerical solution.

4.4.1 Classical Nyström Method

Subtraction of the CNM numerical solution (4.3.6) from the exact solution (4.3.2) yields the error in the form

$$u - u_M = \lambda \left(\mathcal{K} u - \mathcal{K}_M u_M \right) \tag{4.4.1}$$

which, by the addition of $\lambda \left(\mathcal{K}_M u - \mathcal{K}_M u \right) = 0$, is equivalently

$$u - u_M = \lambda \mathcal{K}_M \left(u - u_M \right) + \lambda \left(\mathcal{K} - \mathcal{K}_M \right) u. \tag{4.4.2}$$

The quadrature-error term in (3.2.13) gives

$$\left(\mathcal{K} - \mathcal{K}_M \right) u \left(x \right) = (-1)^{\nu(\nu-1)/2} \, \psi_M^{(\nu)} \, \frac{\partial^{\,2M-\nu}}{\partial y^{\,2M-\nu}} \Big[K(x,y) u(y) \Big]_{y=\xi}, \qquad -1 < \xi < 1, \tag{4.4.3}$$

whilst the action of the operator $\mathcal{K}_M$ on the error $u - u_M$ gives

$$\mathcal{K}_M \left(u - u_M \right) (x) = \sum_{j=1}^{M} w_{j,M} \, K(x, y_{j,M}) \left(u(y_{j,M}) - u_M(y_{j,M}) \right). \tag{4.4.4}$$

Therefore combining (4.4.2)–(4.4.4) gives the CNM error, as seen in (4.3.49), as

$$u(x) - u_M(x) = \sum_{j=1}^{M} A_{j,M} \, K(x, y_{j,M}) + B_M \, \frac{\partial^{\,2M-\nu}}{\partial y^{\,2M-\nu}} \Big[K(x,y) u(y) \Big]_{y=\xi}, \tag{4.4.5}$$

wherein

$$A_{j,M} = \lambda \, w_{j,M} \left(u(y_{j,M}) - u_M(y_{j,M}) \right), \qquad j = 1(1)M \tag{4.4.6}$$

and

$$B_M = \lambda\,(-1)^{\nu(\nu-1)/2}\,\psi_M^{(\nu)}, \tag{4.4.7}$$

which demonstrates that the x dependence of the error is dictated by the x component of the kernel $K(x,y)$. Rearranging (4.4.2) yields

$$u - u_M = \lambda\,(\mathcal{I} - \lambda\,\mathcal{K}_M)^{-1}\,(\mathcal{K} - \mathcal{K}_M)\,u \tag{4.4.8}$$

hence the CNM error is bounded according to

$$\|u - u_M\| \leq |\lambda|\,\left\|(\mathcal{I} - \lambda\,\mathcal{K}_M)^{-1}\right\|\,\|(\mathcal{K} - \mathcal{K}_M)\,u\|\,, \tag{4.4.9}$$

which is the standard form of the Nyström error given by [10, Eq. 4.1.33] and [60, Eq. 4.7.16d].

The immediate problem is that the error bound (4.4.9) is dependent upon the exact solution u; however, since the present work aims to develop computable error bounds based upon the numerical solution u_M, the error (4.4.1) must be manipulated in an alternative way. To this end, addition of $\lambda\,(\mathcal{K}\,u_M - \mathcal{K}\,u_M) = 0$ to (4.4.1) yields, instead of (4.4.2),

$$u - u_M = \lambda\,\mathcal{K}\,(u - u_M) + \lambda\,(\mathcal{K} - \mathcal{K}_M)\,u_M, \tag{4.4.10}$$

which can be rearranged to

$$u - u_M = \lambda\,(\mathcal{I} - \lambda\,\mathcal{K})^{-1}\,(\mathcal{K} - \mathcal{K}_M)\,u_M. \tag{4.4.11}$$

Therefore the CNM error is bounded in terms of the numerical solution u_M according to

$$\|u - u_M\| \leq |\lambda|\,\left\|(\mathcal{I} - \lambda\,\mathcal{K})^{-1}\right\|\,\|(\mathcal{K} - \mathcal{K}_M)\,u_M\| \tag{4.4.12}$$

which, by (4.3.6), is equivalently

$$\|u - u_M\| \leq \left\|(\mathcal{I} - \lambda\,\mathcal{K})^{-1}\right\|\,\|u_M - \lambda\,\mathcal{K}\,u_M - f\|\,. \tag{4.4.13}$$

Since u is the unique solution of the FIE (4.3.2), the operator $(\mathcal{I} - \lambda\,\mathcal{K})^{-1}$ in (4.4.12) and (4.4.13) exists and is bounded [83, Thm. 3.4]. The bound in (4.4.13) avoids the need to compute $\mathcal{K}_M\,u_M$ and also demonstrates, by comparison with (4.3.2), that the error is proportional to the degree to which the numerical solution u_M fails to

satisfy the exact FIE. The bound in (4.4.12) is the basis of an asymptotic analysis in Section 4.4.3.

A bound $\mathcal{F}_{M}$ for the theoretical term $\|(\mathcal{I}-\lambda\,\mathcal{K})^{-1}\|$ in (4.4.12) and (4.4.13) is given [60, Eq. 4.7.17b] as

$$\left\|(\mathcal{I}-\lambda\,\mathcal{K})^{-1}\right\| \leq \mathcal{F}_{M} \equiv \frac{1+|\lambda|\,\|(\mathcal{I}-\lambda\,\mathcal{K}_{M})^{-1}\|\,\|\mathcal{K}\|}{1-\lambda^{2}\,\|(\mathcal{I}-\lambda\,\mathcal{K}_{M})^{-1}\|\,\|(\mathcal{K}-\mathcal{K}_{M})\,\mathcal{K}\|}, \tag{4.4.14}$$

in which both the numerator and denominator are by construction positive (*cf.* [10, Thm. 4.1.1]) since the bound is derived via the geometric series theorem [14, Thm. 1.1]. Additionally, since the quadrature scheme (4.3.4) is convergent for all continuous functions then, for sufficiently large M, $(\mathcal{I}-\lambda\,\mathcal{K}_{M})^{-1}$ exists and is uniformly bounded [10, Thm. 4.1.2]. Although (4.4.14) is given by [60, Eq. 4.7.17b], and in an alternative form by [10, Thm. 4.1.1], it is in neither case developed into a computable quantity. Thus motivated, computable estimates are now developed for the three normed sub-terms in $\mathcal{F}_{M}$ defined by (4.4.14). In supremum-norm-definition form, (4.4.14) is rewritten as

$$\mathcal{F}_{M} = \frac{1+|\lambda|\,\sup\limits_{q\in[-1,1]}\dfrac{\|(\mathcal{I}-\lambda\,\mathcal{K}_{M})^{-1}\,q\|}{\|q\|}\,\sup\limits_{r\in[-1,1]}\dfrac{\|\mathcal{K}\,r\|}{\|r\|}}{1-\lambda^{2}\,\sup\limits_{q\in[-1,1]}\dfrac{\|(\mathcal{I}-\lambda\,\mathcal{K}_{M})^{-1}\,q\|}{\|q\|}\,\sup\limits_{s\in[-1,1]}\dfrac{\|(\mathcal{K}-\mathcal{K}_{M})\,\mathcal{K}\,s\|}{\|s\|}}, \tag{4.4.15}$$

in which unknown functions $\widetilde{q}$, $\widetilde{r}$, $\widetilde{s}\in[-1,1]$ give the required suprema, so that

$$\mathcal{F}_{M} = \frac{\left(\,\|\widetilde{q}\|\,\|\widetilde{r}\|+|\lambda|\,\|(\mathcal{I}-\lambda\,\mathcal{K}_{M})^{-1}\,\widetilde{q}\|\,\|\mathcal{K}\,\widetilde{r}\|\,\right)\|\widetilde{s}\|}{\left(\,\|\widetilde{q}\|\,\|\widetilde{s}\|-\lambda^{2}\,\|(\mathcal{I}-\lambda\,\mathcal{K}_{M})^{-1}\,\widetilde{q}\|\,\|(\mathcal{K}-\mathcal{K}_{M})\,\mathcal{K}\,\widetilde{s}\|\,\right)\|\widetilde{r}\|}. \tag{4.4.16}$$

Since $\widetilde{q}$, $\widetilde{r}$ and $\widetilde{s}$ are unknown, (4.4.16) must instead be computed using near-suprema functions q, r, $s\in[-1,1]$ such that

$$\left\|(\mathcal{I}-\lambda\,\mathcal{K}_{M})^{-1}\right\| \equiv \frac{\|(\mathcal{I}-\lambda\,\mathcal{K}_{M})^{-1}\,\widetilde{q}\|}{\|\widetilde{q}\|} = \frac{\|(\mathcal{I}-\lambda\,\mathcal{K}_{M})^{-1}\,q\|}{\|q\|}+\alpha\,\epsilon, \tag{4.4.17}$$

$$\|\mathcal{K}\| \equiv \frac{\|\mathcal{K}\,\widetilde{r}\|}{\|\widetilde{r}\|} = \frac{\|\mathcal{K}\,r\|}{\|r\|}+\beta\,\epsilon, \tag{4.4.18}$$

and

$$\|(\mathcal{K}-\mathcal{K}_{M})\,\mathcal{K}\| \equiv \frac{\|(\mathcal{K}-\mathcal{K}_{M})\,\mathcal{K}\,\widetilde{s}\|}{\|\widetilde{s}\|} = \frac{\|(\mathcal{K}-\mathcal{K}_{M})\,\mathcal{K}\,s\|}{\|s\|}+\gamma\,\epsilon, \tag{4.4.19}$$

wherein α, β, $\gamma \in \mathbb{R}$ are $O(1)$ constants and $0 < \epsilon \ll 1$. By (3.2.17), $\|(\mathcal{K} - \mathcal{K}_M)\,\mathcal{K}\,s\|$ is bounded by

$$\|(\mathcal{K} - \mathcal{K}_M)\,\mathcal{K}\,s\| \leq \psi_M^{(\nu)}\,\mathbb{S}_{2M-\nu}, \tag{4.4.20}$$

in which (*cf.* (3.2.18))

$$\mathbb{S}_M \equiv \max_{x,y\in[-1,1]} |\mathcal{S}_M(x,y)| \tag{4.4.21}$$

where

$$\mathcal{S}_M(x,y) \equiv \frac{\partial^M}{\partial y^M}\left(K(x,y)\int_{-1}^{1} K(y,z)\,s(z)\,dz\right). \tag{4.4.22}$$

Therefore, for sufficiently large M, provided $\mathbb{S}_{2M-\nu} \sim o(M^{2M})$, (4.4.20) reveals that

$$\|(\mathcal{K} - \mathcal{K}_M)\,\mathcal{K}\| = O(\epsilon). \tag{4.4.23}$$

Sometimes this condition is not met: for example, for the Runge-type kernel

$$K(x,y) = \frac{y-x}{1+(\alpha\,x)^2}, \tag{4.4.24}$$

the norm of successive derivatives increases rapidly (see (2.5.4)–(2.5.5)). Despite this divergence, (4.4.23) holds since [10, Eq. 4.1.19] states that $\|(\mathcal{K} - \mathcal{K}_M)\,\mathcal{K}\| \to 0$ as $M \to \infty$, provided $K(x,y)$ is continuous. That is, the right-hand side of (4.4.20) may diverge whilst the left-hand side converges; this is a result of $\mathcal{S}_M(x,y)$ being maximised over all $y \in [-1,1]$ within $\mathbb{S}_M$ whilst the true error $\|(\mathcal{K} - \mathcal{K}_M)\,\mathcal{K}\,s\|$ is given by some unknown intermediate $y = \xi \in [-1,1]$, as given in (3.2.13). Hence (4.4.16)–(4.4.23) yield

$$\mathcal{F}_M = 1 + \frac{|\lambda|\,\|(\mathcal{I} - \lambda\,\mathcal{K}_M)^{-1}\,q\|\,\|\mathcal{K}\,r\|}{\|q\|\,\|r\|} + O(\epsilon), \qquad M \to \infty. \tag{4.4.25}$$

Therefore, for appropriate near-suprema functions q and r, the computable leading-order bound $\mathcal{F}_M$ is

$$\mathcal{F}_M = 1 + \frac{|\lambda|\,\|Q_M\|\,\|\mathcal{K}\,r\|}{\|q\|\,\|r\|}, \tag{4.4.26}$$

wherein Q_M, the solution of

$$Q_M - \lambda\,\mathcal{K}_M\,Q_M = q, \tag{4.4.27}$$

can be found via the CNM, i.e. u_M and f are replaced by Q_M and q respectively in (4.3.8)–(4.3.10).

It remains to choose suitable norm-maximising functions q and r. The norm $\|\mathcal{K}\,r\|$ is considered first; this term results from approximating $\|\mathcal{K}\|$ in (4.4.14). The norm $\|\mathcal{K}\|$ has previously been defined [10, Eq. 1.2.21] as

$$\|\mathcal{K}\| = \max_{x\in[-1,1]} \int_{-1}^{1} |K(x,y)|\,dy \tag{4.4.28}$$

which differs from the standard form

$$\|\mathcal{K}\| \approx \frac{\|\mathcal{K}\,1\|}{1} = \max_{x\in[-1,1]} \left| \int_{-1}^{1} K(x,y)\,dy \right|. \tag{4.4.29}$$

The definition (4.4.28) is therefore based on the assumption that $r = 1$ and also gives a looser bound than (4.4.29) due to the modulus signs being on the integrand rather than the integral. Thus motivated, the ratio $\|\mathcal{K}\,r\| \,/\, \|r\|$ is computed using $r = 1$, which is compared to alternative choices of readily available functions $r = f$ and $r = u_{\scriptscriptstyle M}$ in Table 4.3 for the four test problems outlined in Table 4.2. In the following results, the norms $\|\mathcal{K}\,r\|$ in (4.4.26) have been computed using the standard "external" form

$$\|\mathcal{K}\,r\| = \max_{x\in[-1,1]} \left| \int_{-1}^{1} K(x,y)\,r(y)\,dy \right|, \tag{4.4.30}$$

rather than an "internal" form suggested by (4.4.28).

Problem	$r = 1$	$r = f$	$r = u_{10}$	$r = u_{15}$	$r = u_{20}$
1	10.00	1.245	3.318	3.318	3.318
2	58.00	10.77	6.470	6.560	6.547
3	4.000	1.000	0.6250	0.6250	0.6250
4	8.000	0.04385	0.1739	0.1765	0.1765

Table 4.3: Comparison of the magnitude of $\|\mathcal{K}\,r\| \,/\, \|r\|$ computed using trial functions $r = 1$, $r = f$ and $r = u_{\scriptscriptstyle M}$, computed using Gauss-Legendre nodes, for $M = 10$, 15, 20. For all problems $\|\mathcal{K}\,r\| \,/\, \|r\|$ is maximised using $r = 1$.

Table 4.3 shows that $\|\mathcal{K}\,r\| \,/\, \|r\|$ is maximised for all four test problems when $r = 1$ and so this choice of r is used in the error factor $\mathcal{F}_{\scriptscriptstyle M}$ in (4.4.26); in this case, $\|\mathcal{K}\|$ is computed by (4.4.29) directly.

The remaining unknown norm $\|Q_{\scriptscriptstyle M}\| \equiv \|(\mathcal{I} - \lambda\,\mathcal{K}_{\scriptscriptstyle M})^{-1}\,q\|$ in (4.4.26) is approximated in a similar way. The M-dependent ratio $\|Q_{\scriptscriptstyle M}\| \,/\, \|q\|$ is computed using $q = 1$,

$q = f$ and $q = u_M$ for the four test problems outlined in Table 4.2. Note that when $q = f$, (4.3.6) and (4.4.27) are equivalent and so $Q_M = u_M$. The computed ratios $\|Q_M\| / \|q\|$ for various functions q, using Gauss-Legendre nodes, i.e. $\nu = 0$, are presented in Table 4.4 for $M = 10, 15, 20$; results for $\nu = 1, 2$ are qualitatively similar.

	$M = 10$			$M = 15$			$M = 20$		
Problem	$q = 1$	$q = f$	$q = u_M$	$q = 1$	$q = f$	$q = u_M$	$q = 1$	$q = f$	$q = u_M$
1	3.500	0.9378	0.9048	3.500	0.9378	0.9048	3.500	0.9378	0.9048
2	2.162	0.9132	0.9642	2.162	0.9148	0.9652	2.162	0.9146	0.9651
3	1.581	0.8889	0.9306	1.581	0.8889	0.9306	1.581	0.8889	0.9306
4	9.286	0.9586	1.167	9.286	0.9581	1.169	9.286	0.9581	1.169

Table 4.4: Comparison of the magnitude of $\|Q_M\| / \|q\|$ computed via (4.4.27) and the CNM using Gauss-Legendre nodes, for various choices of q. For all problems, $\|Q_M\| / \|q\|$ is maximised using $q = 1$; the dependence on M is moreover observed to be minimal.

Table 4.4 shows that $\|Q_M\| / \|q\|$ converges with increasing M for a given q, although the change with M is minimal. It is also evident that $\|Q_M\| / \|q\|$ is maximised when $q = 1$ therefore this is henceforth used within the error factor $\mathcal{F}_M$.

Since Tables 4.3 and 4.4 have shown $q = 1$ and $r = 1$ are suitable bound-maximising functions to use within the error factor $\mathcal{F}_M$, (4.4.26) becomes

$$\mathcal{F}_M = 1 + |\lambda| \, \|Q_M\| \, \|\mathcal{K}(1)\| , \tag{4.4.31}$$

wherein Q_M is the solution of

$$Q_M - \lambda \mathcal{K}_M Q_M = 1. \tag{4.4.32}$$

The theoretical bound (4.4.13) for the CNM has therefore been developed into the computable bound

$$\|u - u_M\| \leq \mathcal{F}_M \, \|u_M - \lambda \mathcal{K} u_M - f\| , \tag{4.4.33}$$

wherein $\mathcal{F}_M$ is computed by (4.4.31) and the term it multiplies can be computed directly from only the numerical solution u_M. The advantage of (4.4.33) over existing error bounds is that it does not depend upon the exact solution u, which is the very objective of error estimates.

4.4.2 Interpolated Nyström Method

The error analysis for the INM follows in a similar way to that of the CNM. Subtraction of the INM numerical solution (4.3.32) from the exact solution (4.3.2) gives the error as

$$u - \widetilde{u}_{M,N} = \lambda \left(\mathcal{K}\, u - \mathcal{K}_M\, \mathcal{L}_N\, \widetilde{u}_{M,N} \right) \tag{4.4.34}$$

which, by the addition of $\lambda \left(\mathcal{K}_M\, u - \mathcal{K}_M\, u + \mathcal{K}_M\, \mathcal{L}_N\, u - \mathcal{K}_M\, \mathcal{L}_N\, u \right) = 0$, can be rewritten as

$$u - \widetilde{u}_{M,N} = \lambda\, \mathcal{K}_M\, \mathcal{L}_N \left(u - \widetilde{u}_{M,N} \right) + \lambda\, \mathcal{K}_M \left(\mathcal{I} - \mathcal{L}_N \right) u + \lambda \left(\mathcal{K} - \mathcal{K}_M \right) u. \tag{4.4.35}$$

The quadrature error $\left(\mathcal{K} - \mathcal{K}_M \right) u$ is given by (4.4.3), whilst the action of the operator $\mathcal{K}_M$ in (4.3.4) acting upon the Lagrange interpolation error (2.4.1) is given by

$$\mathcal{K}_M \left(\mathcal{I} - \mathcal{L}_N \right) u\,(x) = \frac{u^{(N)}(\xi)}{N!} \sum_{j=1}^{M} w_{j,M}\, K(x, y_{j,M})\, p_N(y_{j,M}), \qquad \xi \in (-1, 1). \tag{4.4.36}$$

The action of the combined operator $\mathcal{K}_M\, \mathcal{L}_N$ acting upon the error $u - \widetilde{u}_{M,N}$ is given by (4.3.30) as

$$\mathcal{K}_M\, \mathcal{L}_N \left(u - \widetilde{u}_{M,N} \right)(x) = \sum_{j=1}^{M} \sum_{k=1}^{N} w_{j,M}\, K(x, y_{j,M})\, L_{k,N}(y_{j,M}) \left(u(x_{k,N}) - \widetilde{u}_{M,N}(x_{k,N}) \right). \tag{4.4.37}$$

Therefore, by (4.4.3), (4.4.36) and (4.4.37), the INM error (4.4.35) can be written, as seen in (4.3.52), as

$$u(x) - \widetilde{u}_{M,N}(x) = \sum_{j=1}^{M} \widetilde{A}_{j,M,N}\, K(x, y_{j,M}) + \widetilde{B}_M\, \frac{\partial^{2M-\nu}}{\partial y^{2M-\nu}} \Big[K(x, y) u(y) \Big]_{y=\xi}, \tag{4.4.38}$$

wherein, for $j = 1(1)M$,

$$\widetilde{A}_{j,M,N} = \lambda\, w_{j,M} \left(\frac{u^{(N)}(\xi)\, p_N(y_{j,M})}{N!} + \sum_{k=1}^{N} L_{k,N}(y_{j,M}) \left(u(x_{k,N}) - \widetilde{u}_{M,N}(x_{k,N}) \right) \right) \tag{4.4.39}$$

and

$$\widetilde{B}_M = \lambda\, (-1)^{\nu(\nu-1)/2}\, \psi_M^{(\nu)}, \tag{4.4.40}$$

which shows that the x component of the kernel $K(x,y)$ fully determines the x dependence of the INM error. Rearranging (4.4.35) yields the error as

$$u - \widetilde{u}_{M,N} = \lambda \left(\mathcal{I} - \lambda \mathcal{K}_M \mathcal{L}_N\right)^{-1} \Big(\mathcal{K}_M \left(\mathcal{I} - \mathcal{L}_N\right) u + \left(\mathcal{K} - \mathcal{K}_M\right) u \Big), \tag{4.4.41}$$

with bound given by

$$\|u - \widetilde{u}_{M,N}\| \leq |\lambda| \left\|\left(\mathcal{I} - \lambda \mathcal{K}_M \mathcal{L}_N\right)^{-1}\right\| \left\|\mathcal{K}_M \left(\mathcal{I} - \mathcal{L}_N\right) u + \left(\mathcal{K} - \mathcal{K}_M\right) u\right\|, \tag{4.4.42}$$

which simplifies to

$$\|u - \widetilde{u}_{M,N}\| \leq |\lambda| \left\|\left(\mathcal{I} - \lambda \mathcal{K}_M \mathcal{L}_N\right)^{-1}\right\| \left\|\left(\mathcal{K} - \mathcal{K}_M \mathcal{L}_N\right) u\right\|. \tag{4.4.43}$$

To develop a different bound to (4.4.43) that is independent of the exact solution u, $\lambda \left(\mathcal{K} \widetilde{u}_{M,N} - \mathcal{K} \widetilde{u}_{M,N} + \mathcal{K}_M \widetilde{u}_{M,N} - \mathcal{K}_M \widetilde{u}_{M,N}\right) = 0$ is added to (4.4.34) to give

$$u - \widetilde{u}_{M,N} = \lambda \mathcal{K} \left(u - \widetilde{u}_{M,N}\right) + \lambda \left(\mathcal{K} - \mathcal{K}_M\right) \widetilde{u}_{M,N} + \lambda \mathcal{K}_M \left(\mathcal{I} - \mathcal{L}_N\right) \widetilde{u}_{M,N} \tag{4.4.44}$$

which can be rearranged to

$$u - \widetilde{u}_{M,N} = \lambda \left(\mathcal{I} - \lambda \mathcal{K}\right)^{-1} \Big(\left(\mathcal{K} - \mathcal{K}_M\right) \widetilde{u}_{M,N} + \mathcal{K}_M \left(\mathcal{I} - \mathcal{L}_N\right) \widetilde{u}_{M,N} \Big). \tag{4.4.45}$$

Therefore (4.4.45) yields the INM error bound

$$\|u - \widetilde{u}_{M,N}\| \leq |\lambda| \left\|\left(\mathcal{I} - \lambda \mathcal{K}\right)^{-1}\right\| \left\|\left(\mathcal{K} - \mathcal{K}_M\right) \widetilde{u}_{M,N} + \mathcal{K}_M \left(\mathcal{I} - \mathcal{L}_N\right) \widetilde{u}_{M,N}\right\| \tag{4.4.46}$$

which simplifies to

$$\|u - \widetilde{u}_{M,N}\| \leq |\lambda| \left\|\left(\mathcal{I} - \lambda \mathcal{K}\right)^{-1}\right\| \left\|\left(\mathcal{K} - \mathcal{K}_M \mathcal{L}_N\right) \widetilde{u}_{M,N}\right\| \tag{4.4.47}$$

which, by (4.3.32), is equivalently

$$\|u - \widetilde{u}_{M,N}\| \leq \left\|\left(\mathcal{I} - \lambda \mathcal{K}\right)^{-1}\right\| \left\|\widetilde{u}_{M,N} - \lambda \mathcal{K} \widetilde{u}_{M,N} - f\right\|. \tag{4.4.48}$$

The bound (4.4.48) avoids computation of $\mathcal{K}_M \mathcal{L}_N \widetilde{u}_{M,N}$ and is interpreted in the same way as the CNM bound (4.4.13); that is, by comparison with (4.3.2), the INM error is directly proportional to the degree to which $\widetilde{u}_{M,N}$ fails to satisfy the exact FIE. The bound (4.4.46) is used in the asymptotic analysis of Section 4.4.3.

The theoretical term $\|(\mathcal{I}-\lambda\,\mathcal{K})^{-1}\|$ within (4.4.46)–(4.4.48) is bounded by $\widetilde{\mathcal{F}}_{M,N}$, which is found by replacing $\mathcal{K}_M$ with $\mathcal{K}_M\,\mathcal{L}_N$ throughout (4.4.14) to yield

$$\left\|(\mathcal{I}-\lambda\,\mathcal{K})^{-1}\right\| \leq \widetilde{\mathcal{F}}_{M,N} \equiv \frac{1+|\lambda|\,\|(\mathcal{I}-\lambda\,\mathcal{K}_M\,\mathcal{L}_N)^{-1}\|\,\|\mathcal{K}\|}{1-\lambda^2\,\|(\mathcal{I}-\lambda\,\mathcal{K}_M\,\mathcal{L}_N)^{-1}\|\,\|(\mathcal{K}-\mathcal{K}_M\,\mathcal{L}_N)\,\mathcal{K}\|}. \tag{4.4.49}$$

The development of the theoretical bound (4.4.49) into a computable quantity is analogous to the analysis shown for the CNM in Section 4.4.1 for the bound (4.4.31). Therefore $\widetilde{\mathcal{F}}_{M,N}$ is computed as

$$\widetilde{\mathcal{F}}_{M,N} = 1+|\lambda|\,\left\|\widetilde{Q}_{M,N}\right\|\,\|\mathcal{K}\,(1)\|\,, \tag{4.4.50}$$

wherein $\widetilde{Q}_{M,N}$ is the solution of

$$\widetilde{Q}_{M,N}-\lambda\,\mathcal{K}_M\,\mathcal{L}_N\,\widetilde{Q}_{M,N}=1 \tag{4.4.51}$$

which is found via the INM, i.e. $\widetilde{u}_{M,N}$ and f are replaced by $\widetilde{Q}_{M,N}$ and 1 respectively within (4.3.33)–(4.3.35). The derivation of (4.4.50) from (4.4.49) is based upon the assumption that the sub-terms within (4.4.49) can be approximated in the same way as the sub-terms in (4.4.14) since, by (2.4.2), $\mathcal{K}_M\,u \approx \mathcal{K}_M\,\mathcal{L}_N\,u$ for all continuously differentiable functions $u \in [-1,1]$.

Therefore the theoretical bound (4.4.48) for the INM has been developed into the computable bound

$$\|u-\widetilde{u}_{M,N}\| \leq \widetilde{\mathcal{F}}_{M,N}\,\|\widetilde{u}_{M,N}-\lambda\,\mathcal{K}\,\widetilde{u}_{M,N}-f\| \tag{4.4.52}$$

in which $\widetilde{\mathcal{F}}_{M,N}$ is computed by (4.4.50); this bound is computable using the numerical solution $\widetilde{u}_{M,N}$ and so it requires no knowledge of the exact solution u.

4.4.3 Asymptotic Convergence Rates

Although (4.4.33) and (4.4.52) are used to bound the CNM and INM errors respectively, the bounds (4.4.12) and (4.4.46) can be used to estimate the CNM and INM convergence rates as $M,N\to\infty$. An asymptotic convergence rate for the CNM is derived from (4.4.12) by noting that, via (3.2.17), the quadrature error term satisfies

$$\|(\mathcal{K}-\mathcal{K}_M)\,u_M\| \leq \psi_M^{(\nu)}\,\mathbb{K}_{2M-\nu}, \tag{4.4.53}$$

wherein

$$\mathbb{K}_{M} \equiv \max_{x,y\in[-1,1]} \left| \frac{\partial^{M}}{\partial y^{M}} \Big(K(x,y)\, u_{M}(y) \Big) \right| . \tag{4.4.54}$$

Therefore comparison of (4.4.12) with (4.4.53) yields the asymptotic CNM error-convergence rate

$$\| u - u_{M} \| \sim \psi_{M}^{(\nu)}\, \mathbb{K}_{2M-\nu}, \quad M \to \infty \tag{4.4.55}$$

which, by (3.2.20), is convergent provided $\mathbb{K}_{2M-\nu} \sim o(M^{2M})$.

An asymptotic convergence rate for the INM is derived from (4.4.46) by first defining $\delta_{M,N}$ as

$$\delta_{M,N} \equiv \| (\mathcal{K} - \mathcal{K}_{M})\, \widetilde{u}_{M,N} + \mathcal{K}_{M}\, (\mathcal{I} - \mathcal{L}_{N})\, \widetilde{u}_{M,N} \| \tag{4.4.56}$$

which is bounded by

$$\delta_{M,N} \leq \| (\mathcal{K} - \mathcal{K}_{M})\, \widetilde{u}_{M,N} \| + \| \mathcal{K}_{M}\, (\mathcal{I} - \mathcal{L}_{N})\, \widetilde{u}_{M,N} \| . \tag{4.4.57}$$

The first term on the right-hand side of (4.4.57) is bounded (*cf.* (4.4.53)) by

$$\| (\mathcal{K} - \mathcal{K}_{M})\, \widetilde{u}_{M,N} \| \leq \psi_{M}^{(\nu)}\, \widetilde{\mathbb{K}}_{2M-\nu} \tag{4.4.58}$$

in which

$$\widetilde{\mathbb{K}}_{M} \equiv \max_{x,y\in[-1,1]} \left| \frac{\partial^{M}}{\partial y^{M}} \Big(K(x,y)\, \widetilde{u}_{M,N}(y) \Big) \right| . \tag{4.4.59}$$

The second term on the right-hand side of (4.4.57) is bounded by

$$\| \mathcal{K}_{M}\, (\mathcal{I} - \mathcal{L}_{N})\, \widetilde{u}_{M,N} \| \leq \| \mathcal{K}_{M} \|\, \| (\mathcal{I} - \mathcal{L}_{N})\, \widetilde{u}_{M,N} \| , \tag{4.4.60}$$

wherein $(\mathcal{I} - \mathcal{L}_{N})\, \widetilde{u}_{M,N}$ is the Lagrange interpolation error (*cf.* (2.4.1)) and

$$\| \mathcal{K}_{M} \| \equiv \sup_{t\in[-1,1]} \frac{\| \mathcal{K}_{M}\, t \|}{\| t \|} = \frac{\| \mathcal{K}_{M}\, t \|}{\| t \|} + \widetilde{\alpha}\, \epsilon, \tag{4.4.61}$$

where $\widetilde{\alpha} \in \mathbb{R}$ is an $O(1)$ constant, $0 < \epsilon \ll 1$, and t is a norm-maximising function. Following the approach in Section 4.4.1 for finding the norm-maximising functions q and r in (4.4.17) and (4.4.18) respectively, $\| \mathcal{K}_{M}\, t \| / \| t \|$ in (4.4.61) is found to be maximised when $t = 1$, so that $\| \mathcal{K}_{M} \|$ is computed by

$$\| \mathcal{K}_{M} \| = \max_{x\in[-1,1]} \left| \sum_{j=1}^{M} w_{j,M}\, K(x, y_{j,M}) \right| . \tag{4.4.62}$$

This again differs, see (4.4.28)–(4.4.29), from the existing definition [10, Eq. 4.1.11]

$$\|\mathcal{K}_M\| \equiv \max_{x\in[-1,1]} \sum_{j=1}^{M} |w_{j,M}\, K(x, y_{j,M})|\,, \tag{4.4.63}$$

in which the modulus signs are within the sum rather than outside it. Substitution of (4.4.62) and the Lagrange interpolation bound (2.4.68) into (4.4.60) then yields the bound

$$\|\mathcal{K}_M\,(\mathcal{I} - \mathcal{L}_N)\,\widetilde{u}_{M,N}\| \le \sigma_N\, \|\mathcal{K}_M\,(1)\|\, \left\|\widetilde{u}^{(N)}_{M,N}\right\| \tag{4.4.64}$$

wherein the node dependent σ_N is given explicitly in Table 2.1. Combining (4.4.57), (4.4.58) and (4.4.64) gives the bound on $\delta_{M,N}$ in (4.4.56) as

$$\delta_{M,N} \le \psi^{(\nu)}_M\, \widetilde{\mathbb{K}}_{2M-\nu} + \sigma_N\, \|\mathcal{K}_M\,(1)\|\, \left\|\widetilde{u}^{(N)}_{M,N}\right\|. \tag{4.4.65}$$

By (3.2.20) $\psi^{(\nu)}_M$ has a leading-order term of $\left(\frac{\mathrm{e}}{4M}\right)^{2M}$ and, by Table 2.1, σ_N has a leading-order term of $\left(\frac{\mathrm{e}}{2N}\right)^{N}$ (or $\left(\frac{2}{N-1}\right)^{N}$ for the regular nodes). Therefore, provided

$$\widetilde{\mathbb{K}}_{2M-\nu} \sim o(M^{2M}) \quad \text{and} \quad \left\|\widetilde{u}^{(N)}_{M,N}\right\| \sim o(N^N), \qquad M, N \to \infty, \tag{4.4.66}$$

the asymptotic convergence of $\delta_{M,N}$ is given by

$$\delta_{M,N} \sim \begin{cases} \psi^{(\nu)}_M\, \widetilde{\mathbb{K}}_{2M-\nu}, & M < \frac{N}{2}, \\[2ex] \sigma_N\, \left\|\widetilde{u}^{(N)}_{M,N}\right\|, & M > \frac{N}{2} \end{cases} \tag{4.4.67}$$

which, by comparison with (4.4.46) and (4.4.56), yields the asymptotic INM error-convergence rate

$$\|u - \widetilde{u}_{M,N}\| \sim \begin{cases} \psi^{(\nu)}_M\, \widetilde{\mathbb{K}}_{2M-\nu}, & M < \frac{N}{2}, \\[2ex] \sigma_N\, \left\|\widetilde{u}^{(N)}_{M,N}\right\|, & M > \frac{N}{2}. \end{cases} \tag{4.4.68}$$

The dependence upon M and N of the INM convergence shown by (4.4.68) corroborates the observations from Figure 4.3.5 that the INM error is predominantly dependent upon M for $M < \frac{N}{2}$ and upon N for $M > \frac{N}{2}$, provided the conditions in (4.4.66) are not violated. Furthermore, setting $M = N$ in both the CNM and INM convergence rates, (4.4.55) and (4.4.68) respectively, yields

$$\|u - u_N\| \ll \|u - \widetilde{u}_{N,N}\| \tag{4.4.69}$$

since $\psi_N^{(\nu)} \ll \sigma_N$. The norms in (4.4.66) can be approximated by

$$\widetilde{\mathbb{K}}_{2M-\nu} \approx \left\| (K\,u)^{(2M-\nu)} \right\| \quad \text{and} \quad \left\| \widetilde{u}_{M,N}^{(N)} \right\| \approx \left\| u^{(N)} \right\|, \tag{4.4.70}$$

wherein the bracketed superscripts denote the order of partial differentiation with respect to y. Using the approximations in (4.4.70) it is possible to determine whether the conditions in (4.4.66) have been met and hence determine whether (4.4.67)–(4.4.69) hold. Table 4.5 shows the leading-order asymptotic limits of $\left\| (K\,u)^{(2M)} \right\| / M^{2M}$ and $\left\| u^{(N)} \right\| / N^N$ as $M, N \to \infty$ for the four test problems outlined in Table 4.2. Without loss of generality $\nu = 0$ has been fixed in $\left\| (K\,u)^{(2M-\nu)} \right\|$ since this does not affect the ratio as $M \to \infty$.

Problem	$\left\| (K\,u)^{(2M)} \right\| / M^{2M}$	$\left\| u^{(N)} \right\| / N^N$
1	$10\,M/M^{2M}$	$(1/N)^N$
2	$2\sqrt{\pi\,M}\,(10/\mathrm{e})^{2M}$	$\sqrt{2\,\pi\,N}\,(5/\mathrm{e})^N$
3	$(M+8)\,\mathrm{e}^{12}\,(12/M)^{2M}$	$\mathrm{e}^{12}\,(12/N)^N$
4	$(2\,M)^5\,(10/M)^{2M}$	$(10/N)^N$

Table 4.5: Leading-order asymptotic limits as $M, N \to \infty$ of the problem-specific ratios determining, via the approximations in (4.4.70), whether or not the conditions in (4.4.66) are met.

The ratios in Table 4.5 for problems 1, 3 and 4 tend to 0 as $M, N \to \infty$. Therefore, for these problems, the conditions (4.4.66) are met and so (4.4.67)–(4.4.69) hold. Hence, by (4.4.69), when $M = N$ the INM errors in problems 1, 3 and 4 are much greater than those of the CNM, as shown in Figure 4.3.1 (a), (c) and (d). In contrast, both ratios for problem 2 are divergent with increasing M and N and so (4.4.68) does not hold. Figure 4.3.1 (b) shows that the CNM and INM are convergent with increasing $M = N$, with the exception of the INM on the regular nodes, which demonstrates that (4.4.55) and (4.4.65) are inaccurate over-estimates of the true errors. This is a result of the terms in (4.4.54), (4.4.59) and $\left\| \widetilde{u}_{M,N}^{(N)} \right\|$ in (4.4.64) being maximised over $y \in [-1, 1]$ when in practice, it is some unknown intermediate value $y = \xi \in [-1, 1]$ that gives the true error. In contrast to the other three problems, the problem 2 ratios satisfy $\left\| (K\,u)^{(2M)} \right\| / M^{2M} \gg \left\| u^{(N)} \right\| / N^N$ when $M = N$, hence the problem 2 INM error is dictated by the quadrature error. For

this reason the problem 2 CNM and INM errors converge at the same rate, as seen in Figure 4.3.1 (b).

4.4.4 Numerical Results

The CNM bound (4.4.33) and INM bound (4.4.52) are tested on the four problems summarised in Table 4.2. Figure 4.4.1 presents the newly predicted bounds, denoted by b_N; the true CNM errors $e_N = \|u - u_N\|$ using different quadrature-node distributions; and the true INM errors $e_N = \|u - \widetilde{u}_{N,N}\|$ using Gauss-Legendre quadrature and different interpolation-node distributions.

Figure 4.4.1 shows that the error bounds (4.4.33) and (4.4.52) yield spectrally accurate approximations of the true errors for all four problems, three of which are designed to be challenging to approximation methods; the tightest bounds are observed for the non-challenging problem 1. For each problem the bounds converge at the same rate as the computational errors and therefore are predicted to provide accurate approximations of the true error as $N \to \infty$. The CNM and INM convergence rates (4.4.55) and (4.4.68) can also be used to predict the errors as $N \to \infty$; the errors presented in Figure 4.4.1 are compared to these asymptotic convergence rates in Figure 4.4.2.

It is evident from Figure 4.4.2 that (4.4.55) and (4.4.68) accurately predict the convergence rates of the errors for problems 1, 3 and 4 as $N \to \infty$. For problem 2 the predicted rates are divergent and hence fail to portray the convergent errors, as discussed in the text following Table 4.5.

Problems 3 and 4 have been designed to demonstrate the accuracy of the CNM, the INM, and both their error predictions on problems whose solutions are challenging to approximate. Modified problems 3 and 4 with solutions $u(x) = \mathrm{e}^{\beta x}$ and $u(x) = \sin \beta x$ respectively are now considered to determine the accuracy of the CNM, INM and their bounds as β increases, yielding steeper and more oscillatory solutions. Figure 4.4.3 shows the CNM and INM errors and bounds for $M = N = 15$ and $M = N = 30$ with varying β; since Figure 4.4.1 has demonstrated that results are qualitatively similar using each of the collocation-node sets, for simplicity only the CNM Gauss-Legendre and INM Chebyshev results are displayed.

Figure 4.4.3 shows that the accuracy of the CNM and INM is reduced when approximating steeper and more oscillatory solutions; however, despite this, the

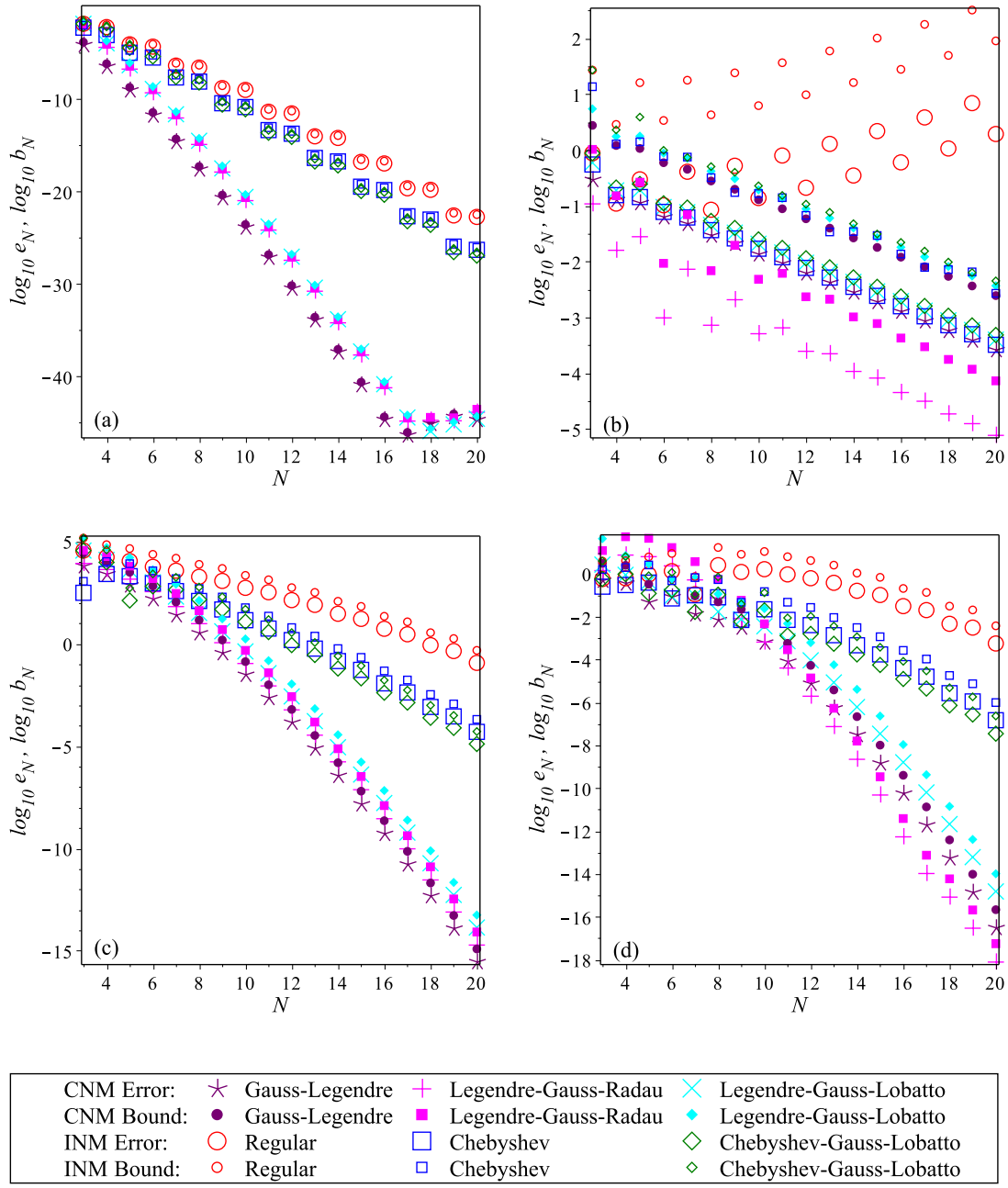

Figure 4.4.1: Semilog plots of the true, computational CNM and INM errors $e_N = \|u - u_N\|$ and $e_N = \|u - \widetilde{u}_{N,N}\|$ with their respective newly predicted bounds b_N computed using (4.4.33) and (4.4.52) for problems (a) 1 ("smooth"), (b) 2 ("Runge"), (c) 3 ("steep") and (d) 4 ("oscillatory") collocated on a variety of node sets.

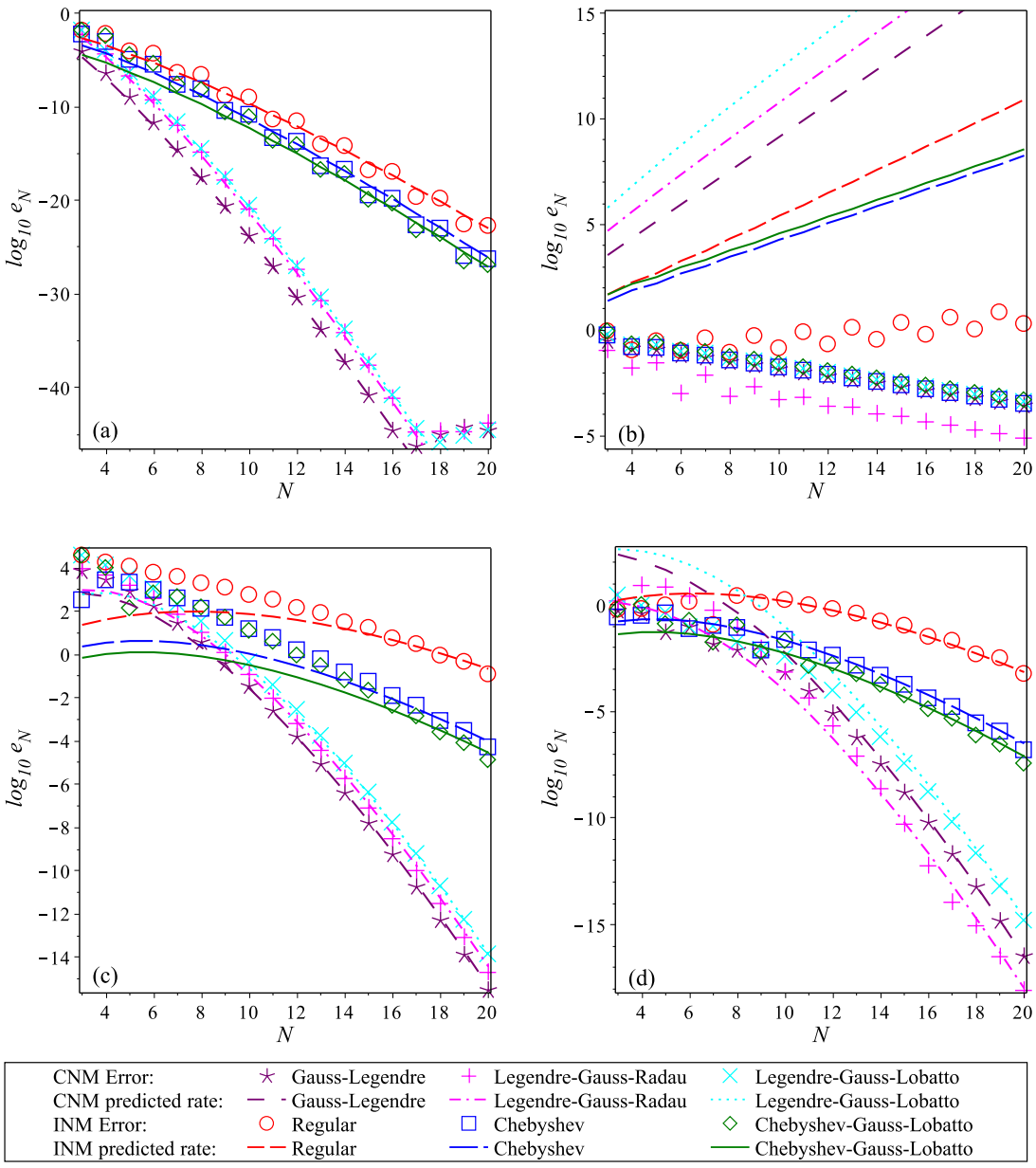

Figure 4.4.2: Semilog plots of the true, computational CNM and INM errors $e_N = \|u - u_N\|$ and $e_N = \|u - \widetilde{u}_{N,N}\|$ with newly predicted convergence rates (4.4.55) and (4.4.68), scaled by appropriate constants, for problems (a) 1 ("smooth"), (b) 2 ("Runge"), (c) 3 ("steep") and (d) 4 ("oscillatory") collocated on a variety of node sets.

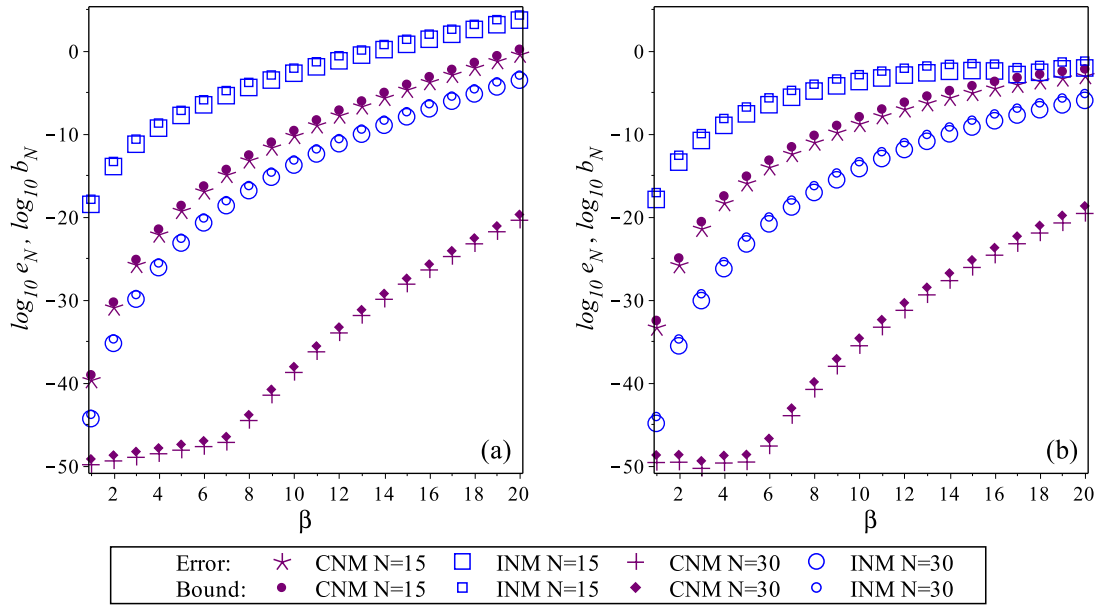

Figure 4.4.3: Semilog plots of the true, computational CNM and INM errors $e_N = \|u - u_N\|$ and $e_N = \|u - \widetilde{u}_{N,N}\|$ with respective bounds b_N for $N = 15$ and $N = 30$ computed using (4.4.33) and (4.4.52) for (a) modified problem 3 with solution $u(x) = \mathrm{e}^{\beta x}$ and (b) modified problem 4 with solution $u(x) = \sin \beta x$, in which β is varied. The observed "elbow" in the CNM results for $N = 30$ at $\beta = 7$ (left) and $\beta = 5$ (right) is due to rounding errors for the 50-digits arithmetic used.

error bounds remain accurate approximations of the true errors. The loss of accuracy of the CNM and INM as β increases is not a limitation since the accuracy can be improved simply by increasing M and N.

4.5 Summary

In this chapter, methods have been developed for solving integral equations both analytically and numerically. The well-known Nyström method has been analysed and extended by incorporating the interpolation techniques introduced in Chapter 2. Both Lagrange and barycentric interpolation have been considered within the new interpolated Nyström method; however, despite offering a computational advantage in terms of workload, the barycentric implementation is restricted in terms of the freedom of nodes on which it can be based. The interpolated Nyström method has

been developed in preparation for an extension, in Chapter 5, for solving integro-differential equations, in which the error can be minimised by using those nodes that minimise the differentiation error, which is orders of magnitude greater than the Gaussian quadrature error.

The integral-equation numerical methods in this chapter have been fully validated on a diverse set of test problems, some of which were designed to be challenging, and both the classical and interpolated Nyström methods were shown to be spectrally accurate. However, it has been shown that the accuracy of the classical Nyström method is far superior to that of the interpolated Nyström method, since the accuracy of the former is dictated by the error in Gaussian quadrature, and the accuracy of the latter is dictated by the, much larger, error in Lagrange interpolation. Since interpolation is unavoidable in the spectral differentiation detailed in Chapter 3, the larger errors incurred in the interpolated Nyström method are not considered a disadvantage in its intended ultimate application: that of solving integro-differential equations (in Chapter 5).

Novel error analyses have been developed from an existing, theoretical framework for both the classical Nyström method and its new interpolated counterpart. Specifically, the theoretical bound [60, Eq. 4.7.17b] forms the basis of new computable error bounds that provide spectrally accurate approximations of the true error on a range of qualitatively diverse problems; this contradicts the statement in [9, p. 282] that the Nyström error is *"difficult to estimate"*, and the assertion in [83, p. 188] that computable error bounds *"will be difficult to evaluate in applications"*. Furthermore, the newly derived error bounds are explicitly computable using only the numerical solution, and so require no knowledge of the exact solution. This is a distinctive feature of the present approach since many existing Nyström error bounds, for example [60, Eqns. 4.7.16c–4.7.16d] and [10, Eq. 4.1.33], are based upon the exact solution, and those based on the numerical solution, for example [4, Eq. 5.15, p. 15] and [60, Eq. 4.7.17c], have never before been developed into computable quantities.

In addition to the error bounds, asymptotic error estimates have been developed from the interpolation and quadrature error analyses examined in Chapters 2 and 3. The asymptotic error analysis quantifies the observed disparity between the errors of the classical and interpolated Nyström methods.

Chapter 5

Integro-Differential Equations

An *integro-differential equation* (IDE) is an equation that contains both the integral and derivative(s) of an unknown function. Due to their inherent differential components, IDEs must be augmented by boundary conditions (BCs). As for integral equations, IDEs arise in the modelling of a wide range of physical problems such as, *inter alia*, neural networks [73]; the dynamics of an elastic aircraft [71]; option pricing [36]; the response of a population of tumor cells to periodic treatment with chemotherapy [74]; the spread of diseases [94]; and glucose-insulin dynamics of diabetes [90].

Due to the many applications of IDEs, there has been much research into their solution, which most commonly is determined numerically due to the complexity invited by the modelling of realistic applications. The diverse range of numerical methods for obtaining the approximate solution of an IDE includes Tau methods with Chebyshev and Legendre bases [69]; approximation in terms of Taylor polynomials [137]; piecewise-linear and polynomial collocation using Gaussian quadrature on an infinite interval of integration [73]; Legendre-polynomial solutions whose coefficients are found via a Legendre collocation matrix method [138]; Legendre spectral collocation using a combination of Gaussian quadrature and Lagrange interpolation [108]; use of sine-cosine wavelets to reduce an IDE to a system of algebraic equations [121]; a Galerkin scheme [12] that is a generalisation of IE methods [43, 44]; and a Sinc method that reformulates an IDE into a discrete system [106].

Despite the considerable literature devoted to the numerical solution of IDEs, the development of corresponding error analyses continues to be relatively rare. For example, in the aforementioned numerical approaches, only [69, 138, 12] contain a

brief discussion of errors, not a single one of which offer a method for obtaining spectrally accurate computable error bounds. In [69] the error estimate is itself subject to an unquantified error; in [138] the error is estimated throughout the domain but only bounded at the Legendre collocation nodes; and, in [12] it is stated that *"for large values of λ [the parameter that multiplies the integral term] the computed error is sometimes larger than the estimated error"*.

Accordingly, the aim of this chapter is to develop not only spectrally accurate numerical methods for approximating the solution of an IDE, but also spectrally accurate error predictions for its numerical solution that are explicitly computable in the absence of an exact solution. Since error bounds of this form are, as discussed above, absent from the existing literature this is a unique and distinctive feature of the present work.

In this thesis, only *Fredholm Integro-Differential Equations* (FIDEs) are considered; these are introduced in Section 5.1. The analytical solution of an FIDE with a degenerate kernel is then considered in Section 5.2; this follows the integral-equation approach of Section 4.2. In Section 5.3, both the classical and interpolated Nyström methods, introduced in Sections 4.3.1 and 4.3.2 respectively, are extended by incorporating the spectral-differentiation methods outlined in Section 2.2 and the resulting differentiation matrices presented in Section 3.1. Two distinct sub-procedures are considered for implementing the associated FIDE boundary condition, and the resulting errors are compared. In the error analyses of Section 5.4, error bounds and asymptotic error estimates are developed, for both Nyström-type methods, that are computable using only the numerical solution. This enables the accuracy of the numerical solution to be quantified in the absence of an exact solution.

An alternative numerical method for approximating the solution of FIDEs is developed in Section 5.5, in which FIDEs are first converted into hybrid Volterra-Fredholm integral equations (VFIEs) following the approach in [87]. This procedure is expected to improve upon the accuracy achieved in Section 5.3 by circumventing the need for the ill-conditioned numerical differentiation matrices, which are discussed in Section 3.1. The solution of VFIEs can be approximated in many ways: for example, by collocation and Galerkin methods [64]; moving-least-square methods and Chebyshev polynomials [84]; Taylor-expansion methods [34]; shifted Legendre polynomials [97]; and iterative methods [25]. The present approach uses a novel

method to solve the resulting VFIE that employs a combination of Lagrange interpolation and Gaussian quadrature, thereby building on the methods introduced in Sections 2.1 and 3.2 respectively. By incorporating these spectrally accurate approximation techniques into the VFIE solution, this new approach will dramatically improve upon the accuracy achieved in [87], in which the VFIE is solved to only quadratic order in the number N of Simpson's-rule panels used. The recovery of an approximate FIDE solution from the approximate VFIE solution is then discussed. In the error analysis that follows, error bounds and asymptotic error estimates are derived for the error in the numerical FIDE solution that are explicitly computable using only the numerical VFIE solution, and so require no knowledge of the exact solution.

All of the newly developed numerical methods and error bounds are tested and validated on a range of test problems with qualitatively distinct solutions. The errors incurred in the Nyström-type method and the VFIE reformulation method, presented in Sections 5.3 and 5.5 respectively, are compared both theoretically and numerically, and the advantages of each method are discussed.

5.1 Fredholm Integro-Differential Equations

Integro-differential equations can be classified in a similar way to integral equations; IDEs with a variable limit of integration are known as Volterra IDEs and those with fixed limits of integration are known as Fredholm IDEs. An IDE is said to be of nth order when the highest derivative of its unknown function is of order n.

In this Chapter, only Fredholm first-order integro-differential equations of the second kind (hereafter IDEs) are considered: when scaled onto the interval $[-1, 1]$, these have the canonical form

$$u(x) - \mu(x)\,\frac{du}{dx} - \lambda \int_{-1}^{1} K(x, y)\, u(y)\, dy = f(x), \qquad x \in [-1, 1], \tag{5.1.1}$$

in which the kernel $K : [-1, 1] \times [-1, 1] \to \mathbb{R}$, coefficient function $\mu : [-1, 1] \to \mathbb{R}$, source function $f : [-1, 1] \to \mathbb{R}$ and constant $\lambda \in \mathbb{R}$ are known and $u(x)$ is the unknown function to be determined on $[-1, 1]$. Additionally, IDE (5.1.1) is augmented by the boundary condition (BC)

$$u(\xi) = \zeta, \tag{5.1.2}$$

which contains known constants $\xi \in [-1, 1]$ and $\zeta \in \mathbb{R}$. The corresponding symbolic form of (5.1.1) is

$$u - \mu\,\mathcal{D}\,u - \lambda\,\mathcal{K}\,u = f, \tag{5.1.3}$$

wherein the operators $\mathcal{D}$ and $\mathcal{K}$ are defined by (2.2.1) and (4.3.3) respectively. It is convenient to define the linear operator $\mathcal{A}$ as

$$\mathcal{A} \equiv \mu\mathcal{D} + \lambda\mathcal{K} \tag{5.1.4}$$

so that the IDE (5.1.3) can be written in the more succinct form

$$u - \mathcal{A}u = f. \tag{5.1.5}$$

As discussed above, many problems arising in engineering, biology and medicine can be modelled by an equation of this form [23]. In addition to these, the most well-known incarnation of a Fredholm IDE is the neutron-transport equation of particle physics [3, 111], in which $u(x)$ is the angular flux and $K(x, y)$ the angular distribution of scattered neutrons [122].

5.2 Degenerate Kernel: Analytical Solution

In the specific case that the coefficient function $\mu(x)$ is a constant, i.e. $\mu(x) = \mu$, and $K(x, y)$ is the simplest degenerate kernel of the form $K(x, y) = P(x)\,Q(y)$, the IDE (5.1.1) can be solved analytically following a similar method to that shown in Section 4.2. The constant C is first defined as

$$C \equiv \int_{-1}^{1} Q(y)\,u(y)\,dy, \tag{5.2.1}$$

using which IDE (5.1.1) can then be written as

$$\frac{du}{dx} - \frac{1}{\mu}\,u(x) = -\frac{1}{\mu}\Big(f(x) + \lambda\,P(x)\,C\Big). \tag{5.2.2}$$

When multiplied by the integrating factor $\mathrm{e}^{-x/\mu}$, (5.2.2) becomes

$$\frac{d}{dx}\Big(\mathrm{e}^{-x/\mu}\,u(x)\Big) = -\frac{\mathrm{e}^{-x/\mu}}{\mu}\Big(f(x) + \lambda\,P(x)\,C\Big), \tag{5.2.3}$$

integration of which gives the solution

$$u(x) = \mathrm{e}^{x/\mu}\left(\alpha - \frac{1}{\mu}\int_{-1}^{x} \mathrm{e}^{-t/\mu}\left(f(t) + \lambda\, P(t)\, C\right) dt\right), \tag{5.2.4}$$

wherein α is a constant of integration. Equivalently, (5.2.4) can be written as

$$u(x) = \mathrm{e}^{x/\mu}\left(\alpha - \frac{\mathcal{I}(x)}{\mu}\right), \tag{5.2.5}$$

in which $\mathcal{I}(x)$ is defined as the integral

$$\mathcal{I}(x) \equiv \int_{-1}^{x} \mathrm{e}^{-t/\mu}\, g(t)\, dt \tag{5.2.6}$$

and

$$g(t) = f(t) + \lambda\, P(t)\, C. \tag{5.2.7}$$

In certain cases it will be possible to evaluate $\mathcal{I}(x)$ exactly so that (5.2.5) yields the exact IDE solution, in which α is determined by the BC in (5.1.2) and C is found from substitution of (5.2.5) into (5.2.1). However, in general $\mathcal{I}(x)$ must be approximated, and methods are now presented for approximating this integral, whereafter an approximate semi-analytical solution of the IDE can be constructed.

5.2.1 Integration by parts: method 1

Integrating (5.2.6) by parts gives

$$\begin{aligned}
\mathcal{I}(x) &= \left[-\mu\, \mathrm{e}^{-t/\mu}\, g(t)\right]_{-1}^{x} + \mu\int_{-1}^{x} \mathrm{e}^{-t/\mu}\, g'(t)\, dt \\
&= \left[-\mu\, \mathrm{e}^{-t/\mu}\, g(t) - \mu^2\, \mathrm{e}^{-t/\mu} g'(t)\right]_{-1}^{x} + \mu^2\int_{-1}^{x} \mathrm{e}^{-t/\mu}\, g''(t)\, dt \\
&= \left[-\mu\, \mathrm{e}^{-t/\mu}\, g(t) - \mu^2\, \mathrm{e}^{-t/\mu} g'(t) - \mu^3\, \mathrm{e}^{-t/\mu}\, g''(t)\right]_{-1}^{x} + \mu^3\int_{-1}^{x} \mathrm{e}^{-t/\mu}\, g^{(3)}(t)\, dt,
\end{aligned} \tag{5.2.8}$$

continuation of which process yields

$$\mathcal{I}(x) = \beta - \mathrm{e}^{-x/\mu}\sum_{k=0}^{\infty} \mu^{k+1}\, g^{(k)}(x), \tag{5.2.9}$$

wherein $g^{(k)}(x)$ refers to the kth derivative of $g(x)$ and

$$\beta = \mathrm{e}^{1/\mu} \sum_{k=0}^{\infty} \mu^{k+1}\, g^{(k)}(-1). \tag{5.2.10}$$

The series in (5.2.9) and (5.2.10) are uniformly convergent provided, via the Weierstrass M-test [5, p. 278] and ratio test [5, p. 264],

$$|\mu| < \lim_{k\to\infty} \frac{\left\|g^{(k)}\right\|}{\left\|g^{(k+1)}\right\|}, \tag{5.2.11}$$

in which case (5.2.9) can be substituted into (5.2.5) to yield

$$u(x) = \gamma\, \mathrm{e}^{x/\mu} + \sum_{k=0}^{\infty} \mu^k\, g^{(k)}(x), \tag{5.2.12}$$

wherein $\gamma = \alpha - \beta/\mu$. Setting $x = \xi$ in (5.2.12) yields, via the BC (5.1.2),

$$\gamma = \mathrm{e}^{-\xi/\mu} \left(\zeta - \sum_{k=0}^{\infty} \mu^k\, g^{(k)}(\xi) \right) \tag{5.2.13}$$

which, when substituted into (5.2.12), yields the IDE solution

$$u(x) = \left(\zeta - \sum_{k=0}^{\infty} \mu^k\, g^{(k)}(\xi) \right) \mathrm{e}^{(x-\xi)/\mu} + \sum_{k=0}^{\infty} \mu^k\, g^{(k)}(x). \tag{5.2.14}$$

Provided the convergence condition (5.2.11) holds, the IDE solution can be found explicitly from (5.2.14). To find the constant C in $g(x)$, (5.2.14) is substituted into (5.2.1) and $g(x)$ is expanded using (5.2.7) to give

$$C = \left(\zeta - \sum_{k=0}^{\infty} \mu^k \left(f^{(k)}(\xi) + \lambda\, C\, P^{(k)}(\xi) \right) \right) \sigma + \sum_{k=0}^{\infty} \mu^k \left(\phi_k + \lambda\, C\, \psi_k \right), \tag{5.2.15}$$

wherein

$$\phi_k = \int_{-1}^{1} Q(y)\, f^{(k)}(y)\, dy, \qquad \psi_k = \int_{-1}^{1} Q(y)\, P^{(k)}(y)\, dy, \qquad k \geq 0, \tag{5.2.16}$$

and

$$\sigma = \int_{-1}^{1} Q(y)\, \mathrm{e}^{(y-\xi)/\mu}\, dy. \tag{5.2.17}$$

Rearranging (5.2.15) then gives

$$C = \frac{\sigma\,\zeta + \sum_{k=0}^{\infty} \mu^k \left(\phi_k - \sigma\, f^{(k)}(\xi)\right)}{1 - \lambda \sum_{k=0}^{\infty} \mu^k \left(\psi_k - \sigma\, P^{(k)}(\xi)\right)}. \tag{5.2.18}$$

Provided the denominator of (5.2.18) is non-zero, (5.2.7), (5.2.14) and (5.2.18) together give the unique IDE solution. The solution (5.2.14) is made up of two parts: the (separable) particular integral

$$\sum_{k=0}^{\infty} \mu^k\, g^{(k)}(x), \tag{5.2.19}$$

which by itself will satisfy the ODE (5.2.2); and the (separable) complementary function

$$\left(\zeta - \sum_{k=0}^{\infty} \mu^k\, g^{(k)}(\xi)\right) \mathrm{e}^{(x-\xi)/\mu}, \tag{5.2.20}$$

which satisfies the homogeneous version of the ODE (5.2.2). However, since both the complementary function and the particular integral are contained within C in (5.2.18), the particular integral (5.2.19) will not alone satisfy the IDE (5.1.1).

If the functions $f(x)$, $P(x)$ and $Q(y)$ are finitely differentiable, then the infinite sums within $u(x)$ and C, (5.2.14) and (5.2.18) respectively, will terminate for some $m < \infty$. However, if these functions are infinitely differentiable, then provided the convergence condition (5.2.11) holds, the solution $u(x)$ can be approximated by $u_M(x)$, in which the latter terminates each of the infinite sums at $k = M$. The approximate IDE solution is therefore given by

$$u_M(x) = \left(\zeta - \sum_{k=0}^{M} \mu^k\, g_M^{(k)}(\xi)\right) \mathrm{e}^{(x-\xi)/\mu} + \sum_{k=0}^{M} \mu^k\, g_M^{(k)}(x), \tag{5.2.21}$$

wherein

$$g_M(x) = f(x) + \lambda P(x)\, \frac{\sigma\,\zeta + \sum_{k=0}^{M} \mu^k \left(\phi_k - \sigma\, f^{(k)}(\xi)\right)}{1 - \lambda \sum_{k=0}^{M} \mu^k \left(\psi_k - \sigma\, P^{(k)}(\xi)\right)}, \tag{5.2.22}$$

which converges to the exact solution $u(x)$ provided (5.2.11) holds. Since (5.2.11) provides an upper limit on $|\mu|$ then, for fixed functions $P(x)$, $Q(y)$ and $f(x)$, the solution $u_M(x)$ will be accurate only for sufficiently small $|\mu|$.

An alternative integration by parts method is now presented for IDEs whose components do not satisfy the condition (5.2.11).

5.2.2 Integration by parts: method 2

In this method, $\mathcal{I}(x)$ in (5.2.6) is again integrated by parts; however, in each step, $\mathrm{e}^{-x/\mu}$ is now differentiated and $g(x)$ integrated. Let

$$G_0(x) = g(x) \qquad \text{and} \qquad G_{k+1}(x) = \int_{-1}^{x} G_k(t)\,dt, \quad k \geq 0, \tag{5.2.23}$$

so that $G_k(x)$ is $g(x)$ integrated k times, then $\mathcal{I}(x)$ is evaluated as

$$\begin{aligned}
\mathcal{I}(x) &= \mathrm{e}^{-x/\mu}\,G_1(x) + \frac{1}{\mu}\int_{-1}^{x} \mathrm{e}^{-t/\mu}\,G_1(t)\,dt \\
&= \mathrm{e}^{-x/\mu}\,G_1(x) + \frac{1}{\mu}\,\mathrm{e}^{-x/\mu}\,G_2(x) + \frac{1}{\mu^2}\int_{-1}^{x} \mathrm{e}^{-t/\mu}\,G_2(t)\,dt \\
&= \mathrm{e}^{-x/\mu}\,G_1(x) + \frac{1}{\mu}\,\mathrm{e}^{-x/\mu}\,G_2(x) + \frac{1}{\mu^2}\,\mathrm{e}^{-x/\mu}\,G_3(x) + \frac{1}{\mu^3}\int_{-x}^{x} \mathrm{e}^{-t/\mu}\,G_3(t)dt.
\end{aligned} \tag{5.2.24}$$

Continuing to integrate by parts then yields

$$\mathcal{I}(x) = \sum_{k=1}^{\infty} \mu^{1-k}\,\mathrm{e}^{-x/\mu}\,G_k(x), \tag{5.2.25}$$

which is uniformly convergent provided

$$\lim_{k\to\infty} \frac{\|G_{k+1}\|}{\|G_k\|} < |\mu|. \tag{5.2.26}$$

Let the functions $F_k(x)$, $P_k(x)$ and $Q_k(x)$ respectively denote $f(x)$, $P(x)$ and $Q(x)$ integrated k times such that, for $k \geq 0$,

$$F_{k+1}(x) = \int_{-1}^{x} F_k(t)\,dt, \qquad F_0(x) = f(x), \tag{5.2.27}$$

$$P_{k+1}(x) = \int_{-1}^{x} P_k(t)\,dt, \qquad P_0(x) = P(x), \tag{5.2.28}$$

and

$$Q_{k+1}(x) = \int_{-1}^{x} Q_k(t)\,dt, \qquad Q_0(x) = Q(x). \tag{5.2.29}$$

Additionally, let

$$\widetilde{\phi}_k = \int_{-1}^{1} Q(y)\,F_k(y)\,dy, \qquad \widetilde{\psi}_k = \int_{-1}^{1} Q(y)\,P_k(y)\,dy, \qquad k \geq 0, \tag{5.2.30}$$

and let σ be defined as in (5.2.17). Then, using (5.2.27)–(5.2.30), an approximate semi-analytical solution $u_{_M}(x)$ is found from (5.2.25) following a similar method to that shown in Section 5.2.1. Provided the convergence condition (5.2.26) holds, then the approximate solution $u_{_M}(x)$ is given by

$$u_{_M}(x) = \left(\zeta + \sum_{k=1}^{M} \mu^{-k}\,G_{k,_M}(\xi)\right) \mathrm{e}^{(x-\xi)/\mu} - \sum_{k=1}^{M} \mu^{-k}\,G_{k,_M}(x), \tag{5.2.31}$$

in which

$$G_{k+1,_M}(x) = \int_{-1}^{x} G_{k,_M}(t)\,dt, \qquad k \geq 0, \tag{5.2.32}$$

and

$$G_{0,_M}(x) = f(x) + \lambda\,P(x)\,\frac{\widetilde{\sigma}_{_M}\,\zeta + \displaystyle\sum_{k=1}^{M} \mu^{-k}\left(\widetilde{\sigma}_{_M}\,F_k(\xi) - \widetilde{\phi}_k\right)}{1 - \lambda \displaystyle\sum_{k=1}^{M} \mu^{-k}\left(\widetilde{\sigma}_{_M}\,P_k(\xi) - \widetilde{\psi}_k\right)}. \tag{5.2.33}$$

In contrast to the method in Section 5.2.1, the convergence condition (5.2.26) provides a lower limit on $|\mu|$. Hence, for given functions $P(x)$, $Q(y)$ and $f(x)$, the solution $u_{_M}(x)$ will be accurate only for sufficiently large $|\mu|$.

5.2.3 Taylor-Series Expansion

An alternative approach is now considered in which the integral $\mathcal{I}(x)$ in (5.2.6) is approximated using a Taylor-series expansion. The Taylor series for $\mathcal{I}(x)$ about $x = 0$ is given by

$$\mathcal{I}(x) = \sum_{n=0}^{\infty} \frac{x^n}{n!}\,\mathcal{I}^{(n)}(0), \tag{5.2.34}$$

wherein $\mathcal{I}^{(n)}(0)$ denotes the nth derivative of $\mathcal{I}(x)$ evaluated at $x = 0$. Differentiating $\mathcal{I}(x)$ in (5.2.6) yields

$$\mathcal{I}^{(1)}(x) = \mathrm{e}^{-x/\mu}\, g(x), \tag{5.2.35}$$

$$\mathcal{I}^{(2)}(x) = -\frac{1}{\mu}\,\mathrm{e}^{-x/\mu}\, g(x) + \mathrm{e}^{-x/\mu}\, g'(x) \tag{5.2.36}$$

and

$$\mathcal{I}^{(3)}(x) = \left(-\frac{1}{\mu}\right)^2 \mathrm{e}^{-x/\mu}\, g(x) - \frac{2}{\mu}\,\mathrm{e}^{-x/\mu}\, g'(x) + \mathrm{e}^{-x/\mu}\, g''(x) \tag{5.2.37}$$

which, when evaluated at $x = 0$, give

$$\mathcal{I}^{(1)}(0) = g(0), \tag{5.2.38}$$

$$\mathcal{I}^{(2)}(0) = -\frac{1}{\mu}\, g(0) + g'(0) \tag{5.2.39}$$

and

$$\mathcal{I}^{(3)}(0) = \left(-\frac{1}{\mu}\right)^2 g(0) - \frac{2}{\mu}\, g'(0) + g''(0). \tag{5.2.40}$$

Therefore, the general expression for $\mathcal{I}^{(n)}(0)$ is given by

$$\mathcal{I}^{(n)}(0) = \sum_{k=0}^{n-1} \binom{n-1}{k} \left(-\frac{1}{\mu}\right)^{n-k-1} g^{(k)}(0), \qquad n > 0. \tag{5.2.41}$$

Substituting (5.2.41) into (5.2.34) yields

$$\mathcal{I}(x) = \mathcal{I}(0) + \sum_{n=1}^{\infty} \sum_{k=0}^{n-1} \frac{x^n}{n!}\, \frac{(n-1)!}{k!\,(n-k-1)!} \left(-\frac{1}{\mu}\right)^{n-k-1} g^{(k)}(0) \tag{5.2.42}$$

which is convergent for $x \in [-1, 1]$ provided

$$\lim_{n\to\infty} \left| \frac{\mathcal{I}^{(n+1)}(0)}{(n+1)\,\mathcal{I}^{(n)}(0)} \right| < 1. \tag{5.2.43}$$

By (5.2.41) the convergence condition (5.2.43) is equivalently

$$\lim_{n\to\infty} \left| \frac{n \displaystyle\sum_{k=0}^{n} \frac{(-\mu)^k\, g^{(k)}(0)}{k!\,(n-k)!}}{(n+1) \displaystyle\sum_{k=0}^{n-1} \frac{(-\mu)^k\, g^{(k)}(0)}{k!\,(n-k-1)!}} \right| < |\mu|, \tag{5.2.44}$$

the left-hand side of which satisfies

$$\lim_{n\to\infty}\left|\frac{n\displaystyle\sum_{k=0}^{n}\frac{(-\mu)^k\,g^{(k)}(0)}{k!\,(n-k)!}}{(n+1)\displaystyle\sum_{k=0}^{n-1}\frac{(-\mu)^k\,g^{(k)}(0)}{k!\,(n-k-1)!}}\right|<1 \tag{5.2.45}$$

provided

$$(-\mu)^n\,g^{(n)}(0)\sim o(n^n),\qquad n\to\infty. \tag{5.2.46}$$

Therefore, given (5.2.46), a sufficient condition for convergence of (5.2.42) is

$$1<|\mu|. \tag{5.2.47}$$

If (5.2.44) holds then (5.2.42) can be substituted into (5.2.5) to give the general solution

$$u(x)=\mathrm{e}^{x/\mu}\left(\widetilde{\alpha}+\sum_{n=1}^{\infty}\sum_{k=0}^{n-1}\frac{x^n}{n\,k!\,(n-k-1)!}\left(-\frac{1}{\mu}\right)^{n-k}g^{(k)}(0)\right), \tag{5.2.48}$$

wherein $\widetilde{\alpha}=\alpha-\mathcal{I}(0)/\mu$. Setting $x=\xi$ in (5.2.48) and using the BC (5.1.2) gives

$$\widetilde{\alpha}=\zeta\,\mathrm{e}^{-\xi/\mu}-\sum_{n=1}^{\infty}\sum_{k=0}^{n-1}\frac{\xi^n}{n\,k!(n-k-1)!}\left(-\frac{1}{\mu}\right)^{n-k}g^{(k)}(0) \tag{5.2.49}$$

which, upon substitution into (5.2.48), yields the IDE solution as

$$u(x)=\zeta\,\mathrm{e}^{(x-\xi)/\mu}+\mathrm{e}^{x/\mu}\sum_{n=1}^{\infty}\sum_{k=0}^{n-1}\frac{x^n-\xi^n}{n\,k!(n-k-1)!}\left(-\frac{1}{\mu}\right)^{n-k}g^{(k)}(0). \tag{5.2.50}$$

To find the constant C within $g(x)$ in (5.2.7), the solution (5.2.50) is substituted into (5.2.1) and $g(x)$ expanded, to give

$$C=\zeta\,\sigma\,\mathrm{e}^{-\xi/\mu}+\sum_{n=1}^{\infty}\sum_{k=0}^{n-1}\frac{\widetilde{\sigma}_n-\xi^n\,\sigma}{n\,k!(n-k-1)!}\left(-\frac{1}{\mu}\right)^{n-k}\Big(f^{(k)}(0)+\lambda\,C\,P^{(k)}(0)\Big), \tag{5.2.51}$$

wherein

$$\sigma=\int_{-1}^{1}Q(y)\,\mathrm{e}^{y/\mu}\,dy,\quad\text{and}\quad\widetilde{\sigma}_n=\int_{-1}^{1}Q(y)\,\mathrm{e}^{y/\mu}\,y^n\,dy,\quad n>1. \tag{5.2.52}$$

The right-hand side of (5.2.51) is convergent if (5.2.44) holds, in which case (5.2.51) can be rearranged to give

$$C = \frac{\zeta\,\sigma\,\mathrm{e}^{-\xi/\mu} + \displaystyle\sum_{n=1}^{\infty}\sum_{k=0}^{n-1} \frac{(\widetilde{\sigma}_n - \xi^n\,\sigma)\,f^{(k)}(0)}{n\,k!(n-k-1)!}\left(-\frac{1}{\mu}\right)^{n-k}}{1 - \lambda\displaystyle\sum_{n=1}^{\infty}\sum_{k=0}^{n-1} \frac{(\widetilde{\sigma}_n - \xi^n\,\sigma)\,P^{(k)}(0)}{n\,k!(n-k-1)!}\left(-\frac{1}{\mu}\right)^{n-k}}. \tag{5.2.53}$$

Together, (5.2.7), (5.2.50) and (5.2.53) give the IDE solution, provided the convergence condition (5.2.44) holds, in which case the solution $u(x)$ in (5.2.50) can again be approximated by $u_{\scriptscriptstyle M}(x)$, in which the infinite sums in the latter are terminated at $n = M$. Therefore, the approximate IDE solution is given by

$$u_{\scriptscriptstyle M}(x) = \zeta\,\mathrm{e}^{(x-\xi)/\mu} + \mathrm{e}^{x/\mu}\sum_{n=1}^{M}\sum_{k=0}^{n-1} \frac{x^n - \xi^n}{n\,k!(n-k-1)!}\left(-\frac{1}{\mu}\right)^{n-k} g_{\scriptscriptstyle M}^{(k)}(0), \tag{5.2.54}$$

wherein

$$g_{\scriptscriptstyle M}(x) = f(x) + \lambda P(x)\,\frac{\zeta\,\sigma\,\mathrm{e}^{-\xi/\mu} + \displaystyle\sum_{n=1}^{M}\sum_{k=0}^{n-1} \frac{(\widetilde{\sigma}_n - \xi^n\,\sigma)\,f^{(k)}(0)}{n\,k!(n-k-1)!}\left(-\frac{1}{\mu}\right)^{n-k}}{1 - \lambda\displaystyle\sum_{n=1}^{M}\sum_{k=0}^{n-1} \frac{(\widetilde{\sigma}_n - \xi^n\,\sigma)\,P^{(k)}(0)}{n\,k!(n-k-1)!}\left(-\frac{1}{\mu}\right)^{n-k}}. \tag{5.2.55}$$

Since the convergence condition for (5.2.54), like that in Section 5.2.2, provides a lower limit for $|\mu|$, (5.2.54) will be accurate only for sufficiently large $|\mu|$.

5.2.4 Numerical Experiments

The integration by parts approximations in (5.2.21) and (5.2.31), and the Taylor-series approximation in (5.2.54) are validated on an IDE with components

$$P(x) = \cos x, \quad Q(y) = y\,\sin y, \quad \lambda = -\frac{1}{2}, \quad u(x) = \mathrm{e}^{a\,x}, \quad a \in \mathbb{R}, \tag{5.2.56}$$

using which $f(x)$ is computed directly from (5.1.1) for varying values of μ and a. The test IDE with components (5.2.56) is augmented by a boundary condition at $\xi = -1$.

First, the convergence conditions must be checked. By (5.2.2), (5.2.7) and (5.2.56), $g(x)$ is given by

$$g(x) = f(x) + \lambda\, P(x)\, C = u(x) - \mu\, u'(x) = (1 - a\,\mu)\, \mathrm{e}^{a\,x}, \tag{5.2.57}$$

which is differentiated to give

$$g^{(k)}(x) = a^k\, (1 - a\,\mu)\, \mathrm{e}^{a\,x}. \tag{5.2.58}$$

Therefore, the convergence condition (5.2.11) for "method 1" yields

$$|\mu| < \frac{1}{|a|}. \tag{5.2.59}$$

To check the "method 2" condition (5.2.26) it is first noted that, by the Cauchy formula for repeated integration [99, Eq. 2.7.2], $G_k(x)$ in (5.2.23) is equivalently

$$G_k(x) = \frac{1}{(k-1)!} \int_{-1}^{x} (x - t)^{k-1}\, g(t)\, dt, \quad k \geq 1, \tag{5.2.60}$$

which, for $g(x)$ given by (5.2.57), yields

$$G_k(x) = \frac{1 - a\,\mu}{a^k} \left(\mathrm{e}^{a\,x} - \mathrm{e}^{-a} \sum_{n=0}^{k-1} \frac{(x+1)^n\, a^n}{n!} \right). \tag{5.2.61}$$

Since the sum in (5.2.61) is the Maclaurin series expansion for $\mathrm{e}^{a\,(x+1)}$, (5.2.61) can be written as

$$\begin{aligned} G_k(x) &= \frac{1 - \alpha\,\mu}{a^k} \left(\mathrm{e}^{a\,x} - \mathrm{e}^{-a} \left(\mathrm{e}^{a\,(x+1)} + R_{k-1}(x) \right) \right) \\ &= \frac{a\,\mu - 1}{a^k} \left(\mathrm{e}^{-a}\, R_{k-1}(x) \right), \end{aligned} \tag{5.2.62}$$

in which the remainder $R_{k-1}(x)$ is computed using the mean-value theorem [62, p. 29] as

$$R_{k-1}(x) = \frac{(a\,x)^k\, \mathrm{e}^{a x^*}}{k!}, \qquad x^* \in (-1, 1). \tag{5.2.63}$$

Therefore,

$$\frac{\|G_{k+1}\|}{\|G_k\|} = \frac{\|R_k\|}{\|a R_{k-1}\|} = \frac{1}{k+1}, \tag{5.2.64}$$

and so the convergence condition (5.2.26) for "method 2" yields

$$0 < |\mu|. \tag{5.2.65}$$

Finally, the convergence condition (5.2.44) is checked for the Taylor-series method. Substituting $g^{(k)}(0)$, found from (5.2.58), into (5.2.44) yields

$$\lim_{n\to\infty}\left|\frac{n\displaystyle\sum_{k=0}^{n}\frac{(-\mu\,a)^k}{k!\,(n-k)!}}{(n+1)\displaystyle\sum_{k=0}^{n-1}\frac{(-\mu\,a)^k}{k!\,(n-k-1)!}}\right|<|\mu|. \tag{5.2.66}$$

Since the binomial theorem [130, p. 145] gives

$$(1-\mu\,a)^n=\sum_{k=0}^{n}\frac{n!}{k!\,(n-k)!}\,(-\mu\,a)^k, \tag{5.2.67}$$

the left-hand side of (5.2.66) is equivalently

$$\lim_{n\to\infty}\left|\frac{\dfrac{n\,(1-\mu\,a)^n}{n!}}{\dfrac{(n+1)\,(1-\mu\,a)^{n-1}}{(n-1)!}}\right|=\lim_{n\to\infty}\left|\frac{1-\mu\,a}{n+1}\right|=0, \tag{5.2.68}$$

hence (5.2.66) becomes

$$0<|\mu|. \tag{5.2.69}$$

Therefore, solving the IDE with components (5.2.56) using integration by parts "method 2" and the Taylor-series expansion method results in solutions that are convergent for all values of μ. However, integration by parts "method 1" is only convergent for $|\mu|<1/|a|$. These assertions are validated for various μ and fixed $a=4$ in Figure 5.2.1.

Figure 5.2.1 demonstrates that, as predicted by (5.2.59), the errors $e_M=\|u-u_M\|$ for u_M given by (5.2.21) diverge when $|\mu|>1/|a|$ and converge for $|\mu|<1/|a|$ as $M\to\infty$; the rate of convergence/divergence is shown to be slower as $|\mu|\to 1/|a|$. Figure 5.2.1 also demonstrates that both approximate solutions (5.2.31) and (5.2.54) are convergent for all μ, as predicted by (5.2.65) and (5.2.69); however, convergence for u_M given by (5.2.31) is slower as $\mu\to 0$. Provided the convergence conditions are met, the accuracy of the approximate solution u_M increases with increasing M; this is expected since, by construction, $u_M\to u$ as $M\to\infty$.

Figure 5.2.1 shows that the semi-analytical methods are accurate for the test IDE with non-challenging components (5.2.56). However, the convergence conditions

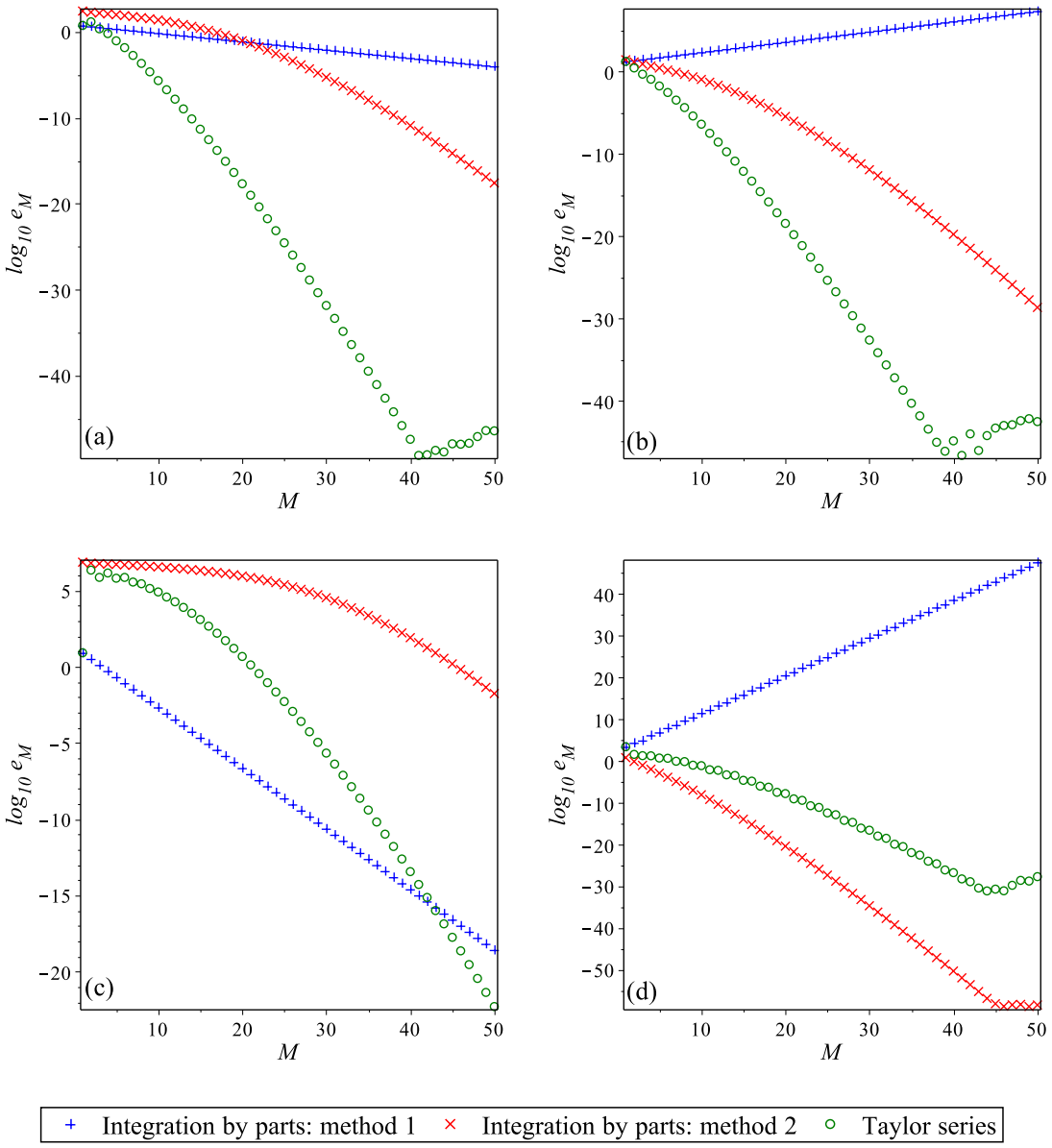

Figure 5.2.1: Semilog plots of the error $e_M = \|u - u_M\|$ as M increases for the IDE (5.1.1) with components (5.2.56) in which $a = 4$ and (a) $\mu = \frac{1}{5}$, (b) $\mu = \frac{1}{3}$, (c) $\mu = \frac{1}{10}$ and (d) $\mu = 2$. The approximate solution u_M is computed by integration by parts method 1 (5.2.21), integration by parts method 2 (5.2.31), and the Taylor-series expansion (5.2.54).

(5.2.11), (5.2.26) and (5.2.44) can in practice be difficult to check for IDEs with more complex components. Furthermore, since the semi-analytical methods are only valid for the subset of IDEs with constant differentiation coefficient $\mu(x) \equiv \mu$ and separable kernel $K(x, y) = P(x)\,Q(y)$, it is necessary to develop methods for solving IDEs numerically.

5.3 Numerical Methods

The previous section demonstrates that even the simplest IDE, with a constant differentiation coefficient $\mu(x) \equiv \mu$ and separable kernel $K(x, y) = P(x)\,Q(y)$, is not straightforward to solve analytically. Therefore, in general, the solution of an IDE must be approximated numerically. Many different numerical methods have been developed in order to solve the IDE (5.1.1). In addition to the methods discussed in this chapter's introduction, these include a differential-transform method [38], variational-iteration methods [24], a backward-difference and repeated-trapezoidal formulae [7], Shannon wavelets [92], a reproducing-kernel Hilbert-space approach [6], and iteration with a Chebyshev series [136]. Each of the methods listed here achieve varying degrees of accuracy on simple degenerate kernel test problems with smooth, non-challenging solutions; however, only [92] is augmented by a brief error analysis, in which error bounds are given for only the first derivative of the solution rather than the solution itself.

Therefore, this work has two aims which set it apart from the existing literature. Firstly, to develop a numerical method that improves upon the accuracy and efficiency of the existing methods, not only for problems with simple smooth solutions, but also for those with solutions that are designed to be challenging. Secondly, to implement an explicit error analysis that yields computable error bounds in terms of only the numerical solution.

In this section, Nyström-type numerical methods are developed that build upon the spectrally accurate FIE Nyström methods presented in Section 4.3. The FIE methods are presently extended by incorporating the Lagrange differentiation approximation (2.2.3) and the differentiation matrices introduced in Section 3.1. Since the Nyström method and Lagrange differentiation both converge exponentially with increasing collocation points, the Nyström-type IDE methods are expected to be

spectrally accurate. Furthermore, since both the Nyström method and Lagrange differentiation admit spectrally accurate and explicitly computable error bounds, so too will the Nyström-type IDE methods.

5.3.1 Extended Classical Nyström Method

Let the differential operator $\mathcal{D}$ in (5.1.3) be approximated by the Lagrange differentiation operator $\mathcal{D}_M$, defined by (2.2.3), and let the integral operator $\mathcal{K}$ be approximated by the Gaussian integral operator $\mathcal{K}_M$, defined by (4.3.4). Then, the approximate solution u_M of the IDE (5.1.3) satisfies

$$u_M - \mu\,\mathcal{D}_M\,u_M - \lambda\,\mathcal{K}_M\,u_M = f, \tag{5.3.1}$$

which is equivalently

$$u_M(x) - \mu(x)\sum_{j=1}^{M} L'_{j,M}(x)\,u_M(y_{j,M}) - \lambda\sum_{j=1}^{M} w_{j,M}\,K(x,y_{j,M})\,u_M(y_{j,M}) = f(x). \tag{5.3.2}$$

Since the integral in the IDE (5.1.1) has unit weight function, the integral operator $\mathcal{K}_M$ in (5.3.1) dictates that the nodes $y_{j,M}$ are Legendre, Legendre-Gauss-Radau or Legendre-Gauss-Lobatto. For simplicity, the linear operator $\mathcal{A}_M$ is defined by

$$\mathcal{A}_M \equiv \mu\mathcal{D}_M + \lambda\mathcal{K}_M, \tag{5.3.3}$$

and the functions $\alpha_{j,M}(x)$ defined by

$$\alpha_{j,M}(x) \equiv \mu(x)\,L'_{j,M}(x) + \lambda\,w_{j,M}\,K(x,y_{j,M}), \qquad j = 1(1)M, \tag{5.3.4}$$

so that

$$\mathcal{A}_M\,u_M = (\mathcal{A}_M\,u_M)(x) \equiv \sum_{j=1}^{M} \alpha_{j,M}(x)\,u_M(y_{j,M}). \tag{5.3.5}$$

Since (2.4.4) and (4.4.3) yield $\mathcal{D}_M u \approx \mathcal{D}u$ and $\mathcal{K}_M u \approx \mathcal{K}u$ respectively, if u is continuously differentiable then, by construction, $\mathcal{A}_M u \approx \mathcal{A}u$, for $\mathcal{A}$ defined by (5.1.4). Using (5.3.3)–(5.3.5), the IDE approximations (5.3.1) and (5.3.2) are equivalently

$$u_M - \mathcal{A}_M\,u_M = f, \tag{5.3.6}$$

and

$$u_M(x) - \sum_{j=1}^{M} \alpha_{j,M}(x)\, u_M(y_{j,M}) = f(x). \tag{5.3.7}$$

Collocating (5.3.7) at nodes $x = y_{i,M}$ yields the $M \times M$ linear system

$$\sum_{j=1}^{M} \Big(\delta_{ij} - \alpha_{j,M}(y_{i,M})\Big)\, u_M(y_{j,M}) = f(y_{i,M}), \qquad i = 1(1)M, \tag{5.3.8}$$

which in matrix form is

$$(\mathbf{I}_M - \mathbf{A}_M)\mathbf{u}_M = \mathbf{f}_M, \tag{5.3.9}$$

wherein

$$\begin{gathered} \{\mathbf{I}_M\}_{i,j} = \delta_{ij}, \quad \{\mathbf{A}_M\}_{i,j} = \alpha_{j,M}(y_{i,M}), \quad \{\mathbf{u}_M\}_i = u_M(y_{i,M}) \\ \{\mathbf{f}_M\}_i = f(y_{i,M}), \quad i,j = 1(1)M. \end{gathered} \tag{5.3.10}$$

It is noted that the matrix $\mathbf{A}_M$ is equivalent to the linear combination

$$\mathbf{A}_M = \mathbf{diag}\{\mu(y_{i,M})\}\, \mathbf{D}_M + \lambda \mathbf{K}_M, \tag{5.3.11}$$

where $\mathbf{D}_M$ is given by (3.1.8) and $\mathbf{K}_M$ is given by (4.3.9), and in which, when $\mu(x)$ is constant, $\mathbf{diag}\{\mu(y_{i,M})\}$ can simply be replaced by the constant μ. By computing $\mathbf{A}_M$ from (5.3.11), rather than from (5.3.10), the computational setup workload can be decreased by utilising the explicit forms of the differentiation matrices for the various node sets derived and discussed in Section 3.1.

The BC can be incorporated into (5.3.8) in one of two ways, depending on whether ξ in (5.1.2) coincides with a quadrature node. This reduces (5.3.8) to an $(M-1) \times (M-1)$ system. For clarity, the notation in (5.3.5) is amended to

$$\mathcal{A}_M\, u^*_M(x) \equiv \sum_{j=1}^{M} \alpha_{j,M}(x)\, u^*_M(y_{j,M}), \tag{5.3.12}$$

in which $u^*_M(y_{j,M})$ indicates a nodal value used only for the purposes of collocation, rather than a nodal value recovered from the numerical solution $u_M(x)$.

5.3.1.1 Case 1: Boundary condition enforced at collocation stage

When ξ coincides with a node, i.e. $\xi = y_{k,M}$ for some $1 \leq k \leq M$, the BC $u(\xi) = \zeta$ can be incorporated directly by assigning

$$u_M^*(y_{k,M}) = \zeta. \tag{5.3.13}$$

Substituting (5.3.13) into (5.3.8), and omitting the redundant equation collocated at $x = y_{k,M}$ gives

$$\sum_{\substack{j=1 \\ j \neq k}}^{M} \Big(\delta_{ij} - \alpha_{j,M}(y_{i,M}) \Big) \, u_M^*(y_{j,M}) = f(y_{i,M}) + \zeta \, \alpha_{k,M}(y_{i,M}), \qquad i = 1(1)M, i \neq k, \tag{5.3.14}$$

so that the reduced $(M-1) \times (M-1)$ system is given by

$$(\check{\mathbf{I}}_M - \check{\mathbf{A}}_M)\check{\mathbf{u}}_M^* = \check{\mathbf{f}}_M, \tag{5.3.15}$$

in which the checked quantities are obtained by removing the kth rows, (and also the kth columns for the matrices) of the matrices and vectors in (5.3.9) and $\check{\mathbf{f}}_M$ is adjusted in accordance with the right-hand side of (5.3.14). The matrix system (5.3.15) is solved for the solution vector $\check{\mathbf{u}}_M^*$ which, via (5.3.7) and (5.3.13), gives the numerical solution for $x \in [-1, 1]$ via the inversion formula

$$u_M(x) = f(x) + \zeta \, \alpha_{k,M}(x) + \sum_{\substack{j=1 \\ j \neq k}}^{M} \alpha_{j,M}(x) \, u_M^*(y_{j,M}). \tag{5.3.16}$$

Setting $x = y_{i,M}$ with $i \neq k$ in (5.3.16) gives, by comparison with (5.3.14), $u_M(y_{i,M}) = u_M^*(y_{i,M})$; however, since (5.3.14) is not collocated at $i = k$, setting $x = y_{k,M} = \xi$ in the inversion formula (5.3.16) does not recover the implemented BC, i.e.

$$u_M(\xi) \neq u_M^*(\xi) = \zeta. \tag{5.3.17}$$

5.3.1.2 Case 2: Boundary condition recovered in numerical solution

This BC implementation can be used whether or not ξ coincides with a node. Substituting the BC $u(\xi) = \zeta$ into (5.3.7) and rearranging for the nodal value $u_M^*(y_{k,M})$,

for some chosen $1 \leq k \leq M$, yields

$$u_M^*(y_{k,M}) = \widehat{\zeta} \equiv \frac{1}{\alpha_{k,M}(\xi)} \left(\zeta - f(\xi) - \sum_{\substack{j=1 \\ j \neq k}}^{M} \alpha_{j,M}(\xi)\, u_M(y_{j,M}) \right), \tag{5.3.18}$$

which gives a pseudo-BC that can be enforced in a similar way as in case 1. Substituting (5.3.18) into (5.3.8) and omitting the redundant equation collocated at $x = y_{k,M}$ gives

$$\begin{aligned} \sum_{\substack{j=1 \\ j \neq k}}^{M} \Big(\delta_{ij} - \alpha_{j,M}(y_{i,M}) \Big)\, u_M^*(y_{j,M}) \quad - \frac{\alpha_{k,M}(y_{i,M})}{\alpha_{k,M}(\xi)} \left(\zeta - f(\xi) - \sum_{\substack{j=1 \\ j \neq k}}^{M} \alpha_{j,M}(\xi)\, u_M^*(y_{j,M}) \right) \\ = f(y_{i,M}), \qquad i = 1(1)M, i \neq k, \end{aligned} \tag{5.3.19}$$

which rearranges to

$$\begin{aligned} &\sum_{\substack{j=1 \\ j \neq k}}^{M} \left(\delta_{ij} - \alpha_{j,M}(y_{i,M}) + \frac{\alpha_{k,M}(y_{i,M})}{\alpha_{k,M}(\xi)}\, \alpha_{j,M}(\xi) \right) u_M^*(y_{j,M}) \\ &\qquad = f(y_{i,M}) + \frac{\alpha_{k,M}(y_{i,M})}{\alpha_{k,M}(\xi)} \Big(\zeta - f(\xi) \Big), \qquad i = 1(1)M, i \neq k. \end{aligned} \tag{5.3.20}$$

In matrix form, (5.3.20) can be written as the $(M-1) \times (M-1)$ system

$$(\widehat{\mathbf{I}}_M - \widehat{\mathbf{A}}_M)\widehat{\mathbf{u}}_M^* = \widehat{\mathbf{f}}_M \tag{5.3.21}$$

in which $\widehat{\mathbf{I}}_M$ and $\widehat{\mathbf{u}}_M$ are obtained by removing the kth rows (and columns) of the matrices in (5.3.9) and the entries of $\widehat{\mathbf{A}}_M$ and $\widehat{\mathbf{f}}_M$ are computed in accordance with the information in (5.3.20). Solving the system (5.3.21) yields the vector $\widehat{\mathbf{u}}_M^*$ which is used, along with (5.3.18), to form the numerical solution for $x \in [-1, 1]$ via the inversion formula

$$u_M(x) = f(x) + \widehat{\zeta}\, \alpha_{k,M}(x) + \sum_{\substack{j=1 \\ j \neq k}}^{M} \alpha_{j,M}(x)\, u_M^*(y_{j,M}). \tag{5.3.22}$$

Setting $x = y_{i,M}$ with $i \neq k$ in (5.3.22) gives, by comparison with (5.3.20), $u_M(y_{i,M}) = u_M^*(y_{i,M})$ and in this case, via (5.3.18), setting $x = \xi$ in (5.3.22) recovers the BC, i.e.

$$u_M(\xi) = \zeta. \tag{5.3.23}$$

However, by an argument analogous to that following (5.3.16), since (5.3.20) is not collocated at $x = y_{k,M}$, the pseudo-BC (5.3.18) is not recovered, i.e.

$$u_M(y_{k,M}) \neq u_M^*(y_{k,M}) = \widehat{\zeta}. \tag{5.3.24}$$

The methods in Sections 5.3.1.1 and 5.3.1.2 will hereafter be referred to respectively as the case-1 and case-2 *extended classical Nyström method* (ECNM).

5.3.2 Extended Interpolated Nyström Method

In order to solve the integral component of an IDE using optimal quadrature nodes, and the differential component using optimal differentiation nodes, the INM, presented in Section 4.3.2, can be extended in a similar way to the extension shown for the CNM in Section 5.3.1. It was for this purpose that the INM was developed, since by combining optimal numerical integration and differentiation, the overall error in the IDE solution can be minimised.

Let the IDE approximation (5.3.1) be adjusted so that the integral operator $\mathcal{K}$ in (5.1.3) is now approximated by $\mathcal{K}_M \mathcal{L}_N$, as in the INM approximation (4.3.30). Therefore, the approximate solution $\widetilde{u}_{M,N}$ of the IDE (5.1.3) satisfies

$$\widetilde{u}_{M,N} - \mu \mathcal{D}_N \widetilde{u}_{M,N} - \lambda \mathcal{K}_M \mathcal{L}_N \widetilde{u}_{M,N} = f, \tag{5.3.25}$$

which is equivalently

$$\begin{aligned} \widetilde{u}_{M,N}(x) \quad &- \quad \mu(x) \sum_{j=1}^{N} L'_{j,N}(x)\, \widetilde{u}_{M,N}(x_{j,N}) \\ &- \quad \lambda \sum_{k=1}^{M} \sum_{j=1}^{N} w_{k,M} K(x, y_{k,M}) L_{j,N}(y_{k,M})\, \widetilde{u}_{M,N}(x_{j,N}) = f(x), \end{aligned} \tag{5.3.26}$$

wherein the integration nodes $y_{k,M}$ are Legendre, Legendre-Gauss-Radau or Legendre-Gauss-Lobatto, and the interpolation nodes $x_{j,N}$ are optimal differentiation nodes

such as Chebyshev or Chebyshev-Gauss-Lobatto. The linear operator $\widetilde{\mathcal{A}}_{M,N}$ is now defined by

$$\widetilde{\mathcal{A}}_{M,N} \equiv \mu \mathcal{D}_N + \lambda \mathcal{K}_M \mathcal{L}_N, \tag{5.3.27}$$

and the functions $\widetilde{\alpha}_{j,M,N}(x)$ defined by

$$\widetilde{\alpha}_{j,M,N}(x) \equiv \mu(x)\, L'_{j,N}(x) + \lambda \sum_{k=1}^{M} w_{k,M} K(x, y_{k,M}) L_{j,N}(y_{k,M}), \quad j = 1(1)N, \tag{5.3.28}$$

so that

$$\widetilde{\mathcal{A}}_{M,N}\, \widetilde{u}_{M,N}(x) \equiv \sum_{j=1}^{N} \widetilde{\alpha}_{j,M,N}(x)\, \widetilde{u}_{M,N}(x_{j,N}). \tag{5.3.29}$$

By an argument analogous to the one following (5.3.5), $\widetilde{\mathcal{A}}_{M,N} u \approx \mathcal{A} u$ when u is continuously differentiable. By (5.3.27)–(5.3.29) the IDE approximations (5.3.25) and (5.3.26) are equivalently

$$\widetilde{u}_{M,N} - \widetilde{\mathcal{A}}_{M,N}\, \widetilde{u}_{M,N} = f \tag{5.3.30}$$

and

$$\widetilde{u}_{M,N}(x) - \sum_{j=1}^{N} \widetilde{\alpha}_{j,M,N}(x)\, \widetilde{u}_{M,N}(x_{j,N}) = f(x). \tag{5.3.31}$$

The derivation of the extended INM now follows in the same way as that of the ECNM, in which $\mathcal{A}_M$ is replaced by $\widetilde{\mathcal{A}}_{M,N}$ and $\alpha_{j,M}(x)$ replaced by $\widetilde{\alpha}_{j,M,N}(x)$ throughout. This yields the case-1 numerical solution

$$\widetilde{u}_{M,N}(x) = f(x) + \zeta\, \widetilde{\alpha}_{k,M,N}(x) + \sum_{\substack{j=1 \\ j \neq k}}^{N} \widetilde{\alpha}_{j,M,N}(x)\, \widetilde{u}^{*}_{M,N}(x_{j,N}), \tag{5.3.32}$$

and the case-2 numerical solution

$$\widetilde{u}_{M,N}(x) = f(x) + \widetilde{\zeta}\, \widetilde{\alpha}_{k,M,N}(x) + \sum_{\substack{j=1 \\ j \neq k}}^{N} \widetilde{\alpha}_{j,M,N}(x)\, \widetilde{u}^{*}_{M,N}(x_{j,N}), \tag{5.3.33}$$

wherein

$$\widetilde{\zeta} \equiv \frac{1}{\widetilde{\alpha}_{k,M,N}(\xi)} \left(\zeta - f(\xi) - \sum_{\substack{j=1 \\ j \neq k}}^{N} \widetilde{\alpha}_{j,M,N}(\xi)\, \widetilde{u}_{M,N}(x_{j,N}) \right). \tag{5.3.34}$$

The solutions (5.3.32) and (5.3.33) are found by solving $(N-1)\times(N-1)$ systems, *cf.* (5.3.15) and (5.3.21). This method will hereafter be referred to as the *extended interpolated Nyström method* (EINM).

5.3.3 Numerical Experiments

The ECNM and EINM are now tested on four problems with known solutions, three of which are designed to be challenging; discussion of problems with challenging kernels is deferred to Section 5.4. The components of the IDE (5.1.1) for the test problems are summarised in Table 5.1.

Problem	Name	Solution $u(x)$	$\mu(x)$	Kernel $K(x,y)$	λ
1	Smooth	$\sin x + x$	$x^3 - 3$	$x^3\, y \cos y$	$\frac{1}{2}$
2	Runge	$\frac{1}{1+25x^2}$	$-x^2 + 3x$	$(x^2+3)(y-2)$	$\frac{1}{3}$
3	Steep	e^{10x}	$x + 2$	$\mathrm{e}^{2x}\, y$	$-\frac{1}{4}$
4	Oscillatory	$\cos 12x$	$-\sin x$	$\sin x^2\, y^2$	-1

Table 5.1: Test problems with known solutions of four qualitatively distinct forms. The Runge function, extreme gradient and highly oscillatory solutions of problems 2, 3 and 4 respectively are known to be challenging to approximation methods. For each problem, the source function $f(x)$ is readily computed directly from (5.1.1).

For the remainder of this chapter, Gauss-Legendre quadrature is used in the EINM since, when the weight function in an integral is unity, it is theoretically the most accurate quadrature method of those considered in Section 3.2.4. Additionally, since the regular nodes have been shown, through numerical experiments and a theoretical error analysis, to yield the least accurate results when used in the INM and numerical differentiation, these nodes will not be used within the EINM. Furthermore, the ECNM and EINM solutions are computed with $M = N$, so that both methods are implemented with N quadrature nodes and N collocation nodes, which enables systems of the same dimension to be compared.

Figure 5.3.1 presents the ECNM errors $e_N = \|u - u_N\|$ and EINM errors $e_N = \|u - \widetilde{u}_{N,N}\|$, with case-1 and case-2 BCs on a variety of nodal distributions. For each test problem the BC is given for $\xi = -1$, and so the case-1 implementation is not

possible on all nodal distributions. The case-2 implementation, which is enforceable on any nodal distribution, is implemented with $k = 1$ in (5.3.18) and (5.3.34).

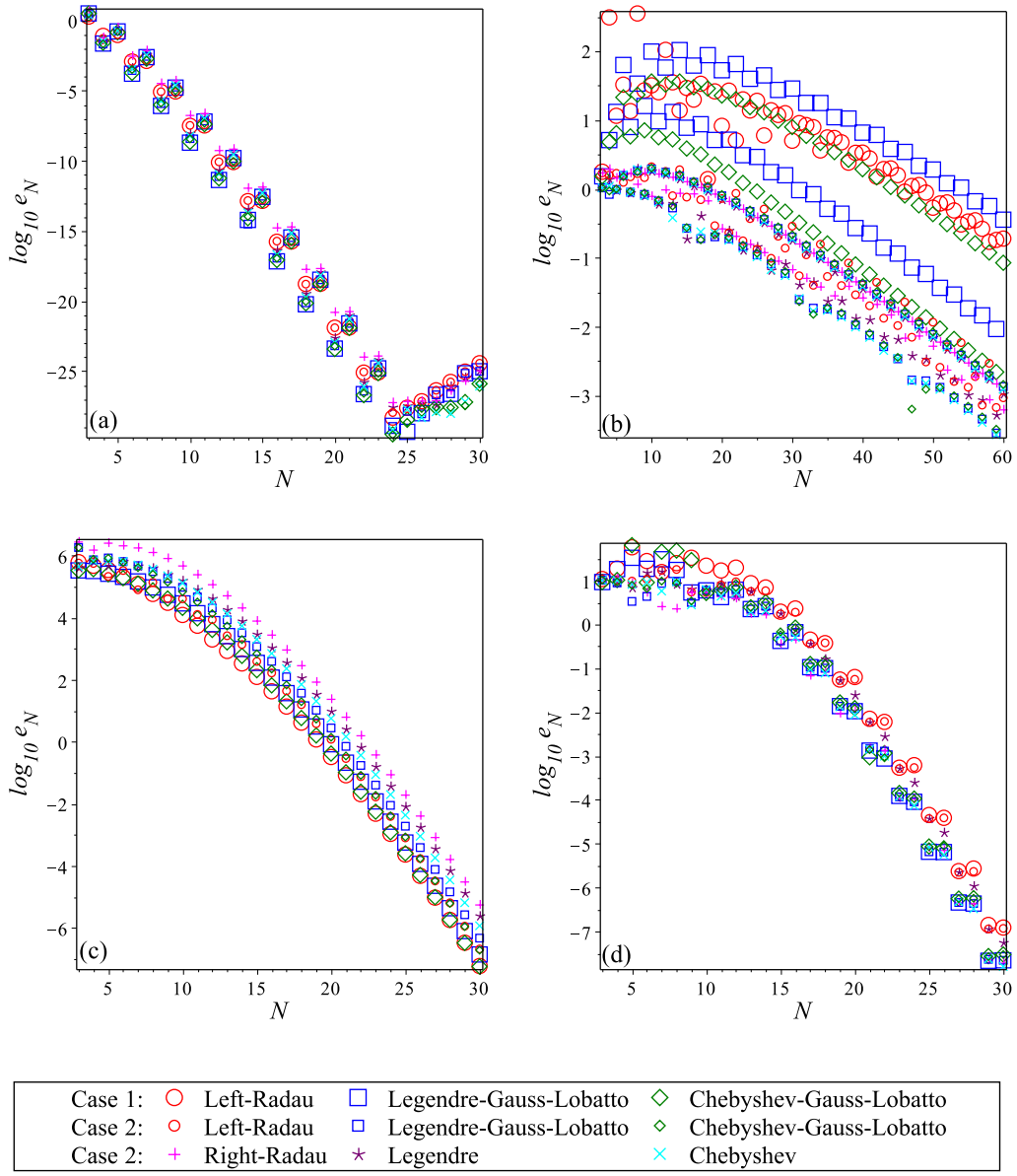

Figure 5.3.1: Logarithmic plots of the ECNM errors (Legendre, Left- and Right-Radau, and Legendre-Gauss-Lobatto) $e_N = \|u - u_N\|$, and EINM errors (Chebyshev and Chebyshev-Gauss-Lobatto) $e_N = \|u - \widetilde{u}_{N,N}\|$, for Problems (a) 1 ("smooth"), (b) 2 ("Runge"), (c) 3 ("steep") and (d) 4 ("oscillatory"), summarised in Table 5.1. Note that N is taken twice as large for problem 2.

The vertical scales of the sub-plots in Figure 5.3.1 show that convergence is fastest for the smooth problem and slowest for the Runge problem; this is expected from the errors shown in Figure 4.3.1 for the IE numerical methods. The steep and oscillatory problems are seen to have errors of approximately the same magnitude for higher values of N; however, the former has large errors for low values of N which shows that the steep gradient of the exact solution cannot be approximated well if the number of collocation nodes is insufficient. For each problem, the ECNM and EINM are shown to converge at the same rate, which demonstrates that the superiority of the CNM over then INM, shown in Figure 4.3.1, is lost in the extended counterparts. Moreover, despite the combination of optimal quadrature and optimal differentiation in the EINM, it has no clear advantage over the ECNM in terms of accuracy, contradicting its intended purpose. Therefore, the EINM is superfluous since not only is it no more accurate than the ECNM, but it is also computationally more expensive due to the intermediate interpolation in its quadrature term. Whether the case-1 or case-2 BC enforcement is more accurate is clearly problem-dependent; the most pronounced difference between case-1 and case-2 errors is observed for problem 2. However, whether the case-1 or case-2 BC enforcement is more accurate cannot be determined a priori because of the complexity of the matrix constructions used to compute the numerical solutions.

The effect of the BC implementation on the absolute-error distribution in $[-1, 1]$ is shown in Figure 5.3.2 for problem 1, solved using Legendre-Gauss-Lobatto nodes in the ECNM and Chebyshev-Gauss-Lobatto nodes in the EINM. Results are qualitatively similar for problems 2, 3 and 4 and for different nodal distributions. The results shown in Figure 5.3.2 confirm the predictions (5.3.17) and (5.3.23) regarding which case recovers the true BC in the inversion formula.

The effect of changing k in the case-2 BCs (5.3.18) and (5.3.34) is shown in Figure 5.3.3; the ECNM and EINM errors are shown for various k between 1 and N for problem 1. The ECNM is again computed using Legendre-Gauss-Lobatto nodes and the EINM using Chebyshev-Gauss-Lobatto nodes; results are qualitatively similar for the other nodal distributions and for problems 2, 3 and 4. The vertical scales in Figure 5.3.3 show that the effect of changing k in (5.3.18) and (5.3.34) is minimal. When N is odd the errors are shown to be largest when the BC is implemented at an end node, whilst when N is even the errors are minimised/maximised when the implementation node is in the vicinity of the BC location.

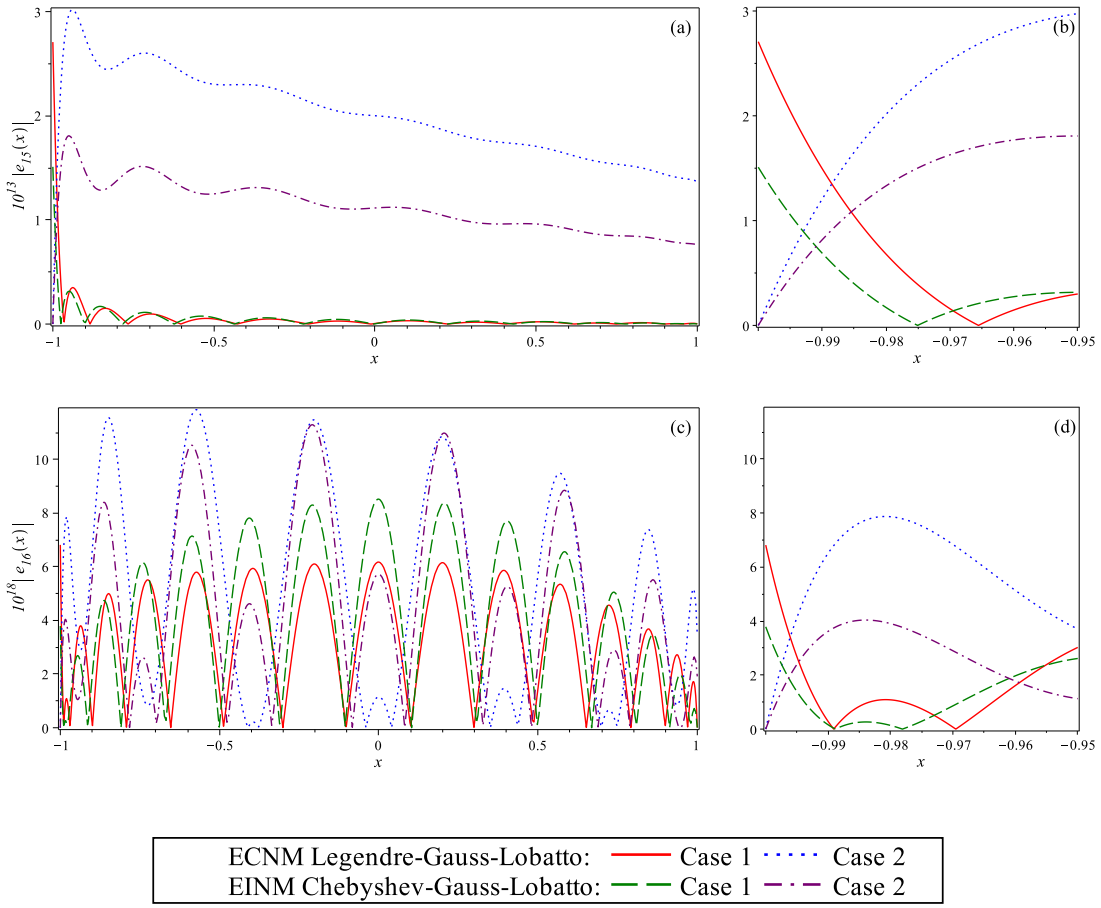

Figure 5.3.2: Plots showing the effect of the case-1 and case-2 BC implementation on the absolute errors $|e_N(x)| = |u(x) - u_N(x)|$ of the ECNM and $|e_N(x)| = |u(x) - \widetilde{u}_{N,N}(x)|$ of the EINM for problem 1. The results shown use Legendre-Gauss-Lobatto nodes in the ECNM and Chebyshev-Gauss-Lobatto nodes in the EINM with (a,b) $N = 15$ and (c,d) $N = 16$; the error profiles are qualitatively similar on other nodal distributions and for other values of N odd and N even. The expanded plots (b) and (d) around the BC location $\xi = -1$ confirm the prediction (5.3.17) that the case-1 approximation fails to recover the true BC and the prediction (5.3.23) that the case-2 approximation recovers the exact BC.

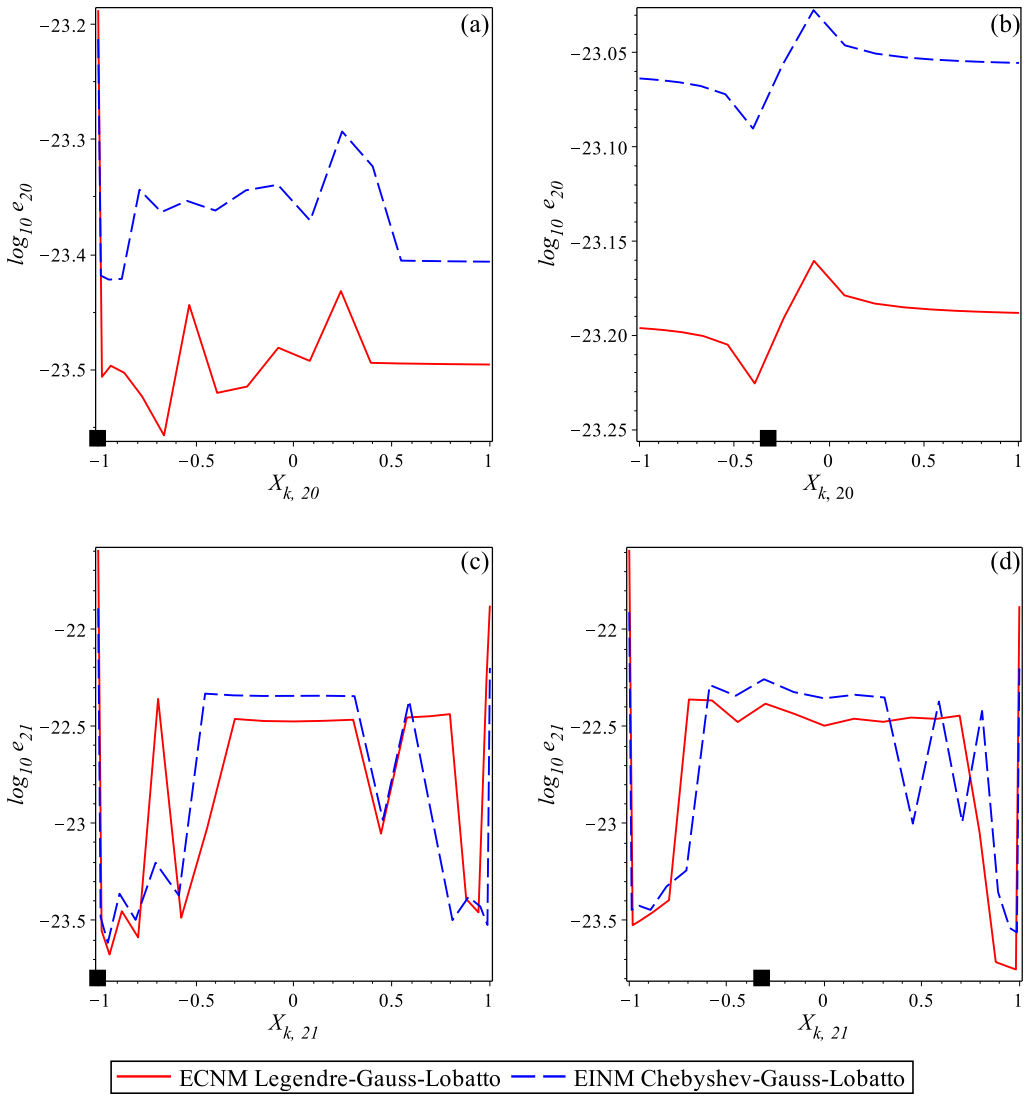

Figure 5.3.3: Logarithmic plots show the effect of varying k in the case-2 pseudo-BCs (5.3.18) and (5.3.34). The horizontal axes show the location of the ECNM node $y_{k,N}$ and EINM node $x_{k,N}$, both denoted by $X_{k,N}$, that the pseudo-BC is implemented and the vertical axes show the ECNM errors $e_N = \|u - u_N\|$ and the EINM errors $e_N = \|u - \widetilde{u}_{N,N}\|$. The errors are shown for problem 1 with (a,b) $N = 20$ and (c,d) $N = 21$ and with BC at (a,c) $\xi = -1$ and (b,d) $\xi = -1/\pi$, the latter irrational number ensuring a case-2 BC implementation. The BC locations are marked by black squares and piecewise-linear curves join the nodal data generated by varying k from 1 to N in (5.3.22) and (5.3.33).

5.4 Error Analysis

With the numerical methods now validated on a range of problems, it remains to find accurate error bounds. The theoretical framework for the error analyses of the extended Nyström methods is based upon the IE error analyses presented in Section 4.4; however, the IE error analyses must be extended to account for the presence of the unbounded differential operator $\mathcal{D}$. Computable error bounds based upon the numerical IDE solution are now derived which circumvent the unboundedness of $\mathcal{D}$ by "puncturing" it at the location of the BC; this is analogous to the procedure noted at the end of Section 3.1 that reduces by one the dimension of the singular differentiation matrix $\mathbf{D}_N$ to account for a BC, thereby yielding a non-singular, invertible matrix.

5.4.1 Extended Classical Nyström Method

The case-1 and case-2 numerical solutions, (5.3.16) and (5.3.22) respectively, can both be written as

$$u_M(x) = f(x) + \sum_{j=1}^{M} \alpha_{j,M}(x)\, u_M^*(y_{j,M}), \tag{5.4.1}$$

wherein $u_M^*(y_{k,M}) = \zeta$ for case 1 and $u_M^*(y_{k,M}) = \widehat{\zeta}$ for case 2. In operator form (5.4.1) is equivalently

$$u_M(x) = f(x) + \mathcal{A}_M\, u_M^*(x), \tag{5.4.2}$$

wherein the action of $\mathcal{A}_M$ on $u_M^*(x)$, which is defined by (5.3.5), is to be interpreted as $\mathcal{A}_M\, u_M^*(x) \equiv (\mathcal{A}_M\, u_M^*)(x)$; this notation is adopted for the action of all linear operators throughout this section. It is noted that the difference between $\mathcal{A}_M\, u_M(x)$ in (5.3.5) and $\mathcal{A}_M\, u_M^*(x)$ in (5.3.12) is

$$\begin{aligned} \mathcal{A}_M\, u_M(x) - \mathcal{A}_M\, u_M^*(x) &= \sum_{j=1}^{M} \alpha_{j,M}(x)\big(u_M(y_{j,M}) - u_M^*(y_{j,M})\big) \\ &= \alpha_{k,M}(x)\big(u_M(y_{k,M}) - u_M^*(y_{k,M})\big), \end{aligned} \tag{5.4.3}$$

since $j = k$ is the only index for which, by (5.3.17) and (5.3.24), the collocated nodal value $u_M^*(y_{j,M})$ is not equal to the solution value $u_M(y_{j,M})$. Therefore, by defining

the *residual* as

$$\rho_M(x) \equiv \alpha_{k,M}(x)\big(u_M(y_{k,M}) - u_M^*(y_{k,M})\big), \tag{5.4.4}$$

the operator form of (5.4.2) that incorporates the BC $u_M^*(y_{k,M}) = \zeta$ or $u_M^*(y_{k,M}) = \widehat{\zeta}$ is

$$u_M(x) = f(x) + \mathcal{A}_M\, u_M(x) - \rho_M(x). \tag{5.4.5}$$

However, the operator form of the exact IDE in (5.1.5) does not incorporate the BC $u(\xi) = \zeta$. Since the operator $\mathcal{A}$ contains the unbounded differentiation operator $\mathcal{D}$, the IDE (5.1.5) admits multiple solutions in the absence of a BC, i.e. two different solutions $u \neq v$ may satisfy $(\mathcal{I} - \mathcal{A})\, u = f$ and $(\mathcal{I} - \mathcal{A})\, v = f$. Therefore, unlike $\mathcal{I} - \lambda\,\mathcal{K}$ in the integral equation analysis of Section 4.4, $\mathcal{I} - \mathcal{A}$ is neither one-to-one nor invertible and so the operator theory used for the IE error analysis cannot be applied in the IDE case. To reformulate the problem in terms of bounded operators, the action of the punctured identity operator $\bar{\mathcal{I}}$ is defined by

$$\bar{\mathcal{I}}\, v(x) \equiv \bar{v}(x) = \begin{cases} v(x) & x \neq \xi \\ 0 & x = \xi. \end{cases} \tag{5.4.6}$$

Acting upon (5.1.5) with $\bar{\mathcal{I}}$ and defining $\bar{\mathcal{A}} = \bar{\mathcal{I}}\mathcal{A}$ yields

$$(\bar{\mathcal{I}} - \bar{\mathcal{A}})\, u(x) = \bar{f}(x), \tag{5.4.7}$$

and acting upon (5.4.5) with $\bar{\mathcal{I}}$ and defining $\bar{\mathcal{A}}_M = \bar{\mathcal{I}}\mathcal{A}_M$ gives

$$(\bar{\mathcal{I}} - \bar{\mathcal{A}}_M)\, u_M(x) = \bar{f}(x) - \bar{\rho}_M(x). \tag{5.4.8}$$

Subtraction of (5.4.8) from (5.4.7) yields the error

$$\bar{\mathcal{I}}\,\big(u(x) - u_M(x)\big) = \bar{\mathcal{A}}\, u(x) - \bar{\mathcal{A}}_M\, u_M(x) + \bar{\rho}_M(x) \tag{5.4.9}$$

which, by the addition of $\bar{\mathcal{A}}\, u_M(x) - \bar{\mathcal{A}}\, u_M(x) = 0$ to the right-hand side, is equivalently

$$(\bar{\mathcal{I}} - \bar{\mathcal{A}})\,\big(u(x) - u_M(x)\big) = (\bar{\mathcal{A}} - \bar{\mathcal{A}}_M)\, u_M(x) + \bar{\rho}_M(x). \tag{5.4.10}$$

The error formula (5.4.10) shows that the error is a combination of the residual incurred by implementing the BC, and the truncation error associated with the discretisation of the differential and integral operators.

Since the BC (5.1.2) is incorporated, (5.4.10) has a unique solution and so, unlike $\mathcal{I} - \mathcal{A}$, the operator $\bar{\mathcal{I}} - \bar{\mathcal{A}}$ is both one-to-one and invertible. This is analogous

to the procedure detailed in Section 3.1.7 which reduces a non-invertible $N \times N$ differentiation matrix to an invertible $N-1 \times N-1$ matrix by removing the row and column that correspond to the location of the given BC. In the context of the present operator theory, this reduction is implemented by puncturing the operator equations at the value of x at which the BC is assigned. Therefore, the inverse of $\bar{\mathcal{I}} - \bar{\mathcal{A}}$ exists and

$$u - u_M = (\bar{\mathcal{I}} - \bar{\mathcal{A}})^{-1}\, \bar{\mathcal{I}} \left((\mathcal{A} - \mathcal{A}_M)\, u_M + \rho_M \right). \tag{5.4.11}$$

By (5.4.8), the error (5.4.11) is equivalently

$$u - u_M = (\bar{\mathcal{I}} - \bar{\mathcal{A}})^{-1}\, \bar{\mathcal{I}}\, (\mathcal{A} u_M - u_M + f). \tag{5.4.12}$$

Therefore, the IDE error can be bounded by either

$$\|u - u_M\| \leq \left\| (\bar{\mathcal{I}} - \bar{\mathcal{A}})^{-1} \right\| \|(\mathcal{A} - \mathcal{A}_M) u_M + \rho_M\| \tag{5.4.13}$$

or

$$\|u - u_M\| \leq \left\| (\bar{\mathcal{I}} - \bar{\mathcal{A}})^{-1} \right\| \|u_M - \mathcal{A} u_M - f\|, \tag{5.4.14}$$

the latter of which reveals that the error is proportional to the residual obtained by substituting the numerical solution $u_M(x)$ into the exact IDE (5.1.5). The bound (5.4.14) also avoids the need to compute $\mathcal{A}_M u_M$ and ρ_M explicitly. In both (5.4.13) and (5.4.14) the second term on the right-hand side is computable; however, the first term is not and so must thus be bounded. Since, by (5.1.4) and (5.3.3), $\bar{\mathcal{A}}$ and $\bar{\mathcal{A}}_M$ are linear operators within which the numerical differentiation and integration schemes are convergent for all continuously differentiable functions, the error theory applied to $\mathcal{K}$ and $\mathcal{K}_M$ in Section 4.4 can be extended such that for sufficiently large M, the inverse $(\bar{\mathcal{I}} - \bar{\mathcal{A}})^{-1}$ exists and is bounded by [10, Thm. 4.1.1]

$$\left\| (\bar{\mathcal{I}} - \bar{\mathcal{A}})^{-1} \right\| \leq \frac{1 + \left\| (\bar{\mathcal{I}} - \bar{\mathcal{A}}_M)^{-1} \right\| \left\| \bar{\mathcal{A}} \right\|}{1 - \left\| (\bar{\mathcal{I}} - \bar{\mathcal{A}}_M)^{-1} \right\| \left\| (\bar{\mathcal{A}} - \bar{\mathcal{A}}_M) \bar{\mathcal{A}} \right\|}. \tag{5.4.15}$$

Following the approach in [10, Eqns. 4.1.13–4.1.17], which was verified for the IE case in Section 4.4, the sub-elements of (5.4.15) can be computed as

$$\left\| (\bar{\mathcal{I}} - \bar{\mathcal{A}}_M)^{-1} \right\| = \left\| (\bar{\mathcal{I}} - \bar{\mathcal{A}}_M)^{-1}(1) \right\|, \tag{5.4.16}$$

$$\left\| \bar{\mathcal{A}} \right\| = \left\| \bar{\mathcal{A}}(1) \right\| = |\lambda| \, \left\| \bar{\mathcal{K}}(1) \right\| \tag{5.4.17}$$

and

$$\left\|(\bar{\mathcal{A}}-\bar{\mathcal{A}}_M)\bar{\mathcal{A}}\right\| = \left\|(\bar{\mathcal{A}}-\bar{\mathcal{A}}_M)\bar{\mathcal{A}}(1)\right\| = |\lambda|\,\left\|(\bar{\mathcal{A}}-\bar{\mathcal{A}}_M)\bar{\mathcal{K}}(1)\right\|. \tag{5.4.18}$$

To compute $(\bar{\mathcal{I}}-\bar{\mathcal{A}}_M)^{-1}(1)$ first define

$$\bar{g}_M \equiv (\bar{\mathcal{I}}-\bar{\mathcal{A}}_M)^{-1}(1), \tag{5.4.19}$$

such that $\bar{g}_M(x)$ satisfies the punctured IDE

$$\bar{g}_M - \bar{\mathcal{A}}_M\, g_M = \bar{1}, \tag{5.4.20}$$

and g_M satisfies the the non-punctured IDE

$$g_M - \mathcal{A}_M\, g_M = 1, \tag{5.4.21}$$

for which there is no specified BC. Imposing a BC and solving the IDE (5.4.21) by either of the methods in Section 5.3 would result in a residual $\widetilde{\rho}_M(x) = \alpha_{k,M}(x)\big(g_M(y_{k,M}) - g^*_M(y_{k,M})\big)$ (*cf.* (5.4.4)) such that

$$g_M - \mathcal{A}_M\, g_M = 1 - \widetilde{\rho}_M. \tag{5.4.22}$$

Comparison of (5.4.21) and (5.4.22) shows that the residual must vanish; this requires $g^*_M(y_{k,M}) = g_M(y_{k,M})$ which occurs only if (5.4.21) is collocated at all nodes, including $x = y_{k,M}$. Therefore, (5.4.21) must be solved without imposing a BC; since only a solution $g_M(x)$ of (5.4.21) is required, this is sufficient. The resulting matrix system is

$$(\mathbf{I}_M - \mathbf{A}_M)\mathbf{g}_M = \mathbf{1}, \tag{5.4.23}$$

in which $\mathbf{I}_M$ is the $M \times M$ identity matrix, $\mathbf{A}_M$ is defined in (5.3.11), and

$$\{\mathbf{g}_M\}_i = g_M(y_{i,M}) \qquad \text{and} \qquad \{\mathbf{1}\}_i = 1. \tag{5.4.24}$$

Solving (5.4.23) yields the nodal values $g_M(y_{i,M})$ from which $g_M(x)$ is then computed by the interpolation formula

$$g_M(x) = 1 + \sum_{j=1}^{M} \alpha_{j,M}(x)\, g_M(y_{j,M}). \tag{5.4.25}$$

Therefore, the theoretical bound on $\left\|(\bar{\mathcal{I}}-\bar{\mathcal{A}})^{-1}\right\|$ in (5.4.15) can be approximated by the computable bound

$$\left\|(\bar{\mathcal{I}}-\bar{\mathcal{A}})^{-1}\right\| \le \frac{1 + |\lambda|\,\|\bar{g}_M\|\,\left\|\bar{\mathcal{K}}(1)\right\|}{1 - |\lambda|\,\|\bar{g}_M\|\,\left\|(\bar{\mathcal{A}}-\bar{\mathcal{A}}_M)\bar{\mathcal{K}}(1)\right\|}. \tag{5.4.26}$$

Substitution of (5.4.26) into (5.4.13) gives the ECNM error bound

$$\|u - u_M\| \leq \frac{1 + |\lambda| \, \|\bar{g}_M\| \, \|\bar{\mathcal{K}}(1)\|}{1 - |\lambda| \, \|\bar{g}_M\| \, \|(\bar{\mathcal{A}} - \bar{\mathcal{A}}_M)\bar{\mathcal{K}}(1)\|} \, \|(\mathcal{A} - \mathcal{A}_M)u_M + \rho_M\| \,, \tag{5.4.27}$$

whilst substitution of (5.4.26) into (5.4.14) gives the ECNM error bound, which is equivalent to (5.4.27), as

$$\|u - u_M\| \leq \frac{1 + |\lambda| \, \|\bar{g}_M\| \, \|\bar{\mathcal{K}}(1)\|}{1 - |\lambda| \, \|\bar{g}_M\| \, \|(\bar{\mathcal{A}} - \bar{\mathcal{A}}_M)\bar{\mathcal{K}}(1)\|} \, \|u_M - \mathcal{A}u_M - f\| \,. \tag{5.4.28}$$

Both (5.4.27) and (5.4.28) are explicitly computable using only the numerical solution and functions that are readily available from the original IDE (5.1.5).

5.4.2 Extended Interpolated Nyström Method

The error analysis for the EINM is analogous to that of the ECNM. The resulting equivalent, computable error bounds (*cf.* (5.4.27), (5.4.28)) are

$$\|u - \widetilde{u}_{M,N}\| \leq \frac{1 + |\lambda| \, \|\bar{\widetilde{g}}_{M,N}\| \, \|\bar{\mathcal{K}}(1)\|}{1 - |\lambda| \, \|\bar{\widetilde{g}}_{M,N}\| \, \|(\bar{\mathcal{A}} - \bar{\widetilde{\mathcal{A}}}_{M,N})\bar{\mathcal{K}}(1)\|} \, \|(\mathcal{A} - \widetilde{\mathcal{A}}_{M,N})\widetilde{u}_{M,N} + \widetilde{\rho}_{M,N}\| \tag{5.4.29}$$

and

$$\|u - \widetilde{u}_{M,N}\| \leq \frac{1 + |\lambda| \, \|\bar{\widetilde{g}}_{M,N}\| \, \|\bar{\mathcal{K}}(1)\|}{1 - |\lambda| \, \|\bar{\widetilde{g}}_{M,N}\| \, \|(\bar{\mathcal{A}} - \bar{\widetilde{\mathcal{A}}}_{M,N})\bar{\mathcal{K}}(1)\|} \, \|\widetilde{u}_{M,N} - \mathcal{A}\widetilde{u}_{M,N} - f\| \,, \tag{5.4.30}$$

wherein the residual $\widetilde{\rho}_{M,N}$ is computed by

$$\widetilde{\rho}_{M,N}(x) \equiv \widetilde{\alpha}_{k,M,N}(x)\big(\widetilde{u}_{M,N}(x_{i,N}) - \widetilde{u}^*_{M,N}(x_{i,N})\big), \tag{5.4.31}$$

and in which $\widetilde{g}_{M,N}$ is the solution of

$$\widetilde{g}_{M,N} - \widetilde{\mathcal{A}}_{M,N}\, \widetilde{g}_{M,N} = 1. \tag{5.4.32}$$

The solution $\widetilde{g}_{M,N}$ in (5.4.32) is found by solving the matrix system

$$(\mathbf{I}_N - \widetilde{\mathbf{A}}_{M,N})\, \widetilde{\mathbf{g}}_{M,N} = \mathbf{1} \tag{5.4.33}$$

wherein, for $i, j = 1(1)N$,

$$\{\widetilde{\mathbf{A}}_{M,N}\}_{i,j} = \widetilde{\alpha}_{j,M,N}(x_{i,N}), \quad \{\widetilde{\mathbf{g}}_{M,N}\}_i = \widetilde{g}_{M,N}(x_{i,N}), \quad \{\mathbf{1}\}_i = 1 \tag{5.4.34}$$

and $\mathbf{I}_N$ is the $N \times N$ identity matrix. The nodal values $\widetilde{g}_{M,N}(x_{i,N})$ found by solving (5.4.33) are then used to compute $\widetilde{g}_{M,N}(x)$ using the interpolation formula

$$\widetilde{g}_{M,N}(x) = 1 + \sum_{j=1}^{N} \widetilde{\alpha}_{j,M,N}(x)\, \widetilde{g}_{M,N}(x_{i,N}). \tag{5.4.35}$$

Note that $\widetilde{g}_{M,N}(x)$ is punctured at $x = \xi$ in (5.4.29) and (5.4.30) yielding $\widetilde{\widetilde{g}}_{M,N}(x)$.

The ECNM bound (5.4.27) and EINM bound (5.4.29) are used for asymptotic error analyses in Section 5.4.3.

5.4.3 Asymptotic Convergence Rates

An asymptotic convergence rate for the ECNM can be derived from the bound (5.4.27). The final term on the right-hand side of (5.4.27) is first bounded by

$$\|(\mathcal{A} - \mathcal{A}_M)u_M + \rho_M\| \leq \Delta_M + \|\rho_M\|, \tag{5.4.36}$$

wherein Δ_M is defined (and bounded) by

$$\Delta_M \equiv \|(\mathcal{A} - \mathcal{A}_M)u_M\| \leq \|\mu\|\, \|(\mathcal{D} - \mathcal{D}_M)u_M\| + |\lambda|\, \|(\mathcal{K} - \mathcal{K}_M)u_M\|. \tag{5.4.37}$$

By (2.4.69) and (4.4.53) the bound (5.4.37) yields

$$\Delta_M \leq \|\mu\| \left(\phi_M \left\| u_M^{(M)} \right\| + \frac{\sigma_M \left\| u_M^{(M+1)} \right\|}{M+1} \right) + |\lambda|\, \psi_M^{(\nu)}\, \mathbb{K}_{2M-\nu}, \tag{5.4.38}$$

wherein ϕ_M and σ_M are given for different node sets in Table 2.1, $\psi_M^{(\nu)}$ is given by (3.2.14)–(3.2.16) for $\nu = 0, 1, 2$, and $\mathbb{K}_M$ is defined in (4.4.54). Since asymptotic limits in Table 2.1 and (3.2.20) yield

$$\phi_M \to \widetilde{\phi}_M \sim \left(\frac{\mathrm{e}}{2M}\right)^M, \quad \sigma_M \to \widetilde{\sigma}_M \sim \left(\frac{\mathrm{e}}{2M}\right)^M \quad \text{and} \quad \psi_M^{(\nu)} \to \widetilde{\psi}_M^{(\nu)} \sim \left(\frac{\mathrm{e}}{4M}\right)^{2M},$$

$$M \to \infty, \tag{5.4.39}$$

and since Table 2.1 additionally shows that $\phi_M > \sigma_M$ then, provided

$$\left\| u_M^{(M)} \right\| \sim o(M^M) \quad \text{and} \quad \mathbb{K}_{2M-\nu} \sim o(M^{2M}), \qquad M \to \infty, \tag{5.4.40}$$

the bound in (5.4.38) can be approximated by

$$\Delta_M \sim \phi_M \, \mathbb{U}_M, \qquad M \gg 1. \tag{5.4.41}$$

wherein

$$\mathbb{U}_M = \max\left(\left\| u_M^{(M)} \right\|, \left\| u_M^{(M+1)} \right\| \right). \tag{5.4.42}$$

Since both $u_M(y_{k,M})$ and $u_M^*(y_{k,M})$ in the residual ρ_M defined in (5.4.4) are given by a Nyström process whose convergence rate is given by (5.4.41), the difference $u_M(y_{k,M}) - u_M^*(y_{k,M})$ is proportional to the same rate, and so

$$\rho_M \sim \phi_M \, \mathbb{U}_M, \qquad M \to \infty. \tag{5.4.43}$$

Therefore, (5.4.27) and (5.4.36)–(5.4.43) together yield the asymptotic ECNM error-convergence rate

$$\|u - u_M\| \sim \phi_M \, \mathbb{U}_M, \qquad M \to \infty, \tag{5.4.44}$$

provided conditions (5.4.40) are met. By defining

$$\kappa(x) \equiv \int_{-1}^{1} K(x,y)\, dy \qquad \text{and} \qquad \mathbb{L}_M \equiv \max_{x,y\in[-1,1]} \left| \frac{\partial^M}{\partial y^M} \Big(K(x,y)\, \kappa(y) \Big) \right| \tag{5.4.45}$$

and using the arguments leading to (5.4.40) it is seen that, provided

$$\left\| \kappa^{(M)} \right\| \sim o(M^M) \quad \text{and} \quad \mathbb{L}_{2M-\nu} \sim o(M^{2M}), \qquad M \to \infty, \tag{5.4.46}$$

then (5.4.18) and a modified (5.4.41) reveal that the denominator in (5.4.26) behaves as $1 + O(M^{-M})$ as $M \to \infty$. Therefore the bound in (5.4.26) is positive, as required by the theory from which it is constructed, see [10, Thm. 4.1.1].

The convergence rate of the EINM can be derived from the bound (5.4.29), whose final term on the right-hand side is bounded by

$$\left\| (\mathcal{A} - \widetilde{\mathcal{A}}_{M,N}) \widetilde{u}_{M,N} + \widetilde{\rho}_{M,N} \right\| \le \widetilde{\Delta}_{M,N} + \|\widetilde{\rho}_{M,N}\|, \tag{5.4.47}$$

wherein $\widetilde{\Delta}_{M,N}$ is defined (*cf.* (5.4.37)) by

$$\widetilde{\Delta}_{M,N} \equiv \left\| (\mathcal{A} - \widetilde{\mathcal{A}}_{M,N}) \widetilde{u}_{M,N} \right\| \tag{5.4.48}$$

and bounded by

$$\widetilde{\Delta}_{M,N} \le \|\mu\| \, \|(\mathcal{D} - \mathcal{D}_N)\widetilde{u}_{M,N}\| + |\lambda| \left(\|(\mathcal{K} - \mathcal{K}_M)\widetilde{u}_{M,N}\| + \|\mathcal{K}_M(\mathcal{I} - \mathcal{L}_N)\widetilde{u}_{M,N}\| \right). \tag{5.4.49}$$

By (2.4.69), (4.4.58) and (4.4.64), the bound in (5.4.49) yields

$$\widetilde{\Delta}_{M,N} \leq \|\mu\| \left(\phi_N \left\| \widetilde{u}_{M,N}^{(N)} \right\| + \frac{\sigma_N \left\| \widetilde{u}_{M,N}^{(N+1)} \right\|}{N+1} \right) + |\lambda| \left(\psi_M^{(\nu)} \widetilde{\mathbb{K}}_{2M-\nu} + \sigma_N \left\| \mathcal{K}_M(1) \right\| \left\| \widetilde{u}_{M,N}^{(N)} \right\| \right), \tag{5.4.50}$$

wherein the node-dependent ϕ_N and σ_N are given explicitly in Table 2.1, $\psi_M^{(\nu)}$ is given by (3.2.14)–(3.2.16) for $\nu = 0, 1, 2$, and $\widetilde{\mathbb{K}}_M$ is defined in (4.4.59). The asymptotic limits in Table 2.1 and (3.2.20) give

$$\phi_N \to \widetilde{\phi}_N \sim \left(\frac{\mathrm{e}}{2N}\right)^N, \quad \sigma_N \to \widetilde{\sigma}_N \sim \left(\frac{\mathrm{e}}{2N}\right)^N \quad \text{and} \quad \psi_M^{(\nu)} \to \widetilde{\psi}_M^{(\nu)} \sim \left(\frac{\mathrm{e}}{4M}\right)^{2M},$$

$$M, N \to \infty, \tag{5.4.51}$$

and Table 2.1 shows also that $\phi_N > \sigma_N$. Therefore, provided

$$\left\| \widetilde{u}_{M,N}^{(N)} \right\| \sim o(N^N) \quad \text{and} \quad \widetilde{\mathbb{K}}_{2M-\nu} \sim o(M^{2M}), \qquad M, N \to \infty, \tag{5.4.52}$$

$\widetilde{\Delta}_{M,N}$ can be approximated by

$$\widetilde{\Delta}_{M,N} \sim \begin{cases} \psi_M^{(\nu)} \widetilde{\mathbb{K}}_{2M-\nu}, & \frac{N}{2} > M \gg 1, \\ \phi_N \widetilde{\mathbb{U}}_{M,N}, & M > \frac{N}{2} \gg 1, \end{cases} \tag{5.4.53}$$

wherein

$$\widetilde{\mathbb{U}}_{M,N} = \max\left(\left\| \widetilde{u}_{M,N}^{(N)} \right\|, \left\| \widetilde{u}_{M,N}^{(N+1)} \right\| \right). \tag{5.4.54}$$

For the reasons following (5.4.40), $\|\widetilde{\rho}_{M,N}\|$ in (5.4.47) also converges at the rates given in (5.4.53). Therefore, (5.4.29) and (5.4.47)–(5.4.53) yield the asymptotic EINM error-convergence rates

$$\|u - \widetilde{u}_{M,N}\| \sim \begin{cases} \psi_M^{(\nu)} \widetilde{\mathbb{K}}_{2M-\nu}, & \frac{N}{2} > M \gg 1, \\ \phi_N \widetilde{\mathbb{U}}_{M,N}, & M > \frac{N}{2} \gg 1, \end{cases} \tag{5.4.55}$$

provided conditions (5.4.52) are met. Finally, by arguments analogous to those following (5.4.45), provided

$$\left\| \kappa^{(N)} \right\| \sim o(N^N) \quad \text{and} \quad \mathbb{L}_{2M-\nu} \sim o(M^{2M}), \qquad M, N \to \infty, \tag{5.4.56}$$

wherein $\kappa(x)$ and $\mathbb{L}_{2M-\nu}$ are defined by (5.4.45), then the bounds in (5.4.29) and (5.4.30) are positive by construction.

When $M = N$, as in the numerical experiments in Section 5.3.3, the asymptotic rate in (5.4.55) reduces to

$$\|u - \widetilde{u}_{N,N}\| \sim \phi_N \, \widetilde{\mathbb{U}}_{N,N}, \qquad N \to \infty. \tag{5.4.57}$$

Therefore, when $M = N$, comparison of the numerical differentiation error (2.4.69) with the error-convergence rates (5.4.44) and (5.4.57) shows that both the ECNM and EINM errors are dictated by the error in the numerical differentiation. Furthermore, comparison of the ECNM error-convergence rate in (5.4.44) with the EINM error-convergence rate in (5.4.57) corroborates the observations from Figure 5.3.1; that the ECNM and EINM errors converge at the same rate since, as outlined in Table 2.1, $\phi_N \sim \left(\frac{\mathrm{e}}{2N}\right)^N$ for all clustered-node distributions. Since the EINM enables IDEs to be solved using nodes that are optimal for differentiation, theoretically it should yield errors that converge at the same rate as those of the ECNM but which are smaller in magnitude; it was for this reason that the EINM was developed. However, Figure 5.3.3 shows that computationally this is not necessarily the case. That is, despite the inclusion of both optimal differentiation and optimal integration nodes, there is no advantage in solving an IDE by the EINM; moreover, the computationally expensive interpolation between the nodes in the EINM means that the ECNM is favourable.

5.4.4 Numerical Results

The ECNM bound (5.4.28) and EINM bound (5.4.30) are tested on the problems summarised in Table 5.1; the newly predicted bounds b_N are presented along with the true computational case-1 and case-2 errors in Figure 5.4.1. Also shown is the quantity $\phi_N \left\|u^{(N)}\right\|$ that approximates both case-1 and case-2 asymptotic convergence rates, given by (5.4.44) and (5.4.57) for the ECNM and EINM respectively; the problem 2 convergence rate is omitted since $\left\|u^{(N)}\right\|$ is divergent when $u(x)$ is the Runge function (see (2.5.4) – (2.5.5)). The ECNM is solved on Legendre-Gauss-Lobatto nodes, and the EINM is solved with $M = N$ on Chebyshev-Gauss-Lobatto nodes, with the BC enforced at $\xi = -1$; results using other nodal distributions were found to be qualitatively similar.

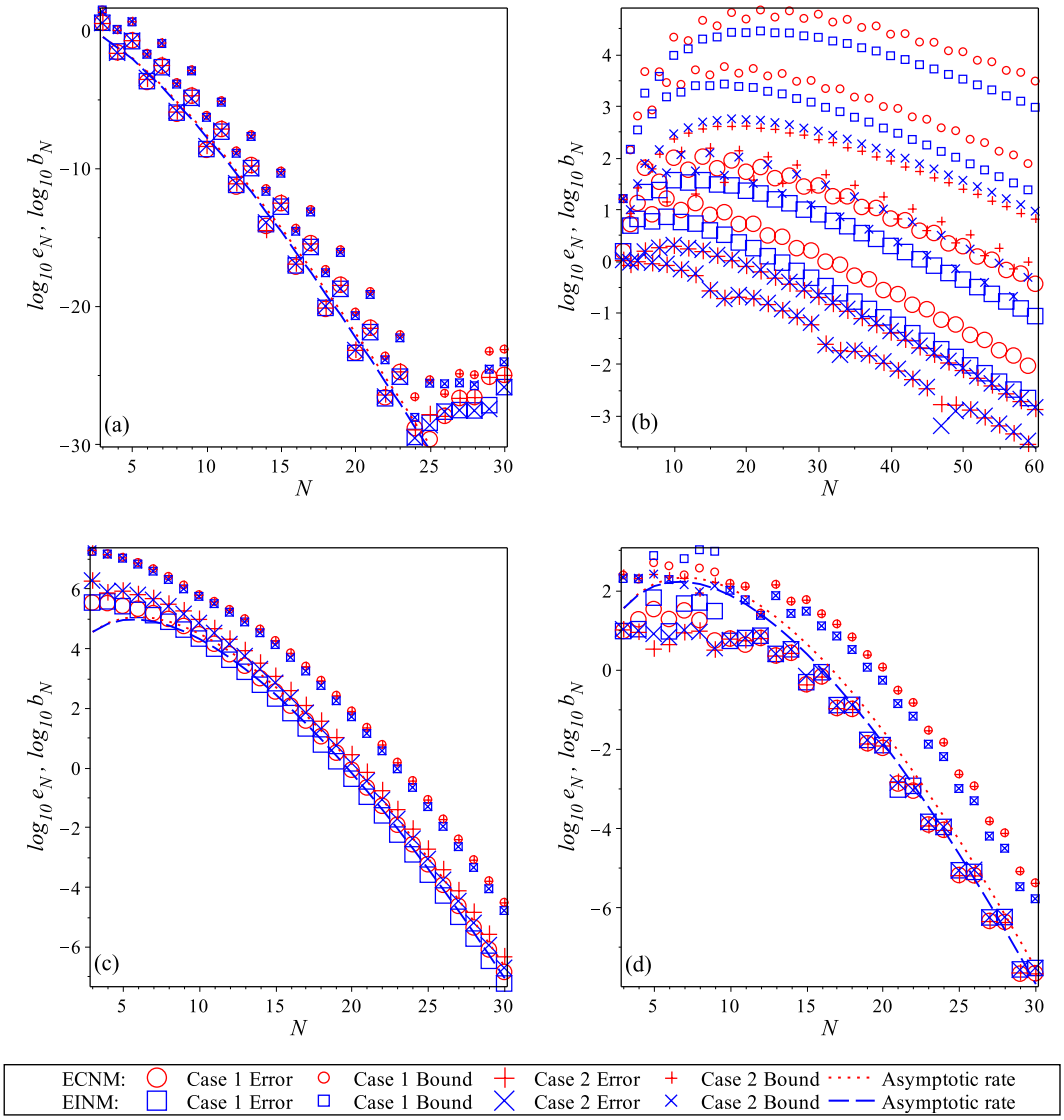

Figure 5.4.1: Logarithmic plots of the ECNM errors $e_N = \|u - u_N\|$ using Legendre-Gauss-Lobatto nodes, and the EINM errors $e_N = \|u - \widetilde{u}_{N,N}\|$ using Chebyshev-Gauss-Lobatto nodes, for both case-1 and case-2 BC implementations, and respective bounds b_N given by (5.4.28) and (5.4.30) for Problems (a) 1 ("smooth"), (b) 2 ("Runge"), (c) 3 ("steep") and (d) 4 ("oscillatory"), summarised in Table 5.1. The errors and bounds are compared to $\phi_N \left\|u^{(N)}\right\|$, scaled by an appropriate constant, which approximates the asymptotic convergence rates of both the ECNM and EINM errors, (5.4.44) and (5.4.57) respectively. Note the extended range of N in (b) invited by the slower convergence.

Figure 5.4.1 shows spectrally accurate agreement between the true computational errors and the newly computed error bounds; the strongest agreement is shown for the smooth problem and the weakest for the Runge problem. This is expected since larger errors in the numerical solution are magnified in the right-most term of the bounds (5.4.28) and (5.4.30). Despite the varying levels of agreement, the bounds capture well the rate of convergence to zero of the true errors. The agreement between the true errors and bounds validates the proposition that the sub-elements of (5.4.15) can be accurately computed by (5.4.16)–(5.4.18). This is additionally supported by further experiments which revealed that, in some cases, if (5.4.16)–(5.4.18) were computed with "1" replaced by some other function, then the resulting bounds do not necessarily exceed, as required, the errors. The bounds remain accurate when the location k of the case-2 BC is changed (see Figure 5.3.3), since the minor perturbations in the errors are reflected in the corresponding bounds: that is, the errors and bounds either increase or decrease together so that the relative accuracy of the bounds is maintained. Figure 5.4.1 also shows that the asymptotic estimates accurately predict the rate of convergence of the errors with increasing N; the exceptions to this are the (omitted) asymptotic rates, for the Runge problem, which are divergent (*cf.* Figure 4.4.2(b)).

The problems analysed in this section, which are summarised in Table 5.1, were designed to have challenging solutions and smooth kernels. Problems which have a smooth solution and a challenging kernel pose a potential limitation to the ECNM and EINM theory. For example, the numerical experiments were repeated on problems with smooth solutions but challenging kernels, these were: (a) $K(x,y) = \mathrm{e}^{\omega\,(x-y)^2}$ (isolated peak along the diagonal for $\omega \in \mathbb{R}^+$); (b) $K(x,y) = y^2/(1+25x^2)$ (Runge); (c) $K(x,y) = x^2\,\mathrm{e}^{20y}$ (steep), and; (d) $K(x,y) = x^2\cos 20\,y$ (highly oscillatory). For each of the challenging-kernel problems the ECNM and EINM errors converge with increasing N; however, the bound theory fails for problems (a) and (c), though for different reasons. The bound for problem (a) cannot be computed due to the term $\bar{\mathcal{A}}\,\bar{\mathcal{K}}(1)$ in (5.4.26)–(5.4.30), since it is not possible to perform the double integration in $\bar{\mathcal{A}}\,\bar{\mathcal{K}}(1)$ as a closed-form function of x. The bound for problem (c) is negative due to the denominator in (5.4.26) and its EINM counterpart; this is because the condition *cf.* [10, Eq. 4.1.22]

$$\left\|(\bar{\mathcal{A}} - \bar{\mathcal{A}}_{_M})\bar{\mathcal{A}}\right\| < \frac{1}{\left\|(\bar{\mathcal{I}} - \bar{\mathcal{A}}_{_M})^{-1}\right\|} \tag{5.4.58}$$

that is required for (5.4.15) to hold is violated by using the approximation (5.4.18). Although in (a) it is possible to bound the uncomputable term in the ECNM bound by a modified (5.4.38) and the uncomputable term in the EINM bound by a modified (5.4.50), this also yields negative error predictions since the second condition in (5.4.46) and (5.4.56) is violated. Despite the kernel in problem (b) yielding a value of $\kappa(x)$ of a "Runge" form thus violating the first condition in (5.4.46) and (5.4.56), e.g.

$$\kappa(x) = \frac{2}{3(1+25x^2)} \qquad \left\|\kappa^{(M)}\right\| = O(M^M), \tag{5.4.59}$$

the ECNM and EINM bounds are in fact computable and positive. This is because the denominators in (5.4.26)–(5.4.30) are computed exactly rather than bounded *cf.* (5.4.38) and (5.4.50).

5.5 Conversion from Fredholm Integro-Differential Equation to Volterra-Fredholm Integral Equation

The asymptotic error analysis in Section 5.4.3 revealed that the ECNM and EINM both have a global error that is dominated by the error in the numerical differentiation procedure. In order to circumvent the need for numerical differentiation, and hence to minimise the error in numerical IDE solutions, a method is now presented that first transforms an IDE into a Volterra-Fredholm integral equation (VFIE). This can be done when the BC (5.1.2) augmenting the IDE (5.1.1) is given for $\xi = \pm 1$; the details of this conversion for $\xi = -1$ follow a method in [87] and are as follows. Let

$$u'(x) = v(x) \tag{5.5.1}$$

so that

$$u(x) = \zeta + \int_{-1}^{x} v(y)\,dy, \tag{5.5.2}$$

using which the IDE (5.1.1) becomes

$$\zeta + \int_{-1}^{x} v(y)\,dy - \mu(x)\,v(x) - \lambda \int_{-1}^{1} K(x,y)\left(\zeta + \int_{-1}^{y} v(z)\,dz\right) dy = f(x). \tag{5.5.3}$$

The order of double integration in the final term on the left-hand side of (5.5.3) can be changed so that (5.5.3) can be written as the VFIE

$$v(x) = g(x) + \frac{1}{\mu(x)} \int_{-1}^{x} v(y)\, dy - \lambda \int_{-1}^{1} k(x,y)\, v(y)\, dy, \tag{5.5.4}$$

in which the modified source function $g(x)$ is given by

$$g(x) = \frac{1}{\mu(x)} \left(\zeta - \lambda\, \zeta \int_{-1}^{1} K(x,y)\, dy - f(x) \right), \tag{5.5.5}$$

and the modified kernel $k(x,y)$ by

$$k(x,y) = \frac{1}{\mu(x)} \int_{y}^{1} K(x,z)\, dz. \tag{5.5.6}$$

In symbolic form, the VFIE (5.5.4) is written as

$$v = g + \frac{\mathcal{V}\, v}{\mu} - \lambda\, \mathcal{F}\, v, \tag{5.5.7}$$

in which the action of the *Volterra integral operator* $\mathcal{V}$ on a function $v : [-1,1] \to \mathbb{R}$ is defined by

$$\mathcal{V}\, v = (\mathcal{V}\, v)(x) \equiv \int_{-1}^{x} v(y)\, dy, \tag{5.5.8}$$

and the action of the *Fredholm integral operator* $\mathcal{F}$ on $v : [-1,1] \to \mathbb{R}$ is defined by

$$\mathcal{F}\, v = (\mathcal{F}\, v)(x) \equiv \int_{-1}^{1} k(x,y)\, v(y)\, dy. \tag{5.5.9}$$

The conversion of an IDE with a BC for $\xi = +1$ to a VFIE follows analogously by replacing integrals $\int_{-1}^{x}$ with $\int_{x}^{1}$ in (5.5.2), (5.5.3), (5.5.4) and (5.5.8) and replacing $\int_{y}^{1}$ with $\int_{-1}^{y}$ in (5.5.6).

5.5.1 Numerical Solution of the VFIE

Using N-node Lagrange interpolation (2.1.1), the VFIE solution $v(x)$ can be approximated by

$$v(x) \approx (\mathcal{L}_N v)(x) \equiv \sum_{j=1}^{N} L_{j,N}(x) v(y_{j,N}). \tag{5.5.10}$$

Therefore, by defining the *Volterra-Lagrange operator* $\mathcal{V}_N \equiv \mathcal{V}\mathcal{L}_N$, application of the operator $\mathcal{V}$ to both sides of (5.5.10) yields

$$(\mathcal{V}v)(x) \approx (\mathcal{V}_N v)(x) \equiv \sum_{j=1}^{N} \tau_{j,N}(x) v(y_{j,N}), \tag{5.5.11}$$

in which the functions $\tau_{j,N}(x)$ are defined by

$$\tau_{j,N}(x) \equiv \mathcal{V}L_{j,N}(x). \tag{5.5.12}$$

This differs from the approach in [87], in which the Volterra integral is approximated using Simpson's rule, and hence to only inverse-quadratic order in the number N of Simpson's-rule panels used.

The Fredholm integral in (5.5.4) can be approximated using the *Fredholm-Gauss operator* $\mathcal{F}_N$ that represents N-node Gaussian quadrature, i.e.

$$\mathcal{F}v \approx \mathcal{F}_N v = (\mathcal{F}_N v)(x) \equiv \sum_{j=1}^{N} w_{j,N}\, k(x, y_{j,N})\, v(y_{j,N}), \tag{5.5.13}$$

in which $w_{j,N}$ and $y_{j,N}$ are respectively the weights and abscissae of the rule, as detailed in Section 3.2. Since the weight function in the integral in $\mathcal{F}v$ is unity, the nodes $y_{j,N}$ can be Legendre, Legendre-Gauss-Radau or Legendre-Gauss-Lobatto. Note that the nodal values $v(y_{j,N})$ in (5.5.13) do not need to be expressed in terms of the Lagrange interpolant (5.5.10) since, by construction, (2.1.2) gives $L_{j,N}(y_{i,N}) = \delta_{ij}$, wherein δ_{ij} is the Kronecker delta defined in (2.3.12); as a result, $v(y_{i,N}) \equiv (\mathcal{L}_N v)(y_{i,N})$ for $i = 1(1)N$.

Using (5.5.11) and (5.5.13), a discrete approximation to the VFIE (5.5.4) is obtained as

$$v_N(x) = g(x) + \frac{1}{\mu(x)} \sum_{j=1}^{N} \tau_{j,N}(x) v_N(y_{j,N}) - \lambda \sum_{j=1}^{N} w_{j,N}\, k(x, y_{j,N})\, v_N(y_{j,N}), \tag{5.5.14}$$

which is collocated at nodes $x = y_{i,N}$ to yield the matrix system

$$(\mathbf{I}_N - \mathbf{M}_N)\mathbf{v}_N = \mathbf{g}_N, \tag{5.5.15}$$

wherein matrix and vector entries are given by

$$\{\mathbf{I}_N\}_{i,j} = \delta_{ij}, \quad \{\mathbf{M}_N\}_{i,j} = \frac{\tau_{j,N}(y_{i,N})}{\mu(y_{i,N})} - \lambda\, w_{j,N}\, k(y_{i,N}, y_{j,N}),$$

$$\{\mathbf{v}_N\}_i = v_N(y_{i,N}) \quad \text{and} \quad \{\mathbf{g}_N\}_i = g(y_{i,N}). \tag{5.5.16}$$

Inversion of (5.5.15) yields the N nodal values $v_N(y_{i,N})$ which, when substituted back into the inversion formula (5.5.14), give the approximate solution $v_N(x)$ of the VFIE (5.5.4), whose symbolic form is

$$v_N = g + \frac{\mathcal{V}_N\, v_N}{\mu} - \lambda\, \mathcal{F}_N\, v_N. \tag{5.5.17}$$

Since [50, Fig. 10.1] and Figure 4.3.1 both demonstrated that an inversion formula is more accurate, the numerical solution v_N is computed via the inversion formula (5.5.14) instead of the Lagrange interpolant (5.5.10).

By (5.5.2), the exact solutions of the VFIE and IDE satisfy, in symbolic form,

$$u = \zeta + \mathcal{V} v. \tag{5.5.18}$$

Therefore, there are two cases to consider when recovering the numerical IDE solution u_N from its derivative v_N. Firstly, if $v_N(x)$ is integrable (case 1), the numerical IDE solution is computed as

$$\widetilde{u}_N = \zeta + \mathcal{V} v_N. \tag{5.5.19}$$

Second, if functions $\mu(x)$, $K(x,y)$ and $f(x)$ in IDE (5.1.1) yield a function v_N in (5.5.17) that is not integrable (case 2), then the numerical IDE solution must be computed as

$$\widehat{u}_N = \zeta + \mathcal{V}_N v_N, \tag{5.5.20}$$

which, note, gives the solution $\widehat{u}_N(x)$ as a polynomial of degree N in x. Here, non-integrable means that the integral of v_N is not expressible directly in terms of elementary functions; for example, if $\mu(x) = \sum_{j=0}^{m} a_j\, x^j, m > 0$ and either $f(x)$ or $K(x,y)$ contains a trigonometric or exponential function of x. Note that the case-2 solution can be found without computing $v_N(x)$ in (5.5.17), since, via (5.5.11), only its nodal values, given by the solution vector $\mathbf{v}_N$ of (5.5.15), are required to compute $\widehat{u}_N(x)$. The fact that v_N may not be integrable is no more restrictive than solving an ODE by the integrating-factor method.

5.5.2 Error Analysis

A brief error analysis is presented for the VFIE approach in [87], which considers only the convergence rate of the error $\|v - v_N\|$ in the VFIE solution (and not the error in the IDE solution); even then, it requires knowledge of an exact solution.

In the following analysis, bounds are developed for the error in the numerical IDE solutions $\widetilde{u}_N$ and $\widehat{u}_N$ that are explicitly computable without knowledge of an exact solution. The error analyses for the case-1 (5.5.19) and case-2 (5.5.20) solutions are now presented.

5.5.2.1 Case 1: $v_N(x)$ integrable

Let the linear operators $\mathcal{S}$ and $\mathcal{S}_N$ be respectively defined as

$$\mathcal{S} \equiv \frac{\mathcal{V}}{\mu} - \lambda\,\mathcal{F} \tag{5.5.21}$$

and

$$\mathcal{S}_N \equiv \frac{\mathcal{V}_N}{\mu} - \lambda\,\mathcal{F}_N, \tag{5.5.22}$$

so that the exact inversion formula (5.5.7) for the VFIE (5.5.4) can be written as

$$v = g + \mathcal{S}\,v, \tag{5.5.23}$$

and the numerical inversion formula (5.5.17) can be written as

$$v_N = g + \mathcal{S}_N\,v_N. \tag{5.5.24}$$

Subtraction of (5.5.24) from (5.5.23) yields the error

$$v - v_N = \mathcal{S}\,v - \mathcal{S}_N\,v_N \tag{5.5.25}$$

which, through the addition of $\mathcal{S}\,v_N - \mathcal{S}\,v_N = 0$ to the right-hand side, is equivalently

$$v - v_N = \mathcal{S}\,(v - v_N) + (\mathcal{S} - \mathcal{S}_N)\,v_N. \tag{5.5.26}$$

Since $v = \mathcal{D}\,u$ by (5.5.1) and $v_N = \mathcal{D}\,\widetilde{u}_N$ by (5.5.19), the error (5.5.26) can be rearranged as

$$(\mathcal{I} - \mathcal{S})\,\mathcal{D}\,(u - \widetilde{u}_N) = (\mathcal{S} - \mathcal{S}_N)\,v_N, \tag{5.5.27}$$

inversion of which yields the IDE error in terms of the computed v_N as

$$u - \widetilde{u}_N = (\mathcal{D} - \mathcal{S}\,\mathcal{D})^{-1}\,(\mathcal{S} - \mathcal{S}_N)\,v_N. \tag{5.5.28}$$

Therefore, a bound on (5.5.28) is

$$\|u - \widetilde{u}_N\| \leq \left\|(\mathcal{D} - \mathcal{S}\,\mathcal{D})^{-1}\right\|\,\Phi_N \tag{5.5.29}$$

wherein

$$\Phi_N = \left\| \left(\mathcal{S} - \mathcal{S}_N \right) v_N \right\| . \tag{5.5.30}$$

By (5.5.24), Φ_N is equivalently

$$\Phi_N = \left\| \mathcal{S}\, v_N - v_N + g \right\| , \tag{5.5.31}$$

which demonstrates that the IDE error is proportional to the residual obtained when the numerical VFIE solution $v_N(x)$ is inserted into the exact VFIE (5.5.4). Since Φ_N is computable using the numerical VFIE solution v_N, it remains only to find a bound on $\left\| (\mathcal{D} - \mathcal{S}\,\mathcal{D})^{-1} \right\|$, which is equivalent to

$$\left\| (\mathcal{D} - \mathcal{S}\,\mathcal{D})^{-1} \right\| = \left\| \Big((\mathcal{I} - \mathcal{S})\,\mathcal{D} \Big)^{-1} \right\| = \left\| \mathcal{D}^{-1} \left(\mathcal{I} - \mathcal{S} \right)^{-1} \right\| = \left\| \mathcal{V} \left(\mathcal{I} - \mathcal{S} \right)^{-1} \right\| , \tag{5.5.32}$$

and hence bounded by

$$\left\| (\mathcal{D} - \mathcal{S}\,\mathcal{D})^{-1} \right\| \leq \left\| \mathcal{V} \right\| \, \left\| (\mathcal{I} - \mathcal{S})^{-1} \right\| . \tag{5.5.33}$$

Since (5.5.8) yields

$$\mathcal{V}(1) = \int_{-1}^{x} dy = x + 1, \tag{5.5.34}$$

using the approach of [10, Eqns. 4.1.13–4.1.17], which was verified in Section 4.4, $\left\| \mathcal{V} \right\|$ is computed as

$$\left\| \mathcal{V} \right\| = \left\| \mathcal{V}(1) \right\| = 2. \tag{5.5.35}$$

By (5.5.21) and (5.5.22), $\mathcal{S}$ and $\mathcal{S}_N$ are linear operators. Therefore, the error theory applied to $\mathcal{K}$ and $\mathcal{K}_M$ in Section 4.4 can be extended to $\mathcal{S}$ and $\mathcal{S}_N$. Since the Lagrangian interpolation and Gaussian quadrature upon which $\mathcal{S}$ and $\mathcal{S}_N$ are based are, by the error definitions (2.4.2) and (3.2.17), convergent for all continuous functions then, for sufficiently large N, $(\mathcal{I} - \mathcal{S})^{-1}$ exists and is uniformly bounded [10, Thm. 4.1.1] by

$$\left\| (\mathcal{I} - \mathcal{S})^{-1} \right\| \leq \frac{1 + \left\| (\mathcal{I} - \mathcal{S}_N)^{-1} \right\| \, \left\| \mathcal{S} \right\|}{1 - \left\| (\mathcal{I} - \mathcal{S}_N)^{-1} \right\| \, \left\| (\mathcal{S} - \mathcal{S}_N)\,\mathcal{S} \right\|}, \tag{5.5.36}$$

which has to be positive by construction, *cf.* [10, Eq. 4.1.22]. Let $s = \mathcal{S}(1)$ such that, by (5.5.9), (5.5.21) and (5.5.34),

$$s(x) = \frac{x+1}{\mu(x)} - \lambda \int_{-1}^{1} k(x,y)\, dy, \tag{5.5.37}$$

using which the sub-elements on the right-hand side of (5.5.36) are computed by again using the approach in [10, Eqns. 4.1.13–4.1.17] as

$$\|\mathcal{S}\| = \|\mathcal{S}(1)\| = \|s\|\,, \tag{5.5.38}$$

$$\|(\mathcal{S} - \mathcal{S}_N)\,\mathcal{S}\| = \|(\mathcal{S} - \mathcal{S}_N)\,\mathcal{S}(1)\| = \|(\mathcal{S} - \mathcal{S}_N)\,s\| \tag{5.5.39}$$

and

$$\left\|(\mathcal{I} - \mathcal{S}_N)^{-1}\right\| = \left\|(\mathcal{I} - \mathcal{S}_N)^{-1}(1)\right\| = \|r_N\|\,, \tag{5.5.40}$$

wherein $r_N(x)$ in (5.5.40) is the solution of

$$r_N - \mathcal{S}_N\, r_N = 1. \tag{5.5.41}$$

Therefore, by (5.5.16), the nodal values of $r_N(x)$ are found by solving the linear system

$$(\mathbf{I}_N - \mathbf{M}_N)\,\mathbf{r}_N = \mathbf{1}, \tag{5.5.42}$$

in which $\mathbf{I}_N$ and $\mathbf{M}_N$ are given by (5.5.16) and the entries of the vectors $\mathbf{r}_N$ and $\mathbf{1}$ are given by

$$\{\mathbf{r}_N\}_i = r_N(y_{i,N}) \qquad \text{and} \qquad \{\mathbf{1}\}_i = 1. \tag{5.5.43}$$

Solving (5.5.42) gives the nodal values $r_N(y_{i,N})$ that are substituted into the inversion formula

$$r_N(x) = 1 + \frac{1}{\mu(x)} \sum_{j=1}^{N} \tau_{j,N}(x)\, r_N(y_{j,N}) - \lambda \sum_{j=1}^{N} w_{j,N}\, k(x, y_{j,N})\, r_N(y_{j,N}), \tag{5.5.44}$$

from which $\|r_N\|$ in (5.5.40) can be computed. By (5.5.35)–(5.5.44), the theoretical bound (5.5.33) can be replaced by the computable bound

$$\left\|(\mathcal{D} - \mathcal{S}\,\mathcal{D})^{-1}\right\| \le \frac{2\,(1 + \|r_N\|\,\|s\|)}{1 - \|r_N\|\,\|(\mathcal{S} - \mathcal{S}_N)\,s\|}, \tag{5.5.45}$$

whence (5.5.29) and (5.5.45) give the case-1 error bound as

$$\|u - \widetilde{u}_N\| \le \frac{2\,(1 + \|r_N\|\,\|s\|)}{1 - \|r_N\|\,\|(\mathcal{S} - \mathcal{S}_N)\,s\|}\, \|\mathcal{S}\,v_N - v_N + g\|\,, \tag{5.5.46}$$

which is explicitly computable in terms of only the derivative v_N of the numerical case-1 IDE solution $\widetilde{u}_N$.

5.5.2.2 Case 2: $v_N(x)$ not integrable in terms of elementary functions

Subtraction of (5.5.20) from (5.5.19) yields

$$\widetilde{u}_N - \widehat{u}_N = (\mathcal{V} - \mathcal{V}_N)\, v_N, \tag{5.5.47}$$

which, by the addition of $u - u = 0$ to the right-hand side, gives

$$\widetilde{u}_N - u + u - \widehat{u}_N = (\mathcal{V} - \mathcal{V}_N)\, v_N. \tag{5.5.48}$$

Therefore, the case-2 error is bounded by

$$\|u - \widehat{u}_N\| \leq \|u - \widetilde{u}_N\| + \|(\mathcal{V} - \mathcal{V}_N)\, v_N\|, \tag{5.5.49}$$

which, by (5.5.46), gives

$$\|u - \widehat{u}_N\| \leq \frac{2\,(1 + \|r_N\|\,\|s\|)}{1 - \|r_N\|\,\|(\mathcal{S} - \mathcal{S}_N)\, s\|}\,\|\mathcal{S}\, v_N - v_N + g\| + \|(\mathcal{V} - \mathcal{V}_N)\, v_N\|. \tag{5.5.50}$$

By (5.5.11), $\|(\mathcal{V} - \mathcal{V}_N)\, v_N\|$ is equivalent to the Volterra operator $\mathcal{V}$ acting upon the standard Lagrange interpolation error (2.4.1), so that

$$(\mathcal{V} - \mathcal{V}_N)\, v_N(x) = \mathcal{V}(\mathcal{I} - \mathcal{L}_N)\, v_N(x) = \frac{\mathcal{V}\, p_N(x)}{N!} v_N^{(N)}(\eta), \quad \eta \in (-1, 1), \tag{5.5.51}$$

in which p_N is the monic polynomial (2.1.3) whose roots are the N integration abscissae $y_{i,N}$. Therefore, (5.5.51) yields

$$\|(\mathcal{V} - \mathcal{V}_N)\, v_N\| \leq Q_N \left\| v_N^{(N)} \right\| \tag{5.5.52}$$

in which

$$Q_N \equiv \frac{\|\mathcal{V}\, p_N\|}{N!}. \tag{5.5.53}$$

As the case-2 solution is computed when $v_N(x)$ is not integrable in terms of elementary functions, $\mathcal{S}\, v_N$ in the bound (5.5.50) is not computable since the operator $\mathcal{S}$ contains the integral operator $\mathcal{V}$. Furthermore, for the same reason, $\mathcal{S}\, s$ in (5.5.50) will also in general be uncomputable. Therefore, $\Phi_N = \|\mathcal{S}\, v_N - v_N + g\|$ and $\|(\mathcal{S} - \mathcal{S}_N)\, s\|$ within (5.5.50) must be bounded. Together, (5.5.21), (5.5.22) and (5.5.30) yield the bound on Φ_N as

$$\Phi_N \leq \frac{\|(\mathcal{V} - \mathcal{V}_N)\, v_N\|}{\|\mu\|} + |\lambda|\,\|(\mathcal{F} - \mathcal{F}_N)\, v_N\|, \tag{5.5.54}$$

wherein $\|(\mathcal{V}-\mathcal{V}_N)\,v_N\|$ is bounded by (5.5.52). Additionally, by (3.2.17), $\|(\mathcal{F}-\mathcal{F}_N)\,v_N\|$ is bounded by

$$\|(\mathcal{F}-\mathcal{F}_N)v_N\| \leq \psi_N^{(\nu)}\,\widetilde{\mathbb{F}}_{2N-\nu}, \tag{5.5.55}$$

in which $\psi_N^{(\nu)}$ is given by (3.2.14)–(3.2.16) for $\nu=0,1,2$ and $\widetilde{\mathbb{F}}_M$ is defined by

$$\widetilde{\mathbb{F}}_M = \max_{x,y\in[-1,1]}\left|\frac{\partial^M}{\partial y^M}\big(k(x,y)\,v_N(y)\big)\right|. \tag{5.5.56}$$

Substitution of (5.5.52) and (5.5.55) into (5.5.54) then gives

$$\Phi_N \leq \frac{Q_N\left\|v_N^{(N)}\right\|}{\|\mu\|} + |\lambda|\,\psi_N^{(\nu)}\,\widetilde{\mathbb{F}}_{2N-\nu} \tag{5.5.57}$$

and, similarly, a bound on $\|(\mathcal{S}-\mathcal{S}_N)\,s\|$ can be found as

$$\|(\mathcal{S}-\mathcal{S}_N)\,s\| \leq \frac{Q_N\left\|s^{(N)}\right\|}{\|\mu\|} + |\lambda|\,\psi_N^{(\nu)}\,\mathbb{S}_{2N-\nu}, \tag{5.5.58}$$

in which

$$\mathbb{S}_M = \max_{x,y\in[-1,1]}\left|\frac{\partial^M}{\partial y^M}\big(k(x,y)\,s(y)\big)\right|. \tag{5.5.59}$$

Therefore, a computable case-2 error bound is given by

$$\|u-\widehat{u}_N\| \leq \frac{2\,(1+\|r_N\|\,\|s\|)\left(Q_N\left\|v_N^{(N)}\right\| + |\lambda|\,\|\mu\|\,\psi_N^{(\nu)}\,\widetilde{\mathbb{F}}_{2N-\nu}\right)}{\|\mu\| - \|r_N\|\left(Q_N\,\|s^{(N)}\| + |\lambda|\,\|\mu\|\,\psi_N^{(\nu)}\,\mathbb{S}_{2N-\nu}\right)} + Q_N\left\|v_N^{(N)}\right\|. \tag{5.5.60}$$

Exact formulae for computing Q_N in the bound (5.5.60) are derived in Section 5.5.2.3.

5.5.2.3 Explicit Formulae for Q_N

The factor Q_N defined in (5.5.53) can be found explicitly for all of the Legendre, Legendre-Gauss-Radau (Radau) and Legendre-Gauss-Lobatto (Lobatto) nodal distributions using which the VFIE method is implemented.

Let ν again correspond to the number of endpoints included in the distribution, i.e. $\nu=0,1,2$ for Legendre, Radau and Lobatto distributions respectively. Then the monic polynomials associated with each distribution are

$$p_N^{(0)}(x) = \frac{2^N(N!)^2}{(2N)!}P_N(x), \tag{5.5.61}$$

$$p_N^{(1)}(x) = \frac{2^N (N!)^2}{(2N)!}\big(P_{N-1}(x) - P_N(x)\big), \tag{5.5.62}$$

and

$$p_N^{(2)}(x) = \frac{2^N (N!)^2}{(2N)!}\frac{2N-1}{N(N-1)}(x^2-1)\,P'_{N-1}(x), \tag{5.5.63}$$

in which only the Left-Gauss-Radau distribution is considered since both Left- and Right-Radau distributions yield the same Q_N. Using the Legendre-polynomial relationship (2.3.22), along with Bonnet's recursion formula (see Appendix (C.0.13)), $p_N^{(2)}(x)$ in (5.5.63) can be rewritten as

$$p_N^{(2)}(x) = \frac{2^N (N!)^2}{(2N)!}\big(P_N(x) - P_{N-2}(x)\big), \tag{5.5.64}$$

and hence the monic polynomials (5.5.61), (5.5.62) and (5.5.64) can all be expressed in the general form

$$p_N^{(\nu)}(x) = \frac{2^N (N!)^2}{(2N)!}\left((1+\nu-\nu^2)\,P_{N-\nu}(x) + \frac{\nu\,(3-(-1)^\nu)}{4}\,P_N(x)\right). \tag{5.5.65}$$

The integral $\mathcal{V}\,p_N$ in (5.5.53), in which $p_N \equiv p_N^{(\nu)}$ is given by (5.5.65), is computed using the Legendre-polynomial relationship [65, Eq. 6.41]

$$(2N+1)\,P_N(x) = \frac{d}{dx}\big(P_{N+1}(x) - P_{N-1}(x)\big), \tag{5.5.66}$$

so that $Q_N \equiv Q_N^{(\nu)}$ in (5.5.53) yields

$$Q_N^{(\nu)} \leq \frac{2^N (N!)}{(2N)!}\left(\frac{\|P_{N+1-\nu} - P_{N-1-\nu}\|}{2\,(N-\nu)+1} + \frac{\nu(3-(-1)^\nu)}{4}\frac{\|P_{N+1} - P_{N-1}\|}{2N+1}\right). \tag{5.5.67}$$

By inspection,

$$\|P_N - P_{N-2}\| = |P_N(0) - P_{N-2}(0)|, \qquad N \text{ even}, \tag{5.5.68}$$

in which, by the Legendre-polynomial definition (2.4.50), $P_N(0)$ is computed as

$$P_N(0) = \frac{2^N\left(\frac{N-1}{2}\right)!}{\left(\frac{-(N+1)}{2}\right)!\,N!}. \tag{5.5.69}$$

By the half-integer factorial definitions (2.4.53) and (2.4.54), (5.5.69) is equivalently

$$P_N(0) = \frac{(-1)^{N/2} N!}{2^N\left(\left(\frac{N}{2}\right)!\right)^2}, \tag{5.5.70}$$

and hence (5.5.68) and (5.5.70) yield

$$\|P_N - P_{N-2}\| = \frac{(2N-1)\,N!}{(N-1)\,2^N\left(\left(\frac{N}{2}\right)!\right)^2}, \qquad N \text{ even}, \tag{5.5.71}$$

which, by Stirling's formula [9, p.279], becomes

$$\|P_N - P_{N-2}\| \sim \frac{2N-1}{N-1}\sqrt{\frac{2}{\pi N}}, \qquad N\,(\text{even}) \to \infty. \tag{5.5.72}$$

Although there is no closed form for $\|P_N - P_{N-2}\|$ when N is odd, Figure 5.5.1 shows that (5.5.72) provides a good approximation for $\|P_N - P_{N-2}\|$ for all N.

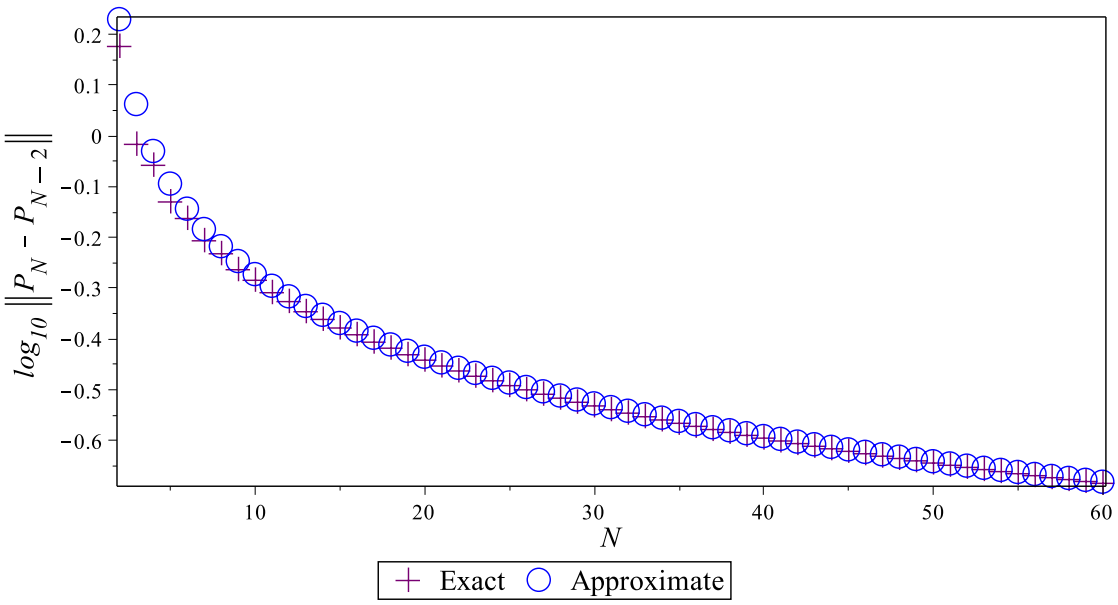

Figure 5.5.1: Logarithmic plot of the exact value of $\|P_N - P_{N-2}\|$ (crosses) and its asymptotic approximation (5.5.72) (circles). The asymptotic approximation clearly holds for both N odd and even.

Together, (5.5.67) and (5.5.72) give the asymptotic formula for $Q_N^{(\nu)}$ as

$$Q_N^{(\nu)} \sim \frac{1}{\sqrt{\pi}}\left(\frac{\mathrm{e}}{2N}\right)^N\left(\frac{1}{(N-\nu)\sqrt{N+1-\nu}} + \frac{\nu(3-(-1)^\nu)}{4N\sqrt{N+1}}\right), \tag{5.5.73}$$

which is shown in Figure 5.5.2 to be an extremely accurate approximation for $\nu = 0, 1$ and 2, for all N.

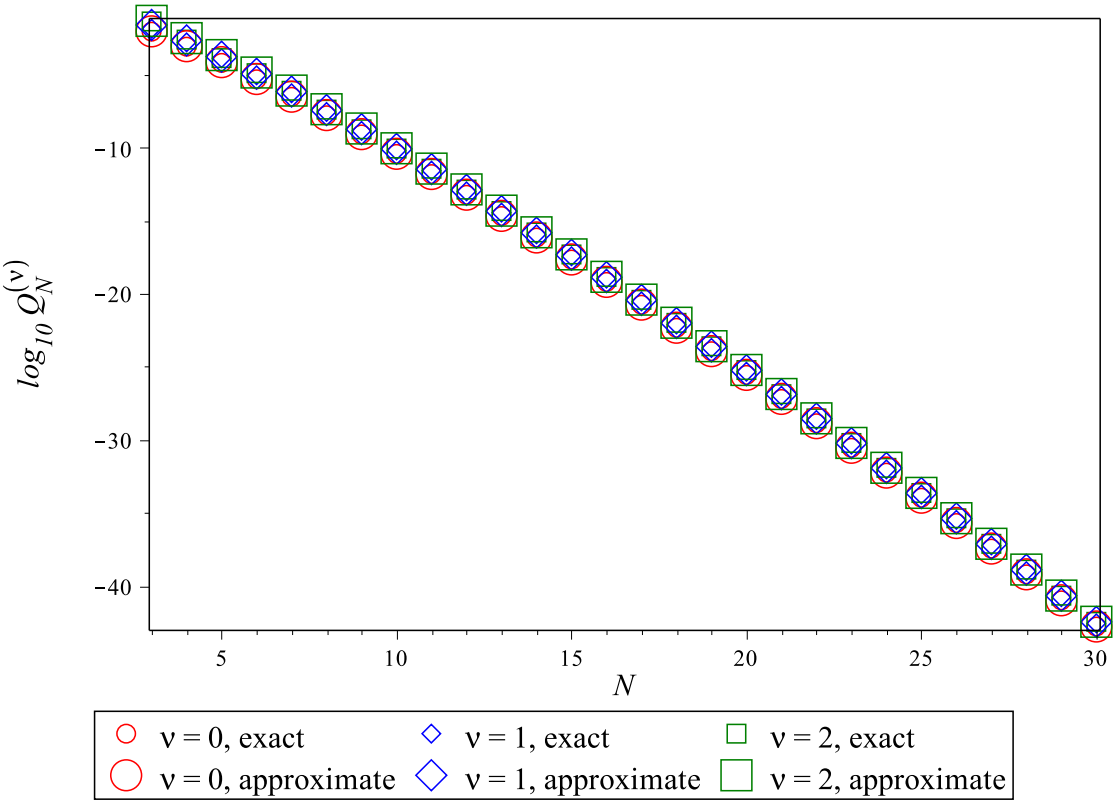

Figure 5.5.2: Logarithmic plot of the exact $Q_N^{(\nu)}$ and its asymptotic approximation (5.5.73) for $\nu = 0, 1, 2$. The asymptotic approximation is accurate for even low values of N.

5.5.2.4 Asymptotic Convergence Rates

The convergence rate of the case-1 error is found by considering that of Φ_N, which is defined in (5.5.31) and bounded, using $\psi_N^{(\nu)}$ and $Q_N^{(\nu)}$, in (5.5.57). The asymptotic rates for $\psi_N^{(\nu)}$ and $Q_N^{(\nu)}$, (3.2.20) and (5.5.73) respectively, yield the ratio

$$\frac{\psi_N^{(\nu)}}{Q_N^{(\nu)}} \sim \frac{\pi\,(4N)^{(2\nu+1)/2}\,(N-\nu)\,\sqrt{(N+1)^2-\nu(N+1)}}{4N\,\sqrt{N+1}+\nu(3-(-1)^\nu)\,(N-\nu)\,\sqrt{N+1-\nu}}\,\left(\frac{\mathrm{e}}{8N}\right)^N \tag{5.5.74}$$

as $N \to \infty$, which reveals that $\psi_N^{(\nu)}/Q_N^{(\nu)} \sim O(N^{-N})$. Therefore, since $Q_N^{(\nu)} \gg \psi_N^{(\nu)}$ as $N \to \infty$, provided that

$$\left\| v_N^{(N)} \right\| \sim o(N^N) \qquad \text{and} \qquad \widetilde{\mathbb{F}}_{2N-\nu} \sim o(N^{2N}), \tag{5.5.75}$$

the bound (5.5.57) can be approximated by

$$\Phi_N \leq \frac{Q_N^{(\nu)} \left\| v_N^{(N)} \right\|}{\|\mu\|}, \qquad N \gg 1, \tag{5.5.76}$$

and hence, by (5.5.29), the asymptotic convergence rate of the case-1 error is

$$\|u - \widetilde{u}_N\| \sim Q_N^{(\nu)} \left\| v_N^{(N)} \right\|, \qquad N \to \infty. \tag{5.5.77}$$

By (5.5.49), (5.5.52) and (5.5.77), the asymptotic convergence rate for the case-2 error is given by

$$\|u - \widehat{u}_N\| \sim Q_N^{(\nu)} \left\| v_N^{(N)} \right\|, \qquad N \to \infty, \tag{5.5.78}$$

so that, irrespective of how the numerical IDE solution is recovered from the numerical VFIE solution, the error-convergence rate is

$$Q_N^{(\nu)} \left\| v_N^{(N)} \right\|, \qquad N \to \infty. \tag{5.5.79}$$

The asymptotic rate (5.5.79) can be used to compare the errors of the VFIE approach to those of the ECNM approach, whose asymptotic convergence rate is given by (5.4.44). The factor ϕ_N in (5.4.44), which is given explicitly for different node sets in Table 2.1, has the asymptotic form

$$\phi_N^{(\nu)} \sim \frac{2^{\nu-3/2}}{N^{(\nu^2-\nu-4)/2}} \left(\frac{\mathrm{e}}{2N}\right)^N, \tag{5.5.80}$$

in which $\nu = 0, 1, 2$ again refer to the Legendre, Radau and Lobatto distributions respectively. The asymptotic forms (5.5.73) and (5.5.80) show that, as $N \to \infty$, $\phi_N^{(\nu)}$ and $Q_N^{(\nu)}$ are of order $O(N^{-N})$. Additionally, the asymptotic forms yield the ratio

$$\begin{aligned} \frac{Q_N^{(\nu)}}{\phi_N^{(\nu)}} &\sim \frac{N^{(\nu^2-\nu-4)/2}}{2^{\nu-3/2}\sqrt{\pi}} \left(\frac{1}{(N-\nu)\sqrt{N+1-\nu}} + \frac{\nu(3-(-1)^\nu)}{4N\sqrt{N+1}} \right) \\ &\sim N^{(\nu^2-\nu-7)/2}, \end{aligned} \tag{5.5.81}$$

which demonstrates that $\phi_N^{(\nu)} > Q_N^{(\nu)}$. Therefore, provided the VFIE norm $\left\| v_N^{(N)} \right\|$ and ECNM norm $\left\| u_N^{(N)} \right\|$ are of the same order, the errors of both the VFIE approach and the ECNM are expected to converge at the same rate, with the former uniformly lower than the latter.

5.5.3 Numerical Examples

The methods and bounds are now validated on four test problems which again feature solutions that are challenging to approximation methods; the test problems are summarised in Table 5.2.

Problem	Name	Solution $u(x)$	$\mu(x)$	Kernel $K(x,y)$	λ
1	Smooth	$\cos x + x^3$	$\sec x$	$(x+2)\,\sin y$	-1
2	Runge	$\frac{1}{1+25x^2}$	$\frac{1}{x-3}$	$(x+2)(y^2-3)$	$\frac{1}{3}$
3	Steep	e^{-13x}	e^{x}	e^{x-y}	1
4	Oscillatory	$\sin 14x$	$\frac{1}{x^2+2}$	$\cos x\,(y^5+1)$	-1

Table 5.2: Test problems with solutions of four qualitatively distinct forms. The source function $f(x)$ can be computed directly from the IDE (5.1.1).

Figure 5.5.3 shows the case-1 and case-2 errors, corresponding respectively to bounds (5.5.46) and (5.5.60), and convergence rate (5.5.79); the ECNM errors are also included for comparison. Since results are qualitatively similar using each nodal distribution, only the Legendre results, for which $\nu = 0$, are shown.

Figure 5.5.3 shows that the case-1 errors are uniformly lower than the case-2 errors, which demonstrates that, as expected, it is more accurate to obtain the numerical IDE solution by integrating the numerical VFIE solution v_N exactly, rather than by integrating its Lagrange interpolant. Furthermore, both the case-1 and case-2 errors are lower than the ECNM errors, as predicted at the end of Section 5.5.2.4; this demonstrates that a more accurate IDE solution can be obtained when the need for numerical differentiation is avoided. The case-1 error bound is shown to be accurate for all four test problems, whilst the case-2 error bound is less accurate for each problem. In particular, it is noted that the case-2 bound is divergent for problem 2, whilst the true errors are convergent. This divergence, and the large discrepancy between the case-2 errors and bounds for problems 1, 3 and 4, is due to the terms $\widetilde{\mathbb{F}}_{2N-\nu}$ and $\left\|v_N^{(N)}\right\|$ within (5.5.60), which may over-estimate the terms that they bound. Specifically, since (5.5.51) is derived via the mean-value theorem, the truncation parameter $\eta \in (-1,1)$ that gives the true value of $(\mathcal{V}-\mathcal{V}_N)\,v_N$ is unknown, so $|v_N^{(N)}(\eta)|$ must be replaced by $\left\|v_N^{(N)}\right\|$ in the bound (5.5.52), the latter

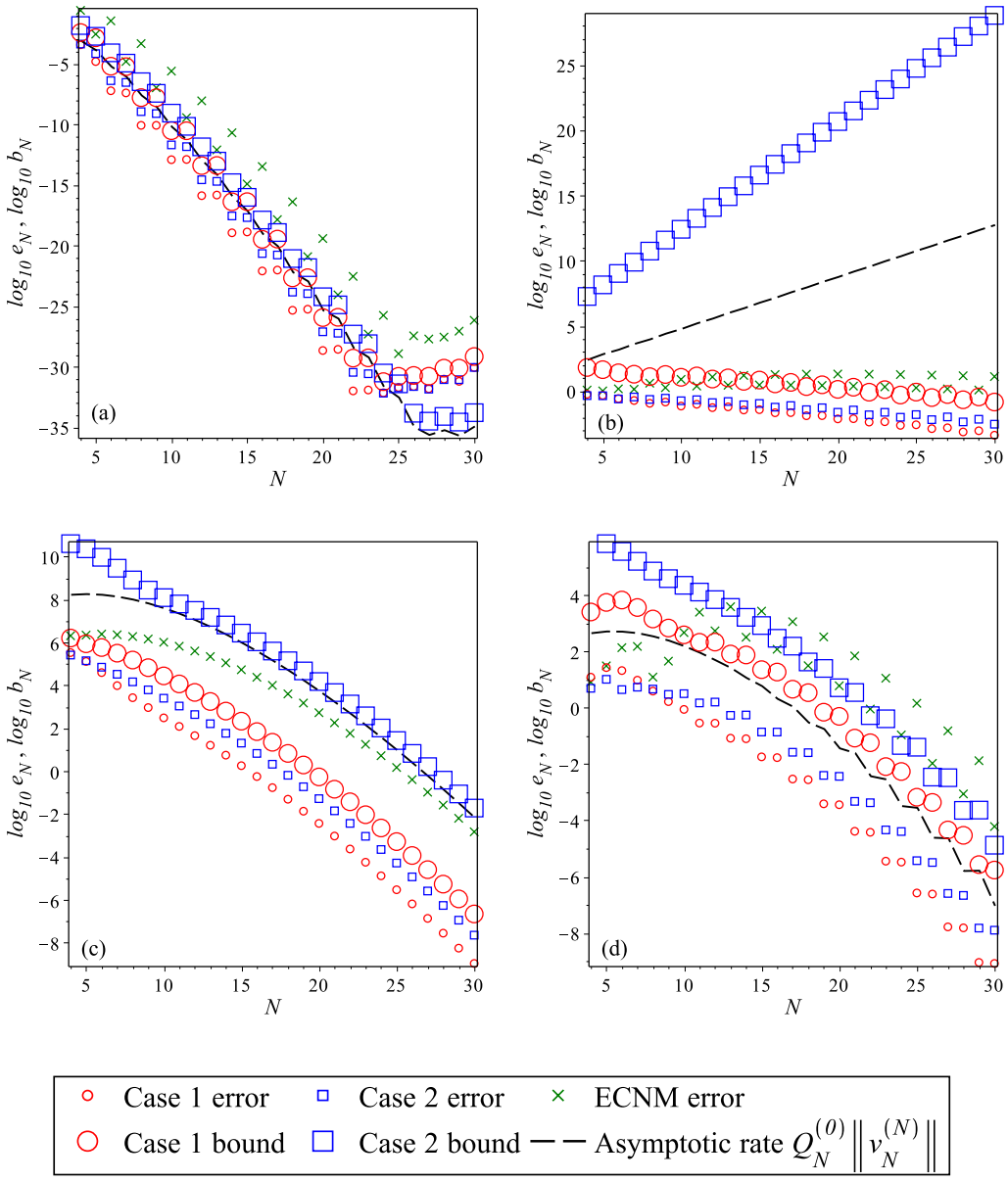

Figure 5.5.3: Logarithmic plots of the case-1 (5.5.19) and case-2 (5.5.20) errors (small symbols) $e_N = \|u - u_N\|$, corresponding bounds (large symbols) b_N (5.5.46) and (5.5.60), and asymptotic convergence rate (dashed lines) (5.5.79), for Problems (a) 1 ("smooth"), (b) 2 ("Runge"), (c) 3 ("steep") and (d) 4 ("oscillatory"), summarised in Table 5.2. The ECNM errors are shown for comparison; these are uniformly higher than the case-1 and case-2 errors.

of which can be much larger than the former. The same argument applies to $\widetilde{\mathbb{F}}_{2N-\nu}$ in (5.5.55), which is computed by maximising over $x, y \in [-1, 1]$ in (5.5.56) as the true values of x and y that give the true quadrature error are unknown. Since the asymptotic rate (5.5.79) also contains the term $\left\| v_N^{(N)} \right\|$, this over-estimation causes the asymptotic rate to be greater than the true case-1 and case-2 errors, as shown in Figure 5.5.3; it is moreover divergent for problem 2. Despite the discrepancy in magnitude between the asymptotic rate and the true errors, the asymptotic rate accurately predicts the rate at which the problem 1, 3 and 4 errors converge with increasing N.

The numerical experiments were repeated on the challenging kernel problems discussed at the end of Section 5.4.4, these were: (a) $K(x, y) = \mathrm{e}^{\omega\,(x-y)^2}$ (isolated peak along the diagonal for $\omega \in \mathbb{R}^+$); (b) $K(x, y) = y^2/(1 + 25x^2)$ (Runge); (c) $K(x, y) = x^2\,\mathrm{e}^{20y}$ (steep), and; (d) $K(x, y) = x^2 \cos 20\, y$ (highly oscillatory). Similar results as discussed for the ECNM and EINM methods were observed for these problems using the VFIE reformulation method; for each problem the errors converged with increasing N and the error bounds for problems (b) and (d) were computable and provided accurate estimates of the true errors. However, the case-1 bound for problem (a) cannot be computed due to the terms $\mathcal{S}\, v_N$ and $S\, s$ in (5.5.46), since it is not possible to perform the required integrations as closed-form functions of x; the case-2 bound for problem (a), which by (5.5.49) also bounds the case-1 error, is negative due to the denominator in the first term on the right-hand side of (5.5.60). The denominator is negative since the condition *cf.* [10, Eq. 4.1.22]

$$\|(\mathcal{S} - \mathcal{S}_N)\,\mathcal{S}\| < \frac{1}{\|(\mathcal{I} - \mathcal{S}_N)^{-1}\|} \tag{5.5.82}$$

required for (5.5.36) to hold is violated by using the approximation (5.5.58). Similarly, the case-1 and case-2 bounds for problem (c) are negative since the condition (5.5.82) is violated by the approximation (5.5.39).

5.6 Summary

The two main goals of this chapter were to develop and to implement novel numerical methods for solving IDEs that converge exponentially with an increasing number of collocation nodes; and, to develop corresponding error predictions that are explicitly

computable in terms of only the available numerical solution. The accomplishment of the latter goal is a novel aspect of the present work since, in the considerable literature on numerical methods for solving IDEs, not only are computable error bounds scarce, but also even mere discussion of errors is relatively rare. For example, of the aforementioned work in this chapter, [7, 121, 24, 38, 73, 106, 108, 136, 137] contain no discussion of errors, [87, 92] give error bounds for only the first derivative of the solution rather than the solution itself, [69] computes the error as a solution of an IDE that is itself subject to error, [138] estimates the error function which is then not developed into an error bound, [6] proves a convergence theorem which is not used explicitly to analyse errors, and [12] develops computable error estimates which are noted, in some cases, to be exceeded by the true computed error and so cannot be used as error bounds.

The first step towards achieving the goals of this chapter was to extend and to adapt the numerical methods for solving IEs in Section 4.3 into numerical methods for solving IDEs through incorporation of the numerical differentiation detailed in Sections 2.2 and 3.1. It was for this very purpose that the interpolated Nyström method was developed in Section 4.3.2, since the integral in the interpolated Nyström method can be approximated through collocation at *any* set of nodes. This has enabled the IDE to be solved using nodes that are optimal for differentiation in the extended interpolated Nyström method. However, despite combining optimal quadrature with optimal differentiation, the extended interpolated Nyström method was shown, through numerical examples, to have no clear advantage over the extended classical Nyström method.

Novel error analyses for the extended Nyström methods have been presented in Section 5.4, in which the operator theory from the pure-IE error analyses of Section 4.4 has been extended and developed to account for the presence of the unbounded differential operator $\mathcal{D}$ inherent in the extended Nyström approach. The resulting error bounds are explicitly computable using only the numerical IDE solution and hence require no knowledge of the exact solution. A corresponding asymptotic error analysis revealed that the error in the numerical IDE solution is dependent upon the error in numerical differentiation which, due to the ill-conditioned differentiation matrices inherent to the formulation, is considerably less accurate than the use of numerical quadrature alone. Furthermore, the asymptotic analysis confirmed that, since Legendre and Chebyshev distributions yield differentiation errors of the same

order, there is no advantage in extending the computationally expensive interpolated Nyström method, as opposed to extending the classical Nyström method.

Since the asymptotic analysis of the extended Nyström methods revealed that the global IDE error is dictated by the numerical differentiation rather than the numerical integration, this motivated an alternative approach in Section 5.5, which bypasses numerical differentiation by first converting the IDE into a VFIE. Although this conversion was previously considered in [87], the resulting VFIE therein was only ever solved to quadratic order in N; additionally, its so-called "error analysis" demanded knowledge of an exact solution. By implementing the new method developed herein, the VFIE can be solved to spectral accuracy in N, thus improving on the results in [87], and this enables a spectrally accurate IDE solution to be recovered. It has been shown theoretically and numerically on a variety of test problems that the errors in this VFIE approach are smaller in magnitude than those in the extended Nyström approaches of Section 5.3. Therefore, a more accurate numerical IDE solution can be found when the need for numerical differentiation is bypassed by VFIE reformulation. However, the advantage of the extended Nyström methods over the VFIE approach is that they may easily be extended to solve higher-order IDEs by incorporating higher-order differentiation matrices; in contrast, by its construction, the VFIE approach can be used for only first-order IDEs.

The errors incurred in the VFIE approach have been analysed and bounded in Section 5.5.2; unlike the error analysis in [87], the error analysis in the present work yields spectrally accurate error bounds that use only the numerical VFIE solution and so are computable without knowledge of the exact solution.

The numerical methods developed in this chapter are both flexible and widely applicable and have yielded spectrally accurate IDE solutions on a range of test problems. Furthermore, the newly predicted error bounds for both the extended Nyström and VFIE approaches have provided spectrally accurate representations of the true errors. These error bounds are explicitly computable in the absence of an exact solution which, as discussed above, is a novel and distinctive aspect of this work.

Chapter 6

Conclusions

6.1 Motivation

This thesis has been concerned with the numerical solution of Fredholm integral- and integro-differential equations of the second kind (respectively FIE2s and FIDEs) which, as stated in Chapter 1, arise frequently in the modelling of many real-life problems in applied sciences and engineering. Accordingly, since the accurate approximation of their solution is of practical importance, and since exact solutions to such problems are invariably unknown, there is a genuine need not only to understand but also to quantify the errors incurred in the computation of such approximate solutions. Thus motivated, the development of accurate and computable error estimates and bounds has been the main focus of this thesis. Specifically considered herein has been the analysis and implementation thereof of both spectrally accurate numerical methods for approximating the solution of not only FIE2s and FIDEs but also their respective error analyses, the main focus in the establishment of which was for all error bounds and estimates to be explicitly computable in — a distinctive element of the present work — the absence of an exact solution. This objective was motivated not only by the practical relevance mentioned above, but also by the apparent paucity of existing literature on the prediction of errors for realistically motivated (rather than model) problems. Since detailed summaries are already provided for each chapter, the following conclusions are based only upon the key results and outcomes.

6.2 Summary and Discussion

Chapters 2 and 3 introduced and analysed the fundamental constituent techniques demanded of Nyström methods for approximating the solution of FIE2s and FIDEs to spectral accuracy: interpolation, numerical differentiation and numerical quadrature. Additionally, Chapter 2 provided an overview of a variety of nodal distributions upon which the approximation techniques can be based. A novel detailed comparison of these distributions revealed that interpolation and numerical differentiation are most accurate when collocated on Chebyshev-based distributions, thus confirming the well-known optimality [124] of Chebyshev spectral differentiation. However, Chapter 3 demonstrated that the Gauss-Legendre nodal distribution is invariably used when implementing quadrature to approximate a definite integral whose weight function is unity. Therefore, one of the aims of this thesis was to develop a numerical method that combined the optimality of Chebyshev differentiation with that of Gauss-Legendre quadrature and so to minimise the total error in approximation of FIDE solutions. This aim was achieved by first considering the projection between optimal-quadrature nodes and optimal-differentiation nodes within the context of numerical methods for FIE2s.

By studying the errors associated with each approximation technique in Chapters 2 and 3, it was possible to determine how these errors contributed to the overall error in numerical solutions of FIE2s and FIDEs. Specifically, the explicit node-dependent formulae derived for the errors in interpolation, numerical differentiation, and numerical quadrature provided the basis for asymptotic error analyses of the FIE2 and FIDE methods in the subsequent chapters. Thus, the analysis presented in Chapters 2 and 3, elements of which have never appeared elsewhere despite their fundamental nature, provided the essential framework for the numerical methods and error analyses developed and implemented for FIE2s in Chapter 4 and for FIDEs in Chapter 5.

Chapter 4 introduced the ubiquitous Nyström method for the solution of FIE2s; this was then extended by incorporating Lagrange interpolation into the Nyström-quadrature term in order to solve FIE2s using any set of collocation nodes, rather than only those dictated by the weighting function in the integral term in the FIE2. Since the error analyses in the initial two chapters demonstrated that Lagrange

interpolation is considerably less accurate than Gaussian quadrature, the new interpolated Nyström method was not expected to improve upon the accuracy achieved by the classical Nyström method; this was confirmed both numerically and theoretically. However, by enabling FIE2s to be collocated on any node set, the interpolated Nyström method facilitated a natural extension for solving FIDEs by the incorporation of optimal numerical differentiation. The larger errors attributed to Lagrange interpolation in the interpolated Nyström method were not considered a disadvantage to the intended FIDE extension, since interpolation is inevitable in the numerical differentiation outlined in Chapters 2 and 3.

The most significant achievement of Chapter 4 was the development of novel implementable error analyses for both the classical and interpolated Nyström methods. These error analyses were founded on an existing, theoretical framework that, despite frequent citation in the literature, does not appear to have been developed into computable error bounds before now; moreover, it has even been claimed that [83, p. 188] *"these bounds will be difficult to evaluate in applications"*. Contrary to this assertion, the error bounds derived in this thesis are explicitly computable using only the available numerical solution and other known quantities from the FIE2; this feature is highly distinctive and effectively absent from the literature.

For practical problems wherein the exact solution is unknown, these bounds are an improvement upon the existing Nyström bounds, e.g. [10, Eq. 4.1.33] and [60, Eq. 4.7.16d] that not only contain theoretical terms, but also depend upon the exact solution. Despite the Nyström errors being [9, p. 282] *"difficult to estimate"*, these new error bounds were shown to agree with the true, computed errors with spectral accuracy on a range of test problems. Additionally, spectrally accurate asymptotic error estimates were derived for FIE2s whose solutions are infinitely continuously and boundedly differentiable. These were derived from the interpolation- and quadrature-error formulae presented in Chapters 2 and 3.

In Chapter 5 two novel and distinct methods were developed for the solution of FIDEs. The first approach extended both the classical and interpolated Nyström methods by incorporating the numerical differentiation detailed in Chapters 2 and 3. Although the extended interpolated Nyström method combines optimal numerical differentiation with optimal numerical quadrature, it was shown both theoretically and computationally to have no clear advantage in terms of accuracy over the extended classical Nyström method, but to have a large disadvantage in terms of

computational workload. Thus it was shown to be sufficient to approximate FIDEs using optimal quadrature and near-optimal differentiation in order to preclude computationally expensive interpolation between nodal distributions. The discretisation of an FIDE in the extended Nyström methods has similarities to the approach in [108], in which higher-order FIDEs are discretised using a combination of Gauss-Legendre quadrature and Lagrange interpolation. However, the approach in [108] and the FIDE-Nyström methods differ substantially thereafter, since the former determines the unknown nodal values of the FIDE solution using Newton's method, and the latter uses a matrix-inversion system. Furthermore, the FIDE solution is approximated in [108] by Lagrange-interpolating the recovered nodal values: as discussed for the FIE2 numerical methods in Chapter 4, this approach does not achieve the spectral accuracy of the inversion formulae used in this thesis.

An asymptotic analysis of the extended Nyström method errors revealed that the error is dictated by the error in numerical differentiation, which is orders of magnitude larger than the error in numerical quadrature, as demonstrated in Chapters 2 and 3. This motivated the second FIDE approach, in which numerical differentiation is bypassed by transforming an FIDE into a Volterra-Fredholm integral equation (VFIE), following the method in [87]. A new method was presented for solving the resulting VFIE that combines Gaussian quadrature with Lagrange interpolation in order to obtain a spectrally accurate VFIE solution, from which the FIDE solution is recovered. The spectral accuracy of this new approach is far superior to that in [87], in which the VFIE is solved to only quadratic order in N.

Asymptotic error analyses and numerical experiments confirmed that the VFIE approach yields errors smaller than those of the Nyström-type methods. However, despite offering advantages in terms of accuracy, the VFIE approach is less flexible than the Nyström-type methods, since the VFIE approach requires a given boundary condition at $x = \pm 1$, whereas the Nyström-type methods can be implemented when the boundary condition is given anywhere in the domain. Additionally, the VFIE approach, by its very construction, can only solve first-order FIDEs, whilst the Nyström-type methods can be extended easily to solve higher-order FIDEs by incorporating higher-order differentiation matrices. The flexibility, and practical relevance, of the FIDE-Nyström method is demonstrated in [54] on a novel FIDE formulation of a fourth-order, Euler-Bernoulli beam-deflection boundary-value problem with varying flexural rigidity. Therefore, both of the new FIDE approaches

developed in this thesis offer different advantages, hence together they provide a useful framework for approximating the solutions of FIDEs.

Novel error analyses were developed for both the Nyström-type methods and the VFIE approach; in keeping with those presented in Chapter 4 for FIE2s, these error analyses were founded on the fundamental operator theorem [10, Thm. 4.1.1] that underpins the Nyström method error. However, due to the presence of the unbounded differential operator $\mathcal{D}$, the theoretical bound resulting from [10, Thm. 4.1.1] had to be adjusted for the FIDE-Nyström methods. Therefore, a novel "punctured" operator was introduced that is an analogy of the procedure that reduces a singular differentiation matrix, by the removal of one row and column, to yield an invertible matrix that accounts for a given boundary condition, see e.g. [124, p. 125]. For both FIDE approaches, the error bounds derived are explicitly computable without knowledge of the exact solution: the FIDE-Nyström bounds are based upon the numerical FIDE solution, whilst the VFIE-approach bounds are based upon the numerical VFIE solution. Therefore, the error analyses developed are notably different from those in existing literature since, as for FIE2s, error bounds of this form appear to be absent from all literature on FIDEs. For example, existing error estimates for FIDE numerical methods include those that only bound the first derivative of the solution [87, 92], those that are themselves subject to an unquantified error [69, 138, 55], those that prove only convergence [6], and those that do not exceed the true computed errors [12], i.e. they are not bounds in the proper sense.

6.3 Future Work

The FIDE error bounds have been shown to provide spectrally accurate error predictions on a range of test problems with challenging solutions. However, there is scope for further developments to the error bounds for FIDEs with challenging kernels since, as discussed in Chapter 5, some kernels violate the condition [10, Eq. 4.1.22] required for the theorem [10, Thm. 4.1.1] to hold. Additionally, since the Nyström method requires modifications for FIE2s with singular kernels, as considered in e.g. [100, 80, 8, 77], further research could also be conducted into adapting the FIDE numerical methods to account for singular-kernel FIDEs.

6.4 Final Remarks

The numerical methods developed in this thesis were shown to deliver spectrally accurate solutions of FIE2s and FIDEs on a range of problems. In addition to this, novel error bounds and asymptotic estimates were derived that predict the true computed errors to spectral accuracy. Although the test problems considered in this thesis all had known solutions, this was not a restriction *per se* and was only done to demonstrate the accuracy of the error bounds computed using only the numerical solution. The agreement between the predicted and computed errors suggests that, in practice, the methods developed in this thesis can be used to approximate the solution, and to predict the error therein, of many problems arising in the mathematical modelling of a host of practical problems whose exact solutions lie beyond the reach of analysis.

Appendix A

Proof of explicit formulae for derivatives of Lagrange polynomials

The general formula for $L_{j,N}^{(M)}(x)$ given by (2.2.9) is proved by induction and the nodal values $L_{j,N}^{(M)}(x_{i,N})$ are derived for both $i = j$ and $i \neq j$. It is first noted, from (2.2.4), that (2.2.9) is true for $M = 1$. Assume now that (2.2.9) is true for $M = m$, whence $L_{j,N}^{(m+1)}(x)$ is found by differentiating $L_{j,N}^{(m)}(x)$ to give

$$L_{j,N}^{(m+1)}(x) = \frac{\displaystyle\sum_{k=0}^{m}(-1)^{m+k}\,\frac{m!}{k!}\,(x-x_{j,N})^{k}\Big(k\,(x-x_{j,N})^{-1}\,p_N^{(k)}(x)+p_N^{(k+1)}(x)\Big)}{(x-x_{j,N})^{m+1}\,p'_N(x_{j,N})}$$

$$+\frac{\displaystyle\sum_{k=0}^{m}(-1)^{m+k+1}\,\frac{(m+1)!}{k!}\,(x-x_{j,N})^{k}\,p_N^{(k)}(x)}{(x-x_{j,N})^{m+2}\,p'_N(x_{j,N})} \qquad \text{(A.0.1)}$$

which is equivalently

$$
\begin{aligned}
L_{j,N}^{(m+1)}(x) &= \frac{\displaystyle\sum_{k=0}^{m}(-1)^{m+k}\,\frac{m!}{k!}\,(x-x_{j,N})^{k}\,k\,p_N^{(k)}(x)}{(x-x_{j,N})^{m+2}\,p'_N(x_{j,N})} \\
&\quad + \frac{\displaystyle\sum_{k=0}^{m}(-1)^{m+k}\,\frac{m!}{k!}\,(x-x_{j,N})^{k+1}\,p_N^{(k+1)}(x)}{(x-x_{j,N})^{m+2}\,p'_N(x_{j,N})} \\
&\quad + \frac{\displaystyle\sum_{k=0}^{m}(-1)^{m+k+1}\,\frac{(m+1)!}{k!}\,(x-x_{j,N})^{k}\,p_N^{(k)}(x)}{(x-x_{j,N})^{m+2}\,p'_N(x_{j,N})}. \qquad \text{(A.0.2)}
\end{aligned}
$$

The $k=0$ term vanishes in the first sum in (A.0.2), and the second sum in (A.0.2) is rewritten with $k'=k+1$ so that (A.0.2) becomes

$$
\begin{aligned}
L_{j,N}^{(m+1)}(x) &= \frac{\displaystyle\sum_{k=1}^{m}(-1)^{m+k}\,\frac{m!}{k!}\,(x-x_{j,N})^{k}\,k\,p_N^{(k)}(x)}{(x-x_{j,N})^{m+2}\,p'_N(x_{j,N})} \\
&\quad + \frac{\displaystyle\sum_{k'=1}^{m+1}(-1)^{m+k'-1}\,\frac{m!}{(k'-1)!}\,(x-x_{j,N})^{k'}\,p_N^{(k')}(x)}{(x-x_{j,N})^{m+2}\,p'_N(x_{j,N})} \\
&\quad + \frac{\displaystyle\sum_{k=0}^{m}(-1)^{m+k+1}\,\frac{(m+1)!}{k!}\,(x-x_{j,N})^{k}\,p_N^{(k)}(x)}{(x-x_{j,N})^{m+2}\,p'_N(x_{j,N})}, \qquad \text{(A.0.3)}
\end{aligned}
$$

which is equivalently

$$
\begin{aligned}
L_{j,N}^{(m+1)}(x) \;=\; & \frac{\displaystyle\sum_{k=1}^{m}(-1)^{m+k}\,\frac{m!}{(k-1)!}\,(x-x_{j,N})^{k}\,p_N^{(k)}(x)}{(x-x_{j,N})^{m+2}\,p'_N(x_{j,N})} \\
& - \frac{\displaystyle\sum_{k'=1}^{m}(-1)^{m+k'}\,\frac{m!}{(k'-1)!}\,(x-x_{j,N})^{k'}\,p_N^{(k')}(x)}{(x-x_{j,N})^{m+2}\,p'_N(x_{j,N})} \\
& - \frac{(-1)^{2m+1}\,\dfrac{m!}{m!}\,(x-x_{j,N})^{m+1}\,p_N^{(m+1)}(x)}{(x-x_{j,N})^{m+2}\,p'_N(x_{j,N})} \\
& + \frac{\displaystyle\sum_{k=0}^{m}(-1)^{m+k+1}\,\frac{(m+1)!}{k!}\,(x-x_{j,N})^{k}\,p_N^{(k)}(x)}{(x-x_{j,N})^{m+2}\,p'_N(x_{j,N})}. \qquad \text{(A.0.4)}
\end{aligned}
$$

The first two sums in (A.0.4) now cancel to give

$$
L_{j,N}^{(m+1)}(x) = \frac{(x-x_{j,N})^{m+1}\,p_N^{(m+1)}(x) + \displaystyle\sum_{k=0}^{m}(-1)^{m+k+1}\,\frac{(m+1)!}{k!}\,(x-x_{j,N})^{k}\,p_N^{(k)}(x)}{(x-x_{j,N})^{m+2}\,p'_N(x_{j,N})} \qquad \text{(A.0.5)}
$$

which simplifies to

$$
L_{j,N}^{(m+1)}(x) = \frac{\displaystyle\sum_{k=0}^{m+1}(-1)^{m+k+1}\,\frac{(m+1)!}{k!}\,(x-x_{j,N})^{k}\,p_N^{(k)}(x)}{(x-x_{j,N})^{m+2}\,p'_N(x_{j,N})}. \qquad \text{(A.0.6)}
$$

Therefore if (2.2.9) is true for $M = m$ then it is also true for $M = m+1$: by induction, it is proved that it is also true for all integers $M > 1$, a proof that does not appear to have been explicitly presented in the previous literature.

Having proved (2.2.9), (3.1.14) follows by setting $x = x_{i,N}$ in (2.2.9) to yield

$$
L_{j,N}^{(M)}(x_{i,N}) = \frac{\displaystyle\sum_{k=0}^{M}(-1)^{M+k}\,\frac{M!}{k!}\,(x_{i,N}-x_{j,N})^{k}\,p_N^{(k)}(x_{i,N})}{(x_{i,N}-x_{j,N})^{M+1}\,p'_N(x_{j,N})}, \qquad \text{(A.0.7)}
$$

which expands to

$$L_{j,N}^{(M)}(x_{i,N}) = \frac{(-1)^M M!\, p_N(x_{i,N}) + \sum_{k=1}^{M}(-1)^{M+k}\frac{M!}{k!}(x_{i,N}-x_{j,N})^k\, p_N^{(k)}(x_{i,N})}{(x_{i,N}-x_{j,N})^{M+1}\, p'_N(x_{j,N})}. \tag{A.0.8}$$

By definition, $p_N(x_{i,N}) \equiv 0$ for all $i = 1(1)N$ so that, upon cancellation of $(x_{i,N}-x_{j,N})$ from both numerator and denominator, (A.0.8) becomes

$$L_{j,N}^{(M)}(x_{i,N}) = \frac{\sum_{k=1}^{M}(-1)^{M+k}\frac{M!}{k!}(x_{i,N}-x_{j,N})^{k-1}\, p_N^{(k)}(x_{i,N})}{(x_{i,N}-x_{j,N})^{M}\, p'_N(x_{j,N})}, \tag{A.0.9}$$

proving (3.1.14).

Finally, (3.1.15) is proved by taking the limit $x \to x_{j,N}$ in (2.2.9) and using L'Hôpital's rule to yield

$$\begin{aligned} L_{j,N}^{(M)}(x_{j,N}) &= \lim_{x\to x_{j,N}} \frac{\sum_{k=0}^{M}(-1)^{M+k}\frac{M!}{k!}(x-x_{j,N})^k\, p_N^{(k)}(x)}{(x-x_{j,N})^{M+1}\, p'_N(x_{j,N})} \\ &\overset{LH}{=} \lim_{x\to x_{j,N}} \left(\frac{\sum_{k=0}^{M}(-1)^{M+k}\frac{M!}{k!}\,k\,(x-x_{j,N})^{k-1}\, p_N^{(k)}(x)}{(M+1)\,(x-x_{j,N})^{M}\, p'_N(x_{j,N})} \right. \\ &\qquad \left. + \frac{\sum_{k=0}^{M}(-1)^{M+k}\frac{M!}{k!}(x-x_{j,N})^k\, p_N^{(k+1)}(x)}{(M+1)\,(x-x_{j,N})^{M}\, p'_N(x_{j,N})} \right). \end{aligned} \tag{A.0.10}$$

Since the $k = 0$ term vanishes in the first sum in (A.0.10), the sum is rewritten with

$k' = k - 1$ so that (A.0.10) becomes

$$L_{j,N}^{(M)}(x_{j,N}) = \lim_{x \to x_{j,N}} \left(\frac{\displaystyle\sum_{k'=0}^{M-1} (-1)^{M+k'+1} \frac{M!}{k'!} (x - x_{j,N})^{k'} p_N^{(k'+1)}(x)}{(M+1)(x - x_{j,N})^M p'_N(x_{j,N})} \right.$$
$$\left. + \frac{\displaystyle\sum_{k=0}^{M} (-1)^{M+k} \frac{M!}{k!} (x - x_{j,N})^{k} p_N^{(k+1)}(x)}{(M+1)(x - x_{j,N})^M p'_N(x_{j,N})} \right) \tag{A.0.11}$$

wherein the two sums cancel leaving only the $k = M$ term of the second sum, so that

$$\begin{aligned} L_{j,N}^{(M)}(x_{j,N}) &= \lim_{x \to x_{j,N}} \frac{p_N^{(M+1)}(x)}{(M+1) p'_N(x_{j,N})} \\ &= \frac{p_N^{(M+1)}(x_{j,N})}{(M+1) p'_N(x_{j,N})}, \end{aligned} \tag{A.0.12}$$

which proves (3.1.15).

A. PROOF OF EXPLICIT FORMULAE FOR DERIVATIVES OF LAGRANGE POLYNOMIALS

Appendix B

Proof of bound on monic polynomial based upon regularly spaced nodes

The bound on $\|p_N\|$ given by (2.4.7) for the regular nodes is derived by following the proof given in [41]. It is included here not only for completeness, but also because it is not intuitively obvious. Let x be a point such that $x_{j,N} < x < x_{j+1,N}$, for any $j = 1(1)N-1$, then

$$\begin{aligned} |x - x_{j,N}|\,|x - x_{j+1,N}| &= (x - x_{j,N})(x_{j+1,N} - x) \\ &= -x^2 + (x_{j+1,N} + x_{j,N})\,x - x_{j,N}\,x_{j+1,N}\,. \end{aligned} \tag{B.0.1}$$

By differentiating the right-hand side of (B.0.1) it is clear that $|x - x_{j,N}|\,|x - x_{j+1,N}|$ is maximised when

$$x = X \equiv \frac{1}{2}(x_{j,N} + x_{j+1,N}), \tag{B.0.2}$$

so that

$$|x - x_{j,N}|\,|x - x_{j+1,N}| \le |X - x_{j,N}|\,|X - x_{j+1,N}|\,. \tag{B.0.3}$$

By expressing the regular nodes as in (2.4.14), X in (B.0.2) is equivalently

$$X = \frac{1}{2}\Big(-1 + (j-1)\,h - 1 + jh\Big) = -1 + \left(j - \frac{1}{2}\right)h \tag{B.0.4}$$

which, when substituted into (B.0.3) with (2.4.14), yields

$$|x - x_{j,N}|\,|x - x_{j+1,N}|$$

$$\leq \left|\left(j - \frac{1}{2}\right) h - (j-1)\,h\right| \left|\left(j - \frac{1}{2}\right) h - jh\right| = \left|\frac{h}{2}\right| \left|-\frac{h}{2}\right| \tag{B.0.5}$$

and so

$$|x - x_{j,N}|\,|x - x_{j+1,N}| \leq \frac{h^2}{4}, \qquad j = 1(1)N-1. \tag{B.0.6}$$

Now consider a node $x_{i,N}$ for which $x_{i,N} < x_{j,N} < x < x_{j+1,N}$; this gives

$$|x - x_{i,N}| \leq |x_{j+1,N} - x_{i,N}| = -1 + jh + 1 - (i-1)\,h = (j - i + 1)\,h. \tag{B.0.7}$$

Similarly, a node $x_{i,N}$ for which $x_{j,N} < x < x_{j+1,N} < x_{i,N}$, gives

$$|x - x_{i,N}| \leq |x_{i,N} - x_{j,N}| = -1 + (i-1)\,h + 1 - (j-1)\,h = (i - j)\,h. \tag{B.0.8}$$

The monic polynomial $p_N(x)$ in (2.1.3) satisfies

$$\begin{aligned} |p_N(x)| &\leq \prod_{i=1}^{N} |x - x_{i,N}| \\ &= \left(\prod_{i=1}^{j-1} |x - x_{i,N}|\right) |x - x_{j,N}|\,|x - x_{j+1,N}| \left(\prod_{i=j+2}^{N} |x - x_{i,N}|\right) \end{aligned} \tag{B.0.9}$$

which, by (B.0.6)–(B.0.8), is bounded by

$$|p_N(x)| \leq \left(\prod_{i=1}^{j-1} (j - i + 1)\,h\right) \frac{h^2}{4} \left(\prod_{i=j+2}^{N} (i - j)\,h\right), \tag{B.0.10}$$

wherein

$$\prod_{i=1}^{j-1} (j - i + 1)\,h = j!\,h^{j-1} \tag{B.0.11}$$

and

$$\prod_{i=j+2}^{N} (i - j)\,h = (N - j)!\,h^{N-j-1}. \tag{B.0.12}$$

Therefore, combining (B.0.10)– (B.0.12) yields the bound, for $x \in (x_{j,N}, x_{j+1,N})$,

$$|p_N(x)| \leq j!\,(N - j)!\,\frac{h^N}{4}. \tag{B.0.13}$$

The bound on $|p_N(x)|$ for $x \in [-1, 1]$, equivalently $\|p_N\|$, is determined as the maximum value of the right-hand side of (B.0.13) for $j = 1(1)N - 1$. The binomial coefficient

$$\binom{N}{j} = \frac{N!}{j!\,(N-j)!} \geq 1 \tag{B.0.14}$$

can be rearranged to give

$$N! \geq j!\,(N-j)! \tag{B.0.15}$$

whose right-hand side is maximised when $j = 0$ and $j = N$. In the context of this example, j cannot be 0 or N and so $j!\,(N-j)!$ is maximised at $j = 1$ and $j = N-1$, i.e. $|p_N(x)| = \|p_N\|$ for some $x \in (x_{1,N}, x_{2,N})$ and $x \in (x_{N-1,N}, x_{N,N})$ as shown in Figure 2.4.2, whence

$$j!\,(N-j)! \leq (N-1)!. \tag{B.0.16}$$

Substitution of (B.0.16) into (B.0.13) then gives

$$\|p_N\| \leq (N-1)!\,\frac{h^N}{4} \tag{B.0.17}$$

as asserted in (2.4.7).

B. PROOF OF BOUND ON MONIC POLYNOMIAL BASED UPON REGULARLY SPACED NODES

Appendix C

Legendre Polynomials

There are many different forms by which the Legendre polynomials can be expressed; when expressed in the form

$$P_N(x) = \sum_{k=0}^{N} a_{k,N}\, x^k, \tag{C.0.1}$$

the coefficient of each power of x can be simply found. Although the Legendre polynomial $P_N(x)$ is expressed in this form in (2.4.50), this form does not appear to be given anywhere other than Wikipedia [1] where it is not proved. For completeness, a proof of this form and the explicit derivation of the coefficients $a_{k,N}$ in terms of N and k will now be given.

Substitution of (C.0.1) into Legendre's differential equation (2.3.14) yields

$$(1-x^2)\sum_{k=0}^{N} k(k-1)a_{k,N}\, x^{k-2} - 2x\sum_{k=0}^{N} k\, a_{k,N}\, x^{k-1} + N(N+1)\sum_{k=0}^{N} a_{k,N}\, x^k = 0 \tag{C.0.2}$$

which is expanded to

$$\sum_{k=0}^{N} k(k-1)a_{k,N}\, x^{k-2} \;-\; \sum_{k=0}^{N} k(k-1)a_{k,N}\, x^k - \sum_{k=0}^{N} 2k a_{k,N}\, x^k + N(N+1)\sum_{k=0}^{N} a_{k,N} x^k = 0. \tag{C.0.3}$$

The terms with $k = 0$ and $k = 1$ vanish in the first sum in (C.0.3) and so the sum is rewritten using the substitution $k' = k - 2$; the remaining sums combine to give

$$\sum_{k'=0}^{N-2} (k'+2)(k'+1)a_{k'+2,N}\, x^{k'} - \sum_{k=0}^{N} \Big(k(k-1)+2k-N(N+1)\Big) a_{k,N}\, x^k = 0. \tag{C.0.4}$$

Noting that $k(k-1)+2k-N(N+1)$ factorises to $(k-N)(N+k+1)$, the second sum in (C.0.4) has non-zero terms for only $k = 0(1)N-1$. Therefore, (C.0.4) is rewritten as

$$\sum_{k=0}^{N-2}\Big((k+2)(k+1)\,a_{k+2,N}+(N-k)(N+k+1)\,a_{k,N}\Big)x^k-2Na_{N-1,N}\,x^{N-1}=0. \quad \text{(C.0.5)}$$

Equating powers of x gives

$$a_{N-1,N}=0 \quad \text{(C.0.6)}$$

and

$$a_{k+2,N}=-\frac{(N-k)(N+k+1)}{(k+2)(k+1)}a_{k,N}, \qquad k=0(1)N-2, \quad \text{(C.0.7)}$$

equivalently

$$a_{k,N}=-\frac{(N-k+2)(N+k-1)}{k(k-1)}a_{k-2,N}, \qquad k=2(1)N. \quad \text{(C.0.8)}$$

Evaluating (C.0.8) recursively for even k gives

$$a_{k,N}=\frac{(-1)^{k/2}\,N!!\,(N+k-1)!!}{k!\,(N-k)!!\,(N-1)!!}\,a_{0,N}, \qquad k=2(2)N, \quad \text{(C.0.9)}$$

and for odd k (C.0.8) gives

$$a_{k,N}=\frac{(-1)^{(k-1)/2}(N-1)!!\,(N+k-1)!!}{k!\,(N-k)!!\,N!!}a_{1,N}, \qquad k=3(2)N, \quad \text{(C.0.10)}$$

in which the double factorial of a non-negative integer n represents the product of all integers from 1 to n that are of the same parity as n [5, p. 530]. Hence for an even positive integer $n=2k$ where $k\geq 0$, the double factorial is expressed as

$$n!!=2^k k!=2^{n/2}\left(\frac{n}{2}\right)! \quad \text{(C.0.11)}$$

and for an odd positive integer $n=2k-1$ with $k\geq 1$, the double factorial is expressed as

$$n!!=\frac{(2k)!}{2^k k!}=\frac{(n+1)!}{2^{(n+1)/2}(\frac{n+1}{2})!}. \quad \text{(C.0.12)}$$

As (C.0.9) and (C.0.10) are dependent upon $a_{0,N}$ and $a_{1,N}$, these values must now be found. Bonnet's recursion formula [118, Eq. 3.27] is a three-term recursion formula given by

$$(N+1)P_{N+1}(x)=(2N+1)xP_N(x)-NP_{N-1}(x) \quad \text{(C.0.13)}$$

which is equivalently

$$P_N(x) = \frac{2N-1}{N} x P_{N-1}(x) - \frac{N-1}{N} P_{N-2}(x). \tag{C.0.14}$$

Substituting (C.0.1) into (C.0.14) gives

$$\sum_{k=0}^{N} a_{k,N}\, x^k = \frac{2N-1}{N} \sum_{k=0}^{N-1} a_{k,N-1}\, x^{k+1} - \frac{N-1}{N} \sum_{k=0}^{N-2} a_{k,N-2}\, x^k, \tag{C.0.15}$$

in which the second sum is rewritten with $k' = k+1$ to give

$$\sum_{k=0}^{N} a_{k,N} x^k = \frac{2N-1}{N} \sum_{k'=1}^{N} a_{k'-1,N-1} x^{k'} - \frac{N-1}{N} \sum_{k=0}^{N-2} a_{k,N-2} x^k, \tag{C.0.16}$$

so that the sums on the right-hand side of (C.0.16) combine to give

$$\begin{aligned} \sum_{k=0}^{N} a_{k,N} x^k \quad = \quad & \sum_{k=1}^{N-2} \Big(\frac{2N-1}{N} a_{k-1,N-1} - \frac{N-1}{N} a_{k,N-2} \Big) x^k \\ & + \frac{2N-1}{N} \Big(a_{N-1,N-1} x^N + a_{N-2,N-1} x^{N-1} \Big) - \frac{N-1}{N} a_{0,N-2}. \end{aligned} \tag{C.0.17}$$

Equating the coefficients of x^0 and x^N then gives

$$a_{0,N} = -\frac{N-1}{N}\, a_{0,N-2} \tag{C.0.18}$$

and

$$a_{N,N} = \frac{2N-1}{N} a_{N-1,N-1}. \tag{C.0.19}$$

Evaluating (C.0.18) recursively gives

$$a_{0,N} = -\frac{N-1}{N} \cdot -\frac{N-3}{N-2} \cdot -\frac{N-5}{N-4} \cdots - \frac{1}{2} a_{0,0}, \qquad N \text{ even} \tag{C.0.20}$$

and

$$a_{0,N} = -\frac{N-1}{N} \cdot -\frac{N-3}{N-2} \cdot -\frac{N-5}{N-4} \cdots - \frac{2}{3} a_{0,1}, \qquad N \text{ odd}. \tag{C.0.21}$$

Since $P_0(x) = 1$ and $P_1(x) = x$ give $a_{0,0} = 1$ and $a_{0,1} = 0$, (C.0.20) and (C.0.21) become

$$a_{0,N} = \begin{cases} (-1)^{\frac{N}{2}} \dfrac{(N-1)!!}{N!!} & N \text{ even} \\ 0 & N \text{ odd}. \end{cases} \tag{C.0.22}$$

Therefore (C.0.9) and (C.0.22) give

$$a_{k,N} = \begin{cases} \dfrac{(-1)^{(N-k)/2}(N+k-1)!!}{k!(N-k)!!} & k \text{ even, } N \text{ even} \\ 0 & k \text{ even, } N \text{ odd,} \end{cases} \tag{C.0.23}$$

which, by comparison with (C.0.22), holds for all $k = 0(2)N$. Evaluating (C.0.19) recursively gives

$$a_{N,N} = \frac{2N-1}{N} \cdot \frac{2N-3}{N-1} \cdots \frac{1}{2} a_{0,0} = \frac{(2N-1)!!}{N!} a_{0,0} = \frac{(2N-1)!!}{N!}, \tag{C.0.24}$$

since $a_{0,0} = 1$. When N is odd, setting $k = N$ in (C.0.10) gives

$$a_{N,N} = \frac{(-1)^{(N-1)/2}(N-1)!!\,(2N-1)!!}{N!\,N!!} a_{1,N} \tag{C.0.25}$$

which, upon substitution of (C.0.24), yields

$$\frac{(2N-1)!!}{N!} = \frac{(-1)^{(N-1)/2}(N-1)!!\,(2N-1)!!}{N!\,N!!} a_{1,N}. \tag{C.0.26}$$

Rearranging (C.0.26) then gives

$$a_{1,N} = \frac{(-1)^{(N-1)/2} N!!}{(N-1)!!}, \qquad N \text{ odd.} \tag{C.0.27}$$

When N is even, setting $k = N-1$ in (C.0.10) gives

$$a_{N-1,N} = \frac{(-1)^{(N-2)/2}(N-1)!!\,(2N-2)!!}{(N-1)!\,N!!} a_{1,N} \tag{C.0.28}$$

which rearranges to

$$a_{1,N} = \frac{(-1)^{(N-2)/2}(N-1)!\,N!!}{(N-1)!!\,(2N-2)!!} a_{N-1,N} = 0, \quad N \text{ even,} \tag{C.0.29}$$

since, by (C.0.6), $a_{N-1,N} = 0$. Now substituting (C.0.27) and (C.0.29) into (C.0.10) gives,

$$a_{k,N} = \begin{cases} \dfrac{(-1)^{(N-k)/2}(N+k-1)!!}{k!(N-k)!!} & k \text{ odd, } N \text{ odd} \\ 0 & k \text{ odd, } N \text{ even,} \end{cases} \tag{C.0.30}$$

which, by comparison with (C.0.27) and (C.0.29), holds for all $k = 1(2)N$. The expressions (C.0.23) and (C.0.30) combine to give

$$a_{k,N} = \begin{cases} \dfrac{(-1)^{(N-k)/2}(N+k-1)!!}{k!(N-k)!!} & k+N \text{ even} \\ \\ 0 & k+N \text{ odd}, \end{cases} \tag{C.0.31}$$

wherein, by (C.0.11),

$$(N-k)!! = 2^{(N-k)/2}\left(\frac{N-k}{2}\right)! \tag{C.0.32}$$

and, by (C.0.12),

$$(N+k-1)!! = \frac{(N+k)!}{2^{(N+k)/2}\left(\frac{N+k}{2}\right)!}. \tag{C.0.33}$$

Therefore, combining (C.0.31)–(C.0.33) yields

$$a_{k,N} = \begin{cases} \dfrac{(-1)^{(N-k)/2}(N+k)!}{2^N\, k!\, \left(\frac{N+k}{2}\right)!\left(\frac{N-k}{2}\right)!} & \text{for } N+k \text{ even} \\ \\ 0 & \text{for } N+k \text{ odd}, \end{cases} \tag{C.0.34}$$

which can be written as the single expression

$$a_{k,N} = \Re\left((-1)^{(N-k)/2}\frac{(N+k)!}{2^N k!\left(\frac{N+k}{2}\right)!\left(\frac{N-k}{2}\right)!}\right), \qquad k = 1(1)N, \tag{C.0.35}$$

where $\Re$ denotes the real part.

The Gamma function [2, p. 255] is used to find half-integer factorials as [110, p. 5]

$$\Gamma\left(\frac{1}{2}+n\right) = \left(-\frac{1}{2}+n\right)! = \frac{(2n-1)!!}{2^n}\sqrt{\pi} \tag{C.0.36}$$

and

$$\Gamma\left(\frac{1}{2}-n\right) = \left(-\frac{1}{2}-n\right)! = \frac{(-2)^n}{(2n-1)!!}\sqrt{\pi} \tag{C.0.37}$$

for $n \in \mathbb{N}$ which, by (C.0.12), equivalently give

$$\left(-\frac{1}{2}+n\right)! = \frac{(2n)!}{4^n n!}\sqrt{\pi} \tag{C.0.38}$$

and

$$\left(-\frac{1}{2}-n\right)! = \frac{(-4)^n n!}{(2n)!}\sqrt{\pi}. \tag{C.0.39}$$

Rearranging (C.0.38) gives

$$n! = \frac{(2n)!}{4^n\left(-\frac{1}{2}+n\right)!}\sqrt{\pi} \tag{C.0.40}$$

and rearranging (C.0.39) gives

$$n! = \frac{(2n)!\left(-\frac{1}{2}-n\right)!}{(-4)^n\sqrt{\pi}}. \tag{C.0.41}$$

For $N+k$ even, let $n = \frac{N+k}{2}$ in (C.0.40) and $n = \frac{N-k}{2}$ in (C.0.41), respectively giving

$$\left(\frac{N+k}{2}\right)! = \frac{(N+k)!\sqrt{\pi}}{4^{(N+k)/2}\left(\frac{N+k-1}{2}\right)!} \tag{C.0.42}$$

and

$$\left(\frac{N-k}{2}\right)! = \frac{(N-k)!\left(-\frac{N-k+1}{2}\right)!}{(-4)^{(N-k)/2}\sqrt{\pi}}. \tag{C.0.43}$$

Substituting (C.0.42) and (C.0.43) into (C.0.35) gives

$$a_{k,N} = \Re\left(\frac{(-1)^{(N-k)/2}(N+k)!}{2^N k!}\cdot\frac{4^{(N+k)/2}\left(\frac{N+k-1}{2}\right)!}{(N+k)!\sqrt{\pi}}\cdot\frac{(-4)^{(N-k)/2}\sqrt{\pi}}{(N-k)!\left(-\frac{N-k+1}{2}\right)!}\right) \tag{C.0.44}$$

which simplifies to

$$\begin{aligned} a_{k,N} &= \Re\left(\frac{4^N\left(\frac{N+k-1}{2}\right)!}{2^N\,k!\,(N-k)!\left(-\frac{N-k+1}{2}\right)!}\right) = 2^N\frac{N!}{k!\,(N-k)!}\cdot\Re\left(\frac{\left(\frac{N+k-1}{2}\right)!}{N!\left(-\frac{N-k+1}{2}\right)!}\right) \\ &= 2^N\binom{N}{k}\binom{\frac{N+k-1}{2}}{N}. \end{aligned} \tag{C.0.45}$$

Therefore substituting (C.0.45) into (C.0.1) gives an expression for the Legendre polynomials as

$$P_N(x) = 2^N\sum_{k=0}^{N}\binom{N}{k}\binom{\frac{N+k-1}{2}}{N}x^k. \tag{C.0.46}$$

The factors that multiply the Legendre polynomial and its derivatives within the monic polynomials (2.3.15), (2.3.18), (2.3.19) and (2.3.26) can be readily determined by considering the coefficient of x^N in (C.0.46).

Appendix D

Conversion of BVP to FIE

It is now shown how the FIEs (4.1.13) and (4.1.17) can be derived from the BVP (4.1.11). For convenience, the two-point BVP (4.1.11) is repeated here as

$$y''(x) + A(x)\,y'(x) + B(x)\,y(x) = g(x), \qquad y(a) = \alpha, \qquad y(b) = \beta. \tag{D.0.1}$$

D.1 Derivation of (4.1.13)

The details of the derivation of the FIE (4.1.13) are now given, which are noted to differ from those in the incorrect approach – apparently never before recognised as such – in [104]. Therefore, the resulting proof is augmented with an example that demonstrates the correctness of the present analysis and the error of that presented in [104].

The derivation of FIE (4.1.13) begins with the conversion

$$y''(x) = u(x), \tag{D.1.1}$$

integration of which yields

$$y'(x) = y'(a) + \int_a^x u(t)\,dt. \tag{D.1.2}$$

Integrating (D.1.2) then yields

$$y(x) = y(a) + (x-a)\,y'(a) + \int_a^x \int_a^t u(s)\,ds\,dt \tag{D.1.3}$$

which, upon substituting the boundary condition $y(a) = \alpha$ and evaluating the double integral using integration by parts, is equivalently

$$y(x) = \alpha + (x-a)\,y'(a) + \int_a^x (x-t)\,u(t)\,dt. \tag{D.1.4}$$

Note that (D.1.4) is equivalent to (4.1.12), wherein the latter gives the integral in terms of $y''(t)$. Substitution of (D.1.1), (D.1.2) and (D.1.4) into the original BVP (D.0.1) yields

$$\begin{aligned} u(x) \;+\; & A(x)\left(y'(a) + \int_a^x u(t)\,dt\right) \\ + \; & B(x)\left(\alpha + (x-a)\,y'(a) + \int_a^x (x-t)\,u(t)\,dt\right) = g(x), \end{aligned} \tag{D.1.5}$$

which is rearranged to

$$\begin{aligned} u(x) \;+\; & \alpha B(x) + \Big(A(x) + (x-a)\,B(x)\Big)\,y'(a) \\ + \; & A(x)\int_a^x u(t)\,dt + B(x)\int_a^x (x-t)\,u(t)\,dt \;=\; g(x). \end{aligned} \tag{D.1.6}$$

The unknown constant $y'(a)$ is found by setting $x = b$ in (D.1.4), imposing the boundary condition $y(b) = \beta$ and rearranging to give

$$y'(a) = \frac{\beta - \alpha}{b-a} - \frac{1}{b-a}\int_a^b (b-t)\,u(t)\,dt \tag{D.1.7}$$

which, when substituted into (D.1.6), yields

$$\begin{aligned} u(x) \;+\; & \alpha B(x) + \frac{\beta-\alpha}{b-a}\Big(A(x) + (x-a)\,B(x)\Big) \\ - \; & \frac{1}{b-a}\Big(A(x) + (x-a)\,B(x)\Big)\int_a^b (b-t)\,u(t)\,dt + A(x)\int_a^x u(t)\,dt \\ + \; & B(x)\int_a^x (x-t)\,u(t)\,dt \;=\; g(x). \end{aligned} \tag{D.1.8}$$

Rearranging (D.1.8) then gives

$$\begin{aligned} u(x) &= g(x) - \alpha B(x) - \frac{\beta-\alpha}{b-a}\Big(A(x) + (x-a)\,B(x)\Big) \\ &+ \int_a^x \left(\frac{b-t}{b-a}\Big(A(x) + (x-a)\,B(x)\Big) - A(x) - (x-t)\,B(x)\right) u(t)\,dt \\ &+ \int_x^b \left(\frac{b-t}{b-a}\Big(A(x) + (x-a)\,B(x)\Big)\right) u(t)\,dt, \end{aligned} \tag{D.1.9}$$

in which the kernel in the first integral can be re-expressed as

$$\begin{aligned} \frac{b-t}{b-a}\Big(A(x) &+ (x-a)\,B(x)\Big) - A(x) - (x-t)\,B(x) \\ &= \left(\frac{b-a}{b-a} - 1\right) A(x) + \left(\frac{(b-t)(x-a)}{b-a} - (x-t)\right) B(x) \\ &= \frac{b-t-(b-a)}{b-a}\,A(x) + \frac{(b-t)(x-a)-(x-t)(b-a)}{b-a}\,B(x) \\ &= \frac{a-t}{b-a}\Big(A(x) + (x-b)\,B(x)\Big). \end{aligned} \tag{D.1.10}$$

Therefore (D.1.9) can be written as the FIE

$$u(x) = f(x) + \int_a^b K(x,t)\,u(t)\,dt \tag{D.1.11}$$

wherein

$$f(x) = g(x) - \alpha B(x) - \frac{\beta-\alpha}{b-a}\Big(A(x) + (x-a)\,B(x)\Big) \tag{D.1.12}$$

and

$$K(x,t) = \begin{cases} \dfrac{a-t}{b-a}\Big(A(x) + (x-b)\,B(x)\Big) & a \le t \le x, \\[2ex] \dfrac{b-t}{b-a}\Big(A(x) + (x-a)\,B(x)\Big) & x \le t \le b, \end{cases} \tag{D.1.13}$$

equivalently (4.1.13), (4.1.15) and (4.1.16), thereby completing the derivation. Upon solving the FIE (D.1.11), the solution is substituted into (D.1.7) to find $y'(a)$ which is then substituted, with the FIE solution, into (D.1.4) to recover the solution of the BVP (D.0.1).

In the case that $a = 0$ and $b = 1$ then the kernel (D.1.13) becomes

$$K(x,t) = \begin{cases} -t\left(A(x) + (x-1)\,B(x)\right) & 0 \le t \le x, \\ \\ (1-t)\left(A(x) + x\,B(x)\right) & x \le t \le 1 \end{cases} \tag{D.1.14}$$

which differs from the kernel given by [104, Eq. 1.30]

$$K(x,t) = \begin{cases} (1-x)\left(A(x) + t\,B(x)\right) & 0 \le t \le x, \\ \\ (1-t)\left(A(x) + x\,B(x)\right) & x \le t \le 1, \end{cases} \tag{D.1.15}$$

that augments the FIE (D.1.11) with $f(x)$ defined by (D.1.12). The following example with given quantities $y(x)$, $A(x)$, $B(x)$, from which α, β and $g(x)$ are readily recovered from the BVP (D.0.1), demonstrates that (D.1.14) is correct and (D.1.15) is incorrect. Substitution of the given quantities $y(x)$, $A(x)$, $B(x)$ into the FIE (D.1.11) should yield a source function $f(x)$ that is consistent with the recovered quantities α, β and $g(x)$. Let

$$y(x) = \cos x, \quad A(x) = x^5, \quad \text{and} \quad B(x) = x^2 \tag{D.1.16}$$

which, upon substitution into the BVP (D.0.1), yields

$$\begin{aligned} g(x) &= y''(x) + A(x)\,y'(x) + B(x)\,y(x) \\ \\ &= -\cos x - x^5 \sin x + x^2 \cos x. \end{aligned} \tag{D.1.17}$$

Additionally α and β are found from (D.1.16) as

$$\alpha = y(a) = 1 \quad \text{and} \quad \beta = y(b) = \cos 1. \tag{D.1.18}$$

By (D.1.1) and (D.1.14), the FIE solution and kernel are now found from (D.1.16) as

$$u(x) = y''(x) = -\cos x \tag{D.1.19}$$

and

$$K(x,t) = \begin{cases} -t\,(x^5 + x^3 - x^2) & 0 \le t \le x, \\ \\ (1-t)\,(x^5 + x^3) & x \le t \le 1 \end{cases} \tag{D.1.20}$$

which, upon substitution into the FIE (D.1.11), yields

$$\begin{aligned} f(x) &= u(x) - \int_a^b K(x,t)\,u(t)\,dt \\ &= -\cos x - (x^5 + x^3 - x^2)\int_0^x t\,\cos t\,dt - (x^5 + x^3)\int_x^1 (t-1)\,\cos t\,dt \\ &= -\cos x - (x^5 + x^3 - x^2)\,(\cos x + x\,\sin x - 1) \\ &\quad -(x^5 + x^3)\Big((1-x)\,\sin x - \cos x + \cos 1\Big) \\ &= (x^2 - 1)\,\cos x - x^5 \sin x - (x^5 + x^3)\,\cos 1 + x^5 + x^3 - x^2. \end{aligned} \tag{D.1.21}$$

Substitution of (D.1.16)–(D.1.18) into the definition of the source function (D.1.12) gives

$$\begin{aligned} f(x) &= g(x) - \alpha B(x) - \frac{\beta - \alpha}{b - a}\Big(A(x) + (x-a)\,B(x)\Big) \\ &= -\cos x - x^5\,\sin x + x^2\,\cos x - x^2 - (\cos 1 - 1)\,(x^5 + x^3) \\ &= (x^2 - 1)\,\cos x - x^5 \sin x - (x^5 + x^3)\,\cos 1 + x^5 + x^3 - x^2 \end{aligned} \tag{D.1.22}$$

which is clearly consistent with (D.1.21), thereby validating the FIE representation (D.1.11)–(D.1.13) of the BVP (D.0.1). In contrast, substitution of $A(x)$ and $B(x)$ defined by (D.1.16) into (D.1.15) yields

$$K(x,t) = \begin{cases} (1-x)\,(x^5 + t\,x^2) & 0 \le t \le x, \\ (1-t)\,(x^5 + x^3) & x \le t \le 1 \end{cases} \tag{D.1.23}$$

which, upon substitution into the FIE (D.1.11) with (D.1.19), gives

$$\begin{aligned} f(x) &= u(x) - \int_a^b K(x,t)\,u(t)\,dt \\ &= -\cos x + (1-x)\,x^5 \int_0^x \cos t\,dt + (1-x)\,x^2 \int_0^x t\,\cos t\,dt \\ &\quad -(x^5+x^3)\int_x^1 (t-1)\,\cos t\,dt \\ &= -\cos x + (1-x)\,x^5\,\sin x + (1-x)\,x^2(\cos x + x\sin x - 1) \\ &\quad -(x^5+x^3)\Big((1-x)\,\sin x - \cos x + \cos 1\Big) \\ &= (x^5+x^2-1)\,\cos x - (x^5+x^3)\,\cos 1 + x^3 - x^2. \end{aligned} \tag{D.1.24}$$

Therefore as the source function derived from its definition (D.1.22) is inconsistent with the source function derived from the FIE (D.1.24), the kernel (D.1.15) must be incorrect. The analysis in [104] does not include the intermediate steps between the correct equivalent forms of (D.1.7) and (D.1.8) with $[a,b]=[0,1]$ and the FIE2 (D.1.11) with correct source function (D.1.12) and incorrect kernel (D.1.15). It is therefore assumed that the error occurs in one of the omitted steps.

D.2 Derivation of (4.1.17)

The BVP (D.0.1) can be rearranged to

$$y''(x) = g(x) - A(x)\,y'(x) - B(x)\,y(x) \tag{D.2.1}$$

which, when integrated, yields

$$\begin{aligned} y'(x) = y'(a) &+ \int_a^x g(t)\,dt - A(x)\,y(x) + A(a)\,y(a) \\ &+ \int_a^x A'(t)\,y(t)\,dt - \int_a^x B(t)\,y(t)\,dt \end{aligned} \tag{D.2.2}$$

wherein $A(x)\,y'(x)$ has been integrated by parts. Integrating (D.2.2) then gives

$$\begin{aligned} y(x) = \quad & y(a) \quad + (x-a)\Big(y'(a) + A(a)\,y(a)\Big) + \int_a^x \int_a^t g(s)\,ds\,dt \\ - \quad & \int_a^x A(t)\,y(t)\,dt + \int_a^x \int_a^t \Big(A'(s) - B(s)\Big)\,y(s)\,ds\,dt \end{aligned} \tag{D.2.3}$$

which, upon substituting the boundary condition $y(a) = \alpha$ and evaluating the double integrals using integration by parts, is equivalently

$$\begin{aligned} y(x) = \alpha \quad + \quad & (x-a)\Big(y'(a) + \alpha\,A(a)\Big) + \int_a^x (x-t)\,g(t)\,dt \\ - \quad & \int_a^x A(t)\,y(t)\,dt + \int_a^x (x-t)\Big(A'(t) - B(t)\Big)\,y(t)\,dt. \end{aligned} \tag{D.2.4}$$

By setting $x = b$ in (D.2.4) and imposing the boundary condition $y(b) = \beta$, the unknown constant $y'(a)$ is found as

$$\begin{aligned} y'(a) \quad = \quad & -\alpha\,A(a) + \frac{1}{b-a}\left(\beta - \alpha - \int_a^b (b-t)\,g(t)\,dt\right) \\ & + \frac{1}{b-a}\int_a^b \Big(A(t) - (b-t)\Big(A'(t) - B(t)\Big)\Big)\,y(t)\,dt \end{aligned} \tag{D.2.5}$$

which, when substituted into (D.2.4), yields

$$\begin{aligned} y(x) = \alpha \quad + \quad & \frac{x-a}{b-a}\left(\beta - \alpha - \int_a^b (b-t)\,g(t)\,dt\right) + \int_a^x (x-t)\,g(t)\,dt \\ + \quad & \frac{x-a}{b-a}\int_a^b \Big(A(t) - (b-t)\Big(A'(t) - B(t)\Big)\Big)\,y(t)\,dt \\ - \quad & \int_a^x \Big(A(t) - (x-t)\Big(A'(t) - B(t)\Big)\Big)\,y(t)\,dt. \end{aligned} \tag{D.2.6}$$

Rearranging (D.2.6) then gives

$$\begin{aligned} y(x) = \alpha \quad &+ \quad \frac{x-a}{b-a}\left(\beta - \alpha - \int_a^b (b-t)\, g(t)\, dt\right) + \int_a^x (x-t)\, g(t)\, dt \\ &+ \quad \int_a^x \frac{x-a}{b-a}\Big(A(t) - (b-t)\Big(A'(t) - B(t)\Big)\Big)\, y(t)\, dt \\ &- \quad \int_a^x \Big(A(t) - (x-t)\Big(A'(t) - B(t)\Big)\Big)\, y(t)\, dt \\ &+ \quad \int_x^b \frac{x-a}{b-a}\Big(A(t) - (b-t)\Big(A'(t) - B(t)\Big)\Big)\, y(t)\, dt \end{aligned} \tag{D.2.7}$$

in which the kernels in the integrals on the interval $[a, x]$ can be combined as

$$\begin{aligned} \frac{x-a}{b-a}\Big(\quad A(t) \quad & -(b-t)\Big(A'(t) - B(t)\Big)\Big) - \Big(A(t) - (x-t)\Big(A'(t) - B(t)\Big)\Big) \\ = \quad & \left(\frac{x-a}{b-a} - 1\right) A(t) - \left(\frac{(x-a)(b-t)}{b-a} - (x-t)\right)\Big(A'(t) - B(t)\Big) \\ = \quad & \frac{x-a-(b-a)}{b-a} A(t) - \frac{(x-a)(b-t) - (x-t)(b-a)}{b-a}\Big(A'(t) - B(t)\Big) \\ = \quad & \frac{x-b}{b-a}\Big(A(t) - (a-t)\Big(A'(t) - B(t)\Big)\Big). \end{aligned} \tag{D.2.8}$$

Therefore (D.2.7) can be written as the FIE

$$y(x) = f(x) + \int_a^b K(x,t)\, y(t)\, dt \tag{D.2.9}$$

wherein

$$f(x) = \alpha + \int_a^x (x-t)\, g(t)\, dt + \frac{x-a}{b-a}\left(\beta - \alpha - \int_a^b (b-t)\, g(t)\, dt\right), \tag{D.2.10}$$

and

$$K(x,t) = \begin{cases} \dfrac{x-b}{b-a}\Big(A(t) - (a-t)\Big(A'(t) - B(t)\Big)\Big) & a \le t \le x, \\ \dfrac{x-a}{b-a}\Big(A(t) - (b-t)\Big(A'(t) - B(t)\Big)\Big) & x \le t \le b, \end{cases} \tag{D.2.11}$$

equivalently (4.1.17), (4.1.18) and (4.1.19), and so the derivation is complete.

Appendix E

Proof of Nyström-Matrix Eigenvalues

The formula (4.3.13) for the eigenvalues of the Nyström matrix $\mathbf{K}_M$ based upon the separable kernel $K(x,y) = P(x)\,Q(y)$ is proved by induction using the property (4.3.12).

When $M = 2$ the characteristic polynomial of a 2×2 matrix yields

$$\det(\mathbf{K_2} - \Lambda \mathbf{I_2}) = \Lambda^2 - \Lambda \,\mathrm{Tr}\,(\mathbf{K_2}) + \det(\mathbf{K_2}), \tag{E.0.1}$$

in which by (4.3.12)

$$\det(\mathbf{K_2}) = K_{1,1}\,K_{2,2} - K_{1,2}\,K_{2,1} = 0. \tag{E.0.2}$$

Therefore, since (E.0.1) is equivalently

$$\det(\mathbf{K_2} - \Lambda \mathbf{I_2}) = -\Lambda\,(\mathrm{Tr}\,(\mathbf{K_2}) - \Lambda), \tag{E.0.3}$$

assertion (4.3.13) is true for $M = 2$. Assume now that (4.3.13) is true for $M = m$ so that

$$\det(\mathbf{K_m} - \Lambda \mathbf{I_m}) = (-\Lambda)^{m-1} \left(\sum_{i=1}^{m} K_{i,i} - \Lambda \right) = 0, \tag{E.0.4}$$

using which the $M = m + 1$ case is considered. The matrix $\mathbf{K_{m+1}} - \Lambda \mathbf{I_{m+1}}$ can be written in block form [112] as

$$\mathbf{K_{m+1}} - \Lambda \mathbf{I_{m+1}} = \left[\begin{array}{c|c} \mathbf{K_m} - \Lambda \mathbf{I_m} & \mathbf{l} \\ \hline \mathbf{k} & K_{m+1,\,m+1} - \Lambda \end{array}\right] \tag{E.0.5}$$

wherein $\mathbf{k}$ and $\mathbf{l}$ are respectively the row vector and column vector, each of length m, with entries

$$\{\mathbf{k}\}_{i,j} = K_{m+1,\,j}, \qquad \{\mathbf{l}\}_{i,j} = K_{i,\,m+1}, \qquad i,j = 1(1)m. \tag{E.0.6}$$

Now, noting that

$$\mathbf{k}\,(K_{m+1,\,m+1} - \Lambda)\,\mathbf{I_m} = (K_{m+1,\,m+1} - \Lambda)\,\mathbf{k} \tag{E.0.7}$$

and

$$(\mathbf{K_m} - \Lambda\mathbf{I_m})\,(K_{m+1,\,m+1} - \Lambda)\,\mathbf{I_m} = (K_{m+1,\,m+1} - \Lambda)\,(\mathbf{K_m} - \Lambda\mathbf{I_m}), \tag{E.0.8}$$

it is clear that (E.0.5) satisfies the matrix equation

$$(\mathbf{K_{m+1}} - \Lambda\mathbf{I_{m+1}})\,\widetilde{\mathbf{K}}_{\mathbf{m+1}} = \widetilde{\mathbf{L}}_{\mathbf{m+1}} \tag{E.0.9}$$

in which

$$\widetilde{\mathbf{K}}_{\mathbf{m+1}} = \left[\begin{array}{c|c} (K_{m+1,\,m+1} - \Lambda)\mathbf{I_m} & \mathbf{0} \\ \hline -\mathbf{k} & 1 \end{array}\right] \quad \text{and} \quad \widetilde{\mathbf{L}}_{\mathbf{m+1}} = \left[\begin{array}{c|c} \mathbf{L} & \mathbf{l} \\ \hline \mathbf{0} & K_{m+1,\,m+1} - \Lambda \end{array}\right], \tag{E.0.10}$$

wherein

$$\mathbf{L} = (K_{m+1,\,m+1} - \Lambda)\,(\mathbf{K_m} - \Lambda\mathbf{I_m}) - \mathbf{lk}. \tag{E.0.11}$$

By (4.3.12), the entries of the product $\mathbf{lk}$ in (E.0.11) are

$$\{\mathbf{lk}\}_{i,j} = K_{m+1,\,j}\,K_{i,\,m+1} = K_{m+1,\,m+1}\,K_{i,j}. \tag{E.0.12}$$

Therefore,

$$\mathbf{lk} = K_{m+1,\,m+1}\,\mathbf{K_m} \tag{E.0.13}$$

and so the matrix $\mathbf{L}$ in (E.0.11) is equivalently

$$\mathbf{L} = -\Lambda\,(\mathbf{K_m} - (\Lambda - K_{m+1,\,m+1})\,\mathbf{I_m}). \tag{E.0.14}$$

Since $\widetilde{\mathbf{K}}_{\mathbf{m+1}}$ and $\widetilde{\mathbf{L}}_{\mathbf{m+1}}$ respectively contain a zero column vector and a zero row vector, by Leibniz formula for determinants [33] their determinants are equal to the product of determinants of the blocks on the leading diagonal, so that

$$\det(\widetilde{\mathbf{K}}_{\mathbf{m+1}}) = (K_{m+1,\,m+1} - \Lambda)^m \quad \text{and} \quad \det(\widetilde{\mathbf{L}}_{\mathbf{m+1}}) = \det(\mathbf{L})\,(K_{m+1,\,m+1} - \Lambda) \tag{E.0.15}$$

in which $\det(\mathbf{L})$ is computed from (E.0.4) and (E.0.14) as

$$\det(\mathbf{L}) = (-\Lambda)^m \left(K_{m+1,\,m+1} - \Lambda\right)^{m-1} \left(\sum_{i=1}^{m+1} K_{i,i} - \Lambda\right). \tag{E.0.16}$$

Combining (E.0.9), (E.0.15) and (E.0.16) then yields

$$\det(\mathbf{K_{m+1}} - \Lambda\mathbf{I_{m+1}}) = (-\Lambda)^m \left(\sum_{i=1}^{m+1} K_{i,i} - \Lambda\right) \tag{E.0.17}$$

and so (4.3.13) holds for $m = M + 1$. Since (4.3.13) is true for $M = 2$ it is therefore also true for all integers $M > 2$.

References

[1] Legendre polynomials. https://en.wikipedia.org/wiki/Legendre_polynomials. Accessed: 07-11-2017.

[2] M. Abramowitz and I. A. Stegun. *Handbook of Mathematical Functions: with Formulas, Graphs, and Mathematical Tables*. Dover Publications, New York, 1972.

[3] F. Anli, F. Yaşa, S. Güngör, and H. Öztürk. T_N approximation to neutron transport equation and application to critical slab problem. *J. Quant. Spectrosc. Ra.*, 101(1):129–134, 2006.

[4] P.M. Anselone. Collectively compact operator approximations. *Tech. Rep. 76, Computer Science Dept., Stanford Univ.*, 1967.

[5] G.B. Arfken and H.J. Weber. *Mathematical Methods For Physicists*. Elsevier Academic Press, 2005.

[6] O. A. Arqub, M. Al-Smadi, and N. Shawagfeh. Solving Fredholm integro–differential equations using reproducing kernel Hilbert space method. *Appl. Math. Comput.*, 219(17):8938–8948, 2013.

[7] E. Aruchunan and J. Sulaiman. Quarter-sweep Gauss-Seidel method for solving first order linear Fredholm integro-differential equations. *Matematika*, 27(2):199–208, 2011.

[8] K. Atkinson. Iterative variants of the Nyström method for the numerical solution of integral equations. *Numer. Math.*, 22(1):17–31, 1973.

[9] K.E. Atkinson. *An Introduction to Numerical Analysis*. Wiley, 2nd edition, 1989.

[10] K.E. Atkinson. *The Numerical Solution of Integral Equations of the Second Kind*. Cambridge University Press, New York, 1997.

[11] E. Babolian, J. Biazar, and A.R. Vahidi. The decomposition method applied to systems of Fredholm integral equations of the second kind. *Appl. Math. Comput.*, 148(2):443–452, 2004.

[12] E. Babolian and L.M. Delves. A fast Galerkin scheme for linear integro-differential equations. *IMA J. Numer. Anal.*, 1(2):193–213, 1981.

[13] E. Babolian and A. Shahsavaran. Numerical solution of nonlinear Fredholm integral equations of the second kind using Haar wavelets. *J. Comput. Appl. Math.*, 225:87–95, 2009.

[14] C.T.H. Baker. *The Numerical Treatment of Integral Equations*. Clarendon Press, Oxford, 1977.

[15] R. Baltensperger and J.P. Berrut. The errors in calculating the pseudospectral differentiation matrices for çebyşev-Gauss-Lobatto points. *Comput. Math. Appl.*, 37:41–48, 1999.

[16] R. Baltensperger and M.R. Trummer. Spectral differencing with a twist. *SIAM J. Sci. Comput.*, 24(5):1465–1487, 2003.

[17] V. E. Barlette, M. M. Leite, and S. K. Adhikari. Integral equations of scattering in one dimension. *American Journal of Physics*, 69(9):1010–1013, 2001.

[18] A. Bayliss, A. Class, and B.J. Matkowsky. Roundoff error in computing derivatives using the Chebyshev differentiation matrix. *J. Comput. Phys.*, 116(2):380–383, 1995.

[19] R. Bellman, B. G. Kashef, and J. Casti. Differential quadrature: A technique for the rapid solution of nonlinear partial differential equations. *J. Comput. Phys.*, 10:40–52, 1972.

[20] C.M. Bender and S.A. Orszag. *Advanced Mathematical Methods for Scientists and Engineers I: Asymptotic Methods and Perturbation Theory*. Springer Science & Business Media, 2013.

[21] J.P. Berrut and H. D. Mittelmann. Linear rational interpolation and its application in approximation and boundary value problems. *Rocky Mountain Journal of Mathematics*, 32(2):527–544, 2002.

[22] J.P. Berrut and L. N. Trefethen. Barycentric Lagrange interpolation. *SIAM Rev.*, 46(3):501–517, 2004.

[23] A.H. Bhrawy, E. Tohidi, and F. Soleymani. A new Bernoulli matrix method for solving high-order linear and nonlinear Fredholm integro-differential equations with piecewise intervals. *Appl. Math. Comput.*, 219(2):482–497, 2012.

[24] N. Bildik, A. Konuralp, and S. Yalçinbaş. Comparison of Legendre polynomial approximation and variational iteration method for the solutions of general linear Fredholm integro-differential equations. *Comput. Math. Appl.*, 59:1909–1917, 2010.

[25] A.H. Borzabadi and M. Heidari. A successive numerical scheme for some classes of Volterra-Fredholm integral equations. *Iranian Journal of Mathematical Sciences and Informatics*, 10(2):1–10, 2015.

[26] J. P. Boyd. Defeating the Runge Phenomenon for equispaced polynomial interpolation via Tikhonov regularization. *Appl. Math. Lett.*, 5(6):57–59, 1992.

[27] J. P. Boyd. *Chebyshev and Fourier Spectral Methods*. Dover Publications, New York, 2000.

[28] J. P. Boyd. Exponentially accurate Runge-free approximation of non-periodic functions from samples on an evenly spaced grid. *Appl. Math. Lett.*, 20(9):971–975, 2007.

[29] K.S. Breuer and R.M. Everson. On the errors incurred calculating derivatives using Chebyshev polynomials. *J. Comput. Phys.*, 99:56–67, 1992.

[30] K. Brix, C. Canuto, and W. Dahmen. Legendre-Gauss-Lobatto grids and associated nested dyadic grids. *Aachen Inst. Adv. Study Comput. Eng. Sci. (arXiv:1311.0028).*, 2013.

[31] L. Brutman. An application of the generalized alternating polynomials to the numerical solution of Fredholm integral equations. *Numer. Algorithms*, 5(9):437–442, 1993.

[32] I. W. Busbridge. *The mathematics of radiative transfer*. Cambridge University Press, 1960.

[33] P. Chen. Determinants. http://shannon.cm.nctu.edu.tw/la/la5s09.pdf. Accessed: 15-06-2015.

[34] Z. Chen and W. Jiang. An approximate solution for a mixed linear Volterra–Fredholm integral equation. *Appl. Math. Lett.*, 25:1131–1134, 2012.

[35] C.W. Clenshaw and Curtis A.R. A method for numerical integration on an automatic computer. *Numer. Math.*, 2(1):197–205, 1960.

[36] R. Cont, P. Tankov, and E. Voltchkova. Option pricing models with jumps: integro-differential equations and inverse problems. In P. Neittaanmäki, T. Rossi, S. Korotov, E. Oñate, J. Périaux, and E. Knörzer, editors, *EC-COMAS 2004*, pages 1–20, 2004.

[37] B. Costa and W.S. Don. On the computation of high order pseudospectral derivatives. *Appl. Num. Math.*, 33:151–159, 2000.

[38] P. Darania and A. Ebadian. A method for the numerical solution of the integro-differential equations. *Appl. Math. Comput.*, 188:657–668, 2007.

[39] M.T. Darvishi. Preconditioning and domain decomposition schemes to solve PDEs. *Int. J. Pure Appl. Math.*, 15(4):419–437, 2004.

[40] M.T. Darvishi and F. Ghoreishi. Error reduction for higher derivatives of Chebyshev collocation method using preconditioning and domain decomposition. *Korean J. Comput & Appl. Math.*, 6(2):421–435, 1999.

[41] L.G. Davis. Polynomial Interpolation and Error Analysis. http://www.math.montana.edu/~davis/Classes/MA442/Sp07/Notes/InterpError.pdf. Accessed: 24-01-2015.

[42] M. Dehghan and A. Saadatmandi. Chebyshev finite difference method for Fredholm integro-differential equation. *Int. J. Comput. Math.*, 85(1):123–130, 2008.

[43] L.M. Delves. A Fast Method for the Solution of Fredholm Integral Equations. *J. Inst. Maths Applics*, 20:173–182, 1977.

[44] L.M. Delves, L.F. Abd-Elal, and J.A. Hendry. A fast Galerkin algorithm for singular integral equations. *J. Inst. Maths Applics*, 23:139–166, 1979.

[45] L.M. Delves and J.L. Mohamed. *Computational Methods for Integral Equations*. Cambridge, 1985.

[46] W.S. Don and A. Solomonoff. Accuracy and speed in computing the Chebyshev collocation derivative. *SIAM J. Sci. Comput.*, 16(6):1253–1268, 1995.

[47] W.S. Don and A. Solomonoff. Accuracy enhancement for higher derivatives using Chebyshev collocation and a mapping technique. *SIAM J. Sci. Comput.*, 18(4):1040–1055, 1997.

[48] E.M.E. Elbarbary and S.M. El-Sayed. Higher order pseudospectral differentiation matrices. *Appl. Num. Math.*, 55:425–438, 2005.

[49] G. N. Elnager. Optimal control computation for integro-differential aerodynamic equations. *Math. Meth. Appl. Sci.*, 21:653–664, 1998.

[50] A.I. Fairbairn and M.A. Kelmanson. Computable theoretical error bounds for Nyström methods for Fredholm integral equations of the second kind. In P.J. Harris, editor, *Proc. 10th UK Conf. on Boundary Integral Methods (Brighton, UK)*, pages 85–94, 2015.

[51] A.I. Fairbairn and M.A. Kelmanson. An exponentially convergent Volterra-Fredholm method for integro-differential equations. In D.J. Chappell, editor, *Proc. 11th UK Conf. on Boundary Integral Methods (Nottingham, UK)*, pages 53–63, 2017.

[52] A.I. Fairbairn and M.A. Kelmanson. Spectrally accurate Nyström-solver error bounds for 1-D Fredholm integral equations of the second kind. *Appl. Math. Comput.*, 315:211–223, 2017.

[53] A.I. Fairbairn and M.A. Kelmanson. Error analysis of a spectrally accurate Volterra-transformation method for solving 1-D Fredholm integro-differential equations. *Int. J. Mech. Sci*, 144:382–391, 2018.

[54] A.I. Fairbairn and M.A. Kelmanson. A priori Nyström-method error bounds in approximate solutions of 1-D Fredholm integro-differential equations. *Int. J. Mech. Sci*, 27pp. in press, 2018.

[55] M. Fathy, M. El-Gamel, and M.S. El-Azab. Legendre-Galerkin method for the linear Fredholm integro-differential equations. *Appl. Math. Comput.*, 243:789–800, 2014.

[56] W.-Z. Feng and X.-W. Gao. An interface integral equation method for solving transient heat conduction in multi-medium materials with variable thermal properties. *Int. J. Heat Mass Transfer*, 98:227–239, 2016.

[57] B. Fornberg. *A practical guide to pseudospectral methods*, volume 1. Cambridge University Press, 1998.

[58] S.Z. Fu, Z. Wang, and J.S. Duan. Solution of quadratic integral equations by the Adomian decomposition method. *CMES - Comp. Model. Eng.*, 92(4):369–385, 2013.

[59] D. Gottlieb and S.A. Orszag. *Numerical Analysis of Spectral Methods: Theory and Applications*. Society for Industrial and Applied Mathematics, 1977.

[60] W. Hackbusch. *Integral Equations: Theory and Numerical Treatment*. Birkhäuser Verlag, Basel, Switzerland, 1995.

[61] P.C. Hansen. Analysis of discrete ill-posed problems by means of the L-curve. *SIAM Rev.*, 34(4):561–580, 1992.

[62] J. H. Heinbockel. *Introduction to Finite and Infinite Series and Related Topics*. Trafford Publishing, 2010.

[63] P.W. Hemker and H. Schippers. Multiple grid methods for the solution of Fredholm integral equations of the second kind. *Math. Comput.*, 36(153):215–232, 1981.

[64] F.A. Hendi and A.M. Albugami. Numerical solution for Fredholm–Volterra integral equation of the second kind by using collocation and Galerkin methods. *Journal of King Saud University - Science*, 22:37–40, 2010.

[65] R.L. Herman. *A Course in Mathematical Methods for Physicists*. CRC Press, 2014.

[66] K. Herrebrugh. Solving the incompressible and isothermal problem in elastohydrodynamic lubrication through an integral equation. *Journal of Lubrication Technology*, 90(1):262–270, 1968.

[67] N.J. Higham. The numerical stability of barycentric Lagrange interpolation. *IMA J. Numer. Anal.*, 24:547–556, 2004.

[68] F. B. Hildebrand. *Introduction to Numerical Analysis*. McGraw-Hill, New York, 1974.

[69] S.M. Hosseini and S. Shahmorad. Tau numerical solution of Fredholm integro-differential equations with arbitrary polynomial bases. *Appl. Math. Model.*, 27:145–154, 2003.

[70] P. Huabsomboon, B. Novaprateep, and H. Kaneko. On Taylor-series expansion methods for the second kind integral equations. *J. Comput. Appl. Math.*, 234(5):1466–1472, 2010.

[71] C. Hwang, D. H. Shih, and F. C. Kung. Use of block-pulse functions in the optimal control of deterministic systems. *Int. J. Control*, 44(2):343–349, 1986.

[72] A. Iserles, S. Nørsett, and S. Olver. Highly oscillatory quadrature: The story so far. In *de Castro A.B., Gómez D., Quintela P., Salgado P. (eds) Numerical Mathematics and Advanced Applications.*, Berlin, Heidelberg, 2006. Springer.

[73] Z. Jackiewicz, M. Rahman, and B.D. Welfert. Numerical solution of a Fredholm integro-differential equation modelling neural networks. *Appl. Numer. Math.*, 56(3):423–432, 2006.

[74] H. V. Jain and H. M. Byrne. Qualitative analysis of an integro-differential equation model of periodic chemotherapy. *Appl. Math. Lett.*, 25:2132–2136, 2012.

[75] A. Jerri. *Introduction to Integral Equations with Applications*. Marcel Dekker, Inc., New York, 1985.

[76] H. Kaneko and Y. Xu. Gauss-type quadratures for weakly singular integrals and their application to Fredholm integral equations of the second kind. *Math. Comput.*, 62(206):739–753, 1994.

[77] S.Y. Kang, I. Koltracht, and G. Rawitscher. Nyström-Clenshaw-Curtis quadrature for integral equations with discontinuous kernels. *Math. Comput.*, 72(242):729–756, 2003.

[78] G. E. Karniadakis and S. J. Sherwin. *Spectral/hp Element Methods for Computational Fluid Dynamics*. Oxford University Press, 2005.

[79] M.A. Kelmanson. Lecture notes MATH5476M Modern Numerical Methods. University of Leeds, 2012.

[80] M.A. Kelmanson and M. C. Tenwick. Error reduction in Gauss-Jacobi-Nyström quadrature for Fredholm integral equations of the second kind. *CMES - Comp. Model. Eng.*, 55(2):191–210, 2010.

[81] N. Keyfitz. The integral equation of population analysis. *Review of the International Statistical Institute*, 35(3):213–246, 1967.

[82] D. Kosloff and H. Tal-Ezer. A modified Chebyshev pseudospectral method with an $o(n^{-1})$ time step restriction. *J. Comput. Phys.*, 104:457–469, 1993.

[83] R. Kress. *Linear Integral Equations*. Springer-Verlag, 2nd edition, Berlin, 1999.

[84] H. Laeli Dastjerdi and F.M. Maalek Ghaini. Numerical solution of Volterra–Fredholm integral equations by moving least square method and Chebyshev polynomials. *Appl. Math. Model.*, 36:3283–3288, 2012.

[85] J.L. Lagrange. Leçons élémentaires sur les mathématiques données à l'école normale en 1795. *in Oeuvres VII, Gauthier–Villars, Paris*, pages 183–287, 1877.

[86] S. Larsson, M. Racheva, and F. Saedpanah. Discontinuous galerkin method for an integro-differential equation modeling dynamic fractional order viscoelasticity. *Comput. Metods Appl. Mech. Engrg.*, 283:196–209, 2015.

[87] P. Linz. A method for the approximate solution of linear integro-differential equations. *SIAM J. Numer. Anal.*, 11(1):137–144, 1974.

[88] E. R. Love. The electrostatic field of two equal circular co-axial conducting disks. *The Quarterly Journal of Mechanics and Applied Mathematics*, 2(4):428–451, 1949.

[89] Y. L. Luke. *Special functions and their approximations*, volume 2. Academic Press, 1969.

[90] A. Makroglou, J. Li, and Y. Kuang. Mathematical models and software tools for the glucose-insulin regulatory system and diabetes: an overview. *Appl. Num. Math.*, 56, 2006.

[91] K. Maleknejad, N. Aghazadeh, and M. Rabbani. Numerical solution of second kind Fredholm integral equations system by using a Taylor-series expansion method. *Appl. Math. Comput.*, 175(2):1229–1234, 2006.

[92] K. Maleknejad and M. Attary. An efficient numerical approximation for the linear class of Fredholm integro-differential equations based on Cattani's method. *Commun. Nonlinear Sci. Numer. Simulat.*, 16:2672–2679, 2011.

[93] J. C. Mason and D.C. Handscomb. *Chebyshev Polynomials*. CRC Press, Florida, 2002.

[94] J. Medlock and M. Kot. Spreading disease: integro-differential equations old and new. *Mathematical Biosciences*, 184:201–222, 2003.

[95] A. A. Men. On an integral equation of radiation-conduction heat transfer. *Journal of Engineering Physics and Thermophysics*, 18(3):327–332, 1970.

[96] G. Miano, L. Verolino, and V.G. Vaccaro. A new numerical treatment for Pocklington's integral equation. *IEEE Trans. Magn.*, 32(3):918–921, 1996.

[97] S. Nemati. Numerical solution of Volterra–Fredholm integral equations using Legendre collocation method. *J. Comput. Appl. Math.*, 278:29–36, 2015.

[98] E. J. Nyström. Über die praktische auflösung von integralgleichungen mit anwendungen auf randwertaufgaben. *Acta Math.*, 54(1):185–204, 1930.

[99] K. B. Oldham and J. Spanier. *The Fractional Calculus*. Academic Press, New York, 1974.

[100] K. Orav-Puurand, A. Pedas, and G. Vainikko. Nyström type methods for Fredholm integral equations with weak singularities. *J. Comput. Appl. Math.*, 234:2848–2858, 2010.

[101] N.F. Parsons and P.A. Martin. Scattering of water waves by submerged plates using hypersingular integral equations. *Applied Ocean Research*, 14:313–321, 1992.

[102] R. Piessens and M. Branders. Numerical solution of integral equations of mathematical physics, using Chebyshev polynomials. *J. Comput. Phys.*, 21(2):178–196, 1976.

[103] J. Qiu. Polynomial Interpolation: Error Analysis. https://www.math.uh.edu/~jingqiu/math4364/interp_error.pdf. Accessed: 15-09-17.

[104] M. Rahman. *Integral Equations and their Applications*. WIT Press, 2007.

[105] A. Ralston and P. Rabinowitz. *A First Course in Numerical Analysis*. Dover Publications, Mineola, New York, 2001.

[106] J. Rashidinia and M. Zarebnia. The numerical solution of integro-differential equation by means of the Sinc method. *Appl. Math. Comput.*, 118(2):1124–1130, 2007.

[107] C. Runge. Über empirische funktionen und die interpolation zwischen äquidistanten ordinaten. *Zeitschrift für Mathematik und Physik*, 46:224–243, 1901.

[108] P.K. Sahu and S. Ray. Legendre spectral collocation method for Fredholm integro-differential equation with variable coefficients and mixed conditions. *Appl. Math. Comput.*, 268:575–580, 2015.

[109] H. E. Salzer. Lagrangian interpolation at the Chebyshev points $x_{n,\nu} \equiv \cos(\nu\pi/n)$, $\nu = 0(1)n$; some unnoted advantages. *Comput. J.*, 15(2):156–159, 1972.

[110] P. Sebah and X. Gourdon. Introduction to the gamma function. *American Journal of Scientific Research*, 2002.

[111] C.E. Siewert and M.M.R. Williams. The effect of anisotropic scattering on the critical slab problem in neutron transport theory using a synthetic kernel. *J. Phys. D: Appl. Phys.*, 10(15):2031–2040, 1977.

[112] J.R. Silvester. Determinants of block matrices. *Math. Gaz.*, 84(501):460–467, 2000.

[113] I. H. Sloan. Quadrature methods for integral equations of the second kind over infinite intervals. *Math. Comput.*, 36(154):511–523, 1981.

[114] I. H. Sloan, B. J. Burn, and N. Datyner. A new approach to the numerical solution of integral equations. *J. Comput. Phys.*, 18(1):92–105, 1975.

[115] A. Solomonoff. A fast algorithm for spectral differentiation. *J. Comput. Phys.*, 98:174–177, 1992.

[116] A. Solomonoff and E. Turkel. Global properties of pseudospectral methods. *J. Comput. Phys.*, 81:239–276, 1989.

[117] A. Spence. On the convergence of the Nyström method for the integral equation eigenvalue problem. *Numer. Math.*, 25:57–66, 1975.

[118] V. Spokoiny and T. Dickhaus. *Basics of modern mathematical statistics*. Springer, 2015.

[119] J. L. Stephenson. Theory of transport in linear biological systems: I. Fundamental integral equation. *The bulletin of mathematical biophysics*, 22(1-17), 1960.

[120] J. Stoer and R. Bulirsch. *Introduction to Numerical Analysis*. Springer-Verlag, New York, 2002.

[121] M. Tavassoli Kajani, M. Ghasemi, and E. Babolian. Numerical solution of linear integro-differential equation by using sine–cosine wavelets. *Appl. Math. Comput.*, 180(2):569–574, 2006.

[122] C. Tezcan, A. Kaşkaş, and M.Ç. Güleçyüz. The H_N method for solving linear transport equation: theory and applications. *J. Quant. Spectrosc. Ra.*, 78(2):243–254, 2003.

[123] H.P. Thielman. On a class of singular integral equations occurring in physics. *Quarterly of Applied Mathematics*, 6(4):443–448, 1949.

[124] L. N. Trefethen. *Spectral Methods in MATLAB*. SIAM, Philadelphia, 2000.

[125] L. N. Trefethen. *Approximation Theory and Approximation Practice*. SIAM, Philadelphia, 2013.

[126] L.N. Trefethen and M.R. Trummer. An instability phenomenon in spectral methods. *SIAM J. Numer. Anal.*, 24(5):1008–1023, 1987.

[127] F. Ursell. On the exterior problems of acoustics: II. *Math. Proc. Camb. Phil. Soc.*, 84:545–548, 1978.

[128] G. von Winckel. Legende-Gauss-Lobatto nodes and weights. https://uk.mathworks.com/matlabcentral/fileexchange/4775-legende-gauss-lobatto-nodes-and-weights. Accessed: 25-04-17.

[129] G. Wahba. *Spline Models for Observational Data*. SIAM, Philadelphia, 1990.

[130] W. D. Wallis. *A beginner's guide to discrete mathematics*. Springer Science & Business Media, 2003.

[131] A.M. Wazwaz. *Linear and Nonlinear Integral Equations: Methods and Applications*. Springer, 2011.

[132] B.D. Welfert. Generation of pseudospectral differentiation matrices I. *SIAM J. Numer. Anal.*, 34(4):1640–1657, 1997.

[133] E. T. Whittaker and G.N. Watson. *A Course of Modern Analysis*. Cambridge University Press, Cambridge, 1969.

[134] J.A.C. Wiederman. Numerical Integration of Periodic Functions: A Few Examples. *The American mathematical monthly*, 109(1):21–36, 2002.

[135] L. B. Winrich. Note on a comparison of evaluation schemes for the interpolating polynomial. *Comput. J.*, 12(2):154–155, 1969.

[136] M.A. Wolfe. The numerical solution of non-singular integral and integro-differential equations by iteration with Chebyshev series. *Comput. J.*, 12(2):193–196, 1969.

[137] S. Yalçinbaş and M. Sezer. The approximate solution of high-order linear volterra-fredholm integro-differential equations in terms of taylor polynomials. *Appl. Math. Comput.*, 112:291–308, 2000.

[138] S. Yalçinbaş, M. Sezer, and H. H. Sorkun. Legendre polynomial solutions of high-order linear Fredholm integro-differential equations. *Appl. Math. Comput.*, 210:334–349, 2009.